EXPERIMENTAL STUDY ON TURBULENCE IN VICINITY OF MID-CHANNEL BAR OF BRAIDED RIVER

Ph.D. THESIS

by

MOHAMMAD AMIR KHAN

DEPARTMENT OF WATER RESOURCES DEVELOPMENT & MANAGEMENT
INDIAN INSTITUTE OF TECHNOLOGY ROORKEE
ROORKEE - 247 667 (INDIA)
APRIL, 2018

EXPERIMENTAL STUDY ON TURBULENCE IN VICINITY OF MID-CHANNEL BAR OF BRAIDED RIVER

A THESIS

Submitted in partial fulfilment of the requirements for the award of the degree

of

DOCTOR OF PHILOSOPHY

in

WATER RESOURCES DEVELOPMENT AND MANAGEMENT

by

MOHAMMAD AMIR KHAN

DEPARTMENT OF WATER RESOURCES DEVELOPMENT &MANAGEMENT
INDIAN INSTITUTE OF TECHNOLOGY ROORKEE
ROORKEE - 247 667 (INDIA)
APRIL, 2018

INDIAN INSTITUTE OF TECHNOLOGY ROORKEE
ROORKEE

CANDIDATE'S DECLARATION

I hereby certify that the work which is being presented in the thesis entitled "**EXPERIMENTAL STUDY ON TURBULENCE IN VICINITY OF MID-CHANNEL BAR OF BRAIDED RIVER"** in partial fulfilment of the requirement for the award of the Degree of Doctor of Philosophy and submitted in the Department of Water Resources Development and Management of the Indian Institute of Technology Roorkee, Roorkee is an authentic record of my own work carried out during a period from July, 2013 to April, 2018 under the supervision of Dr. Nayan Sharma, Professor, Department of Water Resources Development and Management, Indian Institute of Technology Roorkee, India , Dr. A. Jacob Odgaard, Professor, Civil and Environmental Engineering, University of Iowa, College of Engineering, Iowa City, United States of America and Dr. Gopal Das Singhal, Assistant Professor, Civil Engineering, School of Engineering, Shiv Nadar University, Uttar Pradesh, India.

The matter presented in this thesis has not been submitted by me for the award of any other degree of this or any other Institution.

(MOHAMMAD AMIR KHAN)

This is to certify that the above statement made by the candidate is correct to the best of our knowledge.

(Nayan Sharma)	(A. Jacob Odgaard)	(Gopal Das Singhal)
Supervisor	Supervisor	Supervisor

Dated 11-April-2018

ABSTRACT

Alluvial streams with braided patterns are frequently encountered in nature. Braided streams are characterized by a random pattern of multi-thread channel networks owing to the appearance of braid bars within the overall waterway of the river. The presence of braid bars increases the total flow resistance and the energy losses along the boundary, thereby promoting the development of networks of hydraulically inefficient channels. The mid channel deposition is considered as one of the main reasons of initiation of braiding. Extensive laboratory investigations and stringent analysis have been carried out to study the turbulence flow hydraulics in the vicinity of mid-channel bar.

Researchers such as Nakagawa and Nezu (1978), Wu and Jiang (2007) observed that the bursting events are more closely associated to the sediment entrainment rather than the total shear stress. Thus for thoroughly understanding the flow behaviour, the conditional technique is used for decomposing the Reynolds stress into the bursting events. Researchers Jennifer et al. (2011), Nezu et al. (1994) observed that only the extreme turbulent events contribute to the turbulent burst. They used the concept of Hole size for segregating the extreme quadrant events from the low intensity quadrant events. The effect of Hole size on the bursting events are studied in details. The velocity fluctuations are modelled using the Gram-Charlier method. The joint probability distribution of quadrant events is analysed. It will help in analysing the structure of turbulent burst generated due to the fluid bar interaction. The Hole size effect on joint probability distribution of velocity fluctuations is also studied. The extreme events are observed at sections near the upstream end of mid-channel bar. These extreme turbulent bursts are generated by the fluid bar interaction. The sweep events are found to be dominant near the boundary and ejection events are observed to be dominant away upward from the boundary. From the results, it was found that the dominance of sweep events decreases as the hyperbolic Hole size increases. The results bring out that the higher stresses are produced mainly due to ejection events.

The transverse component of turbulent kinetic energy is found significant in the vicinity of mid-channel bar. Thus, the three-dimensional bursting analysis is carried out for analysing the turbulent flow structure. The '3-Dimensional Burst Index' (3DBI) and 'Transition Ratio' (TR) parameters are proposed in this work for linking the bursting events with the local stream bed elevation change observed in the vicinity of mid-channel bar. The 3-Dimensional Burst Index and Transition Ratio exhibit linear relationship with the scouring/deposition phenomena observed in the vicinity of mid-

channel bar with their Coefficient of Determination and Pearson R value are found to be above 0.9. The high value of correlation coefficients indicate that these parameters are closely related with the local stream bed elevation change observed in the vicinity of mid-channel bar.

For studying the interaction of sweep and ejection events, a new parameter '3-Dimensional Dominance Function' (3DDF) is proposed in this study. This parameter helps in analysing the kolks-boils phenomenon observed in the vicinity of mid-channel bar.

Researchers have utilized the concept of Hole size for two-dimensional bursting events. The concepts of Hole size for octant events is yet to be developed till now as could be seen from literature. At region where the flow is three dimensional, the Hole size concept for octant events is necessary for segregating the extreme octant events from the low intensity octant events. Thus, for defining the Hole size concept for octant events, the new parameter '3-Dimensional Hole Size' (3DHS) is proposed in this study. The variations of octant events with the 3DHS are analysed. The results indicate that the presence of mid-channel bar leads to the creation of high turbulent burst. The one more notable conclusion drawn from this analysis is that the dominant events becomes more dominant with increase in the 3DHS value.

Three dimensional transitional movements are modelled using the first order Markov chain. The linkage of these transitional movements with the scouring/deposition occurred in the vicinity of mid-channel bar are analysed. The relationship is proposed between the stable transitional movements using the Nonlinear Fit Toolbox of MATLAB Software. The high value of correlation for these expressions indicates that they are correctly predicting the relationship between the stable movements.

The spatial contours of turbulent parameters are studied for bar and no bar conditions. High level turbulent intensities are observed at region near upstream end of mid-channel bar and level of turbulent intensities decreases with increase in distance from the upstream end of mid-channel bar. The high level of turbulent intensities at region near upstream end of mid-channel bar is responsible for occurrence of scouring at that region.

As could be seen from literature, hardly any work had been done on this type of experimental setup. Thus, for validating the experimental results, the laboratory model is developed in the Fluent Software. The Ansys Mesher is used for meshing the simulated model. The Reynolds stress model is used for modelling purpose. The three-dimensional implicit steady pressure-based solver is

utilized for the computation. Discretization of pressure is done using the Presto method. The momentum and Reynolds stress are discretized using the second order upwind scheme.

The depth-wise profile of velocity and turbulent parameters are investigated at locations upstream and downstream of mid-channel bar. The effect of submergence ratio on the flow structure is analysed by closely observing the depth-wise distribution profile of velocity and turbulent parameters. The results indicate that the increase in the height of mid-channel bar causes greater reduction in longitudinal velocity. The vertical velocity is negative at sections upstream of the mid-channel bar. The negative vertical velocity indicates the downflow at these sections. The magnitude of transverse velocity is significant at sections downstream of mid-channel bar. This highlights that the flow structure is three dimensional at downstream region of the mid-channel bar. The increase in height of mid-channel bar causes increase in the magnitude of longitudinal turbulent intensity. Results confirm that the experimental results are correctly validated by the Reynolds stress model simulation of Fluent Software. The deviation of velocity profile from logarithmic law is more discernible for sections located in close vicinity of the mid-channel bar.

The longitudinal turbulent intensity at sections downstream of mid-channel bar is much more pronounced as compared to the upstream sections. This is mainly due to the interaction of surface wave with the downstream flow. The increase in vertical and transverse component of turbulent intensity is observed for higher submergence ratio.

Third order moments of velocity fluctuations transmit the stochastic information of the turbulent fluctuation in terms of flux and advection of turbulent stresses. The behaviour of these third order moments of velocity fluctuations at locations upstream and downstream of mid-channel bar are analysed. The presence of mid-channel bar causes increase of skewness in the longitudinal velocity distribution. The value of S_u is greater for higher submergence ratio. This indicates that the high submergence ratio creates greater skewness of longitudinal velocity. The magnitude of S_w is more at sections in the close vicinity of mid-channel bar. This highlights that the presence of mid-channel bar causes greater skewness in the vertical velocity distribution.

Presence of mid-channel bar causes redistribution of Fku and Fkw coefficients. The magnitude of Fku and Fkw are greater for higher submergence ratio. This indicates that the greater energy transfer takes place for higher submergence ratio.

New parameters are developed in this study for an insight into turbulent flow structure in the vicinity of mid- channel bar. The concept of Hole size is proposed for the octant events in this study. The newly introduced Three-Dimensional Hole Size in this research helps in minutely studying the turbulent flow structure. Not many prominent studies have been done on the flow structure in the vicinity of mid-channel bar. Due to the lack of experimental data on this topic, the Reynolds stress modelling is done for validating the experimental results. The effect of submergence ratio on the turbulent flow structure in the vicinity of mid-channel bar are analysed. Effect of fluid-bar interaction on the third order moments of velocity fluctuations is investigated. The present study contributes towards better comprehension of the intricate linkage of turbulent burst events with the local stream bed elevation changes that are observed in the vicinity of mid-channel bar of braided river.

ACKNOWLEDGEMENT

I wish to express my sincere appreciation to those who have contributed to this thesis and supported me in one way or the other during this amazing journey.

Firstly, I would like to express my sincere gratitude to my supervisors Prof. Nayan Sharma, Prof. A. Jacob Odgaard and Dr. Gopal Das Singhal for their continuous support, encouragement and guidance throughout the Ph.D. study. Their guidance helped me in all the time of research and writing of this thesis. I could not have imagined having a better advisors and mentors for my Ph.D. study.

I am greatly thankful to my research committee members: Prof. S.K. Mishra, Prof. Deepak Khare, Dr. Ashish Pandey and Prof. Zulfequar Ahmad for their insightful comments and encouragement which help me to widen my research area from various perspectives.

I express my heartfelt thanks and indebtedness to the faculty members of the Department of Water Resource and Development and Management, IIT Roorkee for their continuous support and encouragement during the course of the study.

I would like to thank all of my friends; whose love and guidance provide me the motivation for pursuing the research. Most importantly, I wish to thank my loving parents, who provide me the unending positive energy and inspiration.

Finally, I would like to thanks Almighty God for his immeasurable blessing upon my life.

Dated: 11/04/2018

(MOHAMMAD AMIR KHAN)

TABLE OF CONTENTS

LIST OF FIGURES

LIST OF TABLES

LIST OF SYMBOLS

Notation		Description
b	:	Length of minor axis of elliptical bar
B	:	Overall width of flow
Bt	:	Bursting event at time t
d_i	:	Depth of submerged channel
d_{50}	:	Representative bed size
fku	:	Stream wise flux of turbulent kinetic energy
fkw	:	Vertical flux of turbulent kinetic energy
h	:	Depth of flow
h_b	:	Height of bar
H	:	Hole size
H_{st}	:	Hermite polynomial of order (s+t)
k	:	Von Karman's constant
K	:	Octant event
l	:	Length of major axis of elliptical bar
L	:	Length of bar
n	:	Total number of velocity samples
n_i	:	Number of events belonging to octant i at any instant t
n_{ij}	:	Number of transitional movements from octant event i to octant event j
n_K	:	Total number of bursting events present in octant K
N	:	Number of braided channels
N_t	:	Total number of products $u'(t)\, w'(t)$
P_{ij}	:	Probability of transitional movement from octant event i to octant event j
P_K	:	Occurrence probability of bursting event which belongs to the K octant
$P(u', w')$	:	Joint probability function of u' and w' fluctuations
R	:	Hydraulic mean depth of stream

R^2 : Coefficients of determination

RS_i : Reynolds stress contribution from i^{th} quadrant for Zero Hole size

$RS_{i,H}$: Reynolds stress contribution from i^{th} quadrant for H Hole size

S_u : Skewness coefficient in the longitudinal direction

S_w : Skewness coefficient in the vertical direction

T : Top width of flow

Ti_u : Normalized RMS value of longitudinal fluctuating velocity

Ti_v : Normalized RMS value of transverse fluctuating velocity

Ti_w : Normalized RMS value of vertical fluctuating velocity

u : Longitudinal Velocity

u' : Fluctuation in longitudinal velocity

u_c : Critical velocity for sediment movement

u_i : Magnitude of longitudinal velocity for i^{th} velocity sample

u_* : Shear velocity of approach flow

$\overline{u'}$: Mean- value of the longitudinal velocity fluctuation

U : Mean velocity of flow

v : Transverse Velocity

v' : Fluctuation in transverse velocity

v_i : Magnitude of transverse velocity for i^{th} velocity sample

$\overline{v'}$: Mean- value of the transverse velocity fluctuation

w : Vertical Velocity

w' : Fluctuation in vertical velocity

w_i : Magnitude of vertical velocity for i^{th} velocity sample

$\overline{w'}$: Mean- value of the vertical velocity fluctuation

x : Axis For longitudinal direction

x_i : Width of submerged channel

X_Q : Indicator Function for performing conditional averaging procedure

y : Axis For transverse direction

y_0 : Zero velocity level

z : Axis For vertical direction

ϑ : Dynamic viscosity of water

τ	:	Shear Stress
ρ	:	Density of water
$\phi(u', w')$	:	Gaussian distribution function for $u'$and w' variables
$\chi(x, y)$	:	Characteristics function of Joint probability distribution

Abbreviations

CFD	:	Computational Fluid Dynamics
FGI	:	Flow Geometry Index
PFI	:	Plan Form Index
RANS	:	Reynolds-Averaged Navier-Stokes
RMS	:	Root Mean Square Value
RSM	:	Reynolds Stress Model
TKE	:	Turbulent Kinetic Energy
TR	:	Transition Ratio
2DBI	:	Two Dimensional Burst Index
3DBI	:	Three Dimensional Burst Index
3DDF	:	Three Dimensional Dominance Function
3DHS	:	Three Dimensional Hole Size

THIS PAGE IS INTENTIONALLY LEFT BLANK

CHAPTER-1 INTRODUCTION

1.1 Background

Braiding phenomenon is an occurrence usually observed in alluvial rivers. In Indian sub-continent the river Brahmaputra is known for its braiding characteristics. Bar patterns affect the sedimentary characteristics of anabranching and braided rivers (Ferguson 1993; Kleinhans 2010; Kleinhans and van den Berg 2011; Richardson and Thorne 2001). In the past, a lot of work had been done on braided rivers and their channel pattern forms by several researchers such as (Ahrens 2006; Ashworth et al. 1992; Ashworth et al. 2011; Lane 1957; Parker 1976) etc. and yet, when compared to the wealth of literature upon meandering systems, the braided rivers have been comparatively understudied.

Qualitative and geomorphic models have cited mid-channel bar initiation and growth due to stalling of bed load around the channel centreline as a primary process in braiding (Ashmore 1982; Ashworth et al. 1992; Leopold and Wolman 1957; Schumm and Khan 1972; Schumm and Lichty 1963). Mid-channel bar formation, termed 'central bar deposition' by Ferguson (1993) is still recognised as major cause of channel division in many braided rivers. In spite of the significance of mid-channel bar, only few studies have been done on assessing the flow behaviour in the vicinity mid-channel bar.

Understanding the complex fluvial interaction between the fluid and mid-channel bar has continued to pose a challenging task for hydraulic engineers to deal with and for modellers to simulate. Braiding process generally starts with the formation of small mid-channel bar (Ashmore 1982; Ashworth et al. 1992; Ferguson 1993; Flügel 1995, Rice et. al. 2009, Bridge 1993, Bathurst 1985). Initiation of mid-channel bar formation is of serious concern for people living in the flood plain, as it diverts the flow toward outer region which leads to the erosion of bank. Low flow and high sediment discharge lead to the shedding of sediment. The deposition in the mid-channel acts as hindrance to flow, which leads to further deposition. With time, the deposition becomes pronounced and it takes the form of islands (Federici and Paola 2003; Leopold and Wolman 1957; Richardson and Thorne 1998; Schumm and Khan 1972).

A turbulent phenomenon in braided rivers is much more complex than that in straight and meandering rivers. Turbulent flow characteristics around the braid bar are not well known till now (Lu and Willmarth 1973; Parker 1976; Surian 2015). Turbulent flow characteristics around the mid-channel bar are studied in the past. However, the association of deposition and sediment entrainment around the mid-channel bar with the turbulent bursts still remains least understood. The concept of Hole-size (H) is used by researchers mainly for two-dimensional turbulent bursting in order to exclude the extreme bursting events from the low intensity events (Jennifer et al. 2011; Naot et al. 1993). Keshavarzi et al. (2014), Keshavarzi and Gheisi (2006) developed a method of three-dimensional octant analysis to account for the effect of secondary flow. The third-order velocity fluctuations are sensitive to the occurrence of burst–sweep cycles and turbulent flux contributions (Balachandar and Bhuiyan 2007; Barman et al. 2017; Nagano and Tagawa 1988) and it is directly related to coherent structures through turbulence characteristics (Bhosekar et al. 2007; Bhosekar et al. 2011; Gad-el-Hak and Bandyopadhyay 1994).

1.2 Earlier Research

Although recent work has begun to provide quantitative information on bedform and sediment transport dynamics in large sand-bed rivers (Julien & Klaassen 1995; Kostaschuk & Ilersich, 1995; Kostaschuk & Villard 1996; Amsler & Garcia 1997), the flow structure associated with developing mid-channel sand bars (Richardson and Thorne 1998, Richardson and Thorne 2001), and changes in channel morphology (Klaassen 1999; Mosselman 2009), there is still lack of knowledge concerning the nature of bar evolution and aggradation, and the contribution of bed forms to the overall alluvial architecture. The laboratory study of mid-channel bar is vital for understanding the flow structure observed in the vicinity of mid-channel bar (Ashworth et al. 1992). Detailed literature review on the present research is thoroughly discussed in Chapter 2.

1.3 Research Gap

The experimental study on analyzing the turbulent flow structure is necessary for understanding the flow behavior in the vicinity of mid-channel bar. Only few researches have been done on the flow behavior changes observed due to mid-channel bar formation. No literature is available which relates the bursting events to the local stream bed elevation change observed in the proximity of mid-channel bar. In-depth study of turbulent flow structure is necessary to minutely examine the bursts generated due to the fluid bar interaction. Recently researchers have observed that the shear stress

does not directly relate to sediment motion but turbulent bursts (ejection, sweep) are indeed responsible for sediment entrainment. Thus, the decomposition of shear stress into the bursting events is imperative for analysing the flow behavior. Researchers such as Jennifer et al. (2011), Naot et al. (1993) observed that only the high magnitude bursting events contribute to the turbulent burst. Therefore, the Hole-size analysis is required for segregating the extreme bursting events from the low intensity events. Concept of three dimensional burst analysis is relatively new for open channel flow. The Two-Dimensional analysis of the bursting process cannot completely define the turbulent structure of flow (Keshavarzi et al. 2005; Keshavarzy 1997). Therefore, the Three-Dimensional analysis is essential to provide more resolution to the turbulent burst study. Effect of fluid- bar interaction on the third-order velocity fluctuations is not available in literature. A reliable pattern of sediment transport in the vicinity of mid-channel bar robustly relies on resolving the flow structure at different spatial locations. In due course, research is desirable to quantify the turbulent flow field at close proximity of mid-channel bar.

1.4 Objectives of the Study

1. To study the effect of Hole size concept on the turbulent burst generated due to the fluid bar interaction.
2. To study the spatial distribution of Reynolds stress and other turbulent parameters in the vicinity of mid-channel bar.
3. To develop parameters which relate the bursting events with the local stream bed elevation change observed in the vicinity of mid-channel bar.
4. To analyse the interaction of sweep/ejection events and their association with the scouring occurred in proximity of mid-channel bar.
5. To study the three-dimensional burst analysis and model the transition movements using the first order Markov chain.
6. To investigate the concept of Hole size for three-dimensional bursting events.
7. To develop the relationships between the stable transitional movements.
8. To validate the experimental results using the Reynolds stress model.
9. To analyse the depth-wise distribution of velocity components and turbulent parameters in close proximity of mid-channel bar and to study the effect of submergence ratio on the flow behaviour in the vicinity of mid-channel bar

10. To study the effect of fluid- bar interaction on third-order moment of velocity fluctuations.

1.5 Research Contribution

The present study addresses the variation of turbulent flow structure that occurs due to the fluid bar interaction. Although the static mid-channel bar is not precisely an actual representation of the natural prototype bar, the study for fixed bar will undeniably improve the understanding of turbulent structure in the vicinity of mid-channel bar. It will give an insight to the comprehension of the phenomena which are vital for understanding the intrinsic fluvial processes of fluid bar interaction. The deviations of mean velocity and turbulence due to the presence of mid-channel bar need a special attention. The present research is basically a small but important step for enhancement in discerning the turbulent flow structure in the vicinity of mid-channel bar. The main motive of this study is to analyse the changes that occur in turbulent flow due to the fluid bar interaction and to better understand the mechanics of flow which are responsible for sediment entrainment and deposition in the vicinity of mid-channel bar. It is desirable to study the mechanics of turbulence from the data collected using ADV at different locations. The Reynolds stress model is used for validating the experimental results. The '3-Dimensional Burst Index' and 'Transition Ratio' parameters are proposed in this study. These parameters have intimate linkages with the local stream bed elevation changes observed in the vicinity of mid-channel bar. For analysing the sweep and ejection events interaction, another new parameter '3-Dimensional Dominant Function' is developed in this study. Furthermore, the concept of Hole size for three-dimensional bursting events is proposed in this study. Results indicate that the stable movements are associated with the local stream bed changes observed in the vicinity of mid-channel bar. The summation of transitional probability is equal to one, so change in probability of one stable movements leads to the change in the other transitional movements. Thus, the association of stable movements are analysed by developing the relationships using the Nonlinear Fit Toolbox of MATLAB Software. The effect of submergence ratio on the turbulent flow behaviour is also analysed in this study. The Reynolds stress modelling is done for validating the experimental data.

1.6 Limitation of Research work

The changes induced in the turbulent flow due to the fluid bar interaction are analysed in the present study. The experiments were carried out for only one bed material. This study can be extended in future for different sizes of bed material.

1.7 Organisation of the Thesis

The study carried out is organised in the following way:

Chapter-1 Portrayal of preparatory views of the topic studied, fundamental objectives and the setup of the thesis.

Chapter-2 Presents a comprehensive review of literature to provide the knowledge of researches done on the mid-channel bar.

Chapter-3 This Chapter presents the detailed experimental setup, which has been used for the study.

Chapter-4 This chapter deals with the two-dimensional bursting analysis.

Chapter-5 This Chapter provides the detail of spatial distribution of turbulent parameters in the vicinity of mid-channel bar.

Chapter-6 Presents the results of three-dimensional bursting events analysis

Chapter-7 This Chapter provides the detail of Reynolds stress model inbuilt in Fluent Software used for validating the experimental results.

Chapter-8 Presents analysis of the velocity and turbulent parameters distribution in the vicinity of mid-channel bar.

Chapter-9 This chapter presents the depth-wise distribution of third order moment of velocity fluctuations.

Chapter-10 Presentation of summary and conclusions of research work. It also provides the information about scope for future work.

Bibliography

Furthermore, at the end of the thesis two annexes are placed for ready reference.

Annex-1 MATLAB codes for establishing relationships between the stable transitional movements.

Annex-II List of Publications (Published/Communicated).

CHAPTER-2 REVIEW OF LITERATURE

2.1 General

Braiding phenomenon is observed in alluvial rivers with large fluvial energy. In Indian subcontinent the river Brahmaputra is well kno,,wn for its intense braiding characteristics. In the past, a lot of work has been done on braided rivers and their channel pattern forms by many researchers (Callander 1969; Leopold and Wolman 1957; Mosley 1976; Parker 1976; Sharma 2004; Singh et al. 2010; Thorne et al. 1993) etc. and yet, when compared to the wealth of literature upon meandering systems, the braided rivers have been comparatively understudied.

Only few laboratory and field researches have been done on the flow behaviour in braided streams and as a consequence their association with the braided morphology is not adequately understood. Unlike meandering channel, in which important flow processes can be observed over a range of flow stages, in braided stream most of the morphology changes have been occurring at high level of discharges when data collection is extremely difficult (Church and Ferguson 2015; Richardson and Thorne 1998; Rust 1977; Smith 1970). Study of secondary flow in braided channel is mainly restricted to the channel confluences, whereas the effect of secondary flow on bifurcating flow around the braid bar has been mostly neglected (Richardson and Thorne 2001; Sankhua et al. 2005). Braided reaches have complex structure which consists of distributaries and bars in the high energy environment (Bristow and Best 1993; Cant and Walker 1978; Howard et al. 1970). Multi threads braided streams cause high energy dissipation due to the enhancement of total resistance (Richardson and Thorne 2001; Schumm and Lichty 1963).

Braiding of the river is characterized by the division of channel flow around the alluvial island. The growth of the islands starts as the coarser portion of sediment load start depositing. The bar grows downstream and in height due to the continuous deposition of sediment on its surface, deviating the water into the flanking channels, which are to carry the flow, deepens and cut laterally into the original banks. Intensifying of flanking channels lower the water depth and the bar emerges as an island which becomes stabilized by vegetation (Leopold and Wolman 1957).

The braided streams are hydraulically less efficient and the formation of braid bars plays the significant role in adjustment of the energy loss due to friction (Thorne and Tovey 1981). Sharma (2004) had developed Plan Form Index (PFI) and Flow geometry index (FGI) for classifying the

degree of braiding. These indices are more logical as compared to the previous proposed indices due to the incorporation of river hydraulic variables.

Plan Form Index represents the percentage of actual flow width per braided channel.

PFI is computed using the Equation 2.1.

$$PFI=\frac{\frac{T}{B}\times 100}{N} \quad (2.1)$$

With reference to Figure 2.1, T is top width of flow =T1+T2, B is Overall width of flow and N is number of braided channels. This index indicates the fluvial landform with respect to a given water level. Lower value of PFI indicate the high degree of braiding.

Flow geometry Index (FGI) is given by Equation 2.2.

$$FGI = \frac{\sum d_i * x_i}{R * T} \times N \quad (2.2)$$

With reference to Figure 2.2, d_i and x_i represent the depth and width of submerged channel, R represent the hydraulic mean depth of stream, T represents the top width of flow and N is number of braid channel.

The flow geometry index indicates the underwater sub-channel disposition and the hydraulic efficiency of a braided stream. Its higher value signifies the occurrence of higher degree of braiding.

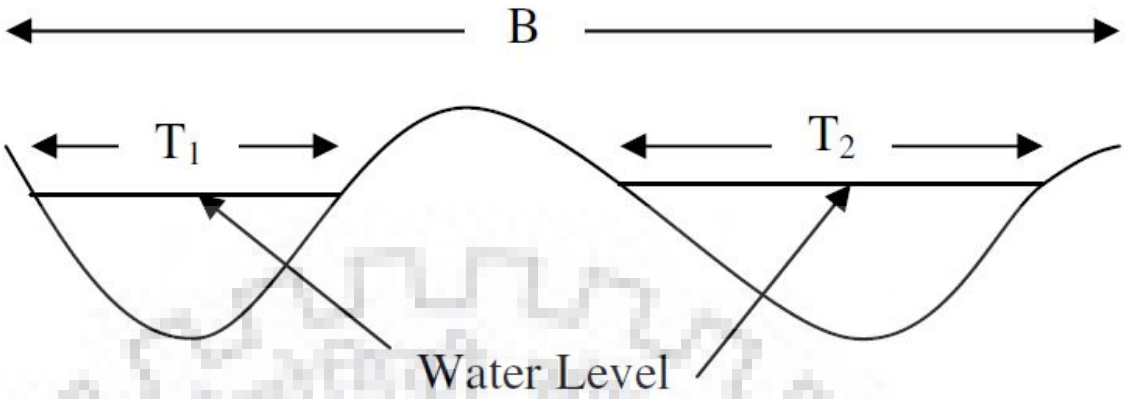

Figure 2.1 A typical flow cross section

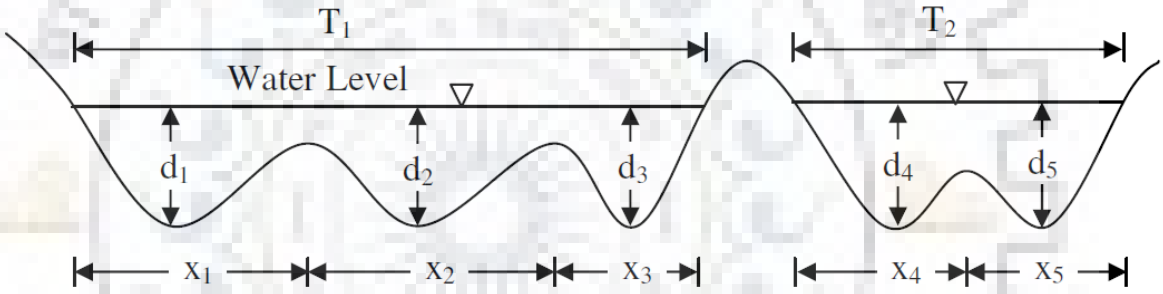

Figure 2.2 Flow geometry

Present knowledge of braiding process and mainly mid-channel bar formation is obtained from only few researches works (Akhtar et al. 2011; Bluck 1979; Ore 1964). The mechanism of mid-channel bar formation is not properly understood (Ferguson 1993; Mosselman 2009; Sapozhnikov and Foufoula-Georgiou 1996; Smith 1970). Mid-channel bar formation is considered as the prominent feature of complex morphology of braided streams. Several researchers have tried to characterize the braided bar pattern by using the criteria such as elongation, symmetry and absence or presence of avalanche face (Chahar 2007; Church and Jones 1982). However, there is not much agreement on these classifications and unambiguous classification is almost impossible (Ashmore 1982; Ashworth et al. 1992; Ashworth 1996). The morphological processes in braided streams are vital for understanding the river engineering and prevent disasters from flood, bank erosion and environmental purposes to maintain river ecosystem. The morphological changes of braided streams are closely related to the bank erosion and deformation due to the mutual interlinking between the sediment transport and water flow. In braided stream, the channel development process is initiated with the bar emergence under certain flow condition due to the widening of initially straight channel (Ashworth et al. 2000; Best 1986; Best et al. 2007; Jang and Shimizu 2007; Sarma and Phukan 2006).

2.2 Study of Mid-Channel Bar Formation

Mid-channel bar formation is primarily responsible for the initiation of braiding process (Ashmore and Parker 1983; Ashmore 1982; Ashworth et al. 1992; Ferguson 1993; Kang et al. 2010). Thus, the literature regarding the morphological structure of mid-channel bar formation is analysed in this section.

Although their appearance is quite similar to that of alternating bars, their occurrence is mainly depending on the local flow conditions which cause deposition and scouring in a non-periodic manner. This is in opposite to the scours that are responsible for the alternate bars which are mostly periodic in nature (Baki and Gan 2012; Coleman 1969). Bristow (1993), Cant and Walker (1978), Hein and Walker (1977), Sarma (2005) observed that the change in local flow condition may generate mid-channel bar in streams. Bar formation is initiated whenever there is decrease in sediment transport capacity.

There is no universal mechanism for bar development. Rather bar development can be initiated either by central deposition or by erosional dissection of topographic highs (Goff and Ashmore 1994; Lunt et al. 2004; Szupiany et al. 2009).

The division of velocity field into the multiple threads and the development of mid-channel bar is crucial for understanding the braiding process (Ashmore 1991; Ashworth 1996; Ashworth et al. 2011; Leopold and Wolman 1957). However, lack of data at the point of braid bar initiation and lack of knowledge concerning the fluvial and sediment processes responsible for braiding have limited the degree to which braiding in alluvial channels can be understood and explained (Ashmore 1991; Bristow et al. 1993; Luchi et al. 2010; Rosgen 1985). It is significant that the process of deposition of bed load at the centre of the channel as pointed out by Ashworth et al. (2011) and Ferguson (1993) is not adequately understood and remains a relevant topic for study.

The factors responsible for mid-channel bar development are not yet completely known. Leopold and Wolman (1957) reported that the mid-channel deposition diverts the flow towards the banks which leads to the erosion and positive feedback then accentuates bar development and widening.

Some researchers have been done in assessing the flow structure in the vicinity of mid-channel bar (Detert et al. 2007; Mahanta 2010; Nelson et al. 1995), which are considered as the precursors to braiding. However, these research works do not analyse the turbulent flow dynamics and may be not apt for the low sinuosity channels that are characteristics of braided channels (Bridge et al. 1986; Klaassen 1999; Lewin 1976).

Ashmore (1982), Ashworth et al. (1992) carried out measurements in flumes and in streams. They had proposed the process-based explanations of mid-channel bar initiation and its growth on the basis of flow behaviour and sediment deposition downstream of the channel confluence. Ashmore and Parker (1983), Ashmore (1988) observed that the initial deposition is caused by the 'slight change in competence near the centre of the channel' which is plausible if the flow is shallow and close to critical. Ferguson (1993) had observed that the high turbulence zone lies in the central region of the channel at location just downstream of confluence, but progressively moves away from the bed and dissipate within a few channel widths downstream. The turbulent kinetic energy redistribution causes decrease in the vertical energy gradient and thus create a zone of high sediment deposition and subsequent bar growth.

Ashworth (1996) had developed a physical model on mid-channel bar growth on the basis of (Ashmore 1991; Ashworth 1996; Leopold and Wolman 1957) works. Figures 2.3 (a-d) are showing the stages of mid-channel bar development at location just downstream of a recently formed confluence.

For unconfined braid plains, channel avulsions are commonly observed and new distributary is often created (Figure 2.3a). For the case of recently formed Y' shaped confluence having almost equal

sediment and water discharge, the deposition occurred at location downstream of the confluence (Figure 2.3b). The distance between the channel confluence and sediment accumulation zone is primarily depends on the total discharge, sediment supply, turbulence discharge ratio (Mosley 1976; Yalin 1992). The bar growth continues by deposition of all sizes of bed load in the low velocity region that is created behind the coarse bar head. With passage of time, the bar becomes quite bigger and it deflects the flow towards the banks (Figure 2.3c), causing reduction in reach average shear stress.

The change in flow behaviour from convergence to divergence leads to shifting of high velocity zone from the centre of channel to the distributaries. The decrease in shear stress caused by the widening of channel promotes further growth of bar (Figure 2.3d). The emergent mid-channel bar may stabilize by the vegetation (Leopold and Wolman 1957).

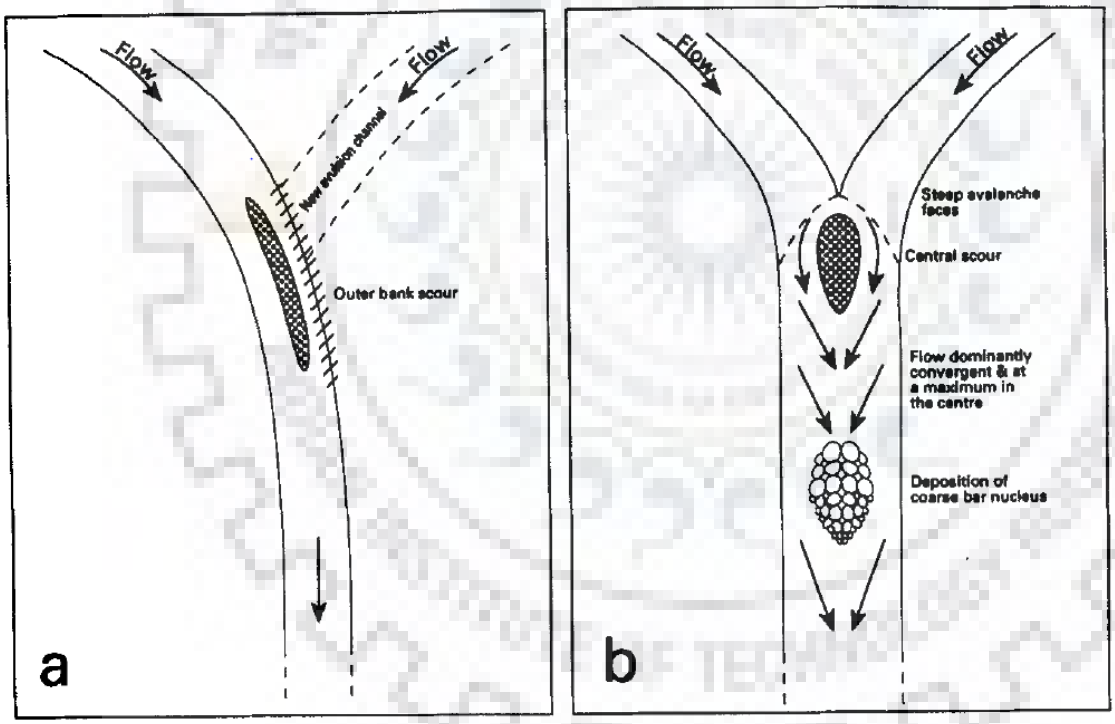

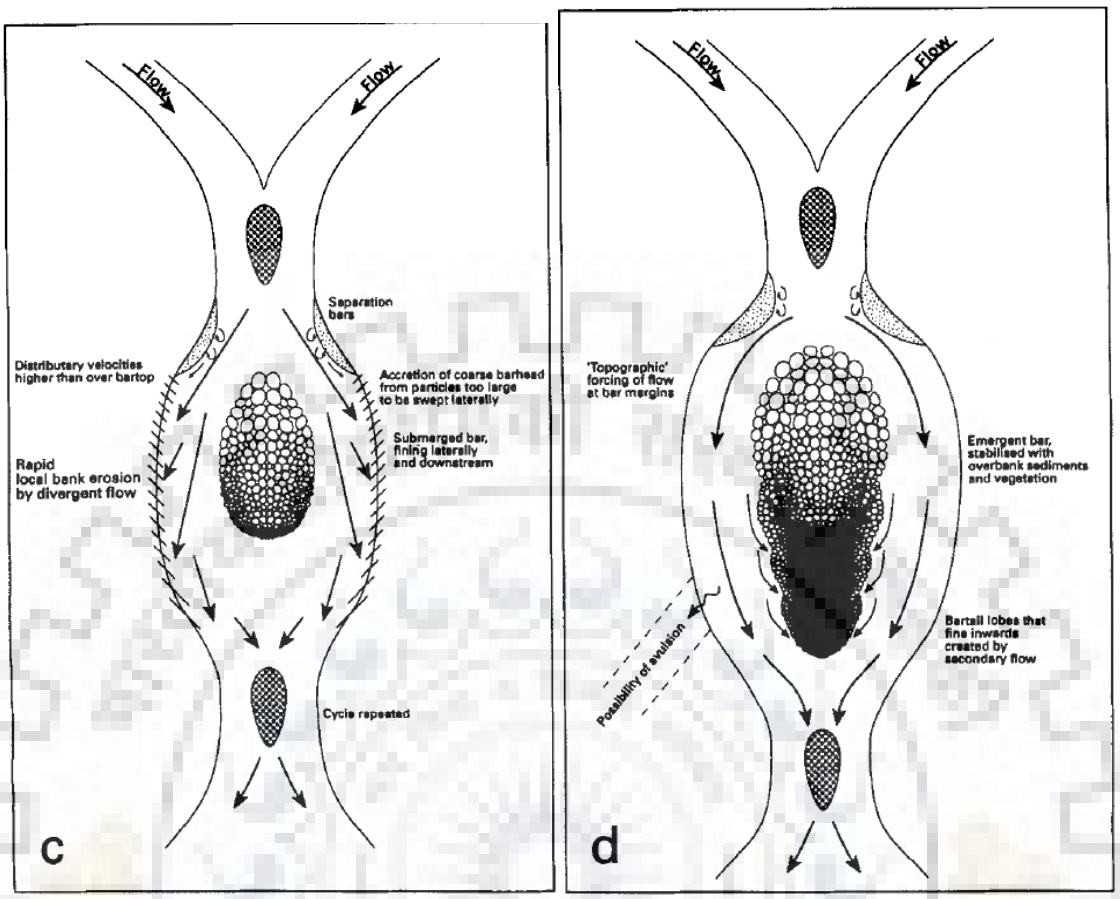

Figure 2.3. (a)-(d) Model of mid-channel bar growth downstream of a confluence proposed by Ashworth (1996). Arrows refer to surface flow direction

The interaction between the fluid and mid-channel bar is a challenging task for hydraulic engineers to deal with and for modellers to simulate (Best 1986; Bhosekar et al. 2011; Izadinia et al. 2013; Bridge et al. 1986; Bridge 1993; Rice et al. 2009). It has greater effects on people living on flood plains. Field data collection for large braided river over long period of time is very tedious and financially challenging task (Crosato et al. 2011; Dobler and Ahrens 2008; Gaur et al. 2011; Van der Wegen and Roelvink 2008). In recent years, many researchers had used physically based models for modelling the fluvial processes. However, limited works have been done on modelling the process of bar evolution (Ashmore 1991; Eaton et al. 2010; Ferguson and Werritty 1983; Lunt and Bridge 2004).

2.3 Study of Turbulent Burst

Several channel patterns such as straight, braided, meandering river exist in the natural conditions. Few research works have been done for analysing the turbulent flow behaviour in the vicinity of mid-channel bar. However, these works are not enough to adequately understand the flow structure around the mid-channel bar (Goel 2008; Mahanta 2010; Murray and Paola 1994; Richardson and Thorne 2001; Roy et al. 2004). The turbulence phenomenon in the braided river is much more complicated as compared to the meandering rivers. Turbulent characteristics of flow in the vicinity of mid-channel bar is not studied much till now (Ferguson 1993; Girija et al. 2007; Joglekar and Gedam 2012; Parker 1976). The literature regarding the characteristics of turbulent burst is discussed in this section.

Braiding network comprises of number of channels which divide and re-join thus forming the complex network around the mid-channel bar. Schumm and Lichty (1963) defined the braided river as a single channel which at low flow season has islands formed by sediment and stabilized by vegetation. Braided river is currently important topic of study, and several scientists are doing research on the complexity of braided river and flow characteristics around mid-channel bar. Turbulent flow characteristics around mid-channel bar are studied in the past; however, the association of deposition and sediment entrainment around mid-channel bar with the turbulent bursts phenomenon still remains not adequately investigated.

The concept of turbulent burst and its impact on near-bed stress generation was first introduced by (Kim 1985; Kline et al. 1967) as a quasi-periodic process which leads to transfer of momentum in the boundary layer. Researchers (Khan et al. 2016; Nakagawa and Nezu 1978; Nakagawa et al. 1975; Nelson et al. 1995; Williams et al. 1989) had studied the 2-D bursting events and observed that the sweep event is primarily responsible for sediment entrainment. Mazumder and Ojha (2007) and Wu and Jiang (2007) found that the shear stress does not directly relate to sediment motion but turbulent bursts (ejection, sweep) are responsible for sediment entrainment.

Nakagawa and Nezu (1978,1981) had performed experiments in a fully developed turbulent open channel flow. They studied the space time correlation structure of the bursting events using the conditional sampling technique. They observed that temporal and spatial scale of sweep events extend more toward downstream than upstream. Bogard and Tiederman (1986) provided seven new methods for detecting bursting events in open channel flow. They had applied the quadrant technique

to single point velocity measurements. They observed that the quadrant technique is able to detect burst. They also found that other algorithms are significantly less accurate for detecting coherent structure in turbulent flow. The effectiveness of those algorithms depends on the so-called threshold levels and the optimum threshold for the quadrant technique was found to be about 1. Sumer and Deigaard (1981) found that the ejection bursting events are primarily responsible for saltation motion of sediment particles in the inner region of flow. In the past few years the research on coherent structure of turbulent flow have significantly increased and have been executed in both natural channels (Goel 2008; Nikora and Goring 2000; Roy and Bergeron 1990), as well as in laboratory flumes (Detert et al. 2007). The proper knowledge of sediment transport process is required for solving various problems such as reservoir sedimentation, soil erosion in catchment, river morphological computation etc. In the alluvial rivers, the sediment transport is accompanied with the formation of various bed forms, thus the turbulent characteristics of such flows are quite different from the flow passing through the plane bed.

The velocity fluctuations are defined as variation of temporal velocities. Algebraically these fluctuations in longitudinal, transverse and vertical directions are defined as $u' = u - \bar{u}$, $v' = v - \bar{v}$, $w' = w - \bar{w}$ respectively. Here, u , v and w are the instantaneous sample velocities in the longitudinal, transverse and vertical directions respectively. $\bar{u}$, $\bar{v}$ and $\bar{w}$ are the temporal mean velocities in the longitudinal, transverse and vertical directions respectively. The temporal mean velocities are defined (Equations 2.3 to 2.5).

$$\bar{u} = \frac{1}{n}\sum_{i=1}^{i=N} u_i \tag{2.3}$$

$$\bar{v} = \frac{1}{n}\sum_{i=1}^{i=N} v_i \tag{2.4}$$

$$\bar{w} = \frac{1}{n}\sum_{i=1}^{i=N} w_i \tag{2.5}$$

here n is the total number of velocity samples. u_i, v_i and w_i are the magnitude of velocity in longitudinal, transverse and vertical directions respectively for ith velocity sample.

The conventional quadrant method involves studying the relationship between temporal fluctuations of velocity components, u' and w', particularly their distribution between four quadrants numbered as shown in Figure 2.4. u' and w' are the velocity fluctuations in longitudinal and vertical direction respectively.

Based on quadrant analysis turbulent phenomenon is characterized into the four quadrants depending on the sign of fluctuating velocity u' and w' (Kline et al. 1967). Figure 2.5 shows the sample velocity fluctuations of longitudinal and vertical velocity with respect to the mean value. The Q1, Q2, Q3 and Q4 in Figure 2.5 represent the quadrants 1, 2 ,3 and 4 respectively.

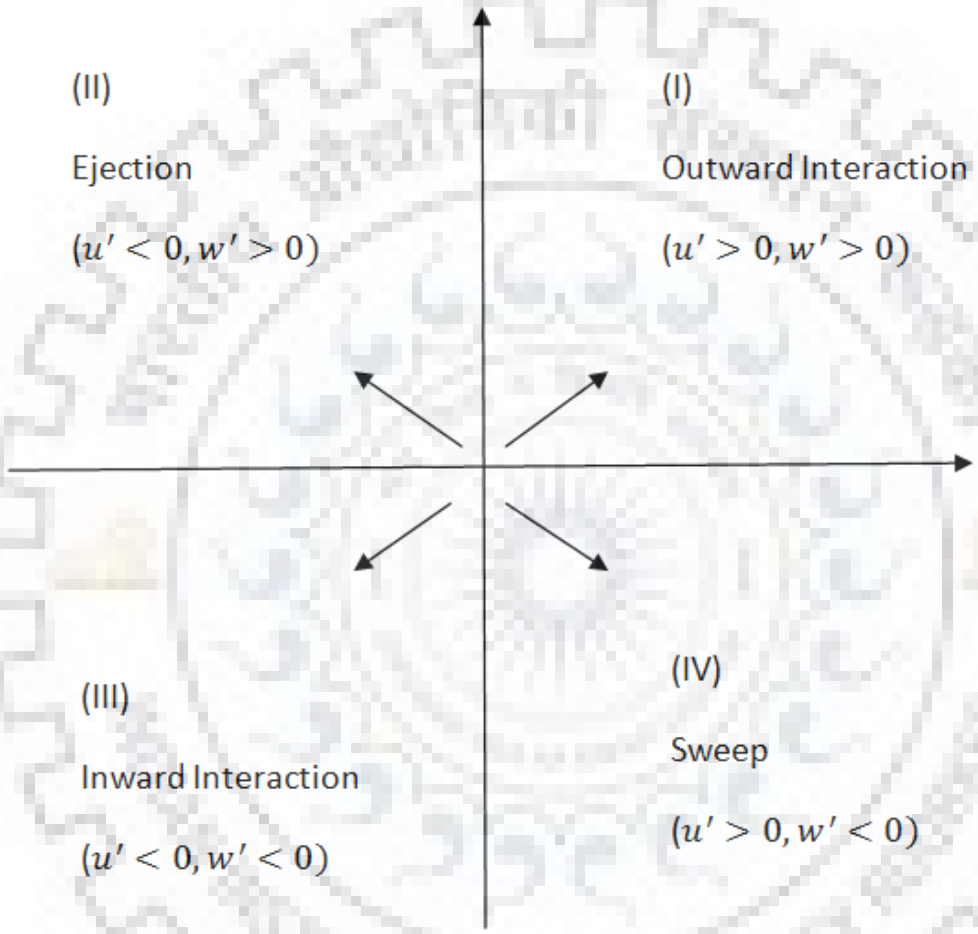

Figure 2.4 showing the four classes of bursting events and the associated quadrant

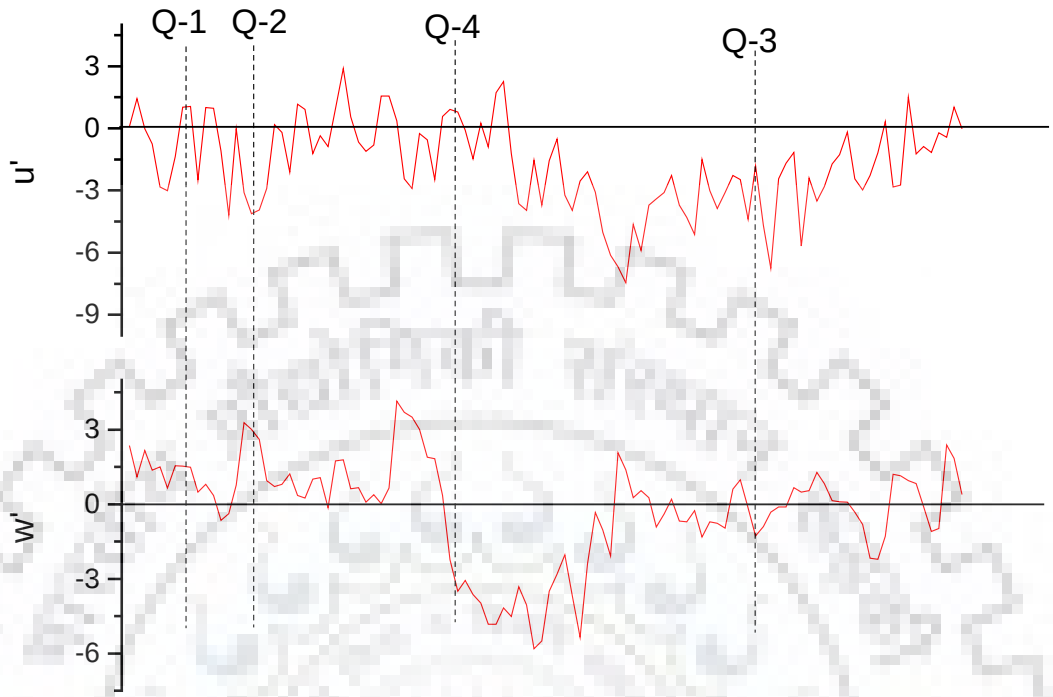

Figure 2.5 Example of the fluctuating components of velocity

Quadrant analysis of bursting events indicates that the sweep events are linked with the high speed fluid moving away from the main flow into the boundary layer (Offen and Kline 1975). Ejection events represent the low speed fluid moving into the main flow away from the boundary layer. The sweep events create many small scale eddies in the boundary layer (Cellino and Lemmin 2004; Cuthbertson and Ervine 2007; Czernuszenko and Rowiński 2008; Dey et al. 1995). Outward interaction events create high velocity pulses moving toward the main flow from the boundary layer and in the flow direction. While, inward interactions events create low velocity pulses moving away from the outer flow region into the boundary layer and opposite to the direction of flow (Katul et al. 1997; Li et al. 1992; Shvidchenko and Pender 2001; Wohl 2000).

Conditional quadrant technique is applied to decompose the instantaneous Reynolds stress, i.e., the product of $u'w'$. For a better detection, a threshold level 'Hole' H is introduced and u'-w' plane is divided into five regions. The additional region is called a 'Hole', and is bounded by the curves $|u'$

w'| = H$\overline{u'}\overline{w'}$ in the plane u'-w', where $\overline{u'}$ and $\overline{w'}$are the mean- values of the longitudinal and vertical components of turbulent velocities. Jennifer et al. (2011), Nezu et al. (1994) observed that only extreme events contribute to the turbulent burst. Therefore, the concept of Hole size (H) is used in order to exclude the extreme bursting events from the low intensity events.

In fluid dynamics, the turbulent kinetic energy (TKE) is the mean kinetic energy per unit mass associated with eddies in turbulent flow. Physically, the TKE is characterized by measured root-mean-square (RMS) value of velocity fluctuations (Afzal et al. 2009; Kozioł 2015; Lien and D'Asaro 2006). The study of TKE is necessary for thoroughly understanding the turbulent structure of flow (Afzal et al. 2009; Bergé et al. 1984; Box and Cox 1964).

The temporal structure of bursting process consists of the movements from one condition to another with time increment. The bursting events are quasi-periodic in nature which occurs randomly in space and time. The position of turbulent events at any instant of time is crucial for sediment entrainment and deposition. Blanckaert and De Vriend (2005), Drake et al. (1988), Hussain (1983) observed that the coherent structure is an aggregation of turbulent eddies which has a rotary motion and bursting processes are evolved from the coherent flow structure during their birth, growth and successive breakdown.

Keshavarzi and Gheisi (2007) found that the flow near the bridge is three dimensional, thus 2D bursting analysis is not apt for analysing the turbulent flow structure. They utilized the 3-D bursting process for analysing the turbulent flow structure in the vicinity of bridge pier. In the 3-D bursting analysis, the effect of transverse velocity fluctuations on the sediment entrainment is also included. In three-dimensional bursting analyses, the bursting events are classified into eight events depending on the sign of longitudinal, vertical and transverse velocity fluctuations (Figure 2.6). The three-dimensional bursting events are also termed as octant events due to the presence of eight different events.

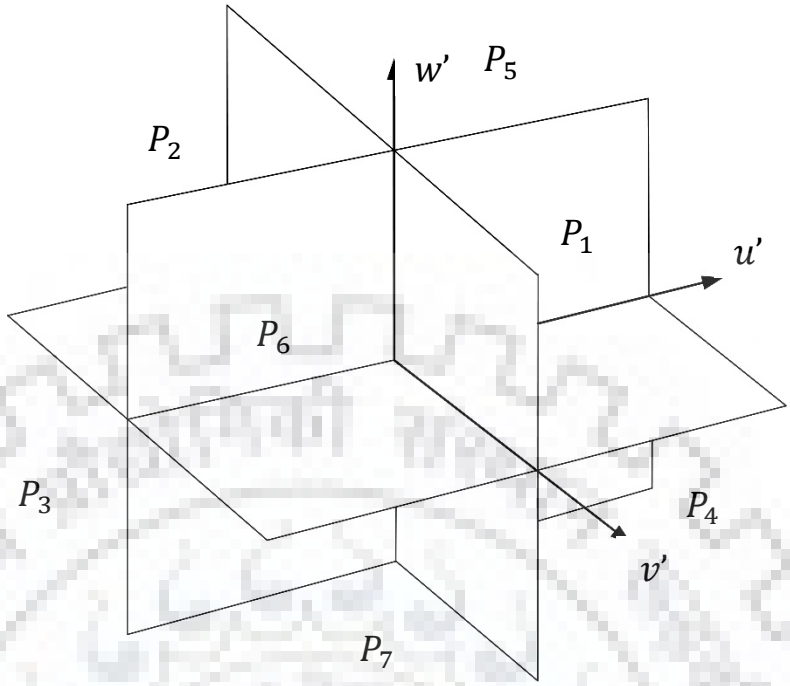

Figure 2.6 Showing the eight classes of bursting events and the associated octant for the three-dimensional bursting analyses

In order to study the stochastic nature of the bursting events, Keshavarzi and Shirvani (2002); Keshavarzi et al. (2005) had utilized the Markov chain process for modelling the transitional movements. Keshavarzi et al. (2014), Keshavarzi and Gheisi (2006) studied the probability of bursting events movements from one condition to another condition. Neary and Odgaard (1993) studied the flow structure at open channel diversion. They observed that the diversion flow is distinctly three-dimensional and have a strong analogy with the bend flow. They also observed that the similarity between diversion flows and bend flows may justify the application of relatively simple bend-flow models to predict the three-dimensional flow features at open-channel diversions. The "kolks" and "boils" phenomenon was first proposed by Matthes (1947). The "kolks" and "boils" are the upward leaning vortices originated from downstream of dune crest. The kolks-boils phenomenon creates negative pressure gradient which leads to the suspension of bed particle.

The higher moments measure the skewness of fluctuating velocity with respect to the mean components of velocity. The negative or positive values of higher moment coefficients represent the skewness in terms of left and right tail respectively (Nagano and Tagawa 1988).

The higher order moments are related to the turbulent flux contributions and burst-sweep cycles and hence, it is closely related to the turbulent burst (Gad-el-Hak and Bandyopadhyay 1994). Third order moment transmits the stochastic information of the fluctuating velocity in the form of advection and flux of the turbulent stresses.

2.4 Concluding Remarks

Researchers such as Leopold and Wolman (1957), Schumm and Lichty (1963) had analysed the patterns of braided rivers. Brice (1960), Howard et al. (1970), Rust (1977), Sharma (2004) had developed indices for classifying the degree of braiding. Most of the researchers have studied the braiding on a macro level with regard to its fluvial landform configuration. The micro level study on the underlying internal mechanism of turbulence generated due to the fluid bar interaction is hardly done till now.

Researchers have done few quantitative studies on the mid-channel bar development process and its association with the flow velocity and shear stress approach. Most of the literature available on the mid-channel bar are based on the shear stress. Researchers such as Mianaei and Keshavarzi (2008), Wu and Jiang (2007) observed that the shear stress does not directly relate to sediment motion but the bursting events stresses are responsible for sediment entrainment. Thus, the bursting events analysis is necessary for minutely analyzing the turbulence structure generated due to the fluid bar interaction. Modelling the fluid bar interaction will be extremely useful, as it holds the clue on the factors causing the mid-channel bar growth in a braided river.

Ashmore and Parker (1983), Ashworth (1996), Ferguson and Werritty (1983) observed that the mid-channel deposition is primarily responsible for initiation of braiding process. Inspite of the importance of mid-channel deposition, only few investigations have been done on the flow behaviour in the vicinity of mid-channel bar. Ashworth (1996) had carried out experiments on the mid-channel bar development in a flume model. He had presented only the direction and magnitude of surface velocity. Detailed analysis of velocity and turbulence parameters in the vicinity of mid-channel bar are required for understanding the mechanism of mid-channel bar growth.

In most of the studies, the transverse component of flow velocity is not considered, although recent researches indicate that the significant secondary flow present at bar sites causes changes in the near bed flow structure. Thus, the three-dimensional bursting analysis is essential for thoroughly understanding the pertinent turbulent flow structure. Notably, Ashworth (1996) observed that the mid-channel bar formation is mainly responsible for initiation of braiding process. The study of flow characteristics in the vicinity of mid-channel bar is vital for unravelling the braiding process. Thus,

it is imperative to undertake research into the turbulent flow hydraulics in the vicinity of mid-channel bar which has hardly been investigated with proper insight.

CHAPTER-3 EXPERIMENTAL PROGRAM

3.1 General

Our ability to distinguish natural processes depends on the experimental methods and observations as well as on fundamental principle of diverse fields. Hydraulic processes are arbitrary and thus the improbability because of variability and may be aptly quantified by means of the experimental and empirical approach.

River morphological processes are among the most complex and least understood phenomena in nature. Due to the fact that they intimately affect our living conditions, scientists and engineers have been looking for better tools to improve our understanding and enhance the quality of our lives ever since the beginning of human civilization (Wang et al. 2012). Understanding flows through open channel is of crucial importance for addressing hydraulic engineering problems. A prerequisite for arriving at such optimal solutions is to comprehend the underlying complex physics of open channel flow.

Traditional approaches for studying the natural river flows and morpho-dynamic study are based on field measurements and laboratory experiments. Owing to site and event specific concerns, field studies of natural open channel flows are very expensive, tedious and time consuming. Laboratory methods are generally based on three steps, namely: experimental design, data collection, rectification and data analysis.

3.2 Specifications of experimental components

3.2.1 Bed Material

Bed material of channel is classified on the basis of grain size distribution. From the grain size distribution curve, representative bed size (d_{50}) was calculated. Sand of d_{50} =0.25 mm was used as the bed material in the present study.

3.2.2 Velocity Measuring Instrument

3.2.2.1 Acoustic Doppler velocimetry

The Acoustic Doppler Velocimetry (ADV) is used to measure the three dimensional velocity components of flow. Measurements are performed by measuring the velocity of particles in a remote sampling volume based upon the Doppler shift effect. The technique employed in ADV is superior

to the other conventional methods, since the actual sampling volume is located at a lower depth (0.05 m below the probe in the present case) than the probe and hence is less disturbed. ADV has been recommended as a capable instrument for characterizing near bed flow, particularly in the first 10 mm above the bed (Finelli et al. 1999). The image of ADV is shown in Figure 3.1.

Figure 3.1 Showing the image of ADV

In most of these cases, Acoustic Doppler Velocimetry is the technique of choice, because it is relatively low in cost, can record at a relatively high frequency up to 100 Hz. The velocity measurements are taken at a frequency of 25 Hz in our experiment; this value is taken on the basis of fact, that the high frequency of measurement may induce spike in velocity measurement (Franca and Lemmin 2006; Voulgaris and Trowbridge 1998). The sample volume is a cylinder of diameter 4.0 mm and height of 5.6 mm. A recent near-bed turbulence measurement by Radice et al. (2009) showed that a typical size of sweep events contributing to bed load motion has a representative length of 0.8cm given the duration of 0.05s and celerity of 16cm/s. This length is the same order of magnitude as that of a typical ADV sampling volume. The measurements of ADV are affected by the noise contributions. Considering the importance of noise, several methodologies have been proposed to detect and remove noise from velocity signals (Nikora and Goring 2000). Phase space threshold method is the most widely accepted technique due to its non-parametric characteristics (Cea et al. 2007; Mori et al. 2007). Therefore, this method is used for removing the signal noise using the WinADV software. Velocity measurements are taken for 4 min duration at each point to ensure that observations become stationary (Kumar et al. 2012).

3.2.2.2 Point Gauge

The measurements of bed levels are done by using the manually adjusted hook and a reading is taken from the vertical movement using a scale. The complete setup of hook and scale is known as Point Gauge. A Vernier Scale on point gauge have a least count of 0.1 mm. The bed levels at measuring points are taken before starting and after completion of the experiments. The differences between the initial bed level and the final bed level after the completion of experiments are calculated, wherein negative values of difference represent the scouring and positive values represent the deposition at those points.

3.2.3 Flume

Flume is essential part of open channel flow experiments. The experiments are conducted in a flume 2.6 m wide, 1 m deep and 10 m long. The sides of the flume are made up of perspex glass. Discharges of the flume have been measured with the calibrated 'V' notch in the River Engineering Laboratory. Accuracy of discharge from 'V' Notch depends on the water head from the crest level. Measurement of water head has been carried out using the point gauge (equipped with Vernier scale).

3.3 Details of Experimental Work

The experiments are carried out at River Engineering Laboratory, Department of Water Resources Development and Management, Indian Institute of Technology Roorkee, India. Depth of flow is maintained using the tailgate. The experiments are performed in clear water condition. The bed slope is kept constant at 0.005 for all experimental runs. The mid-channel bar of elliptical shape is constructed in the mid portion of channel (Figure 3.2). Experiments are performed for two different phases. In first phase, the flow structure at the side of mid-channel bar are studied in detail. In second phase, the flow behavior at the location upstream and downstream of mid-channel bar are investigated.

Figure 3.2 Shows the image of mid-channel bar model constructed in River Engineering Lab IIT Roorkee

3.3.1 First phase of Experiments

First phase experiments are carried out at the flow rate of 0.12 m^3/sec. The details of experiments are given in Table 3.1. The plan and dimensions of mid-channel bar model are shown in Figure 3.3. The velocities are measured at 24 different points for no bar and bar conditions. The effect of fluid bar interaction is more at location in the close vicinity of mid-channel bar. The points at which effect of fluid bar interaction is prominent are named from a to l (Figure 3.3). The present study is mainly focused on these named points.

For each point, the velocity is measured at 16 different vertical distances from the bed. The detail of relative depths at which velocity are measured for each points are shown in Table 3.2. Relative depth is the ratio of vertical distance from bed (z) to the depth of flow (h). In this phase of study, the bursting events are analysed. The effect of bursting events is more predominant in the near bed

region (Kline et al. 1967). Thus, the velocity measurements are done in the near bed region (z/h≤ 0.1). For both experimental runs, the average bed shear stress is kept less than the critical shear stress τ_c for sediment movement. As mentioned, the bed shear stress is less than the critical shear stress. Therefore, the scouring occurs only due to the interaction of fluid and mid- channel bar.

Table 3.3 shows the experimental results of scouring and deposition patterns at 12 main points. The results of first phase of experiments are discussed in Chapters 4 ,5 and 6. In Table 3.1, l and b represent the length of major axis and minor axis of elliptical mid-channel bar respectively and h_b represent the height of mid-channel bar.

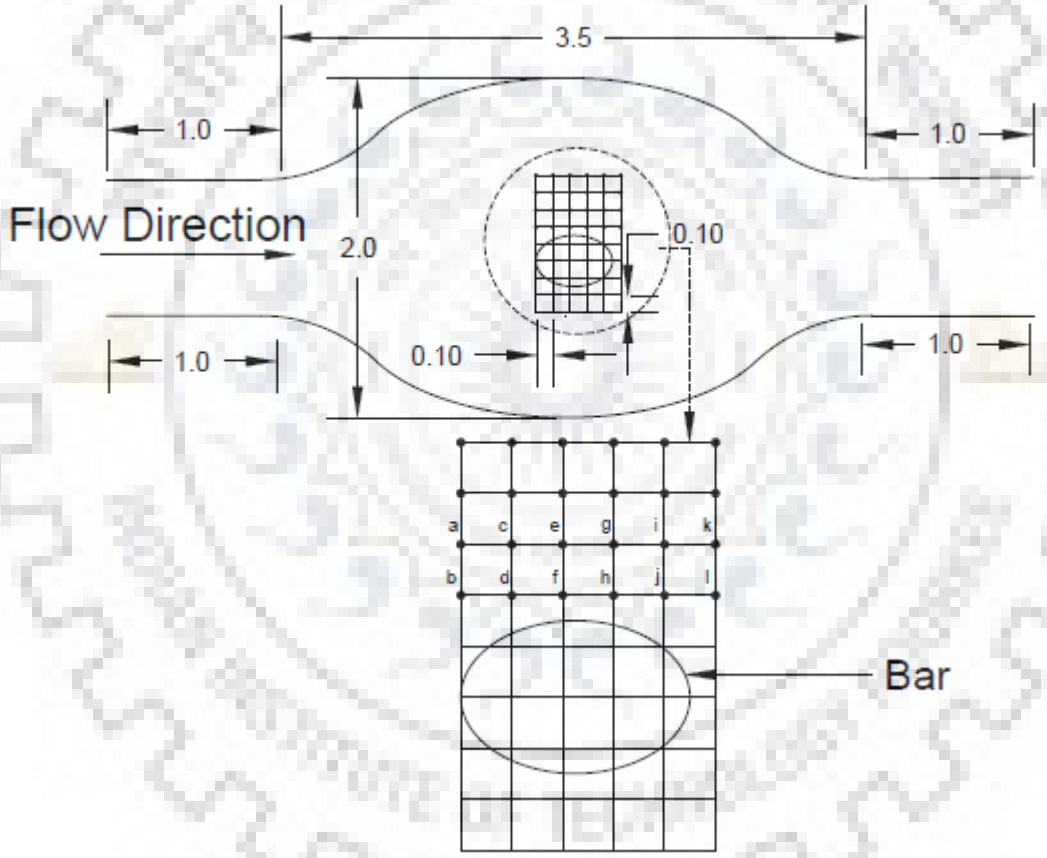

Figure 3.3 Showing the sketch of the mid-channel bar model and measuring points for first phase of experiments (All dimensions in Meters)

Table 3.1 Showing the details for first phase of experiments

Experiment code	Discharge m^3/sec	Bar Size ($l \times b \times h_b$) cm	Condition	Velocity (m/sec)	Depth (cm)
No Bar condition	0.12	No bar	No bar	0.22	26
Bar condition	0.12	90 by 60 by 8	Presence of bar	0.25	26

Table 3.2 Shows the relative depths at which velocity are measured for each point (First phase of experiments)

Relative Depth (z/h)
0.05
0.053
0.055
0.057
0.059
0.061
0.063
0.067
0.071
0.075
0.08
0.084
0.088
0.092
0.096
0.1

Table 3.3 Showing the scouring and deposition patterns at different positions in the vicinity of mid-channel bar (First phase of Experiment)

Points	Scouring/deposition in cm (bar condition)
a	-4.32
b	-5.12
c	-3.45
d	-4.28
e	-0.72
f	-1.21
g	0.22
h	0.41
i	0.43
j	0.81
k	0.92
l	1.10

3.3.2 Second Phase of Experiments

In this experimental phase, the effects of submergence ratio on the flow characteristics in the vicinity of mid-channel bar are analysed. Submergence ratio is the ratio of height of mid-channel bar to the depth of flow. Second phase experiments are carried out at the flow rate of 0.15 m^3/sec. Table 3.4 shows the details of experiments performed in this phase. Dots shown in Figure 3.4, indicate the measurement points. The depth of flow is maintained at 30 cm for all experimental runs using the tail gate.

The velocity is measured at 20 points, 10 of which are upstream and 10 points are present downstream of mid-channel bar (Figure 3.4). For each points, the velocity is measured at 16 different vertical distances from the bed. The detail of relative depths at which velocity are measured for each points are shown in Table 3.5. In this phase, the velocity is measured at locations just upstream and downstream of the mid-channel bar. For all experimental runs, the average bed shear stress is less than the critical shear stress τ_c for sediment movement. The results of second phase of experiments are discussed in Chapters 8 and 9.

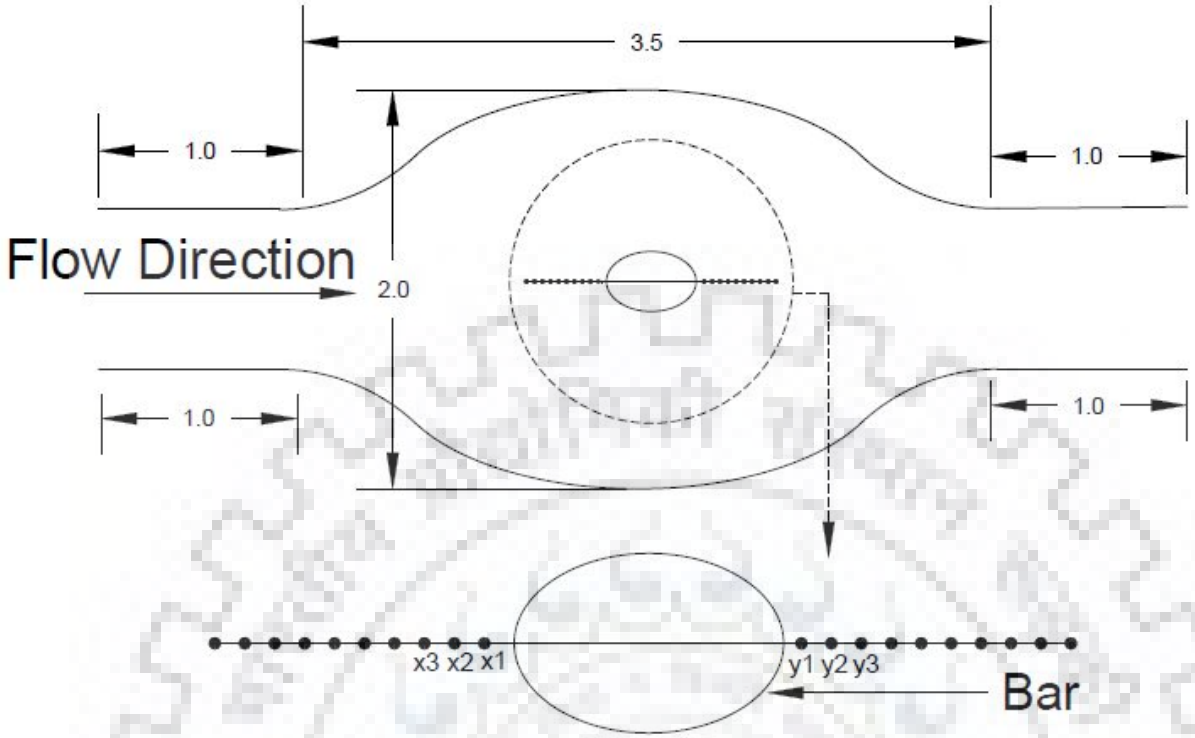

Figure 3.4 Shows the sketch of the mid-channel bar model and measuring points for second phase of experiments (All dimensions in Meters)

Table 3.4 Shows the details for second phase of experiments

Experimental Code	Bar Size ($l \times b \times h_b$)	Discharge m^3/sec	Submergence Ratio (h_b/h)
1R	90 by 60 by 6 cm	0.15	0.2
2R	90 by 60 by 9 cm	0.15	0.3
3R	90 by 60 by 12 cm	0.15	0.4
4R	90 by 60 by 14.5 cm	0.15	0.48
5R	90 by 60 by 16 cm	0.15	0.53
6R	90 by 60 by 18 cm	0.15	0.6
7R	90 by 60 by 21 cm	0.15	0.7
8R	90 by 60 by 23 cm	0.15	0.77
9R	90 by 60 by 25 cm	0.15	0.83

Table 3.5 shows the relative depths at which velocity are measured for each points (Second phase of experiments)

Relative Depth (z/h)
0.03
0.07
0.12
0.17
0.22
0.26
0.31
0.36
0.43
0.48
0.50
0.54
0.57
0.62
0.69
0.70

CHAPTER-4 TWO-DIMENSIONAL BURSTING PROCESS

4.1 General

The bursting process was first introduced by Kline et al. (1967) for describing transfer of momentum between the turbulent and laminar region near the boundary. The rate of sediment entrainment depends on the intensity of quadrant events (Kline et al. 1967). Turbulent bursts have greater influence on the sediment entrainment mechanism (Naot et al. 1993, Cuthbertson and Ervine 2007). Turbulent burst induces a rapid pressure fluctuation on the bed. As soon as the instantaneous pressure becomes lower than the local pressure, sediment particle will be entrained from the bed (Williams et al. 1989).

The two-dimensional bursting process involves studying the relationship between temporal fluctuations of velocity components u' and w', particularly their distribution in the four quadrants (Kline et al. 1967). Here, u' and w' are the velocity fluctuations in longitudinal and vertical direction respectively.

The velocity fluctuations are characterized into four quadrants depending on the sign of fluctuating velocity u' and w' (Figure 2.4).

First quadrant- Outward interaction in which u'>0, w'>0

Second quadrant- Ejection in which u'<0, w'>0

Third quadrant- Inward interaction in which u'<0, w'<0

Fourth quadrant- Sweep in which u'>0, w'<0

Out of these four quadrants events, sweep and ejection events are relatively more important and they are related to the sediment entrainment in river (Nakagawa and Nezu 1981). The approaches given by previous investigators Cellino and Lemmin (2004) indicated that flow structures exhibiting ejection and sweep features are the two main events composing the burst cycle and they may extend over the whole depth of flow. In this chapter, the turbulent flow structures in the vicinity of mid-channel bar are analysed using the Two-Dimensional bursting process. The bursting events are depth-averaged for near bed region ($z/h \leq 0.1$).

4.2 Decomposition of Reynolds stress using the conditional sampling technique

Near bed turbulence occurs due to presence of vortices that are organized in time and space called coherent structures, and they are the major resistance of motion and process (Mazumder and Ojha, 2008). The production of turbulence depends on the bursting events which are demonstrated by the conditional sampling technique (Wallace et al. 1972, Lu and Willmarth 1973). Researchers Wu and Jiang (2007) concluded that the shear stress does not directly relate to sediment motion but turbulent bursts (e.g. sweep, ejection) are responsible for entrainment of sediment particle from the bed. The above discussion indicates that the bursting events play an important role in defining the turbulent structure of flow. Thus, the Conditional Quadrant technique is applied for decomposing the instantaneous Reynolds stress, i.e., the product of $u'w'$ into the quadrant bursting events (Wallace et al. 1972, Lu and Willmarth 1973).

Nakagawa and Nezu (1981) observed that only the extreme bursting events contributes to the occurrence of significant bursting phenomenon causing sediment entrainment. Thus, the concept of Hole size (H) is used in order to exclude the extreme bursting events from the low intensity events. After the application of Hole concept, the u'-w' plane is divided into five regions (Figure 4.1). The Hole region is bounded by the curves $|u'\,w'| = H\overline{u'}\,\overline{w'}$ in the plane u'-w'. Here, $\overline{u'}$ and $\overline{w'}$ are the mean values of turbulence velocity fluctuations in the longitudinal and vertical direction respectively. Hole size (H) is the threshold parameter in the Reynolds stress signal; and this parameter is used to extract the Reynolds stress value which is greater than the H times of its average value.

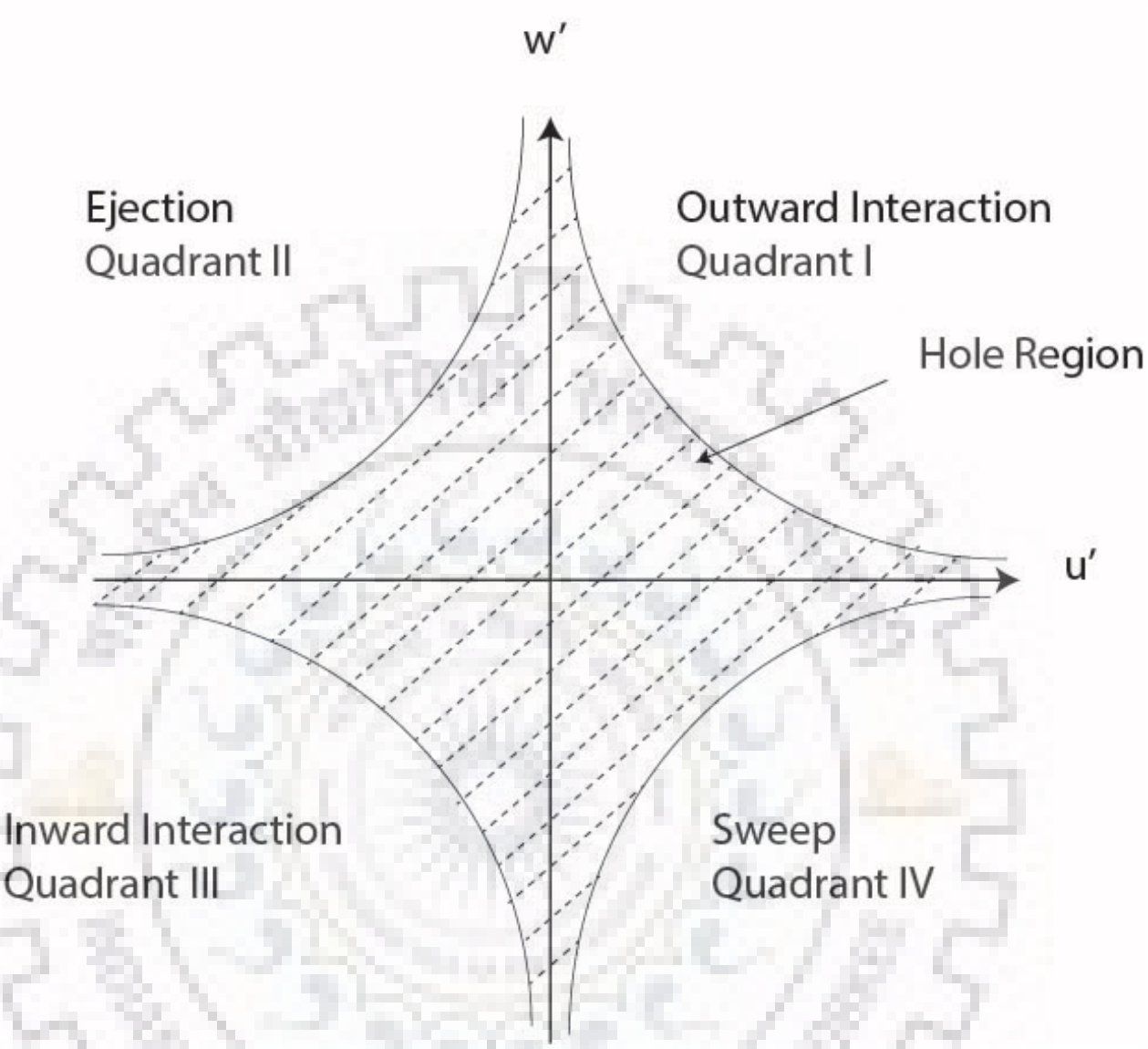

Figure 4.1 Definition sketch of the u'w' plane representing Hole

Contributions to the Reynolds stress from each quadrant for Zero-Hole size are calculated using Equation 4.1.

$$RS_i = -\frac{\rho}{N_t}\sum_{j=1}^{N_t}\left[u'w'_j(t)\right]_i \tag{4.1}$$

Here $\left[u'w'_j(t)\right]_i$ represents product of fluctuating instantaneous velocity in longitudinal and vertical direction belonging to i^{th} quadrant., RS_i is fractional contribution to Reynolds stress from i^{th} coordinate; N_t is the total number of products $u'(t)$ $w'(t)$ and ρ is density of water.

For Hole Size H, fractional Reynolds stress contribution for each quadrant is given by Equation 4.2.

$$RS_{i,H} = -\frac{\rho}{N_t}\sum_{j=1}^{N_t} X_Q\left[u'w'_j(t)\right]_i \quad (4.2)$$

The indicator function X_Q, for performing conditional averaging procedure, is defined in Equation 4.3.

$$X_Q = \begin{Bmatrix} 1 for \left|u'w'_j\right|_i \geq H\sqrt{\overline{u'^2}}\sqrt{\overline{w'^2}} \\ 0 for \left|u'w'_j\right|_i < H\sqrt{\overline{u'^2}}\sqrt{\overline{w'^2}} \end{Bmatrix} \quad (4.3)$$

$$RS_{total} = \sum_{i=1}^{5} RS_i \quad (4.4)$$

In Equation 4.4, RS_{total} is the total stress for the whole observation time related to the chosen pairs of turbulence velocities, $\left|u'w'_j\right|_i$ represents the products of j^{th} fluctuating components of longitudinal and vertical velocities which belongs to quadrant i and j =1,2……. N.

4.3 Variation of Bursting Events with the Hole-size

The contribution to the Reynolds stress from each quadrant events are computed using the Equation 4.2. Small value of Hole-size leads to the selection of both low and high intensity events and large value of Hole size segregate the high intensity events from the low intensity events. The effect of Hole size on the quadrant bursting events are studied in this section. Twelve different Hole sizes are arbitrarily selected for analysing the quadrant events variation with the Hole size. The Hole size values lie from 0 to 7. The variations of quadrant events with the Hole size are computed for all 24 measuring points. As it is not possible to display all the graph. so, only the four points 'b', 'd', 'f' and 'l' are selected for displaying the graph (Figures 4.2 and 4.3).

Figure 4.2 shows the variation of depth-averaged quadrant stresses with the Hole size for bar condition. For 'b', 'd' and 'f' points, the quadrant stresses greatly increase with increase in the Hole size. For 'l' point, the depth-averaged quadrant stresses do not show great variation with the Hole size. This indicates that the extreme events are present at 'b', 'd' and 'f' points (Figure 4.2). These

extreme turbulent bursts are generated by the fluid bar interaction. The effect of this interaction is not visible for ‘l’ point.

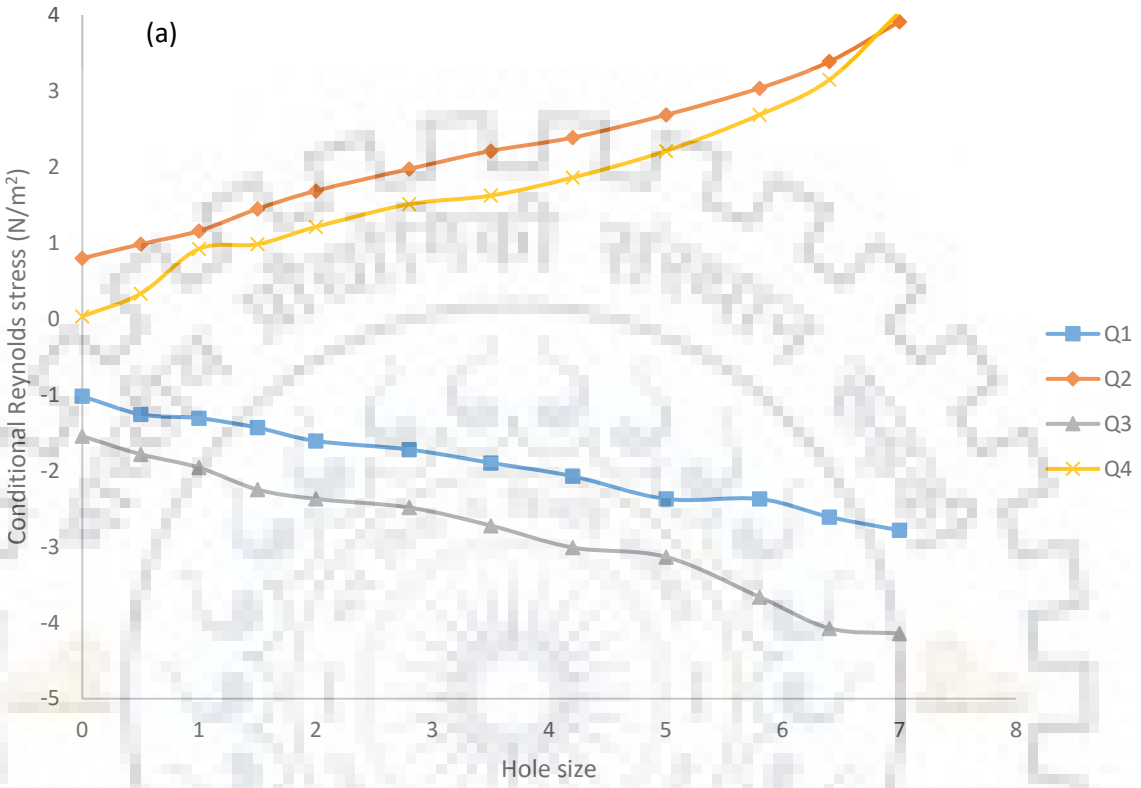

Figure 4.2(a) Showing the variation of depth-averaged quadrant stresses with the Hole size for Point b (bar condition)

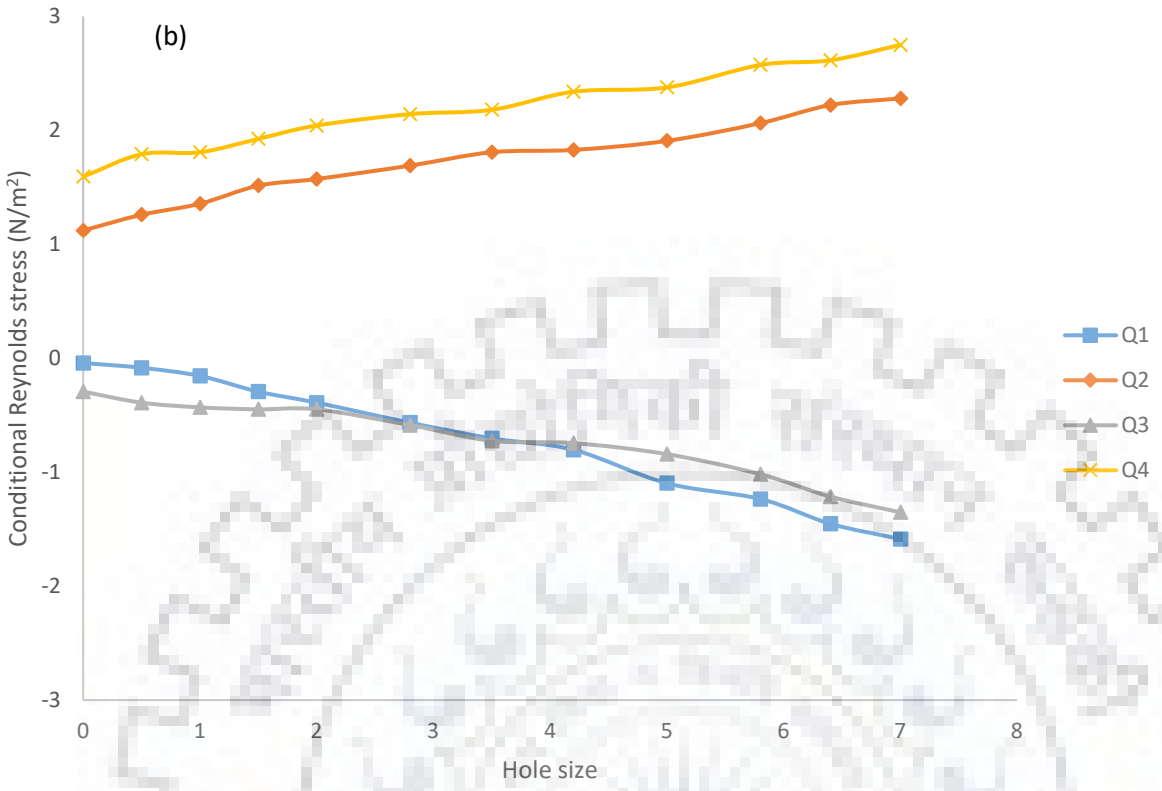

Figure 4.2(b) Showing the variation of depth-averaged quadrant stresses with the Hole size for Point d (bar condition)

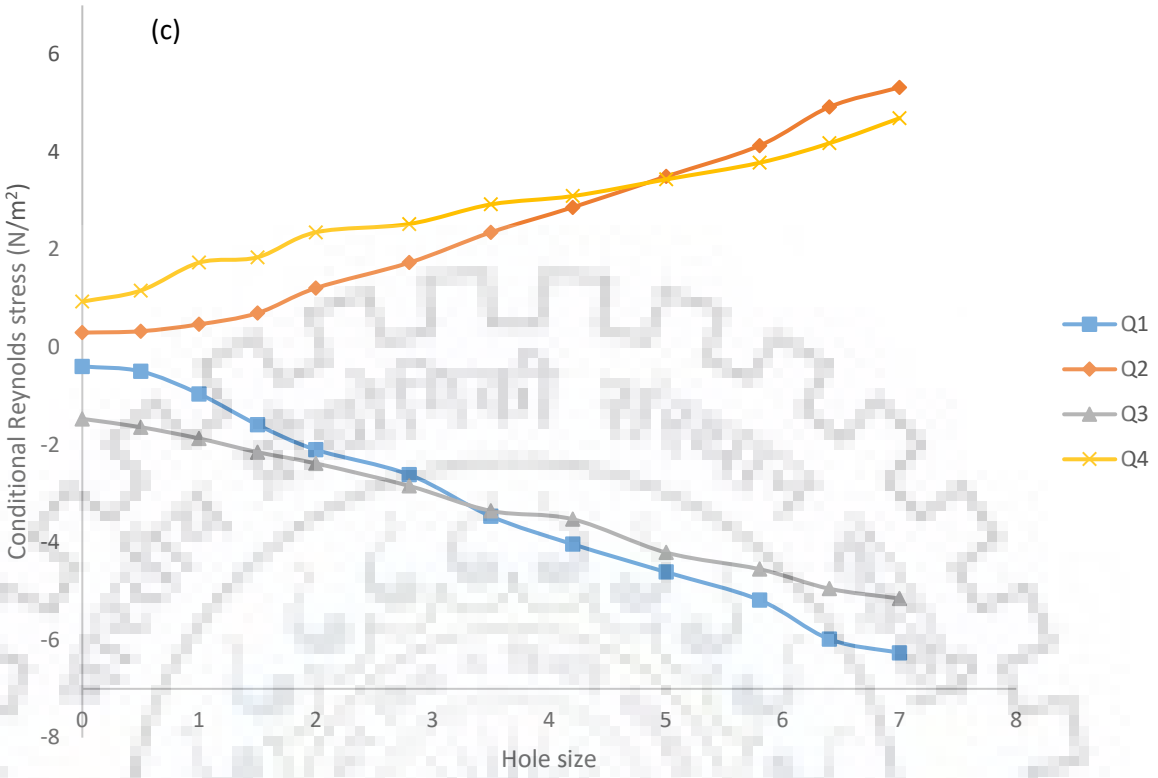

Figure 4.2(c) Showing the variation of depth-averaged quadrant stresses with the Hole size for Point f (bar condition)

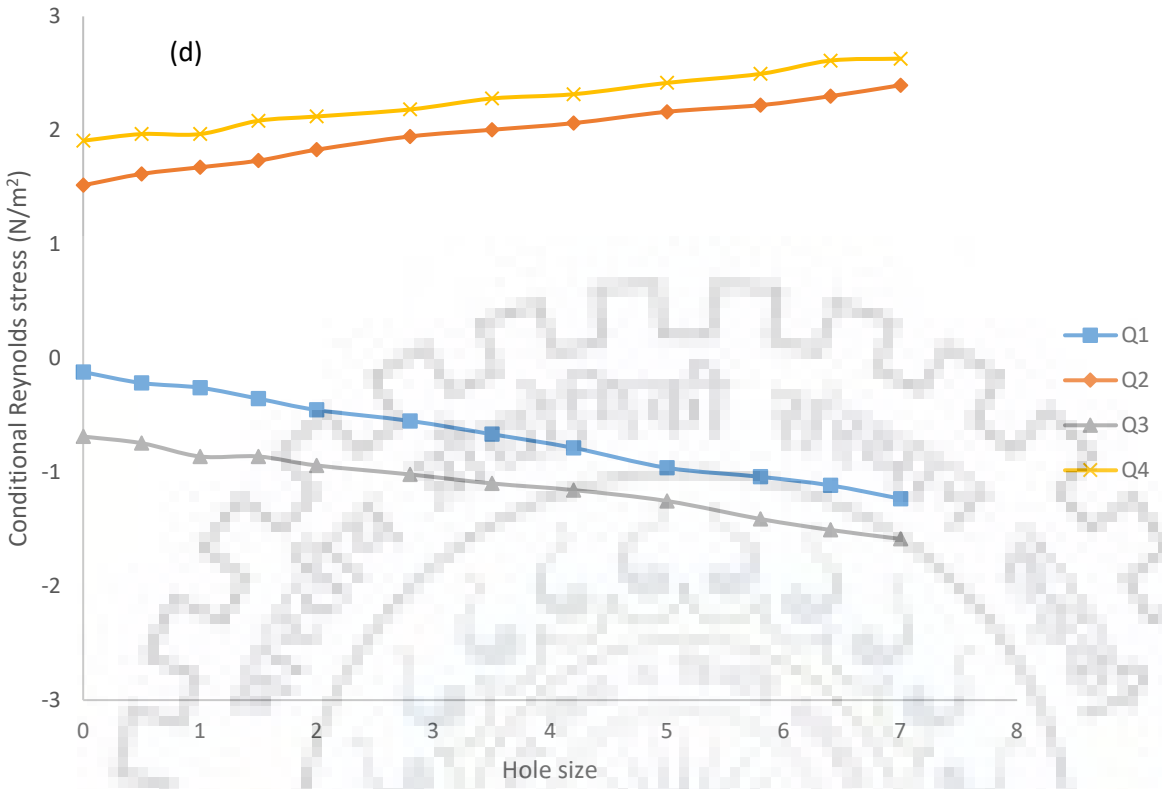

Figure 4.2(d) Showing the variation of depth-averaged quadrant stresses with the Hole size for Point I (bar condition)

Figure 4.3 shows the variation of depth-averaged quadrant stresses with the Hole size for no bar condition. For no bar condition, the increase in depth-averaged quadrant stresses with the Hole size are much lesser as compared to the bar condition. This indicates that the extreme quadrant events are present only for bar condition and effect of fluid bar interaction is dominant at location near upstream end of mid-channel bar.

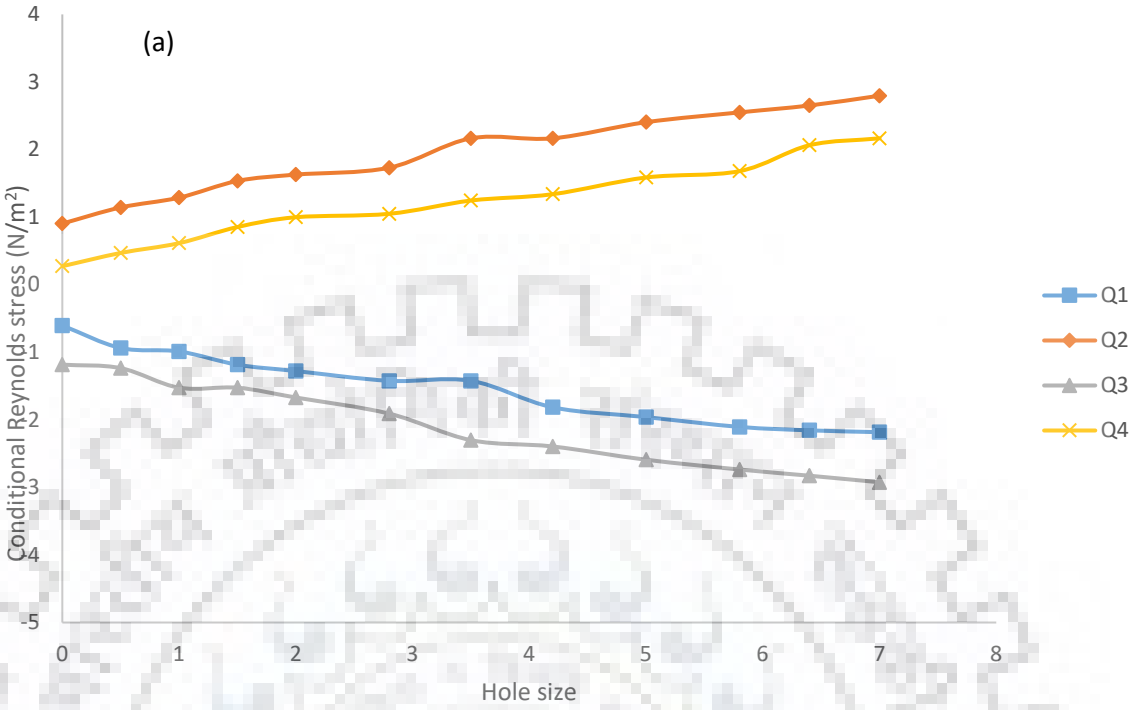

Figure 4.3(a) Showing the variation of depth-averaged quadrant stresses with the Hole size for Point b (no bar condition)

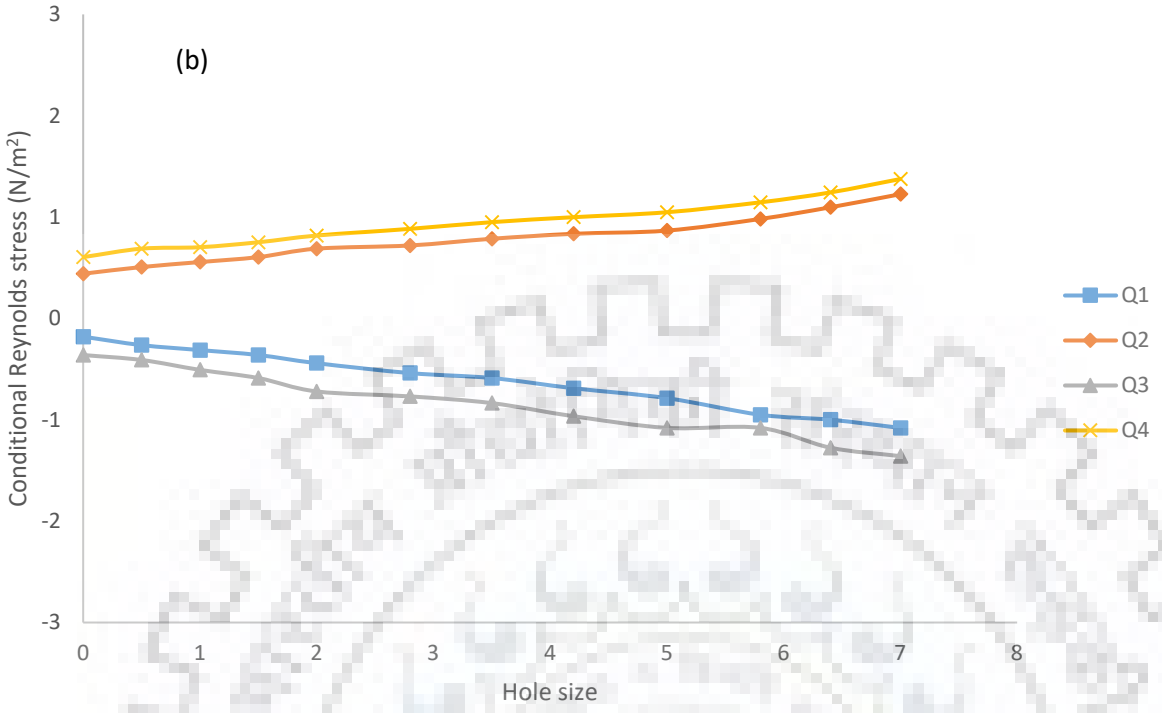

Figure 4.3(b) Showing the variation of depth-averaged quadrant stresses with the Hole size for Point d (no bar condition)

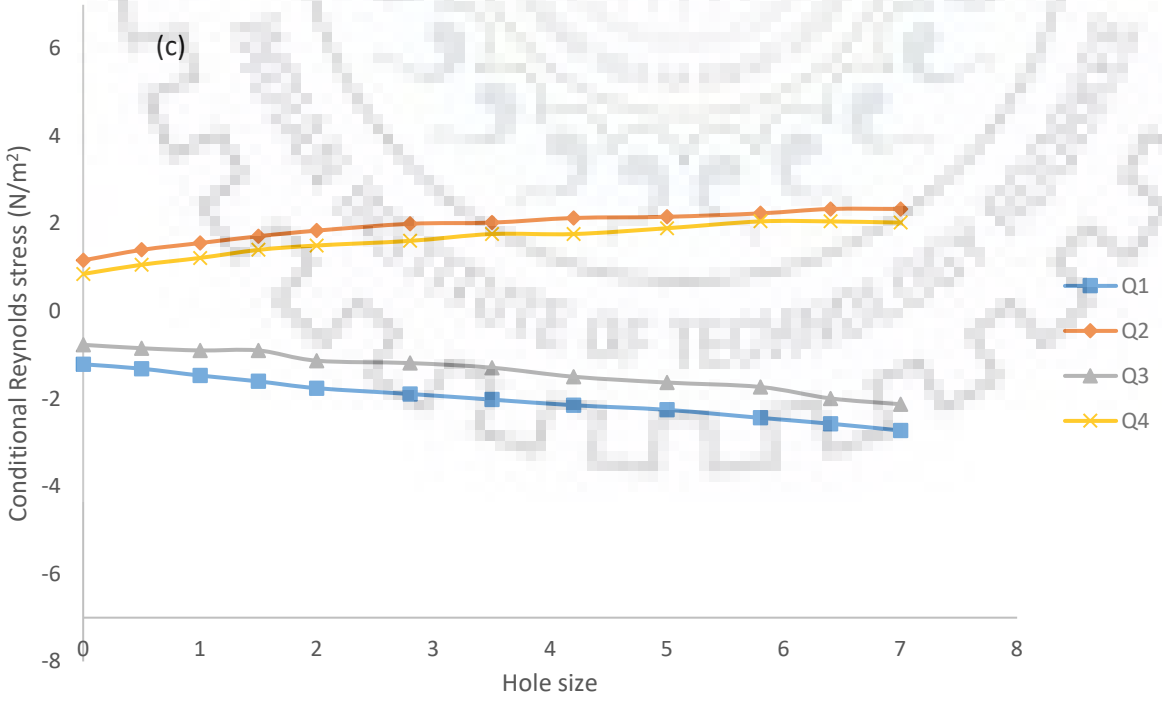

Figure 4.3(c) Showing the variation of depth-averaged quadrant stresses with the Hole size for Point f (no bar condition)

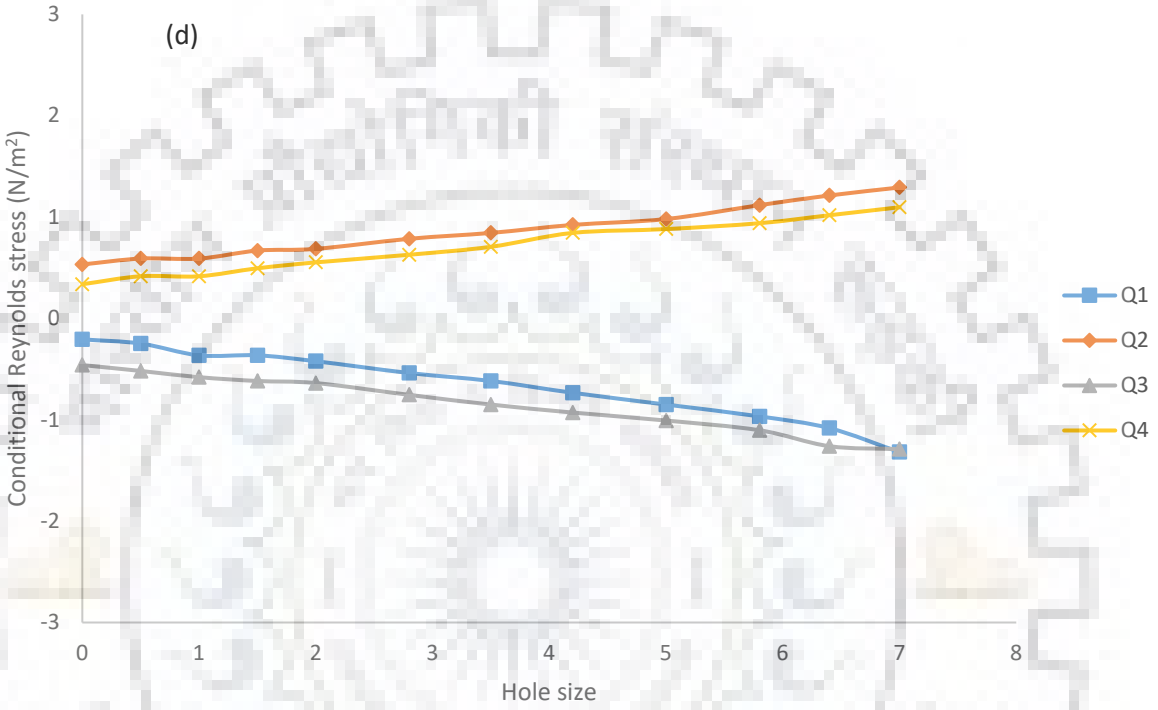

Figure 4.2(d) Showing the variation of depth-averaged quadrant stresses with the Hole size for Point l (no bar condition)

4.4 Sweep/Ejection Interaction

The Reynolds stress contribution of quadrant i for H Hole size is represented by $\langle u'w' \rangle_{i,H}$. Sweep and Ejection events are the main contributors to the turbulent burst (Nakagawa and Nezu 1981). These two events are important for analysing the structure of turbulent burst. For studying the interaction between the sweep and ejection events, we have used the Dominance Function (DF) $=\frac{\langle u'w' \rangle_{2,H}}{\langle u'w' \rangle_{4,,H}}$. It is the ratio of ejection events to the sweep events for Hole size H. It indicates the relative dominance of ejection /sweep events.

Figure 4.4 is showing the location of measurement points. Upstream end of mid-channel bar is set as origin for measuring points. The longitudinal and transverse distances in Figure 4.4 are

normalized by the length of mid-channel bar (L). The depth-wise contours of DF are plotted for bar condition along the dotted line shown in Figure 4.4.

Depth-wise contours of DF are plotted for three different Hole sizes of 0, 2 and 4 for bar condition (Figure 4.5). Arbitrary values of Hole sizes are taken in order to study the effect of Hole size on the coherent structure of flow. These Hole sizes are selected on the basis of pertinent study of Ojha and Mazumder (2010). The longitudinal distance x and vertical distance z in Figure 4.5 are normalized by the length of mid-channel bar (L) and depth of flow (h) respectively.

White region in Figure 4.5, indicate the ejection dominance and black region indicate the sweep dominance. The sweep events are dominant near the boundary and ejection events are dominant events away from the boundary (Figure 4.5). From the Figure 4.5, it was found that the dominance of sweep events decreases as the Hole size increases. This shows that the higher stresses are produced mainly due to ejection events. At the interface of sweep and ejection events dominance, the interaction of these events occurs. The interaction is responsible for the kolk-boil phenomenon (Nezu and Nakagawa 1989). The "kolks" and "boils" are the upward tilting vortices generated by the fluid bar interaction. Near the bed, the area of interaction between the sweep and ejection events is shown by the circle. By referring the Table 3.3 and Figure 4.5, it was observed that the scouring is observed at the area of interaction. Although the scouring is observed at the area of interaction, but the region of highest scouring is located upstream of the area of interaction (Table 3.3 and Figure 4.5). This indicates that the Dominance function is not completely related to the region of high scouring. Therefore, in Chapter 6 the new parameter "3-Dimensional Dominance Function" is proposed for relating the high scouring region with the bursting events.

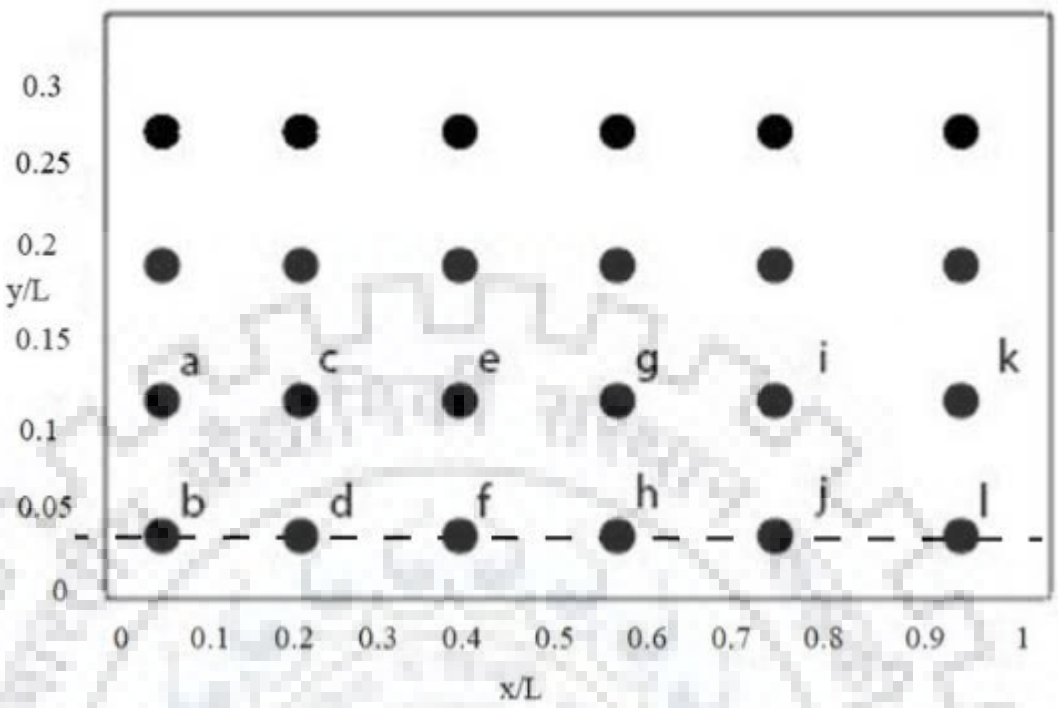

Figure 4.4 Showing the locations of velocity measuring points

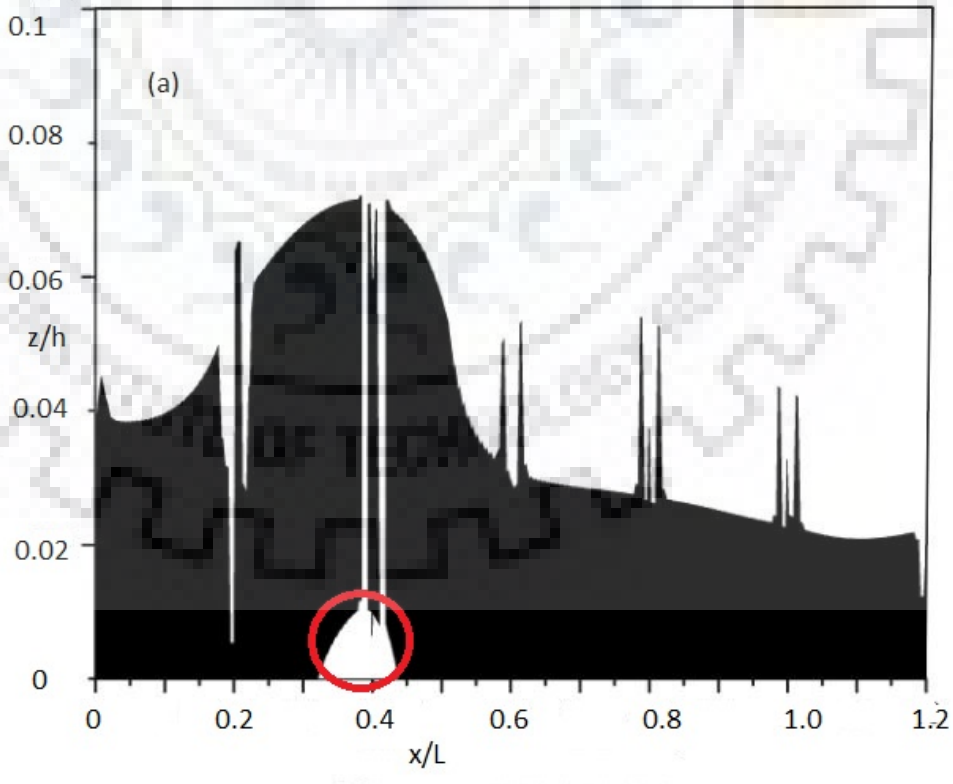

Figure 4.5 (a) Shows the contour of parameter Dominance Function which indicates the relative dominance of sweep / ejection events for 0 Hole size.

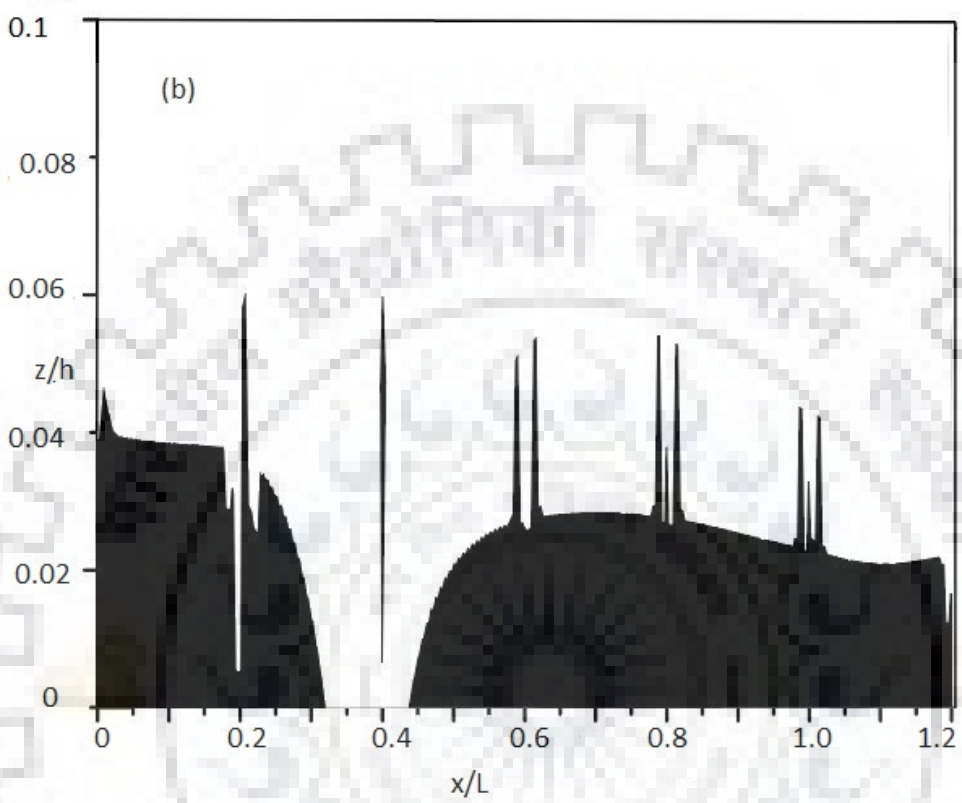

Figure 4.5 (b) Shows the contour of parameter Dominance Function which indicates the relative dominance of sweep / ejection events for 2 Hole size.

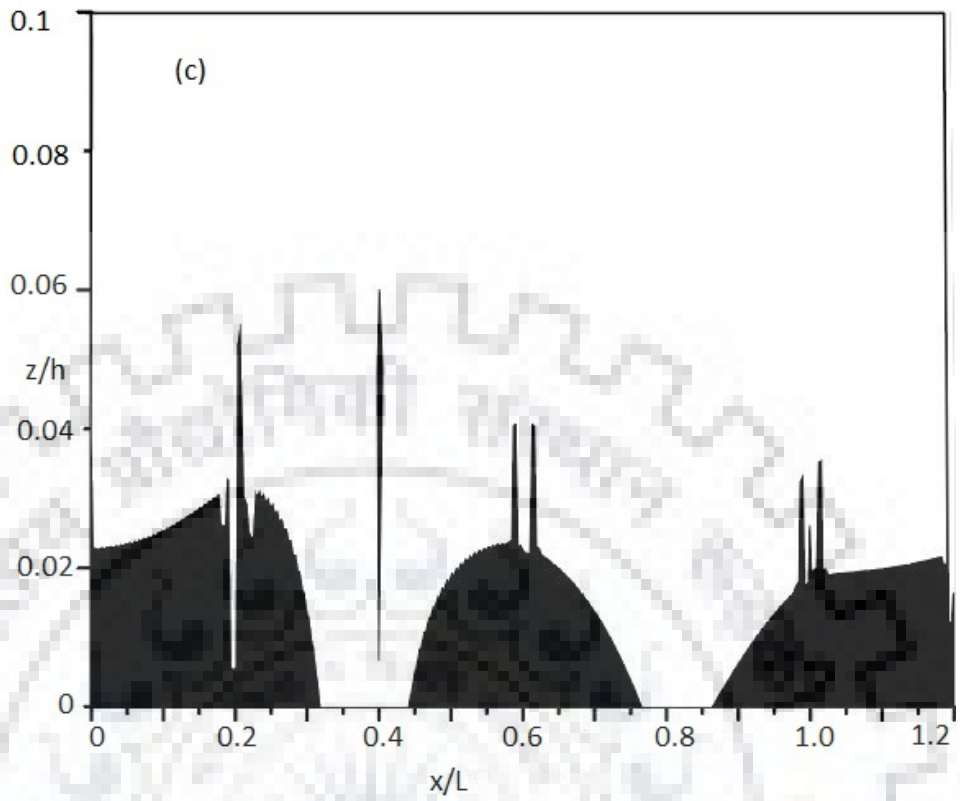

Figure 4.5 (c) Shows the contour of parameter Dominance Function which indicates the relative dominance of sweep / ejection events for 4 Hole size.

4.5 Joint probability distribution of bursting events

Our attention is in particular turned on the evolution of the horizontal bursting sequences, which would be responsible for the alternate bar initiation. The knowledge of the Joint Probability Distribution (JPD) of bursting events helps in better understanding the turbulence bursting phenomenon (Nelson 1995, Afzal et al 2009). In this section, the JPD of bursting events for points in the vicinity of mid-channel bar are analysed.

In order to plot the joint probability distribution of bursting events, the cumulant discard method is utilized (Nakagawa et al. 1975). The joint probability function of u' and w' fluctuations is given by Equation 4.5.

$$P(u', w')=\frac{1}{2\pi}\int_{-\infty}^{+\infty}\int_{-\infty}^{+\infty}\exp[-i(u'x+w'y)]\,\chi(x,y)dxdy \qquad (4.5)$$

Here, $\chi(x,y)$ is the characteristics function of joint probability distribution $P(u', w')$.

$\chi(x,y)$ is defined by Equation 4.6.

$$\chi(x,y) = \int_{-\infty}^{+\infty} \int_{-\infty}^{+\infty} \exp[i(u'x + w'y)] P(u',w')\, du'dw' \quad (4.6)$$

By expanding the integration, the Equation 4.5 can be rewritten as

$$P(u',w') = \phi(u',w') \left[1 + \sum_{s+t=3}^{4} \frac{q_{st}}{s!t!} H_{st}(u',w')\right] \quad (4.7)$$

Here, $\phi(u',w')$ is the Gaussian distribution function for $u'$and w' variables. H_{st} is the Hermite polynomial of order (s+t). In Equation 4.7, the term between the square bracket is an orthogonal polynomial expansion of $P(u',w')/\phi(u',w')$ ratio.

Equation 4.7 represents the Gram-Charlier bivariate joint probability density distribution for u' and w' variables (De Feriet 1966). The JPD graphs are plotted for different points in the vicinity of mid-channel bar.

Figure 4.6 shows the JPD graphs plotted for 'b', 'd', 'h' and 'l' points at relative depth of 0.05 (zero Hole-size, bar condition). At points 'b' and 'd', the graph of JPD is ellipsoidal in shape and eccentric toward the II and IV quadrants. This indicates that the sweep and ejection events are dominant at these points. At point 'h', the zone of high probability lies in the third quadrant. For l point, the high probability zone lies in the first quadrant. The probability distribution graph is eccentric towards the odd quadrants for points 'h' and 'l'. The high probability of sweep and ejection events observed at points located near upstream end of mid-channel bar due to the turbulent burst generated by the fluid bar interaction (Figure 4.6).

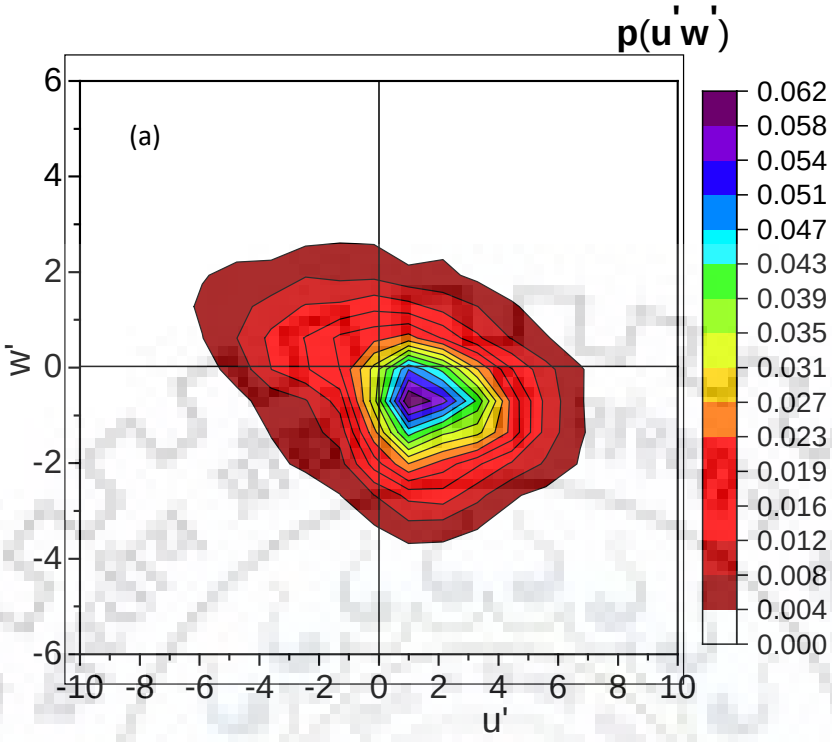

Figure 4.6 (a) shows the joint probability distribution of bursting events for Point 'b' at the relative depth of 0.05 (Hole-size 0, bar condition)

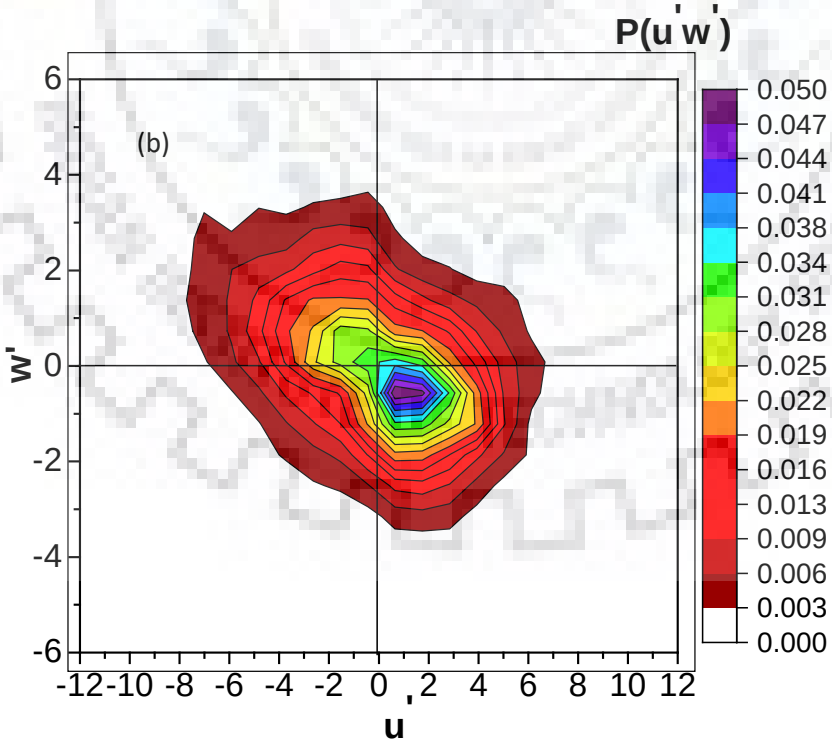

Figure 4.6 (b) shows the joint probability distribution of bursting events for Point 'd' at the relative depth of 0.05 (Hole-size 0, bar condition)

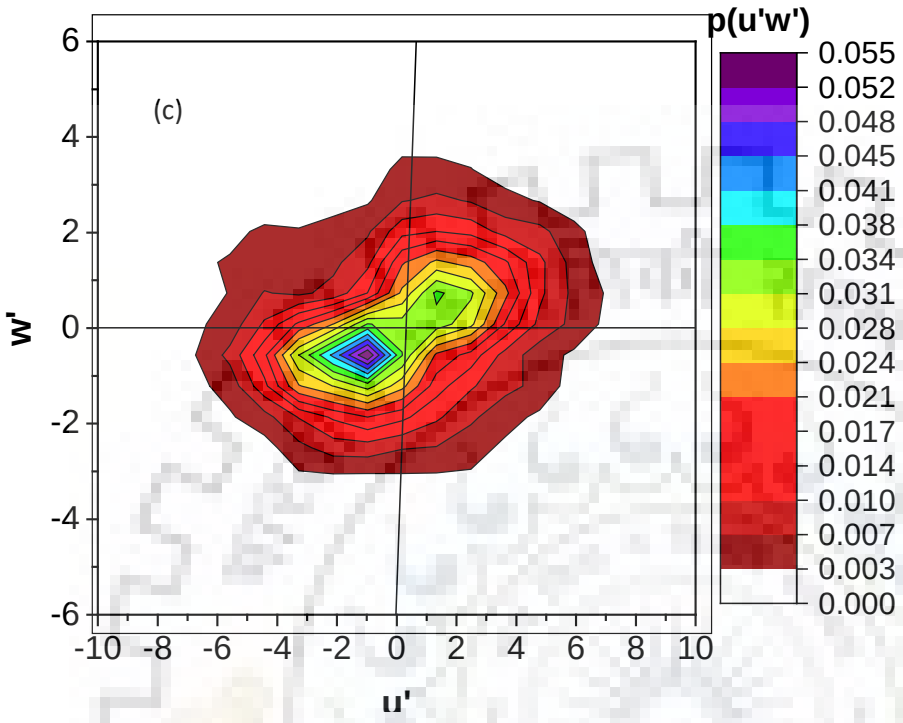

Figure 4.6 (c) shows the joint probability distribution of bursting events for Point 'h' at the relative depth of 0.05 (Hole-size 0, bar condition)

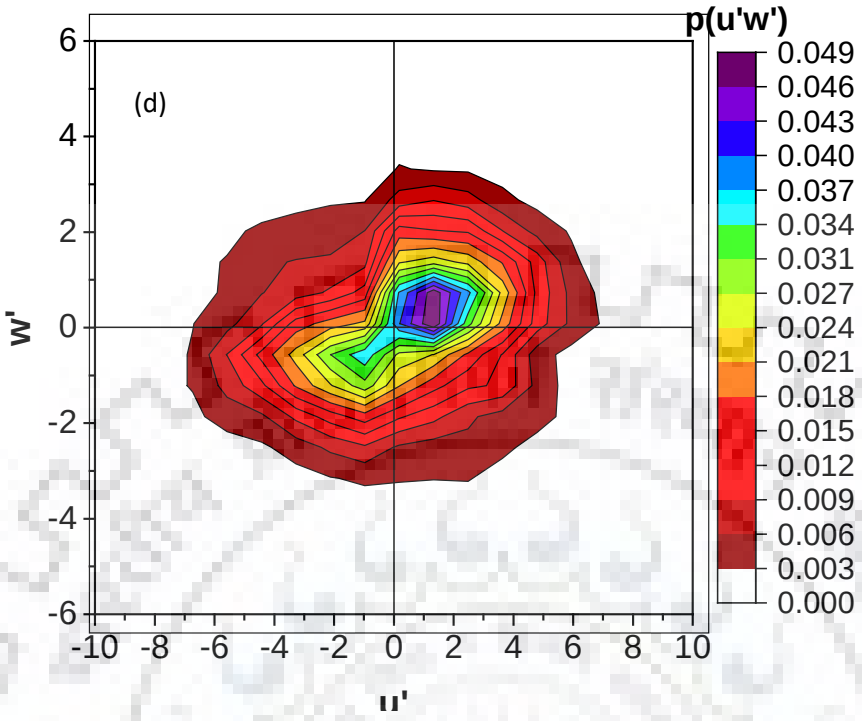

Figure 4.6 (d) shows the joint probability distribution of bursting events for Point 'l' at the relative depth of 0.05 (Hole-size 0, bar condition)

Figure 4.7 shows the JPD graphs plotted for points 'b', 'd', 'h' and 'l' at relative depth of 0.05 (1.5 Hole-size, bar condition). At points 'b', the high probability zone shifted from quadrant 4 to quadrant 2, as the Hole size increases from 0 to 1.5 (Figures 4.6 and 4.7). This indicates that the higher stresses are produced mainly by the ejection events. For point 'h', the area of joint probability graph that comes under the odd quadrants increases, as the Hole size increases from 0 to 1.5 (Figures 4.6 and 4.7). The high probability zone becomes more eccentric toward the dominant quadrants as the Hole size increases from 0 to 1.5.

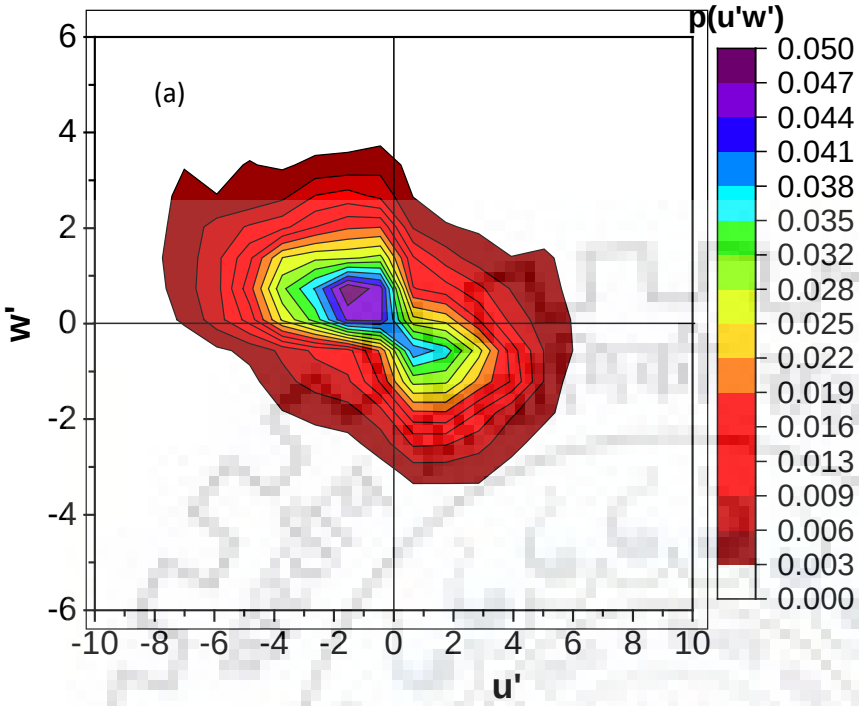

Figure 4.7 (a) shows the joint probability distribution of bursting events for Point 'b' at the relative depth of 0.05 (Hole size 1.5, bar condition)

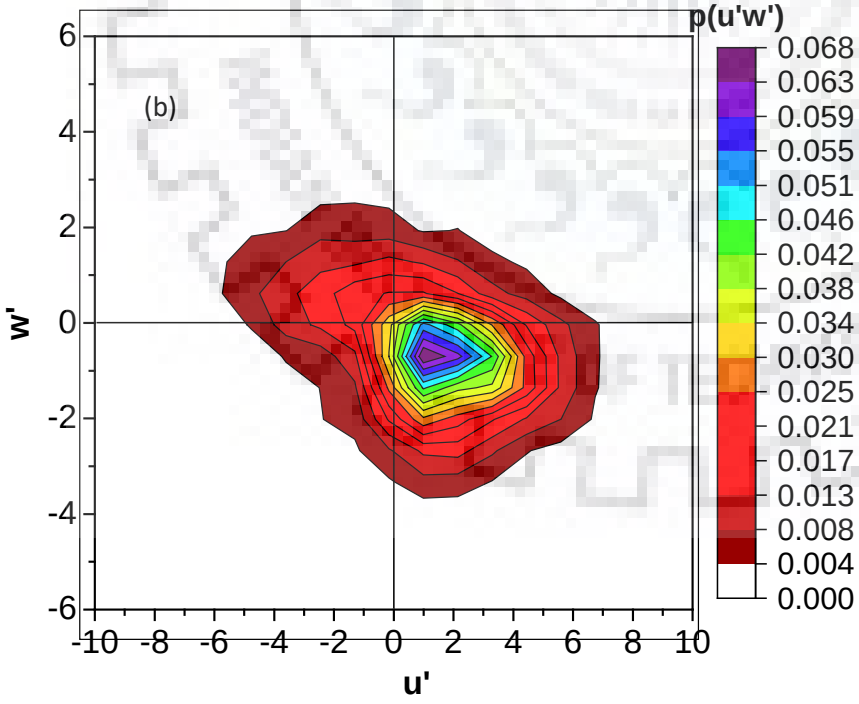

Figure 4.7 (b) shows the joint probability distribution of bursting events for Point 'd' at the relative depth of 0.05 (Hole size 1.5, bar condition)

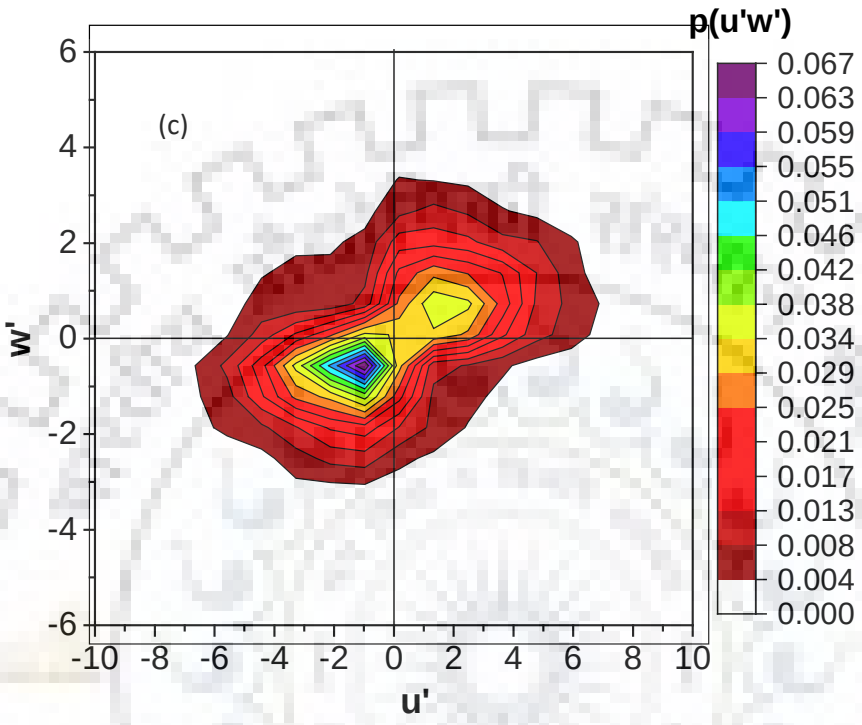

Figure 4.7 (c) shows the joint probability distribution of bursting events for Point 'h' at the relative depth of 0.05 (Hole size 1.5, bar condition)

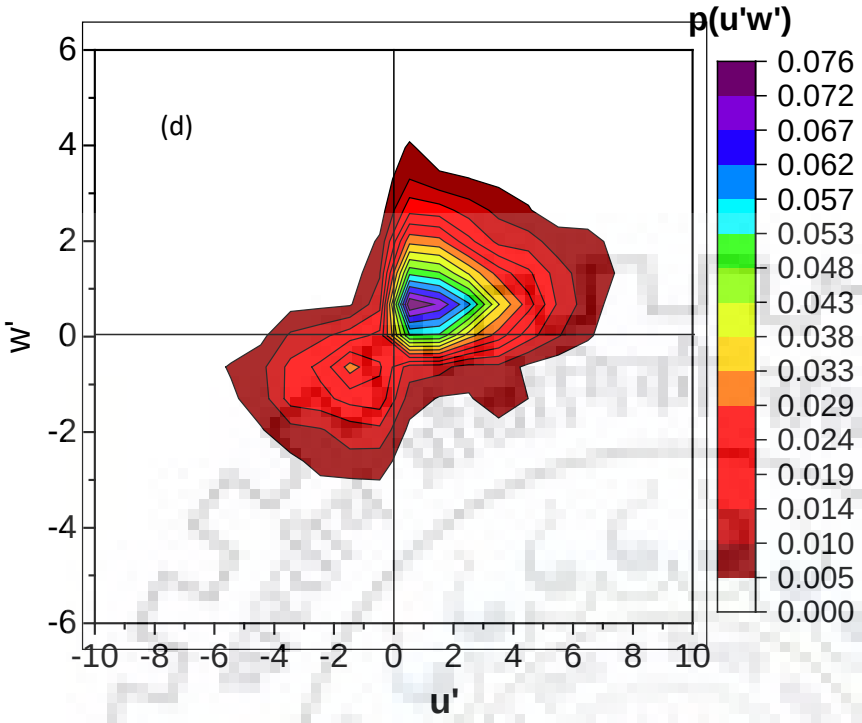

Figure 4.7 (d) shows the joint probability distribution of bursting events for Point 'l' at the relative depth of 0.05 (Hole size 1.5, bar condition)

Figure 4.8 shows the JPD graphs plotted for 'b', 'd', 'h' and 'l' points at relative depth of 0.1 (0 Hole-size, bar condition). Figure 4.8 also shows that the area of probability graph that comes under the II quadrant is highest. This indicates that the ejection event is dominant at greater distance from the bed.

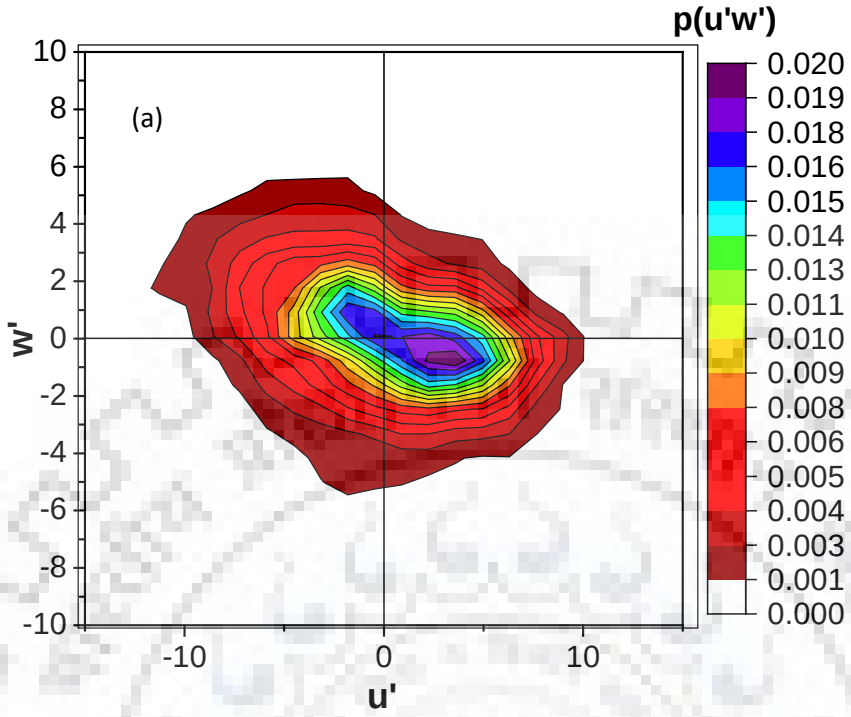

Figure 4.8 (a) shows the joint probability distribution of bursting events for Point 'b' at the relative depth of 0.1 (Hole size 0, bar condition)

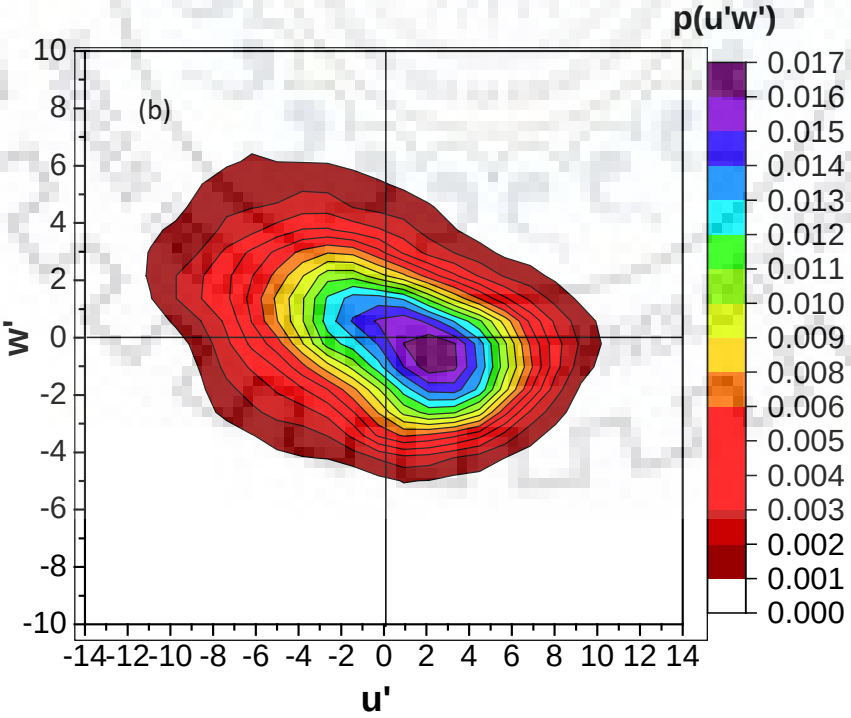

Figure 4.8 (b) shows the joint probability distribution of bursting events for Point 'd' at the relative depth of 0.1 (Hole size 0, bar condition)

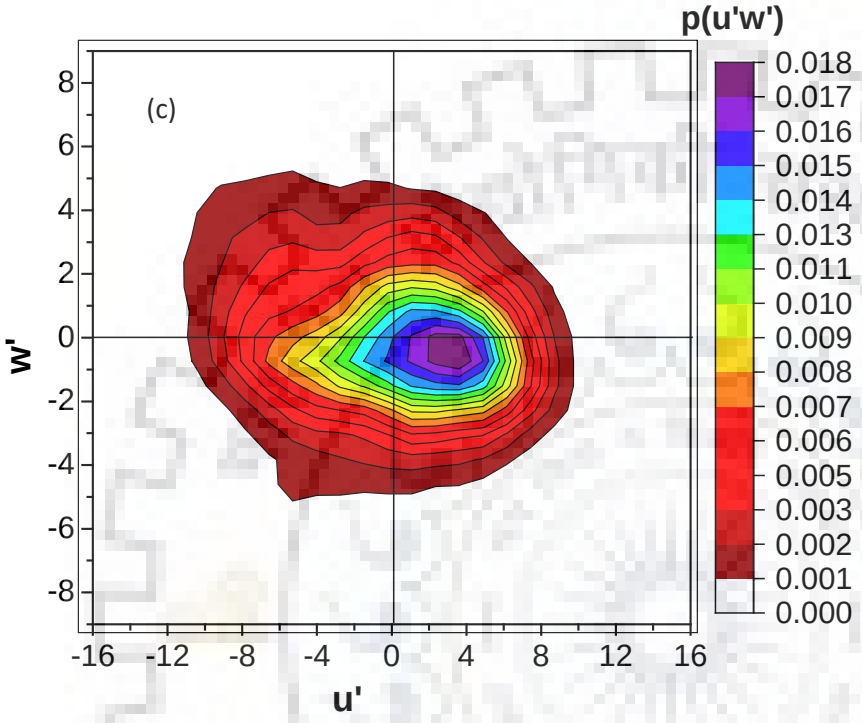

Figure 4.8 (c) shows the joint probability distribution of bursting events for Point 'h' at the relative depth of 0.1 (Hole size 0, bar condition)

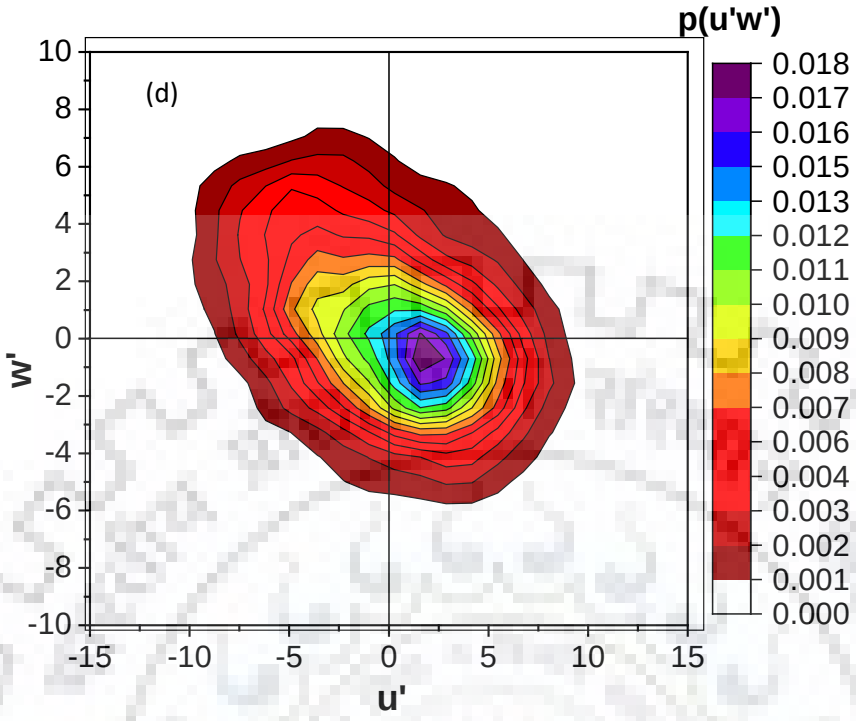

Figure 4.8 (d) shows the joint probability distribution of bursting events for Point 'l' at the relative depth of 0.1 (Hole size 0, bar condition)

Figure 4.9 shows the JPD graphs plotted for 'b', 'd', 'h' and 'l' points at relative depth of 0.05 (0 Hole-size, no bar condition). Figure 4.9 shows that the probability density graphs are evenly distributed among the four quadrants. The levels of turbulence fluctuations are very low as compared to bar condition.

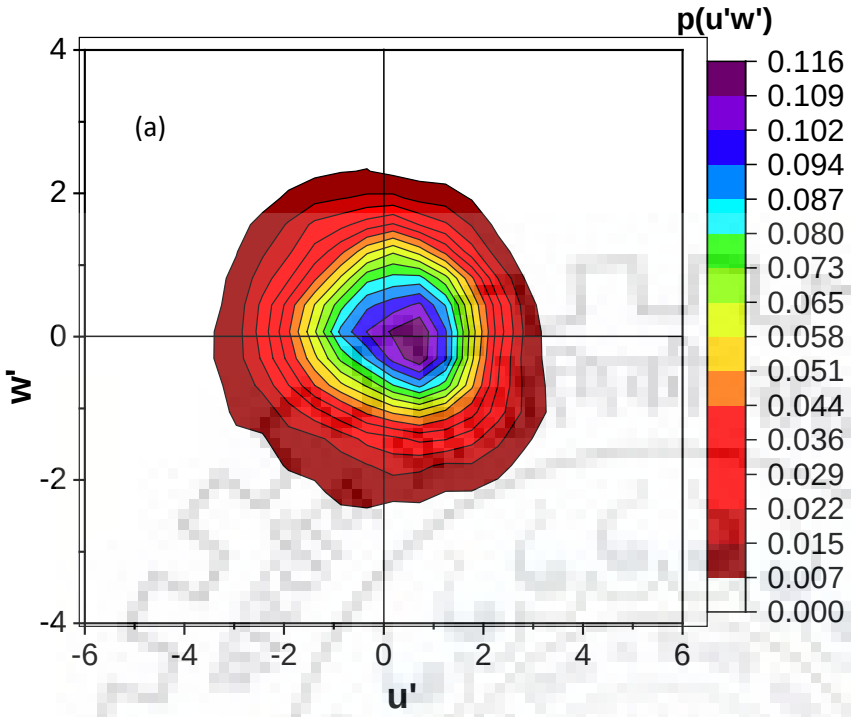

Figure 4.9 (a) shows the joint probability distribution of bursting events for Point 'b' at the relative depth of 0.05 (Hole size 0, no bar condition)

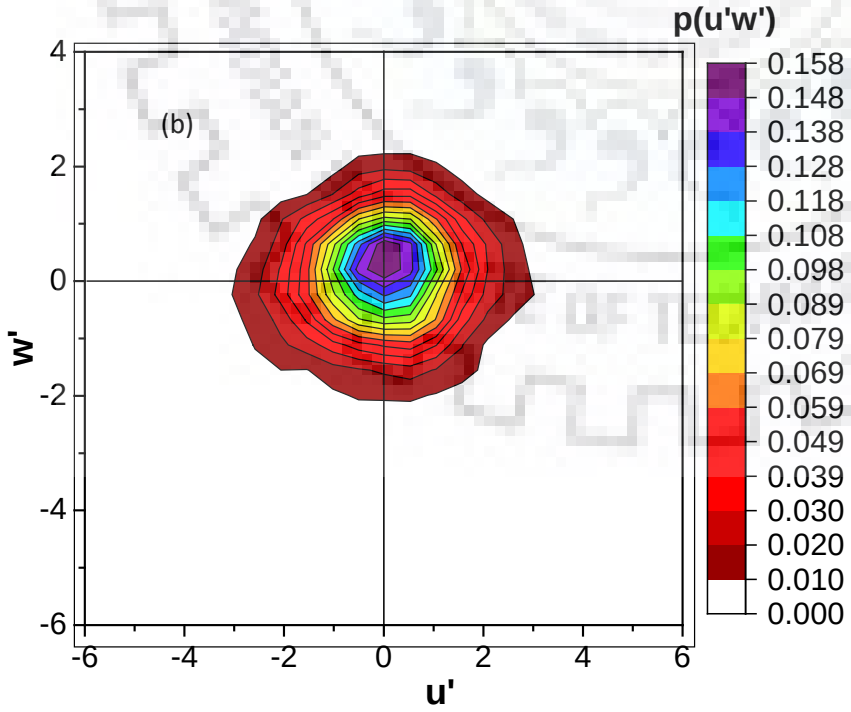

Figure 4.9 (b) shows the joint probability distribution of bursting events for Point 'd' at the relative depth of 0.05 (Hole size 0, no bar condition)

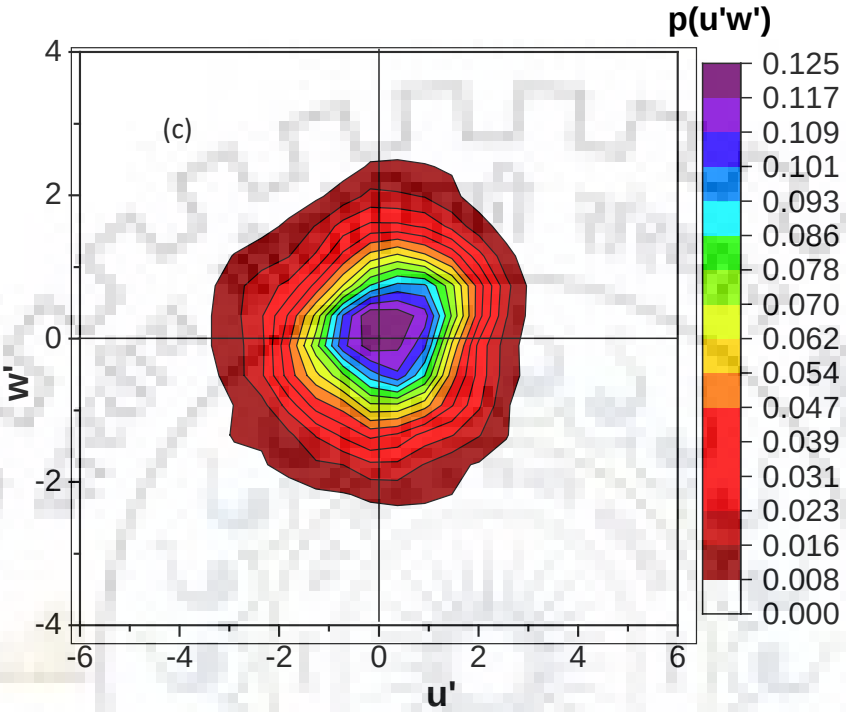

Figure 4.9 (c) shows the joint probability distribution of bursting events for Point 'h' at the relative depth of 0.05 (Hole size 0, no bar condition)

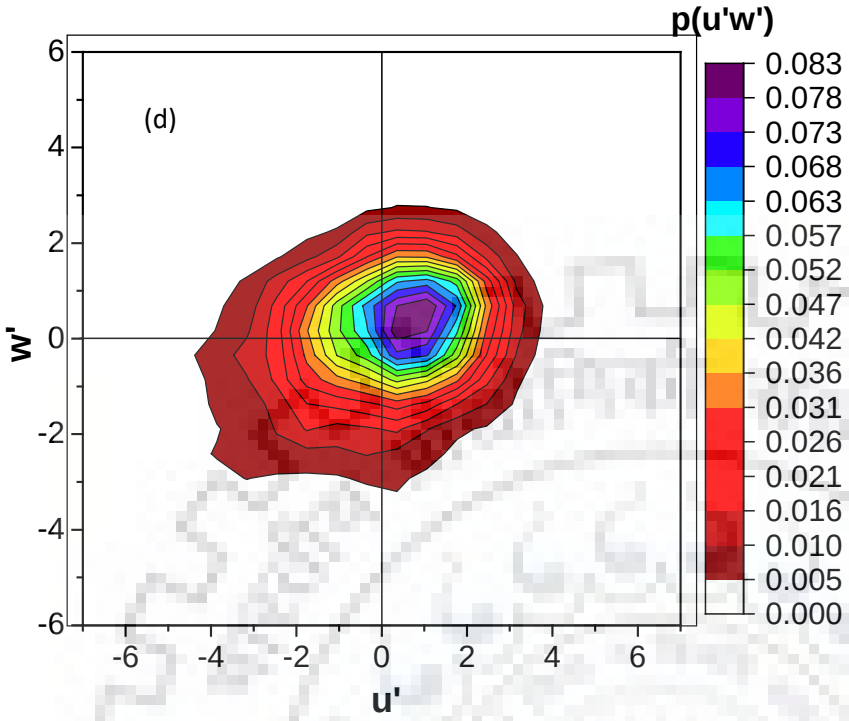

Figure 4.9 (d) shows the joint probability distribution of bursting events for Point 'I' at the relative depth of 0.05 (Hole size 0, no bar condition)

Evidently, the presence of mid-channel bar causes redistribution of turbulent burst with high occurrence probability for even events at location near upstream end of bar. The high magnitude of turbulent burst generated due to the fluid bar interaction causes scouring at these locations (Table 3.3).

CHAPTER-5 ANALYSIS OF SPATIAL DISTRIBUTION OF TURBULENCE PARAMETERS

5.1 General

As observed in Section 4.1, the turbulent stresses are much greater for bar condition as compared to the no bar condition. This indicates that the flow characteristics in the vicinity of bar is greatly affected by the presence of mid-channel bar. Therefore, in this section the depth-averaged contours of turbulence parameters are analysed for bar and no bar conditions. These contours give more details about the turbulent structure of flow in the vicinity of mid-channel bar. Figure 4.4 is showing the points of measurements for plotting the contours. Upstream end of bar is set as origin for measuring points. The turbulence parameters are depth-averaged for near bed region (z/h≤0.1).

5.2 Turbulent Intensity

The root mean squared values of turbulent fluctuating velocity ($u', v' and\ w'$) are normalized by the shear velocity and presented in the form of $Ti_u = \frac{\sqrt{\overline{u'^2}}}{u_*}$ (in the longitudinal direction), $Ti_v = \frac{\sqrt{\overline{v'^2}}}{u_*}$ (in the transverse direction) and $Ti_w = \frac{\sqrt{\overline{w'^2}}}{u_*}$ (in the vertical direction). Here, u_* is the shear velocity of approach flow. The fluctuating velocity $u', v' and\ w'$ are already defined in Chapter 2.

The contours for depth-averaged turbulent intensity components are plotted for bar and no bar conditions. The longitudinal distance x and transverse distance y are normalized by the length of bar (L).

Figure 5.1 shows the depth-averaged contours of Ti_u , Ti_v and Ti_w for bar condition. Figure 5.1 shows that the high values of Ti_u , Ti_v and Ti_w are observed at region near upstream end of mid-channel bar. The values of Ti_u , Ti_v and Ti_w decreases with increase in the x/L value. This indicates that the effect of bar on turbulent intensity components are mostly observed at region close to the upstream end of mid-channel bar.

Figure 5.2 shows the depth-averaged contours of Ti_u , Ti_v and Ti_w for no bar condition. For no bar condition, the turbulent intensities contours have lesser spatial variation. Near the downstream end

of mid-channel bar (x/L=1), the values of Ti_v and Ti_w for bar condition are comparable to the corresponding values for no bar condition (Figures 5.1 and 5.2).

The Ti_u values for bar condition is much greater as compared to the corresponding values for no bar condition. Similarly, Ti_v and Ti_w values are also greater for bar condition (Figures 5.1 and 5.2).

The presence of mid-channel bar had caused non-homogeneity in the turbulent intensities contours. The high level of turbulent intensities is observed at region near upstream end of mid-channel bar and level of turbulent intensities decreases with increase in the distance from the upstream end of mid-channel bar.

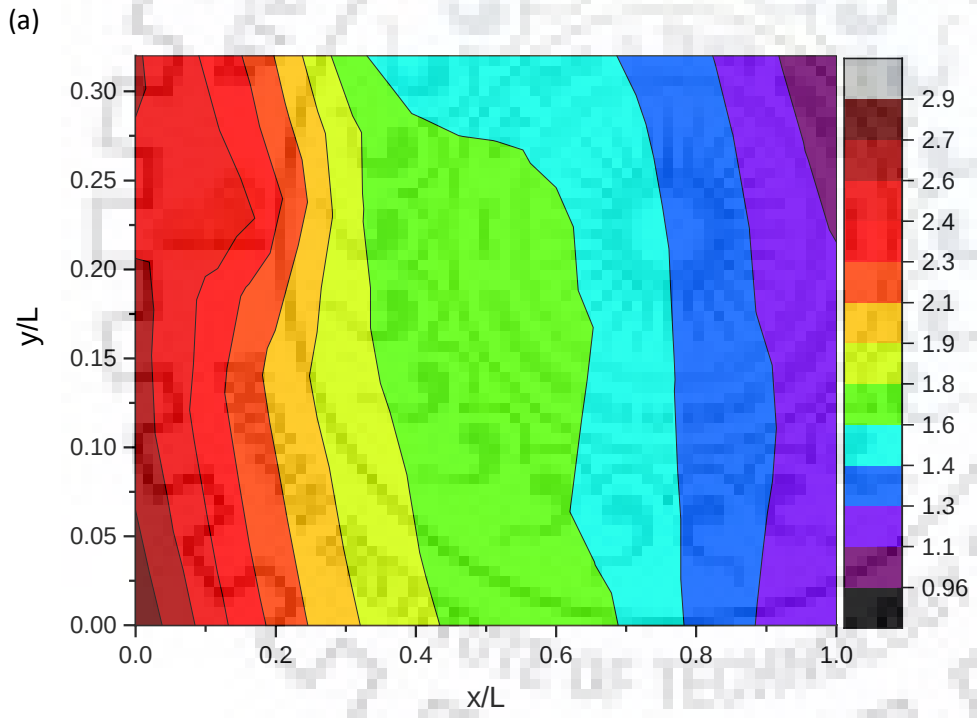

Figure 5.1 (a) showing the depth-averaged contour of normalized longitudinal turbulent intensity for bar condition

(b)

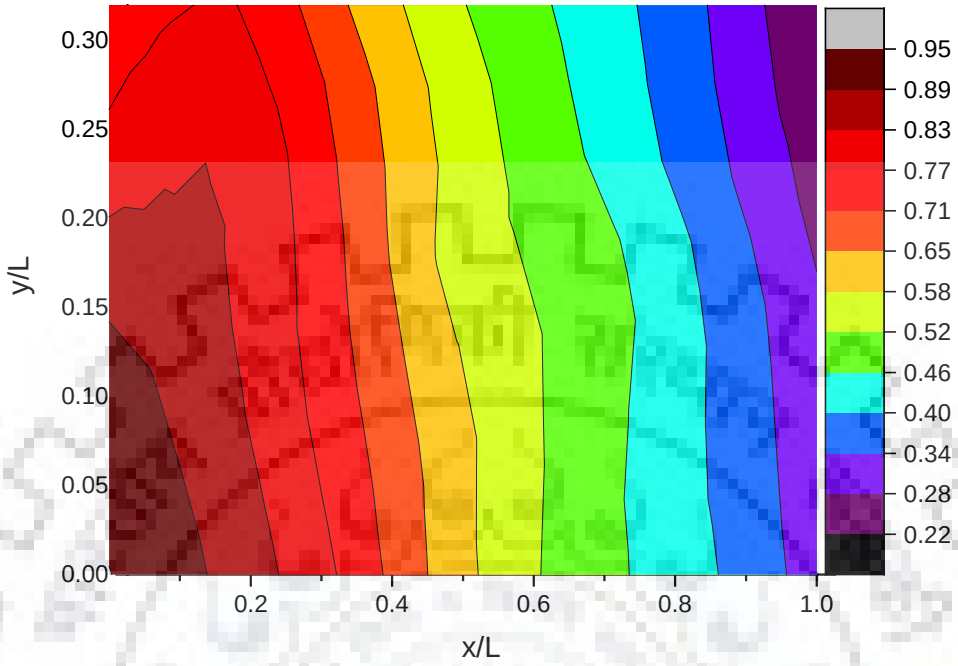

Figure 5.1 (b) showing the depth-averaged contour of normalized transverse turbulent intensity for bar condition

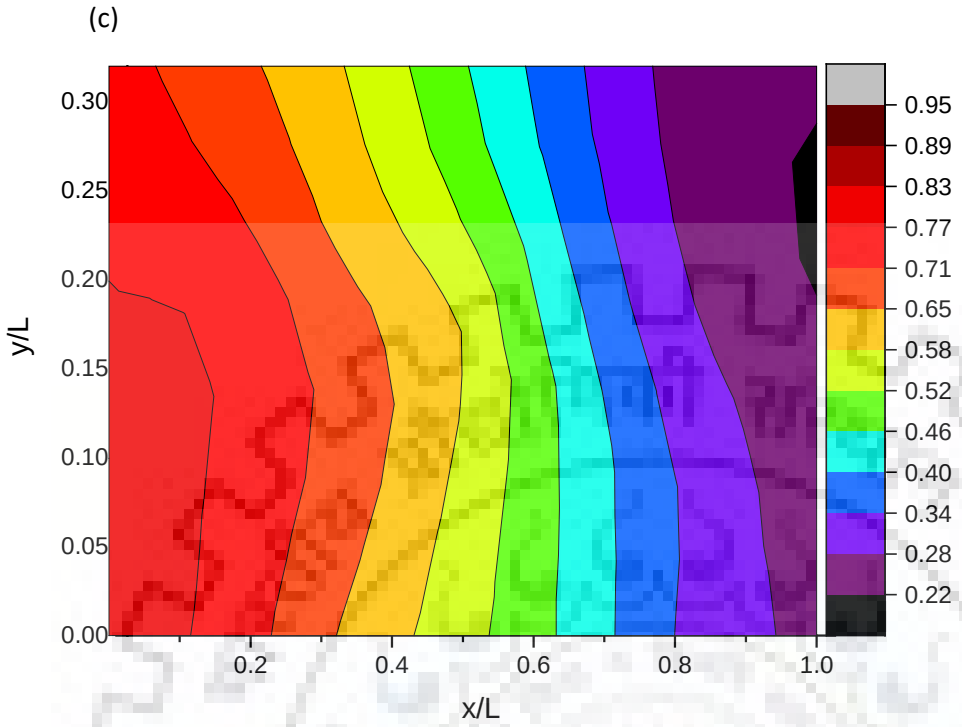

Figure 5.1 (c) showing the depth-averaged contour of normalized vertical turbulent intensity for bar condition

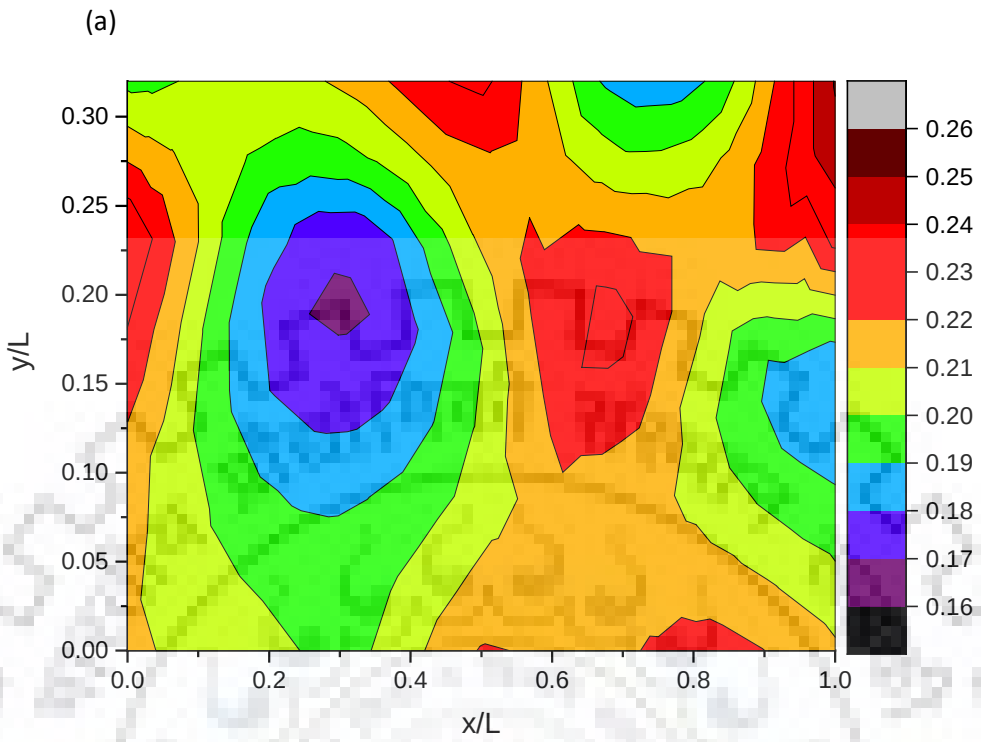

Figure 5.2 (a) showing the contour of depth-averaged normalized longitudinal turbulent intensity for no bar condition

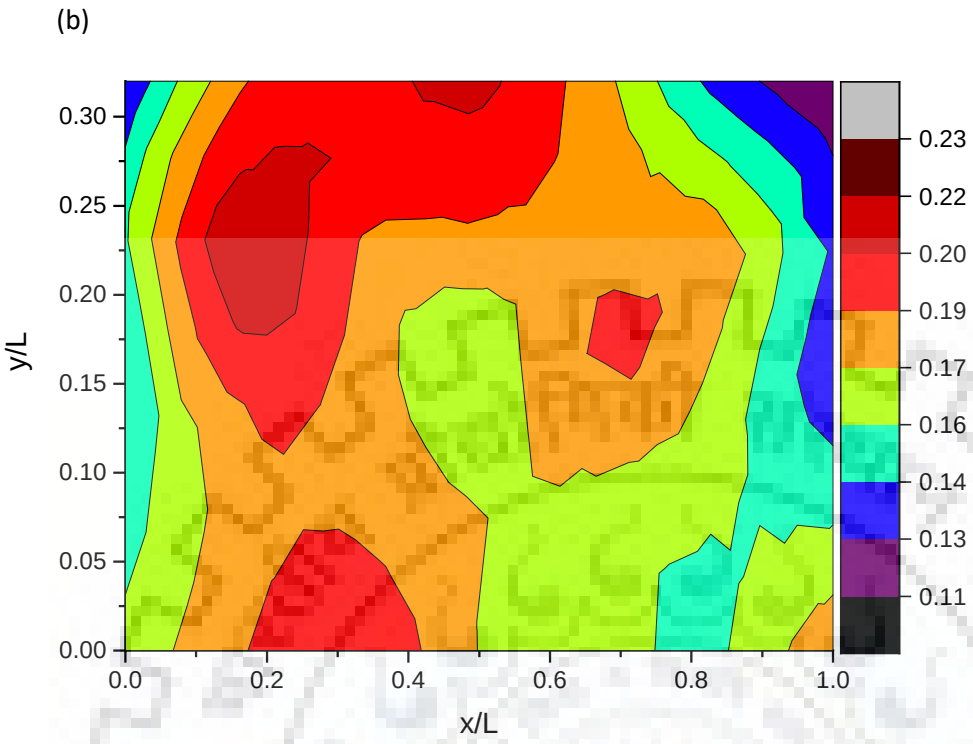

Figure 5.2 (b) showing the contour of depth-averaged normalized transverse turbulent intensity for no bar condition

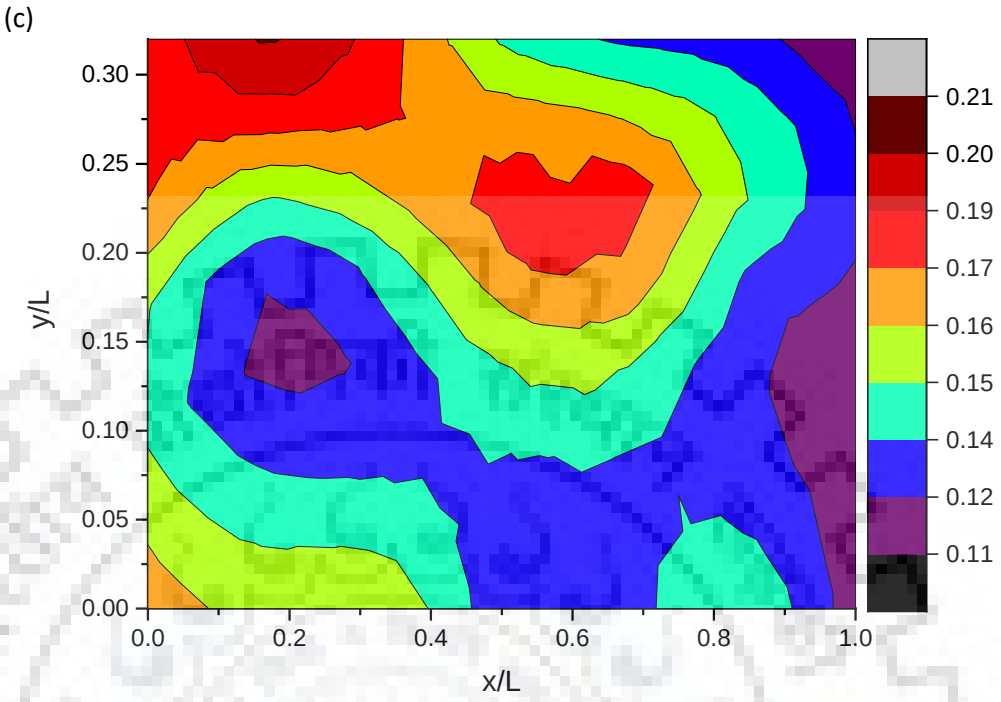

Figure 5.2 (c) showing the contour of depth-averaged normalized vertical turbulent intensity for no bar condition

5.3 Reynolds Shear Stress

The contours for depth-averaged Reynolds stress components are plotted for bar and no bar conditions. Figure 5.3 shows the contours of depth-averaged Reynolds stress components $-\rho u'w'$, $-\rho u'v'$, and $-\rho v'w'$ for bar condition. The values of depth-averaged Reynolds stress components for bar condition are much greater as compared to the no bar condition (Figures 5.3 and 5.4). The presence of mid-channel bar induces a series of critical changes to the turbulent flow structure, where high Reynolds stresses are generated at region near upstream end of mid-channel bar. These high Reynolds stresses may be expected to generate increased bed scouring. The level of Reynolds stress component decreases with increase in the x/L value.

(a)

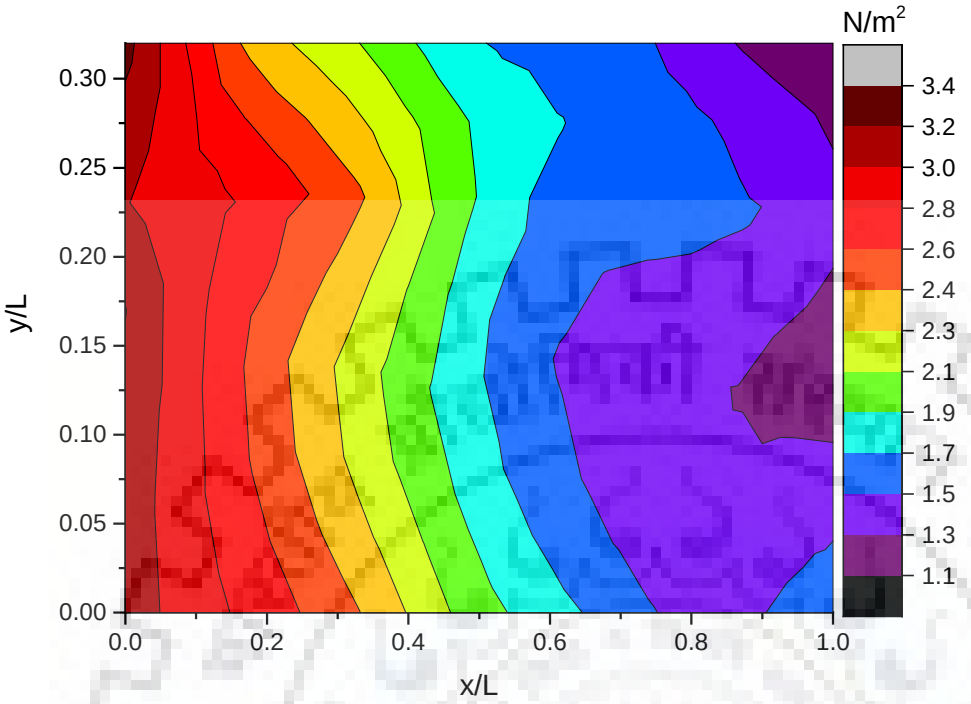

Figure 5.3 (a) showing the depth-averaged contour of -ρu′w′Reynolds stress for bar condition

(b)

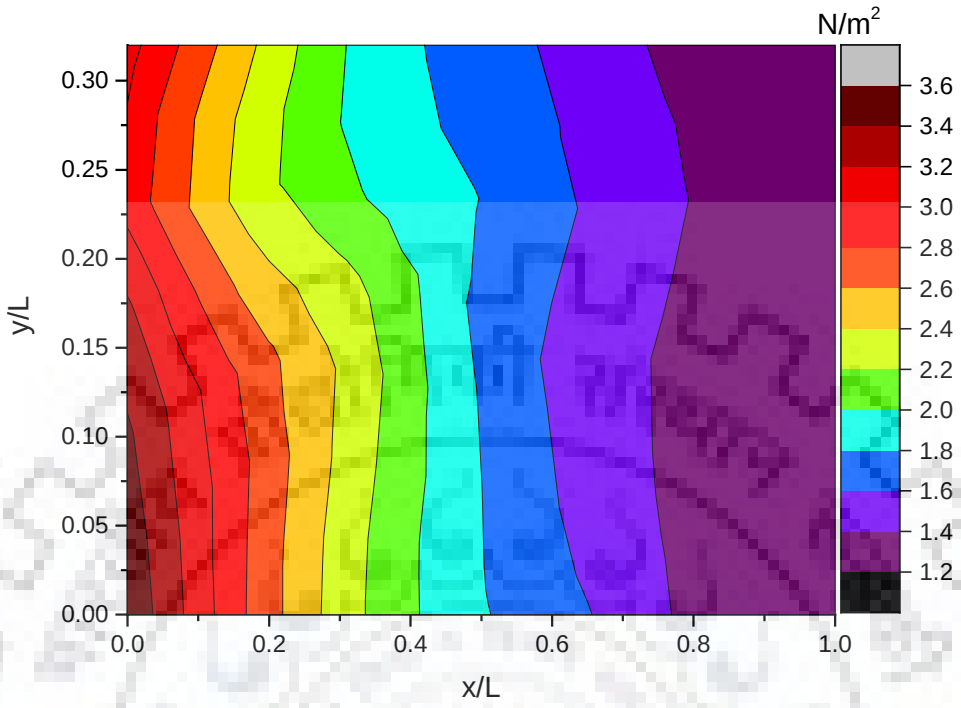

Figure 5.3 (b) showing the depth-averaged contour of -ρu′v′ Reynolds stress for bar condition

(c)

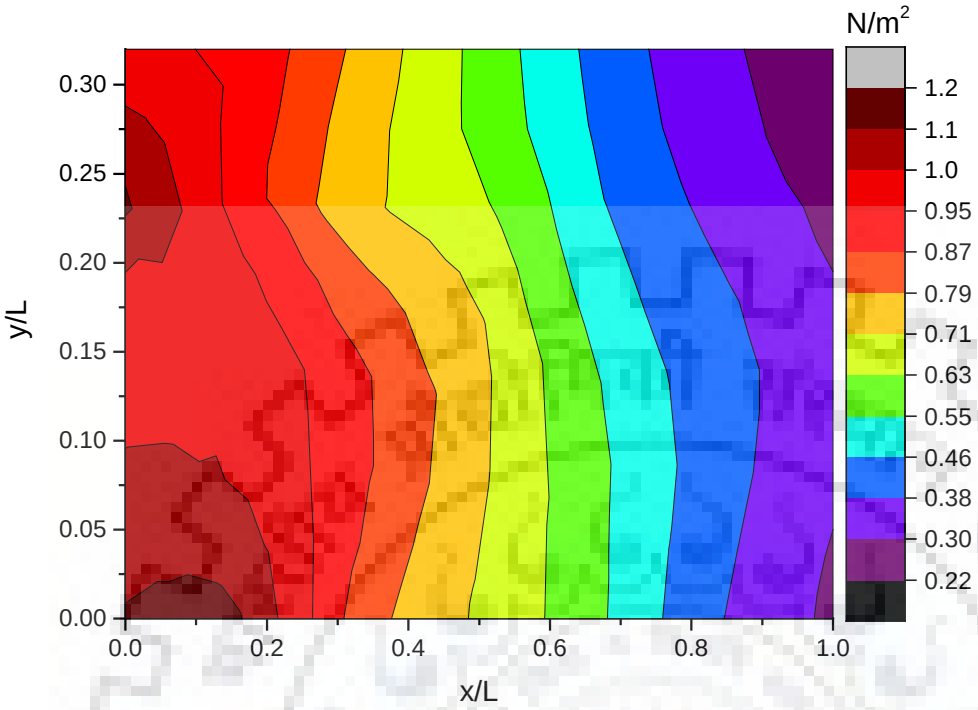

Figure 5.3 (c) showing the depth-averaged contour of -ρv′w′ Reynolds stress for bar condition

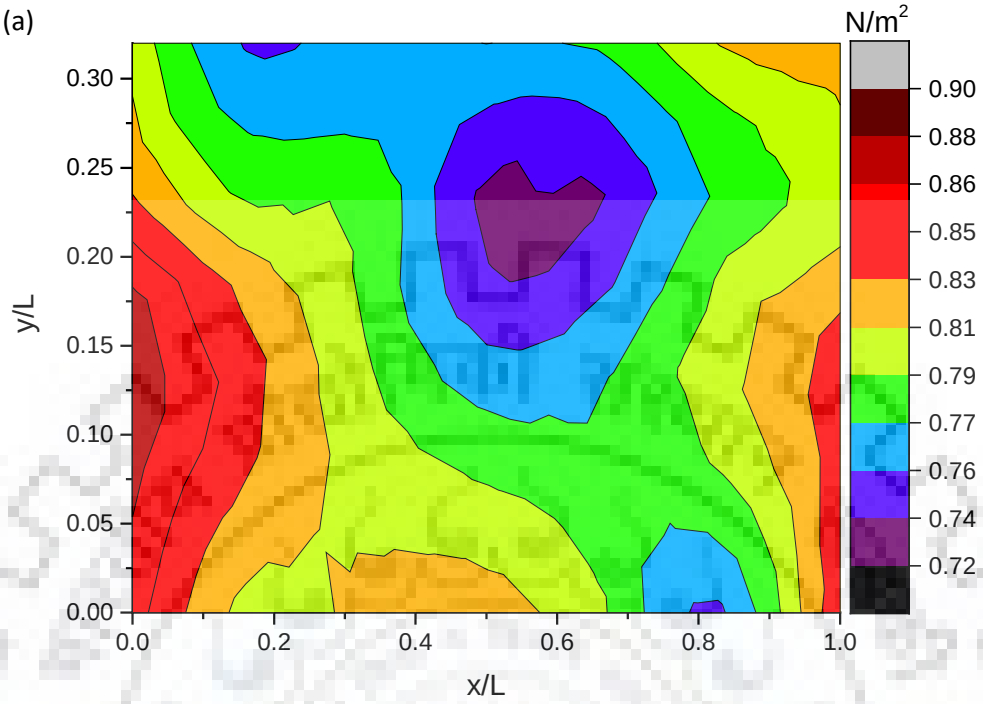

Figure 5.4 (a) showing the depth-averaged contour of -ρu′w′ Reynolds stress for no bar condition

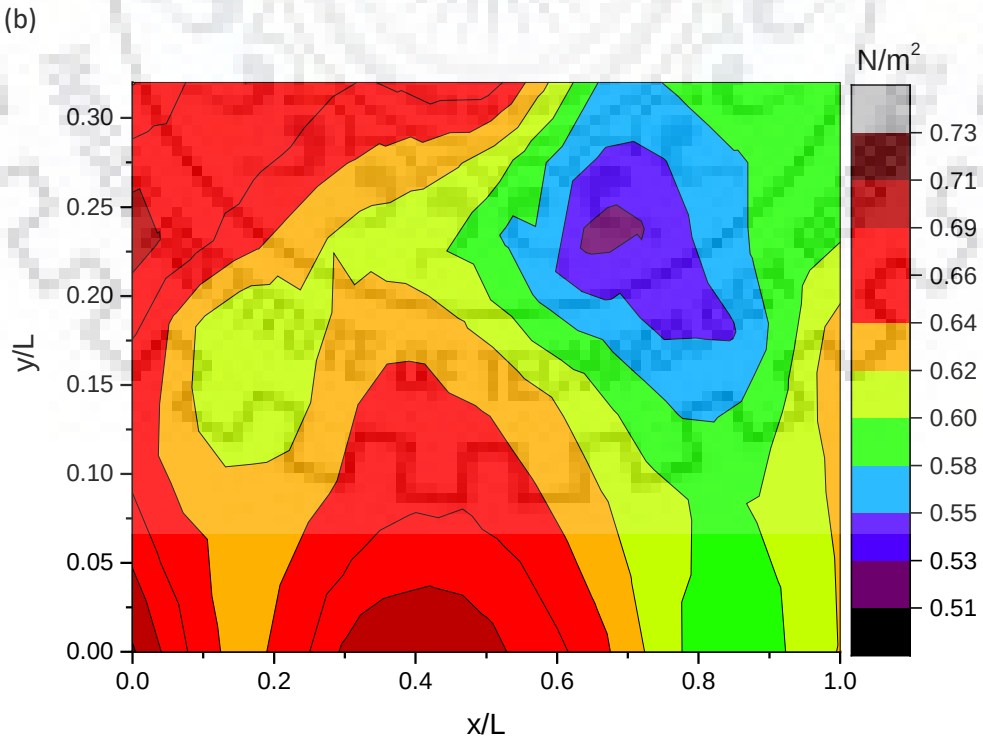

Figure 5.4 (b) showing the depth-averaged contour of -ρu′v′ Reynolds stress for no bar condition

(c)

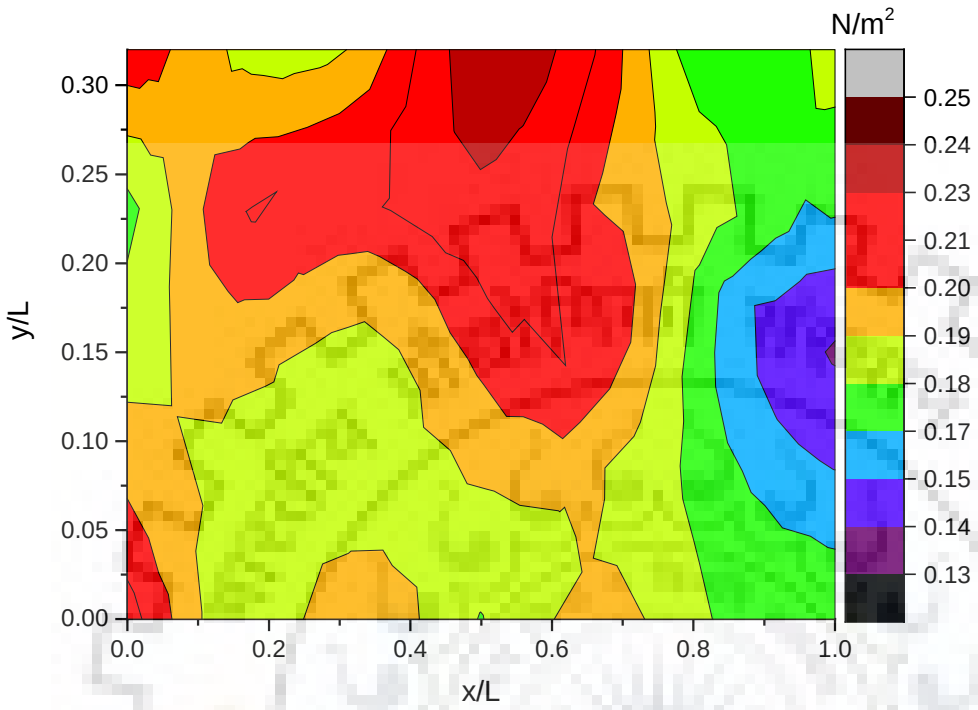

Figure 5.4 (c) showing the depth-averaged contour of -ρv′w′ Reynolds stress for no bar condition

CHAPTER-6 THREE-DIMENSIONAL BURSTING ANALYSIS

6.1 Analysis of Turbulent Kinetic Energy

Turbulent Kinetic Energy (TKE) is characterized by the root mean square values of velocity fluctuations (Lien and D'Asaro 2006, Ali et al. 2013). The total turbulent kinetic energy is given by Equation 6.1.

$$Tke_{Total} = \frac{1}{2}\{\overline{(u')^2} + \overline{(v')^2} + \overline{(w')^2}\} \quad (6.1)$$

The turbulent kinetic energy value for each individual direction was also computed. The TKE for x direction (Tke_x) is equal to $\frac{1}{2} * \overline{(u')^2}$. Similarly, the turbulent kinetic energy for y direction (Tke_y) and z direction (Tke_z) are represented by the $\frac{1}{2} * \overline{(v')^2}$ and $\frac{1}{2} * \overline{(w')^2}$ respectively. x, y and z represent the longitudinal, transverse and vertical directions respectively.

The depth averaged values of the TKE in all three directions (x, y and z) and the total kinetic energy Tke_{Total} are displayed in Figure 6.1 for bar condition. Figure 6.1 shows that the Tke_y has a significant contribution. The percentage contribution of Tke_y lies between 20-28%.

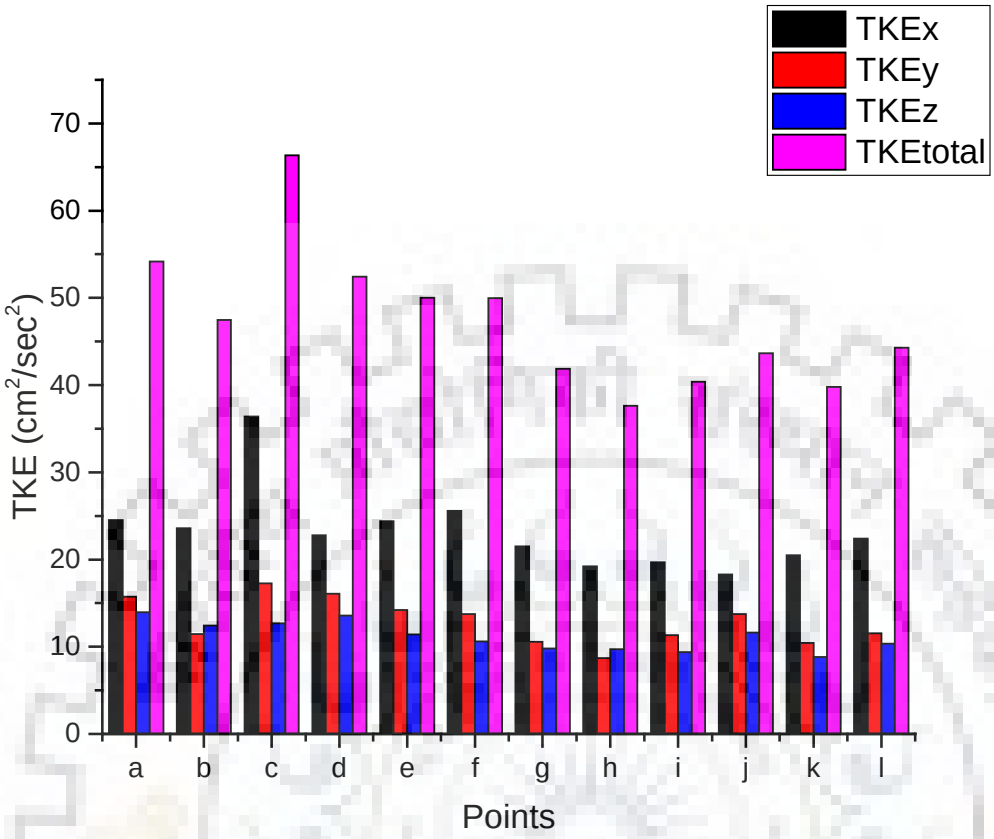

Figure 6.1 shows the depth averaged turbulent kinetic energy contribution for each direction and total turbulent kinetic energy for bar condition

Figure 6.2 displays the contribution of Tke_y for bar and no bar conditions. Figure 6.2 shows that the contribution of Tke_y for bar condition is almost 1.5 times as compared to the no bar condition. The above results show that the transverse flow component has significant contribution for bar condition. Thus the transverse flow component is also taken into account for analysing the turbulent structure in the vicinity of mid-channel bar. Therefore, in the next part the three-dimensional bursting events are analysed in the vicinity of the mid-channel bar.

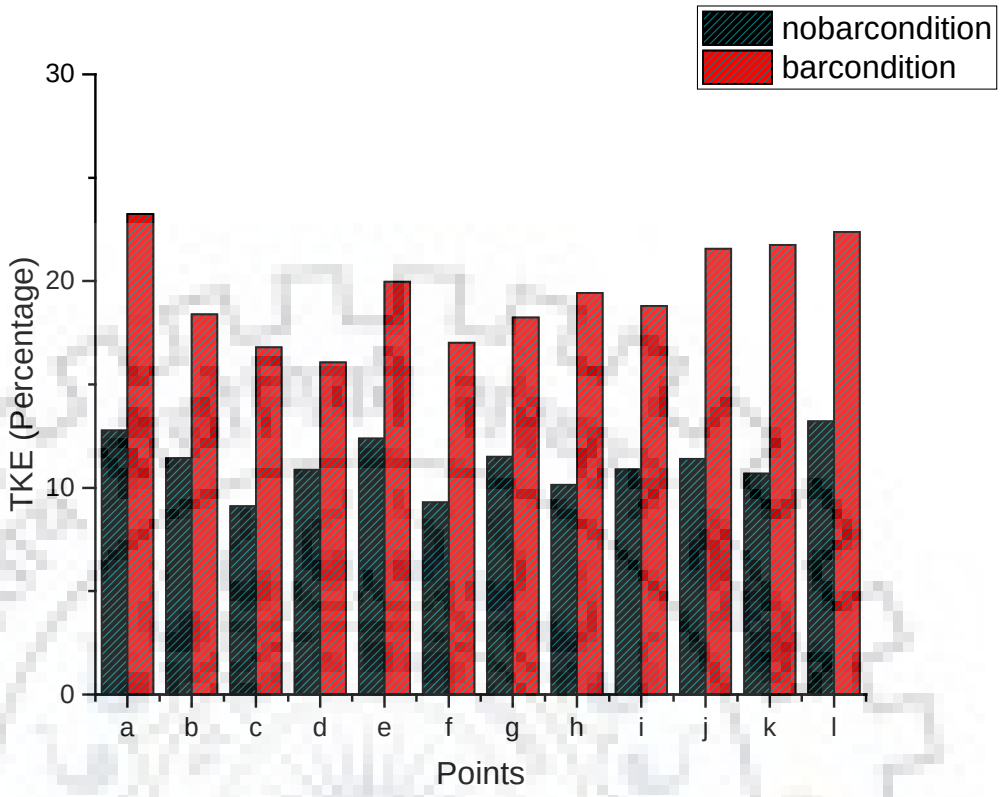

Figure 6.2 shows the percentage contribution of depth averaged transverse turbulent kinetic energy for no bar and bar condition

In Chapter 4, the two-dimensional bursting events are studied in detail. It is very difficult to analyse the joint probability distribution of all three components of velocity from mathematical point of view. Although the three-dimensional analysis will provide the better results but for sake of simplifying the analysis only the longitudinal and vertical components of velocity fluctuations are taken into account.

In this chapter, all three components of velocity are taken into consideration for more precise study of turbulent flow structure. The three-dimensional bursting analysis results are also compared with the two-dimensional bursting analysis results in this chapter.

6.2 Analysis of three-dimensional bursting events

In section 6.1, it was found that the turbulent flow becomes predominantly three dimensional in the vicinity of mid-channel bar. Thus, the three-dimensional turbulent flow characteristics in the vicinity of mid-channel bar is analysed in this section.

On the basis of three-dimensional velocity fluctuations, the bursting events are classified into eight categories (Table 6.1). The bursting events classification are done as per Keshavarzi and Gheisi (2006). The three-dimensional analysis of laboratory experiment would provide greater details regarding the sediment transport mechanism (Tiwari and Sharma 2014). Herein, the octagonal bursting events are analysed at locations in the vicinity of mid-channel bar.

The occurrence probability of each octagonal bursting event is determined by Equation 6.2 (Keshavarzi et al. 2006).

$$P_K = \frac{n_K}{n} \tag{6.2}$$

$$n = \sum_{K=1}^{8} n_K \tag{6.3}$$

Here, P_K is the occurrence probability of bursting event which belongs to the Kth octant. The K values are integer lies from 1 to 8 (Table 6.1). n_K is the total number of bursting events present in octant K and n is the length of velocity sample. n is determined using the Equation 6.3.
Keshavarzi and Gheisi (2006) divided the bursting events into two Zones i.e. Zone A and Zone B. The terminology of each of the eight bursting events have been adopted as per Keshavarzi and Gheisi (2006). For e.g. Internal Outward interaction (I-A) is named as P_1 (Table 6.1).
Primary Y axis in Figure 6.3, shows the values of depth averaged occurrence probability of octant events for twelve points in the vicinity of mid-channel bar. Secondary Y axis in Figure 6.3, shows the scouring /deposition values observed at these twelve points. By comparing the primary and secondary Y Axis of Figure 6.3, it was found that the even events are dominant at scouring points and odd events are dominant at depositional points.

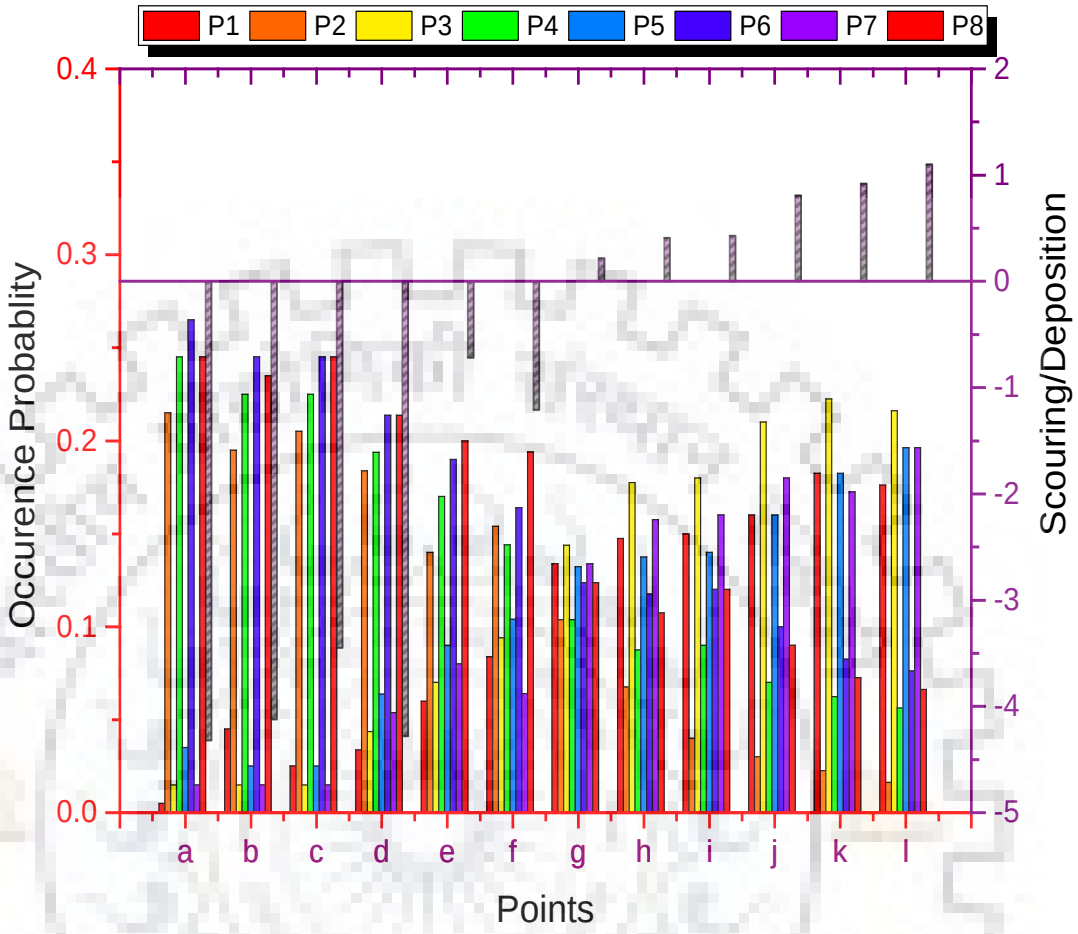

Figure 6.3 Show the variation of depth averaged octant events along-with the magnitude of scouring/deposition in centimeter observed in the vicinity of mid-channel bar (bar condition)

In order to club the effect of bursting events on the turbulent flow characteristics in the vicinity of mid-channel bar, a new parameter 3-Dimensional Burst Index (3DBI) is introduced in the present study (Equation 6.4). It is the ratio of summation of odd events to the summation of even events.

$$3DBI = \left(\frac{P_1+P_3+P_5+P_7}{P_2+P_4+P_6+P_8}\right) \quad (6.4)$$

High values of 3DBI is observed at depositional points and low values for scouring points. Figure 6.4 shows that the 3DBI exhibits linear relationship with the scouring/deposition phenomenon observed in the vicinity of mid-channel bar with Coefficient of Determination R^2 and Pearson R value equal to 0.94 and 0.97 respectively. The high values of correlation coefficients indicate that the 3DBI is closely related with local stream bed elevation change occurred in the proximity of mid-channel bar.

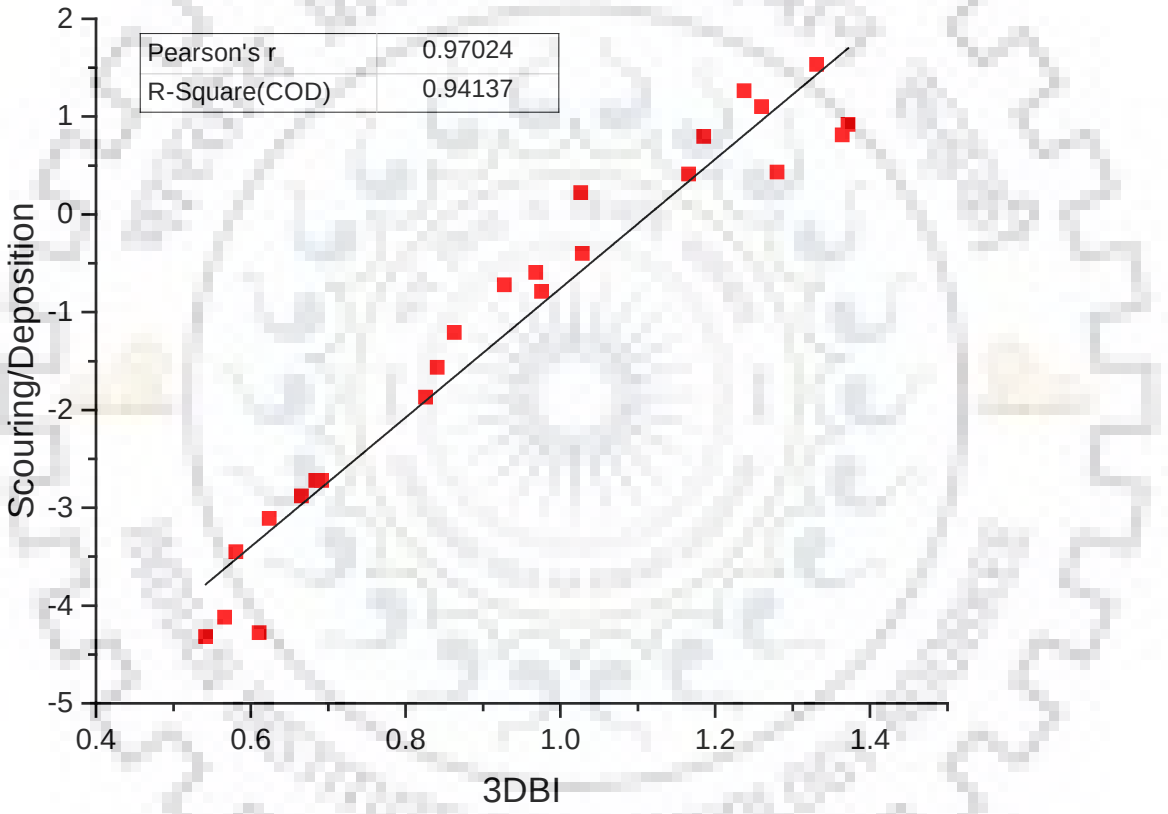

Figure 6.4 Shows the variation of 3-Dimensional Burst Index with the magnitude of scouring/deposition in centimetre observed in the vicinity of mid-channel bar (bar condition)

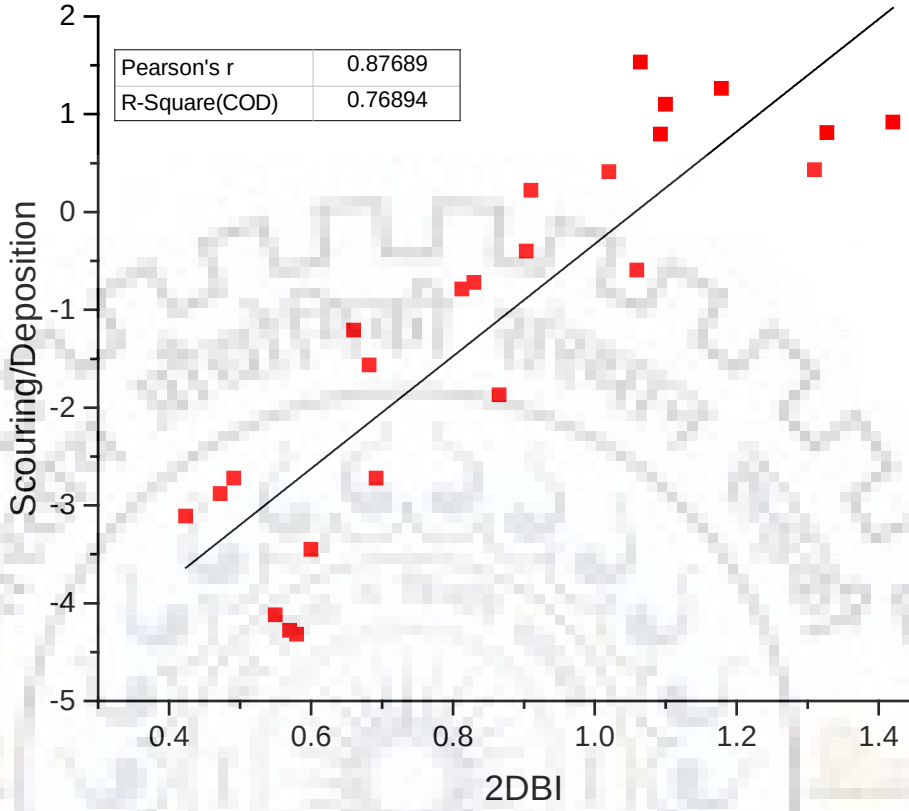

Figure 6.5 Shows the variation of 2-Dimensional Burst Index with the magnitude of scouring/deposition in centimetre observed in the vicinity of mid-channel bar (bar condition)

The average Burst Index for 2-D Quadrant Events is also computed. Two-dimensional Burst Index (2DBI) is defined as the ratio of summation of odd events to the summation of even events (Equation 6.5).

$$2DBI = \left(\frac{P_{outward\ interaction} + P_{inward\ interaction}}{P_{ejection} + P_{Sweep}}\right) \quad (6.5)$$

Figure 6.5 shows the relationship of 2DBI with the scouring/deposition phenomenon observed in the vicinity of mid-channel bar. The linear relationship between the 2DBI and scouring/deposition data has Coefficient of Determination and Pearson R value equal to 0.76 and 087 respectively. Results indicates that the 3DBI parameter is better for analysing the local stream bed elevation change occurred in the vicinity of mid-channel bar.

Table 6.1 Showing the classification for three-Dimensional Octant Bursting Events

Bursting Event Number (k)	Sign of fluctuating velocity			Octant Events	Zone
	u'	v'	w'		
P_1	+	+	+	Internal Outward interaction (I-A)	Zone A
P_2	–	-	+	Internal Ejection (II-A)	
P_3	–	–	–	Internal Inward interaction (III-A)	
P_4	+	+	-	Internal sweep (IV-A)	
P_5	+	-	+	External Outward interaction (I-B)	Zone B
P_6	–	+	+	External Ejection (II-B)	
P_7	–	+	-	External Inward interaction (III-B)	
P_8	+	–	–	External Sweep (IV B)	

6.3 Three-Dimensional Hole Size Analysis

Researches have been done on the effect of Hole size on two-dimensional bursting events. The effect of Hole size concepts for octant events is not studied till now. As the flow is three dimensional in the vicinity of mid-channel bar, thus the Hole size analysis of octant events will be beneficial for analysing the turbulent flow structure.

We have defined the Hole size concept for three-dimensional flow. Three-Dimensional Hole Size (3DHS) is the threshold parameter which extracts the signal greater than the H times the product of the mean values of turbulence fluctuations (Equation 6.6).

$$|u'\ v'\ w'| > H\overline{u'}\,\overline{v'}\,\overline{w'} \qquad (6.6)$$

For Three-Dimensional Hole Size H, octants events for which product |u' v' w'| is less than H*$\overline{u'}\overline{v'}\overline{w'}$ are removed using the 'and' operator in Microsoft excel. $\overline{u'}, \overline{v'}$ and $\overline{w'}$ are the mean values of longitudinal, transverse and vertical velocity fluctuations respectively. The 3DHS helps in segregating the extreme octant events from the low intensity octant events.

The variation of octant events with the 3DHS will be discussed in this section. As observed by Cellino and Lemmin (2004) the effect of Hole size is mainly observed in the boundary region, thus the octant events are depth averaged for near bed region (z/h≤0.06).

The variation of octant events with the 3DHS for bar condition is shown in Figure 6.6. For 'b' and 'd' points, the even events are dominant. The occurrence probability of even events is increasing with increase in the value of 3DHS. The occurrence probability of odd events is decreasing with increase in the 3DHS value (Figure 6.6).

For "h' and 'l' points, the occurrence probabilities of odd events are greater as compared to the even events. The occurrence probabilities of odd events show increasing trend with the 3DHS. For 'h' points, the P_6 and P_8 events do not show much variation with the 3DHS (Figure 6.6).

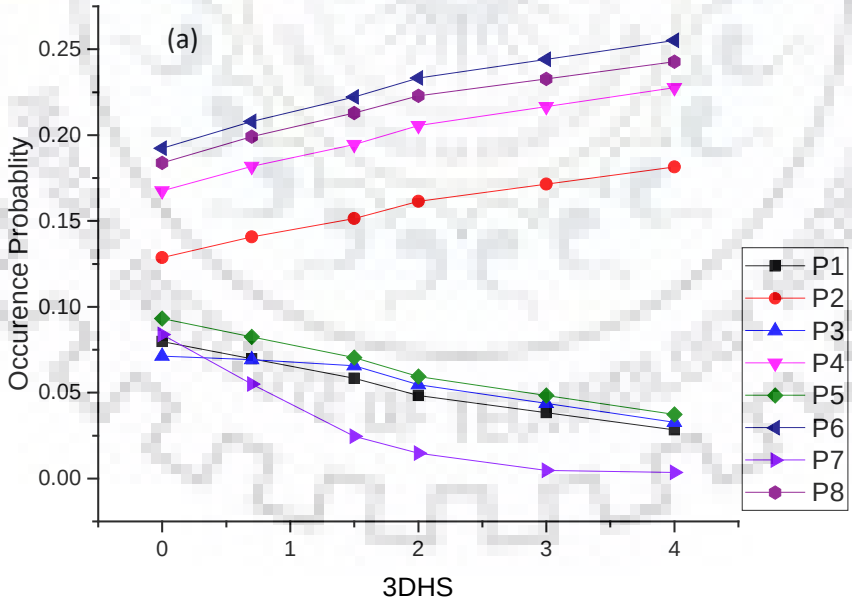

Figure 6.6 (a) shows the variation of depth averaged octant events with the 3DHS for Point 'b' (bar condition)

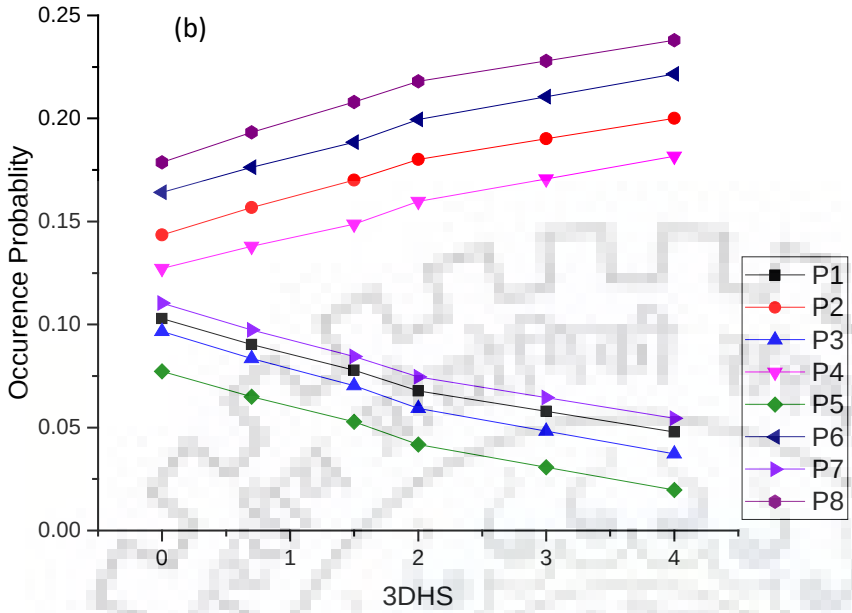

Figure 6.6 (b) shows the variation of depth averaged octant events with the 3DHS for Point 'd' (bar condition)

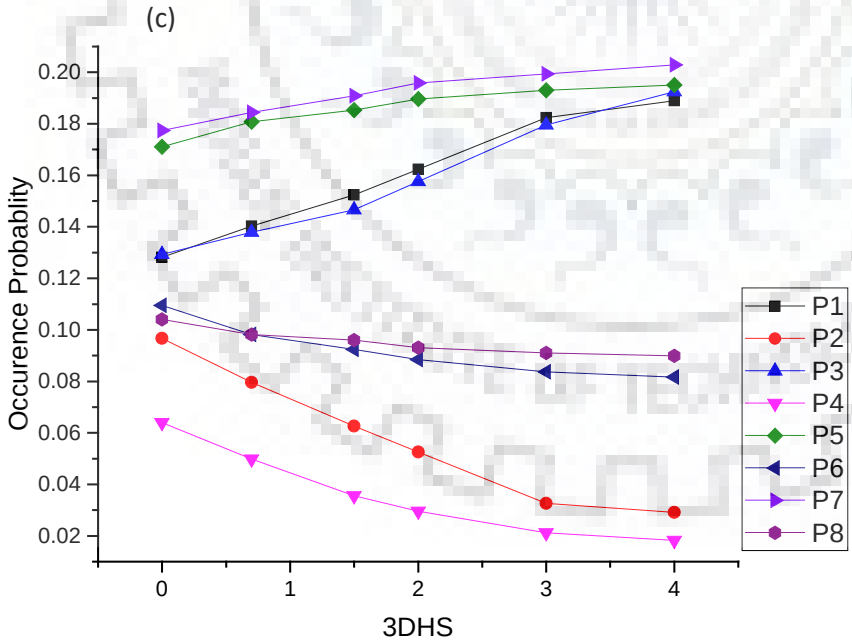

Figure 6.6 (c) shows the variation of depth averaged octant events with the 3DHS for Point 'h' (bar condition)

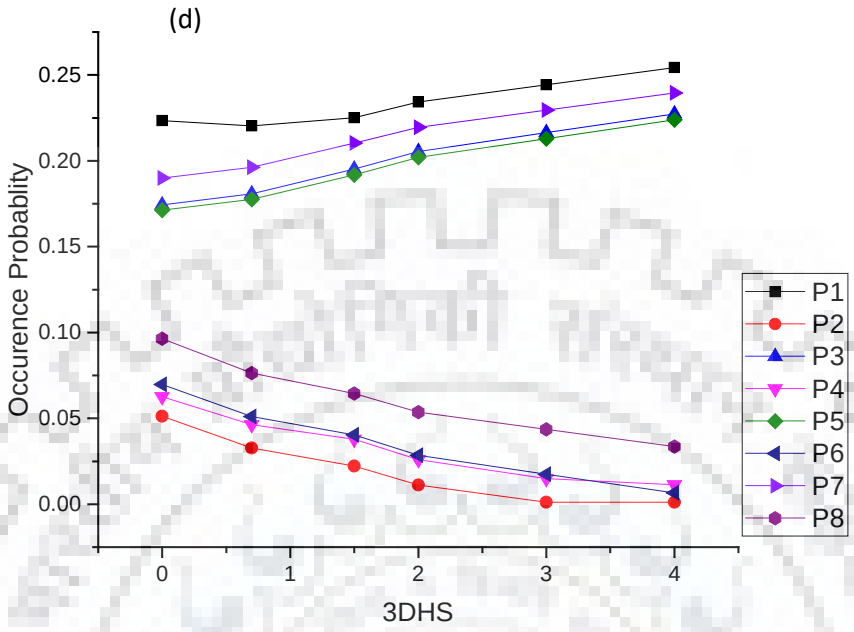

Figure 6.6 (d) shows the variation of depth averaged octant events with the 3DHS for Point 'I' (bar condition)

Figure 6.7 shows the variation of octant events with the 3DHS for no bar condition. Figure 6.7 indicates that the occurrence probabilities of even events are greater as compared to the odd events. The octants events show little variation with the 3DHS. This indicates that the extreme turbulent burst is not observed for no bar condition. In other words, it can be written that the presence of mid-channel bar leads to the creation of high turbulent burst. The one more conclusion drawn from this section is that the dominant events becomes more dominant with increase in the 3DHS value.

(d)

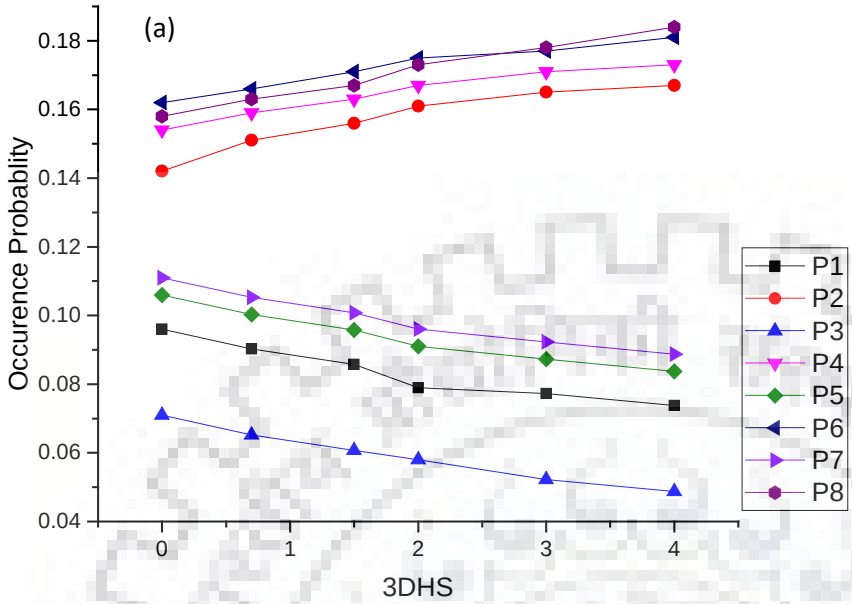

Figure 6.7 (a) shows the variation of depth averaged octant events with the 3DHS for Point 'b' (no bar condition)

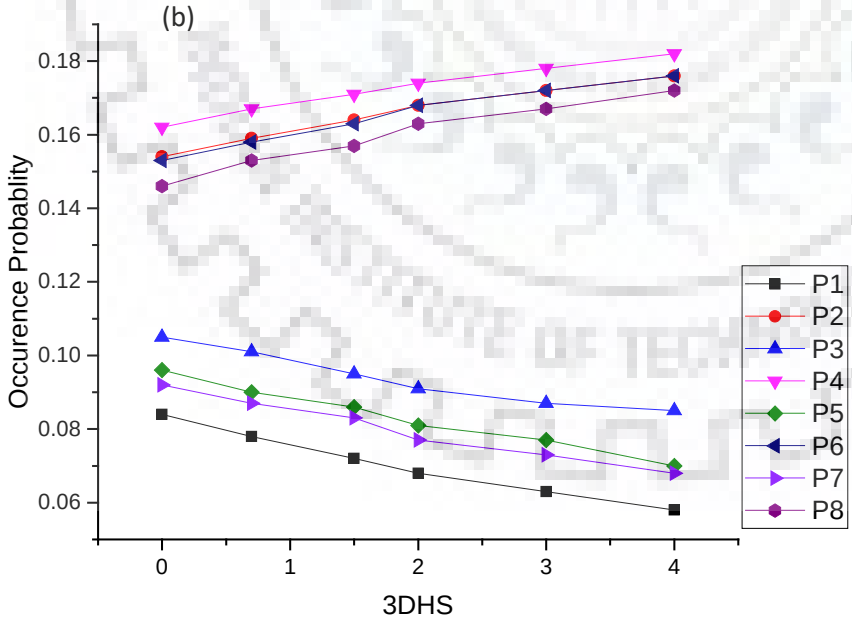

Figure 6.7 (b) shows the variation of depth averaged octant events with the 3DHS for Point 'd' (no bar condition)

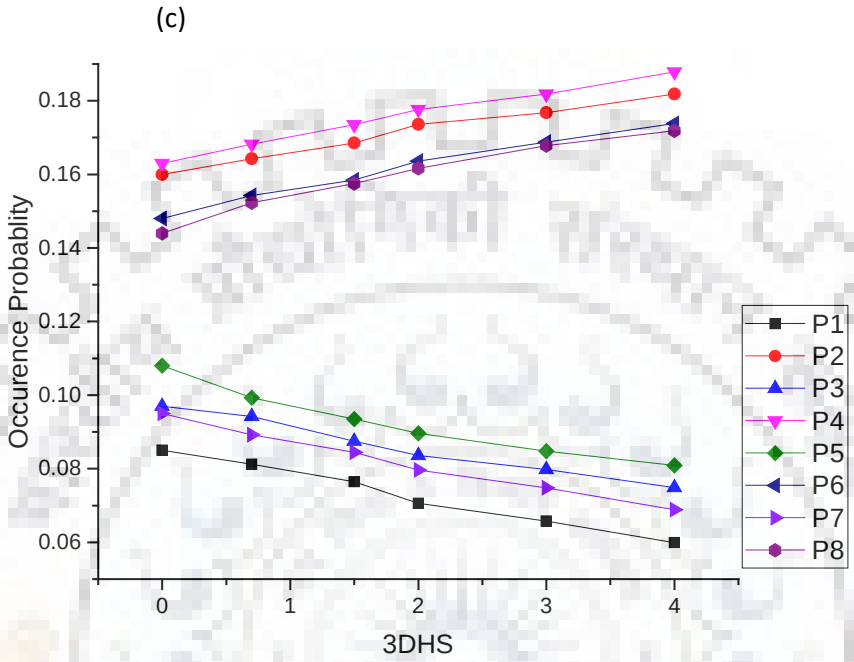

Figure 6.7 (c) shows the variation of depth averaged octant events with the 3DHS for Point 'h' (no bar condition)

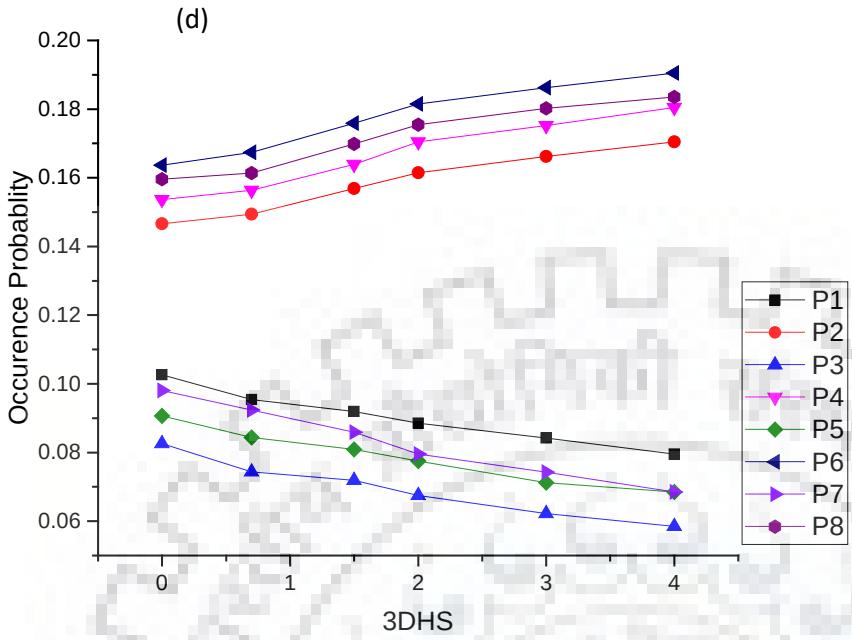

Figure 6.7 (d) shows the variation of depth averaged octant events with the 3DHS for Point 'I' (no bar condition)

6.4 Ejection/Sweep Interaction

In this study, the three-dimensional bursting events responsible for kolks-boils phenomenon are studied in detail. For studying the interaction between the sweep and ejection events, we have introduced a new parameter 3-Dimensional Dominance Function (3DDF)=$\frac{P_{2,H}+P_{6,H}}{P_{4,H}+P_{8,H}}$, which is the ratio of summation of ejection events to the summation of sweep events. $P_{2,H}$ and $P_{6,H}$ represents the occurrence probability of internal ejection (II-A) and external ejection (II-B) events respectively for H Hole size. $P_{4,H}$ and $P_{8,H}$ represent the occurrence probability of internal sweep (IV-A) and external sweep (IV-B) events respectively for H Hole size (Table 6.1).

Figure 4.4 is showing the location of measurement points. Upstream end of bar is set as origin for measuring points. The 3DDF contours are plotted for bar condition in Figure 6.8 along the dotted line indicated in Figure 4.4.

Depth-wise distribution of 3DDF is plotted for bar condition (Figure 6.8). The longitudinal distance (x) and vertical distance (z) in Figure 6.8 are normalized by the length of bar (L) and depth of flow (h) respectively. White region indicates the ejection dominance and black region

indicates the sweep dominance. The Sweep events are dominant near the bed and Ejection events are dominant at greater distance from the bed (Figure 6.8).

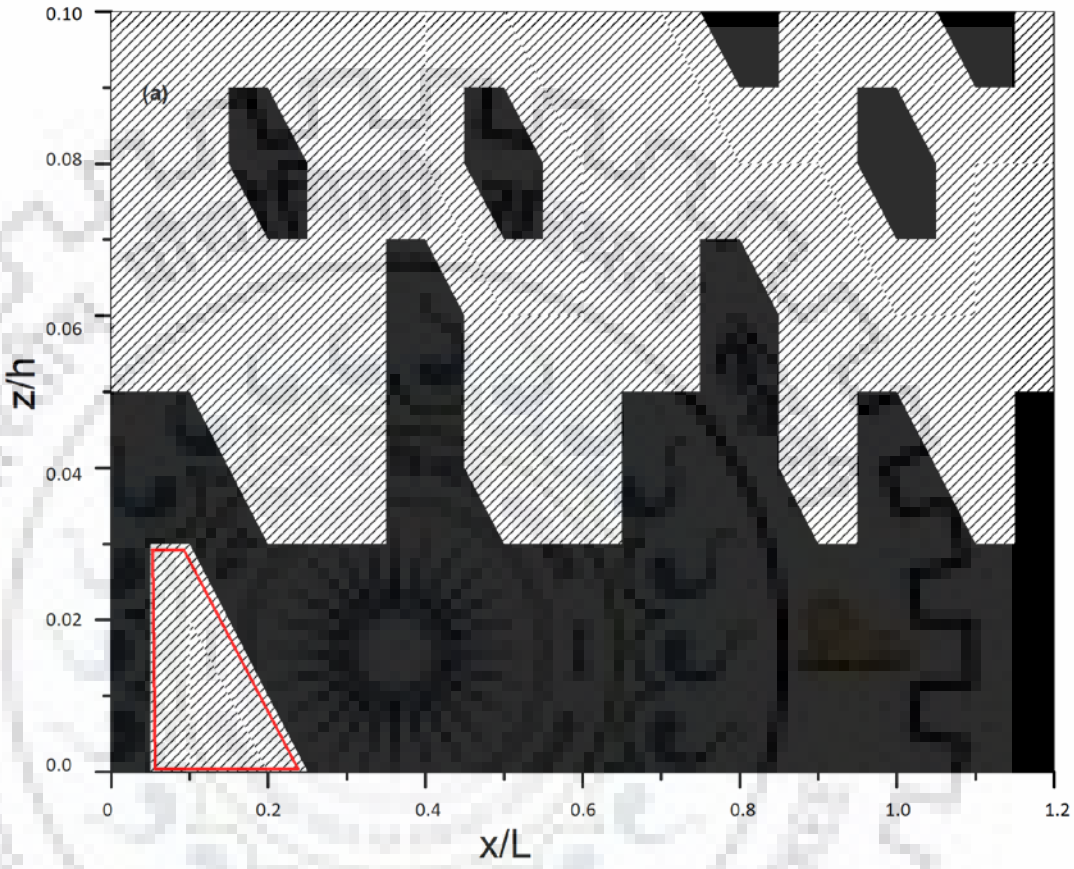

Figure 6.8 (a) Shows the depth-wise distribution of 3-Dimensional Dominance Function parameter for 0 Hole size

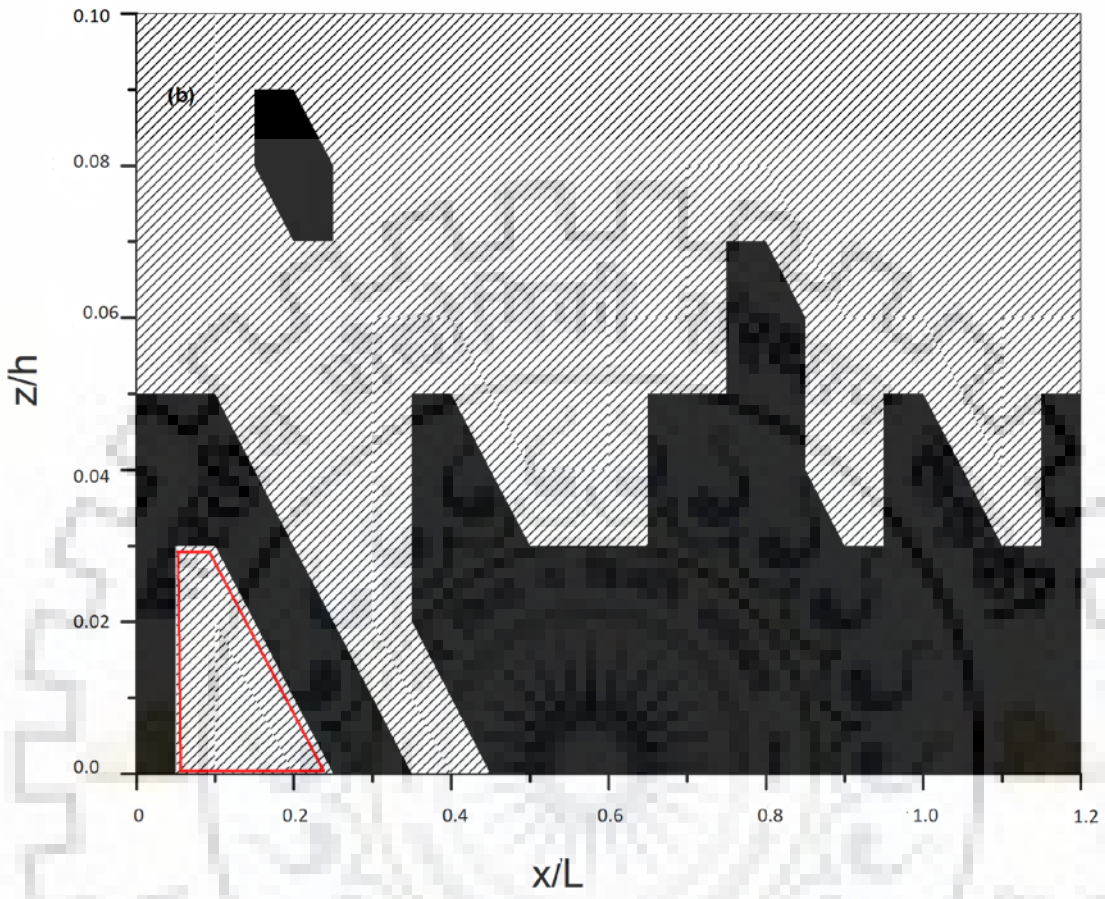

Figure 6.8 (b) Shows the depth-wise distribution of 3-Dimensional Dominance Function parameter for 2 Hole size

It is observed that the region of ejection dominance increases as the Hole size increases from 0 to 2. At the interface of sweep and ejection events dominance, the interaction of these events occurs. The interaction is responsible for the kolks-boils phenomenon (Mao 2003; Matthes 1947). The "kolks" and "boils" are the upward tilting vortices generated by the fluid bar interaction. kolks-boils phenomenon creates negative pressure gradient which leads to the suspension of bed particle. Near the bed, the area of interaction between the sweep and ejection events is shown by the red quadrilateral. By referring the Figure 6.8 and Table 3.3, it was found that the high scouring is observed at the area of interaction. The above discussion indicates that the 3DDF parameter is

successful in predicting the high scouring region. From section 4.4, it was found that the Two-Dimensional Dominance Function is not able to predicts the high scouring region successfully. The main purpose of defining 3DDF parameter is to predict the high scouring region, which is fulfilled as indicated by the above results.

6.5 Three-Dimensional Transitional Movements Modelling

Bursting phenomena consist of quasi-organized and quasi-periodic events that occur randomly in turbulent flow (Kline et al. 1967). These events have spatio-temporal nature. Keshavarzi and Gheisi (2006) observed that the movements of these bursting events from one octant event to an another octant one with time increment play a crucial role in understanding the micro structure of turbulence.

The bursting events can be modelled as continuous or discrete variable. As per Keshavarzi and Gheisi (2007), the bursting events are considered as discrete for modelling the transitional movements. Markov chain process is most commonly used for modelling the time series of discrete variable. Thus, the Markov chain process is used herein for modelling the spatio-temporal transitional movements.

Bt represents the bursting event at time t. At any point of time, the Bt can occur in any of the octant. The change in current state of Bt with respect to time increment is defined as movement (Gheisi et al. 2006). These movements were modelled by Gheisi et al. (2006) using the Markov chain process. The probability of these movements is defined as transition probability. Keshavarzi and Gheisi (2007) modelled transition probability using the zero, first and second order Markov chain. They observed that the first order Markov chain is best for modelling the transition movements. First order Markov chain process is used in this study for transitional movements modelling as per Keshavarzi and Gheisi (2007).

In first order Markov chain process, the next situation depends on the present situation (Gilks et al. 1995). The probability of first order Markov chain transitional movements are calculated with the help of maximum likelihood estimates (Equation 6.7).

$$P_{ij} = \frac{n_{ij}}{n_i} \tag{6.7}$$

$$n_{ij} = n_{i1} + +n_{i2} + n_{i3} + n_{i4} + n_{i5} + n_{i6} + n_{i7} + n_{i8} \tag{6.8}$$

Here $n_{ij}$is the number of transitional movements from octant event i to octant event j (Equation 6.8). n_i is number of events belonging to octant i at any instant t. The P_{ij} is

probability of transitional movement from octant event i at instant time t to octant event j at time t+1.

The $Matrix(A)$ is displaying the location of transitional movements obtained from the first order Markov chain .

$$Matrix(A) = \begin{bmatrix} \boldsymbol{P_{1\to1}} & P_{1\to2} & P_{1\to3} & P_{1\to4} & P_{1\to5} & P_{1\to6} & P_{1\to7} & P_{1\to8} \\ P_{2\to1} & \boldsymbol{p_{2\to2}} & P_{2\to3} & P_{2\to4} & P_{2\to5} & P_{2\to6} & P_{2\to7} & P_{2\to8} \\ P_{3\to1} & P_{3\to2} & \boldsymbol{P_{3\to3}} & P_{3\to4} & P_{3\to5} & P_{3\to6} & P_{3\to7} & P_{3\to8} \\ P_{4\to1} & P_{4\to2} & P_{4\to3} & \boldsymbol{P_{4\to4}} & P_{4\to5} & P_{4\to6} & P_{4\to7} & P_{4\to8} \\ P_{5\to1} & P_{5\to2} & P_{5\to3} & P_{5\to4} & \boldsymbol{P_{5\to5}} & P_{5\to6} & P_{5\to7} & P_{5\to8} \\ P_{6\to1} & P_{6\to2} & P_{6\to3} & P_{6\to4} & P_{6\to5} & \boldsymbol{P_{6\to6}} & P_{6\to7} & P_{6\to8} \\ P_{7\to1} & P_{7\to2} & P_{7\to3} & P_{7\to4} & P_{7\to5} & P_{7\to6} & \boldsymbol{P_{7\to7}} & P_{7\to8} \\ P_{8\to1} & P_{8\to2} & P_{8\to3} & P_{8\to4} & P_{8\to5} & P_{8\to6} & P_{8\to7} & \boldsymbol{P_{8\to8}} \end{bmatrix}$$

$P_{1\to2}$ represents the probability of movement from octant P_1 to octant P_2 . In the similar manner, the remaining elements of above matrix can be defined.

The transitional movements are divided into two main classes. The first class consists of movements that take place between the events that belong to same zone, for e.g. $P_{1\to3}$ or $P_{2\to4}$. The second class contains movements that occur between the events which belong to different zone, for eg. $P_{1\to6}$ or $P_{8\to3}$ (Keshavarzi and Gheisi 2006). The transitional movements that belong to first class are called inner class movements. These inner class movements are further divided into three sub classes mentioned below.

Stable movements: The event stays in the same octant as the time changes from t to t+1. These movements are located at the main diagonal of $Matrix(A)$ highlighted by bold letter. For e.g. $P_{1\to1}$, $P_{8\to8}$. These movements are further classified into the Class A and Class B transitional movements on the basis of their octant Zone (Table 6.1). Class A stable transitional movements are $P_{1\to1}$, $P_{2\to2}$, $P_{3\to3}$ and $P_{4\to4}$. Class B stable transitional movements are $P_{5\to5}$, $P_{6\to6}$, $P_{7\to7}$ and $P_{8\to8}$.

Marginal movements: The event moves to the neighboring event of same zone as the time changes from t to t+1. For e.g. $P_{3\to4}$, $P_{7\to8}$.

Cross movements: The bursting events move to the cross events of same zone as the time changes from t to t+1. For e.g. $P_{2\to4}$, $P_{6\to8}$.

It is difficult to analyse all 64 probable transitional movements. Keshavarzi and Gheisi (2006) found that only inner group movements play significant role in defining the turbulent structure of flow. Therefore, in this research only the inner group movements are analysed.

The depth averaged values of transition probability of stable movements are plotted for bar condition (Figure 6.9). From Figure 6.9, it was found that the higher values of $P_{2\to2}$, $P_{4\to4}$, $P_{6\to6}$, $P_{8\to8}$ observed at scouring points and higher values of $P_{1\to1}$, $P_{3\to3}$, $P_{5\to5}$, $P_{7\to7}$ observed at depositional points. Thus, the odd stable movements are related to deposition and even stable movements are related to the scouring occurred in the vicinity of mid-channel bar.

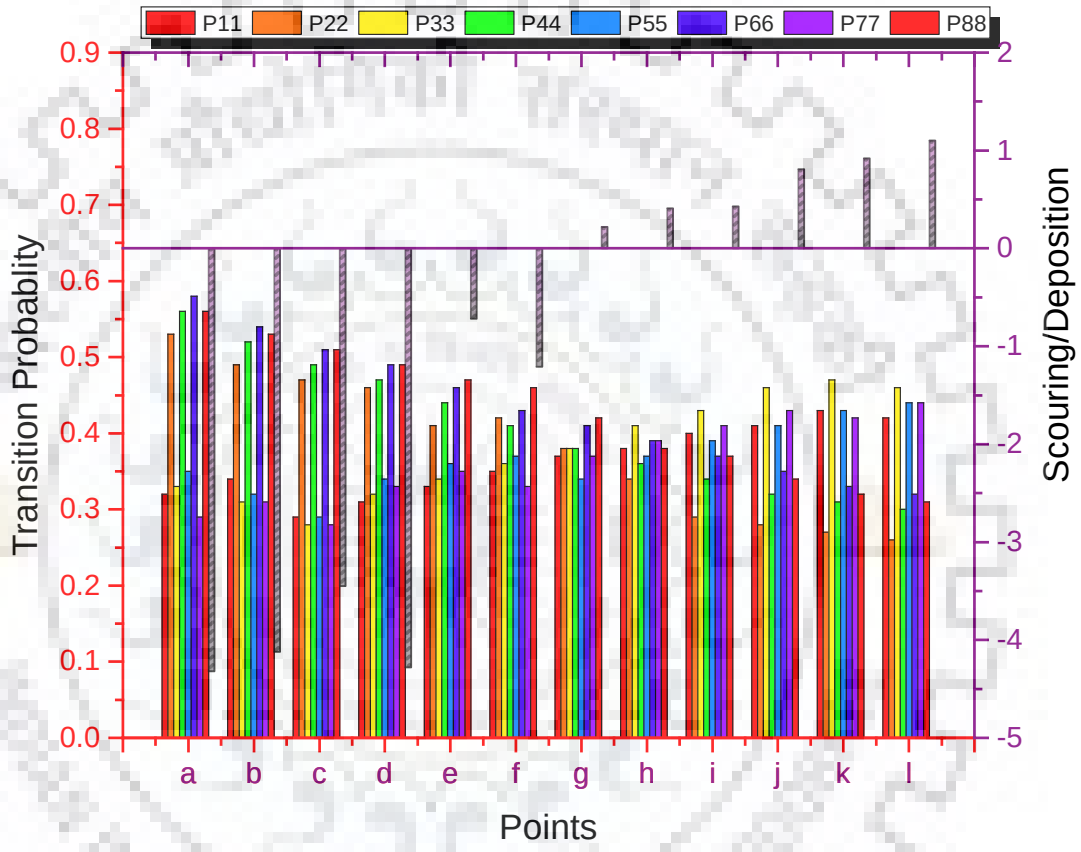

Figure 6.9 Shows the histogram plot of depth averaged stable transition movement along-with the magnitude of scouring/deposition in centimetre observed in the vicinity of mid-channel bar (bar condition)

Keshavarzi and Gheisi (2006) had analysed the stable movements. But they have not proposed any parameter which could summarize the effect of stable movements into one parameter. In the present study, the new parameter Transition Ratio (TR) is proposed. (Equation 6.9). This

parameter has taken into account the effect of stable movements on the local stream bed elevation change occurred in the proximity of mid-channel bar.

It is the ratio of summation of odd stable movement to the summation of even stable movement (Equation 6.9).

$$TR=\frac{P_{1\to1}+P_{3\to3}+P_{5\to5}+P_{7\to7}}{P_{2\to2}+P_{4\to4}+P_{6\to6}+P_{8\to8}} \quad (6.9)$$

Transition Ratio is plotted against the scouring/deposition observed in the vicinity of mid-channel bar (Figure 6.10). Figure 6.10 shows that the Transition Ratio follows linear relationship for the scouring/deposition data with Coefficient of Determination and Pearson R values are equal to 0.89 and 0.94 respectively. The high values of correlation coefficients indicate that the Transition Ratio parameter is closely related with the local stream bed elevation change observed in the vicinity of mid-channel bar. Evidently, the TR values less than unity signify scouring, whereas the values greater than one represent deposition.

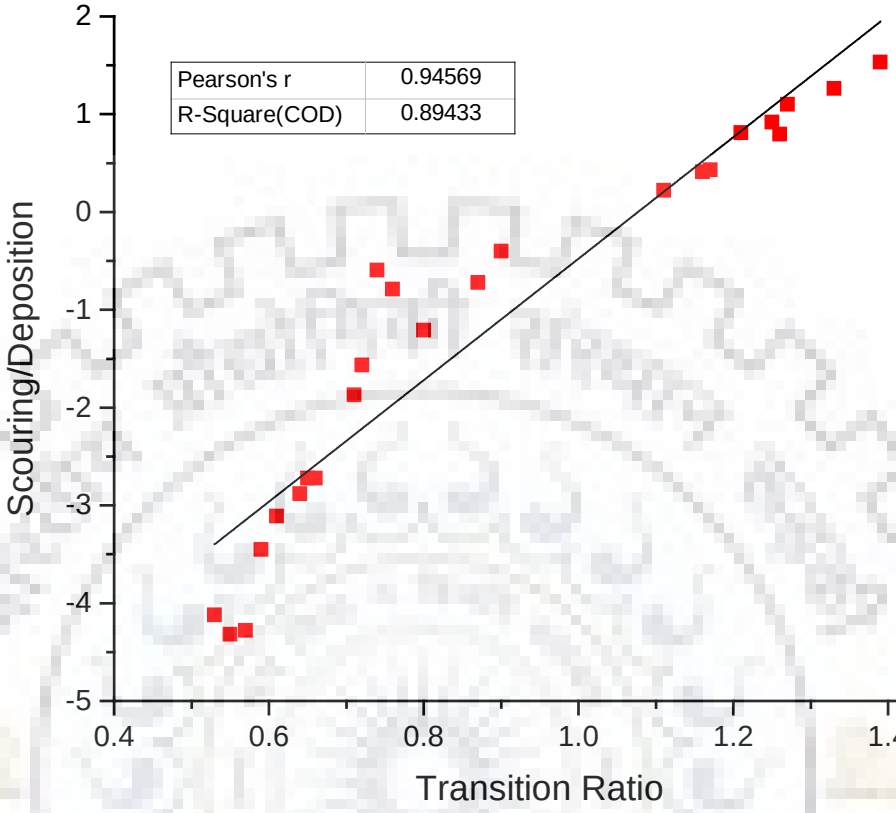

Figure 6.10 Shows the variation of Transition Ratio with the magnitude of scouring/deposition in centimetre observed in the vicinity of mid-channel bar (bar condition)

Depth averaged values of Marginal and Cross movements are also plotted for 12 points for bar condition (Figures 6.11 and 6.12). These transition movements do not show any linkage with scouring and deposition that occurred in the vicinity of the mid-channel bar.

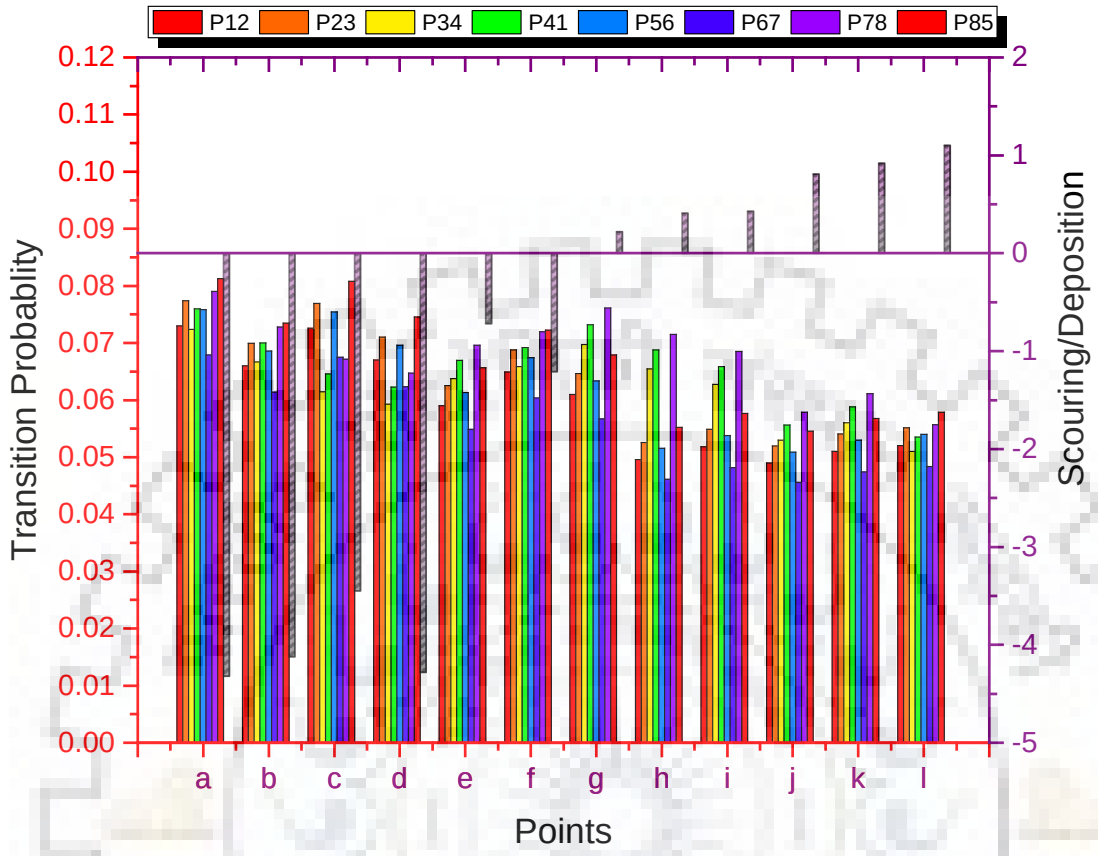

Figure 6.11 Shows the histogram plot of depth averaged marginal transition movements along-with the magnitude of scouring/deposition in centimetre observed in the vicinity of mid-channel bar (bar condition)

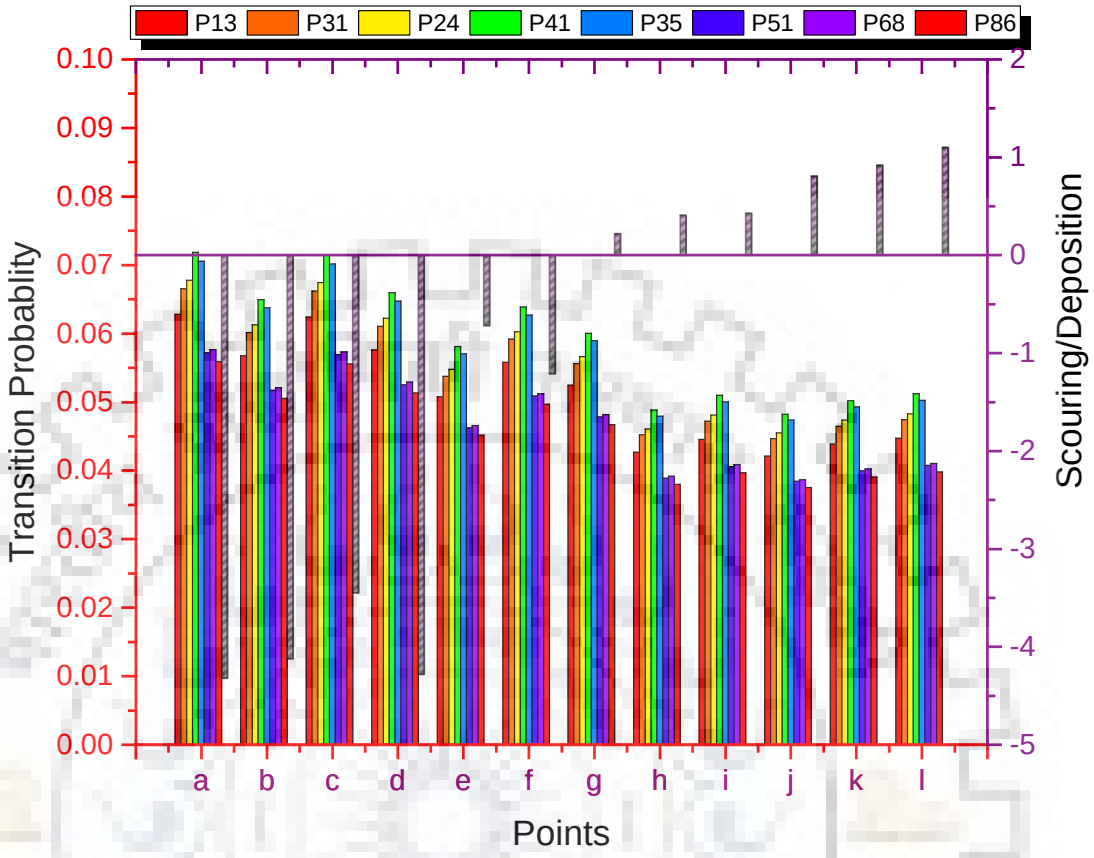

Figure 6.12 Shows the histogram plot of depth averaged cross transition movements along-with the magnitude of scouring/deposition in centimetre observed in the vicinity of mid-channel bar (bar condition)

The results indicate that only the stable transition movements are related to the local stream bed elevation change occurred in the vicinity of mid-channel bar. As we know sum of probabilities is equal to one, so change in probability of one stable movement will cause changes in the other stable movements. Therefore, we modelled a relationship between these stable movements for our experimental dataset. By using the statistical analysis, it was observed that the best mathematical relationships will be obtained if the Class A and Class B transition movements are modelled separately. In this study the relationships have been developed for Class A and Class B stable movements using the Nonlinear Fit toolbox of MATLAB Software (Table 6.2). The high values of correlation for these expressions indicate that they are correctly predicting the relationship

between the stable movements. These mathematical equations are valid only for our experimental data.

Table 6.2 Showing the mathematical relationships for class A and class B stable transition movements

Transition Movements	Mathematical Equations	Correlation (R)
Class A Transition Movement	$P_{1\to1} = -2.52 * P_{2\to2}^{3.27}$ +0.93$* P_{3\to3}^{1.14} + 1.42 * P_{4\to4}^{2.42}$	0.94
	$P_{2\to2} = -0.58 * P_{1\to1}^{0.44}$ +0.51$* P_{3\to3}^{0.54} + 0.98 * P_{4\to4}^{0.87}$	0.93
	$P_{3\to3} = 0.99 * P_{1\to1}^{0.88}$ -0.28$* P_{2\to2}^{-0.71} + 0.24 * P_{4\to4}^{-0.87}$	0.92
	$P_{4\to4} = -0.66 * P_{1\to1}^{0.46}$ +1.04$* P_{2\to2}^{1.18} - 0.57 * P_{3\to3}^{0.57}$	0.94
Class B Transition Movement	$P_{5\to5} = -1.94 * P_{6\to6}^{3.27}$ +0.91$* P_{7\to7}^{1.21} + 1.22 * P_{8\to8}^{2.12}$	0.91
	$P_{6\to6} = -0.08 * P_{5\to5}^{-0.13}$ -0.02$* P_{7\to7}^{3.84} + 0.85 * P_{8\to8}^{1.17}$	0.92
	$P_{7\to7} = 1.2 * P_{5\to5}^{0.97}$ -0.37$* P_{6\to6}^{-0.81} + 0.32 * P_{8\to8}^{-0.95}$	0.89
	$P_{8\to8} = -0.78 * P_{5\to5}^{0.58}$ +1.14$* P_{6\to6}^{1.29} - 0.69 * P_{7\to7}^{0.68}$	0.92

The transition probabilities averaged for 24 points for bar condition are displayed in Table 6.3. The arrangements of transitional movements in Table 6.3 are same as displayed in $Matrix(A)$. The transition movements in bold letters show the stable movements; these movements have the highest transition probability.

Table 6.3 The transition probabilities averaged for 24 Points near the bed around the mid-channel bar in a braided river model

	$P_1(t+1)$	$P_2(t+1)$	$P_3(t+1)$	$P_4(t+1)$	$P_5(t+1)$	$P_6(t+1)$	$P_7(t+1)$	$P_8(t+1)$
$P_1(t)$	**0.31**	0.16	0.09	0.19	0.09	0.04	0.09	0.08
$P_2(t)$	0.15	**0.24**	0.13	0.12	0.09	0.08	0.11	0.13
$P_3(t)$	0.17	0.14	**0.25**	0.14	0.1	0.07	0.09	0.08
$P_4(t)$	0.17	0.11	0.12	**0.17**	0.1	0.14	0.1	0.12
$P_5(t)$	0.09	0.11	0.1	0.1	**0.26**	0.15	0.11	0.09
$P_6(t)$	0.16	0.11	0.12	0.14	0.08	**0.22**	0.19	0.09
$P_7(t)$	0.09	0.08	0.09	0.13	0.14	0.14	**0.18**	0.17
$P_8(t)$	0.12	0.08	0.08	0.14	0.09	0.18	0.19	**0.18**

CHAPTER-7 VALIDATION OF EXPERIMENTAL RESULTS USING THE FLUENT SOFTWARE

7.1 General

The Reynolds stress model (RSM) is one of the most elaborate turbulence model inbuilt in the CFD code Fluent. In RSM, the isotropic eddy-viscosity hypothesis is neglected. The RSM closes the Reynolds-Averaged Navier-Stokes (RANS) equations by solving transport equations for the Reynolds stresses together with an equation for the dissipation rate. This indicates that five more transport equations are required for 2-D flows and seven additional transport equations are required for 3-D closure of RANS equations. The RSM takes into accounts the effects of rotation, swirl, abrupt change in strain rate and stream line curvature in a more effective manner as compared to the one-equation and two equation models. It has a greater accuracy for complex flow (Cambon et al. 1992; Durbin 1993).

The appropriate Reynolds stress equations may be obtained by taking moments of the momentum equation. In this process the momentum equations are multiplied by the fluctuating property, then the Reynolds average of the product is computed. In Reynolds stress model, the individual Reynolds stress components are computed using the differential transport equations. The computed Reynolds stresses are used for obtaining closure of the Reynolds-averaged momentum equation.

7.2 Details of Meshing

Structured meshing is done using the Ansys Mesher. The view of the mesh is shown in Figure 7.1. Face sizing method is used for meshing the area in the vicinity of the mid-channel bar. The element size for face sizing is kept at 0.001mm for region in the vicinity of mid-channel bar. For the remaining portion of the model, the element size is kept at 0.01mm. The low value of element size in the vicinity of mid-channel bar is taken in order to study the velocity and turbulence parameters precisely at region close to the mid-channel bar. The experiments performed in second phase of study are validated using the Fluent Software.

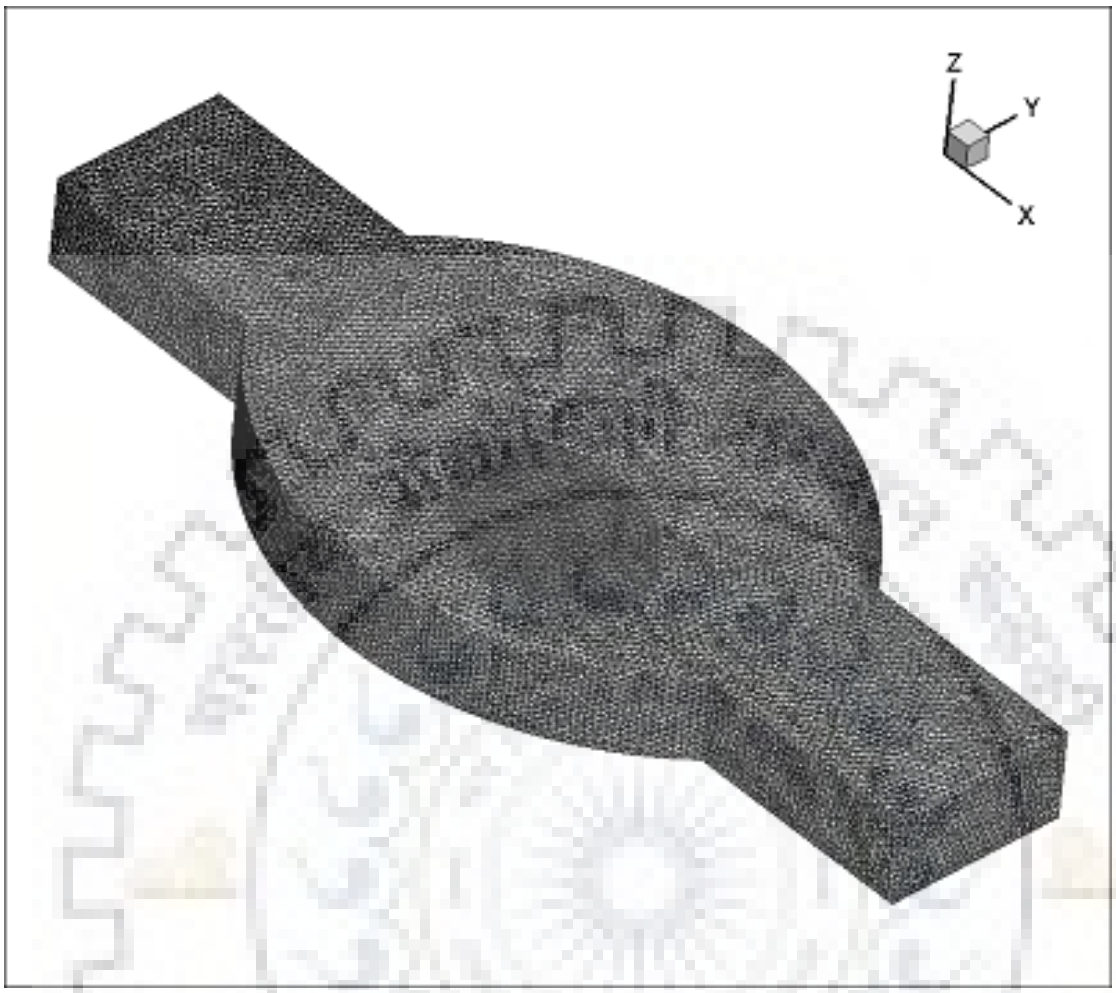

Figure 7.1 Showing the mesh of three dimensional model developed in Fluent Software

7.3 Details of Modelling

As could be seen from literature, hardly any work had been done on this type of experimental setup. Thus, for validating the experimental results, the laboratory model is developed in the Fluent Software. Steady state simulations are carried out using the Reynolds stress model of Fluent Software on the basis of the study by Sarkar and Ratha (2014). The three dimensional implicit steady pressure based solver is utilized for the computation. Air and water are considered as two immiscible fluids. The implicit volume of fluid model and channel boundary conditions are used for solving the momentum equation and track the volume fraction of each of the fluids over the computational domain. The velocity boundary condition is applied at the inlet, whereas velocity outlet and velocity inlet boundary conditions are utilized for the outlet. The turbulence parameters are computed using the SIMPLE pressure velocity coupling. Discretization of pressure is done using the Presto method.

The momentum and Reynolds stress are discretized using the second order upwind scheme. The convergence criteria for the residual of all the parameters are kept at 1×10^{-8}.The number of iterations were kept at 1×10^{6}. The Initialization of solution was done using the standard initialization toolbox in Fluent software. The comparison of experimental data with the results obtained from the Fluent simulation will be discussed in the Chapter 8.

CHAPTER-8 STUDY OF TURBULENT FLOW CHARACTERISTICS IN THE VICINITY OF MID-CHANNEL BAR

8.1 General

Shamloo et al. (2001), Sarkar and Ratha (2014) had observed the down-flow at locations just upstream and wake at locations downstream of the submerged structure. Dey et al. (2008) found that the down-flow occurred at upstream of the submerged cylinder to act as a main scouring agent. They also observed that the vortex formed at the top of the submerged cylinder joins the main flow downstream of the cylinder. As discussed above, the flow at locations upstream and downstream of the submerged structure have great importance. Thus in this experimental phase, the flow structure at locations upstream and downstream of the mid-channel bar is studied (Figure 3.4). The experiments are performed for different submergence ratios (Table 3.4). The aim of performing experiments is to analyse the effect of mid-channel bar on the flow structure at locations upstream and downstream of mid-channel bar and to study the effect of bar height on the turbulent structure of flow in the vicinity of mid-channel bar.

The velocity is measured at 20 points, 10 of which are upstream and 10 points are present downstream of mid-channel bar (Figure 3.4). The depth-wise distributions of velocities and turbulence parameters are computed for all 20 points. The results indicate that the effect of mid-channel bar is observed only for points that are present in the close proximity of mid-channel bar. Thus the velocity and turbulence parameters are only displayed for six points (x1, x2, x3, y1, y2 and y3), three of which are upstream of the mid-channel bar and remaining three points of which are located downstream of mid-channel bar (Figure 3.4).

8.2 Depth wise Distribution of Flow Parameters

8.2.1 Velocity Distributions

The depth-wise profile of velocity distribution helps in understanding the behaviour of flow in the vicinity of mid-channel bar. The depth-wise distributions of all three velocity components are plotted for 3R, 5R and 7R experimental runs (Table 3.4). For each point, the velocity is measured at 16 different vertical distances from the bed. The velocities are normalized by the approach flow

velocity. The normalized velocities are plotted against the relative depth of flow (z/h). The depth-wise distribution of normalized longitudinal velocity is shown in Figures 8.1 and 8.2. The deceleration occurs at points just upstream of the mid-channel bar (Figure 8.1). The deceleration is more for point 'x1' because this point is in close proximity of mid-channel bar. The deceleration was also reported by Shamloo et al. (2001). The longitudinal velocity is lesser for higher submergence ratio. This indicates that the increase in the height of mid-channel bar causes reduction in the longitudinal velocity. For points downstream of mid-channel bar, the flow velocity is lesser as compared to the upstream points (Figure 8.2).

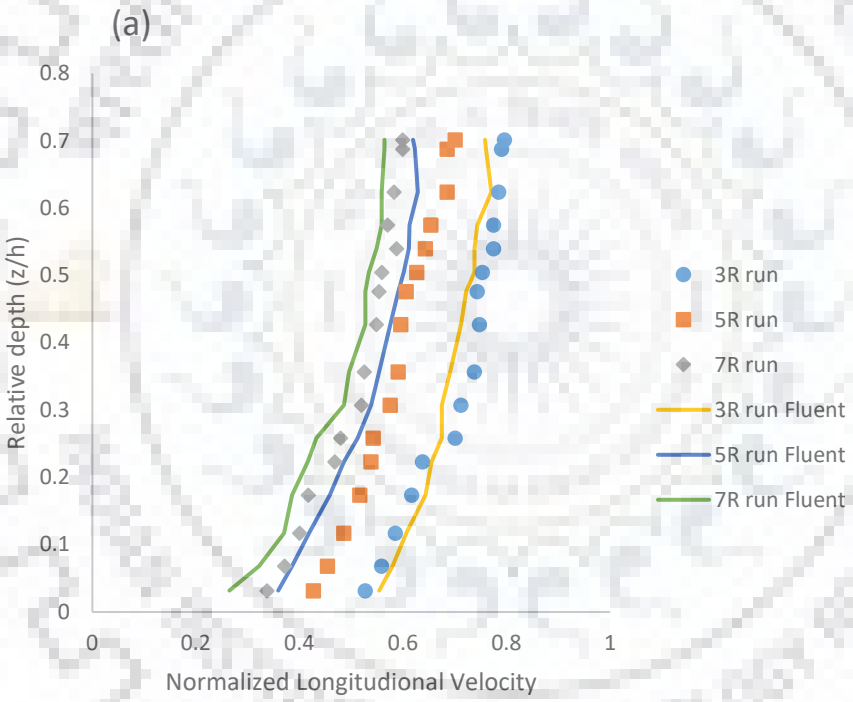

Figure 8.1 (a) Shows the depth-wise variation of normalized longitudinal velocity for 'x1', point (Experimental and Simulation)

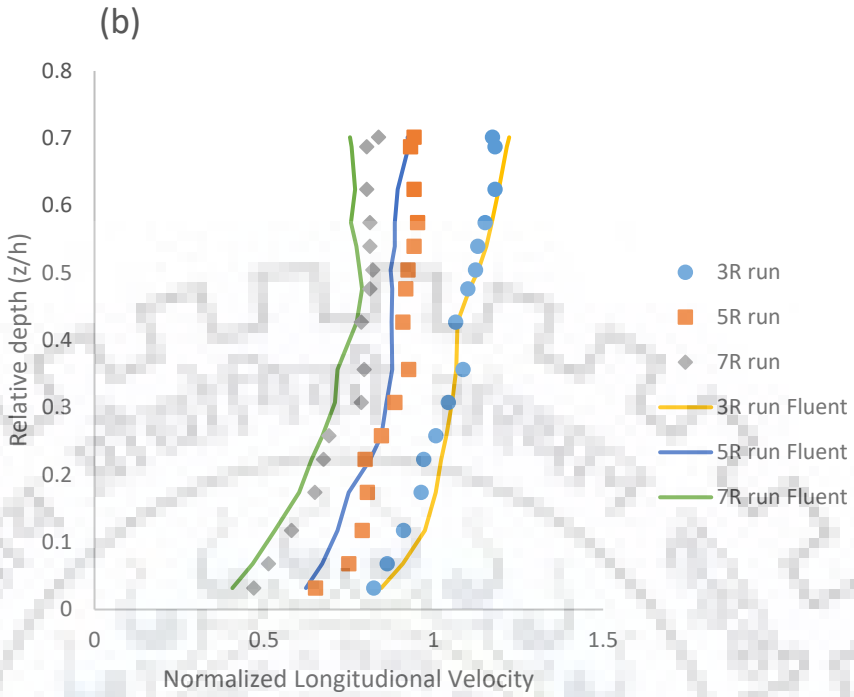

Figure 8.1 (b) Shows the depth-wise variation of normalized longitudinal velocity for 'x2', point (Experimental and Simulation)

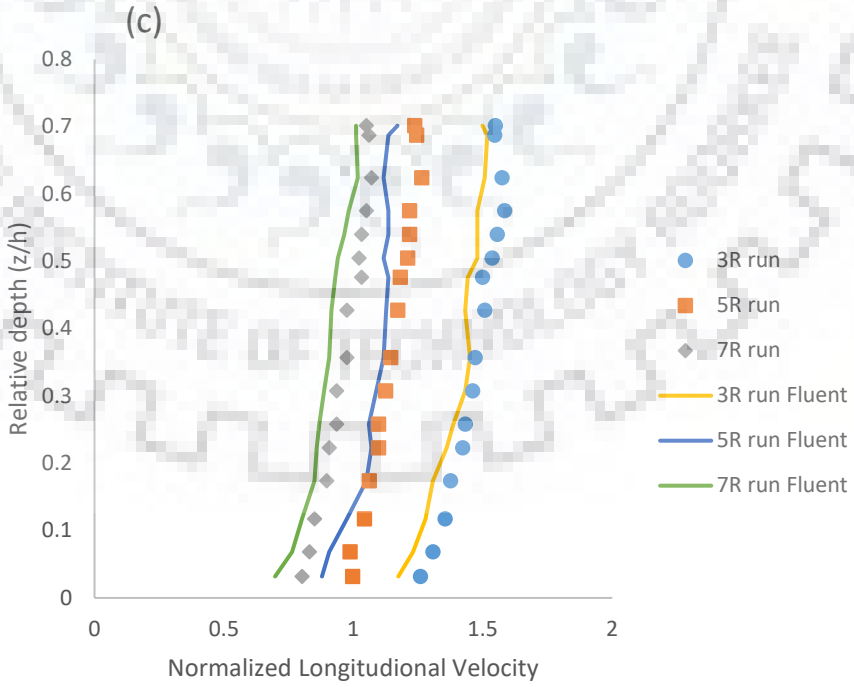

Figure 8.1 (c) Shows the depth-wise variation of normalized longitudinal velocity for 'x3', point (Experimental and Simulation)

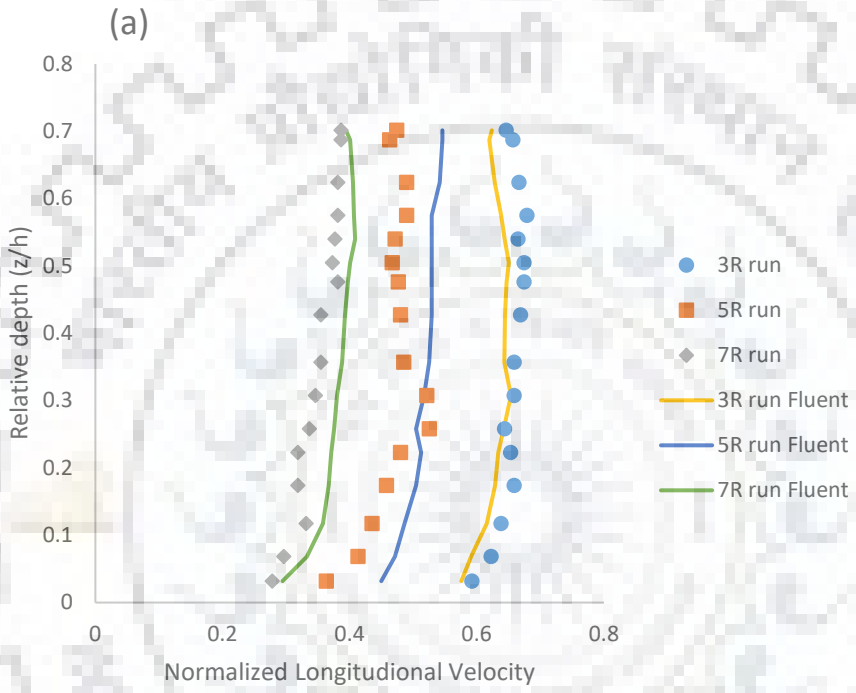

Figure 8.2 (a) Shows the depth-wise variation of normalized longitudinal velocity for 'y1', point (Experimental and Simulation)

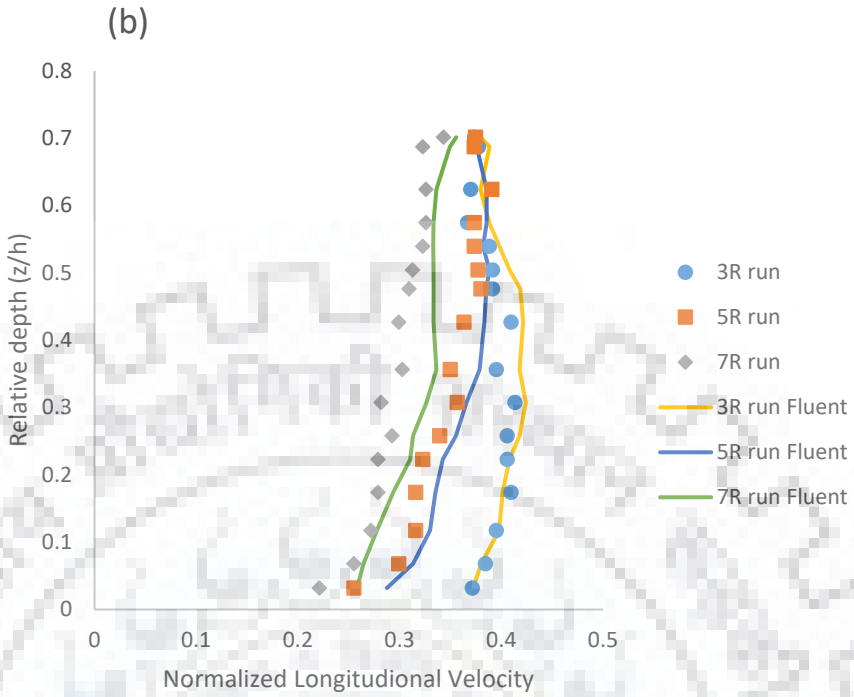

Figure 8.2 (b) Shows the depth-wise variation of normalized longitudinal velocity for 'y2', point (Experimental and Simulation)

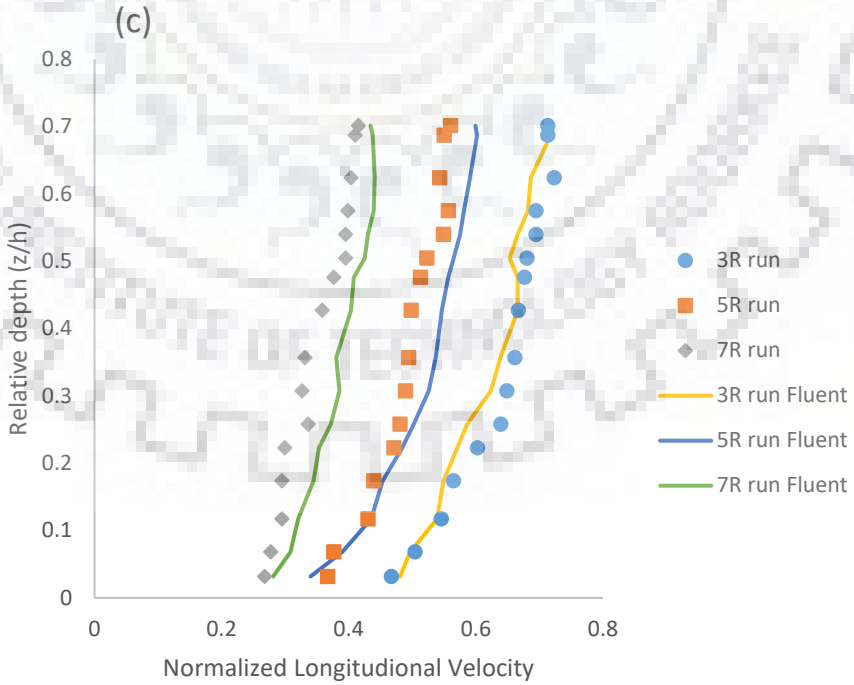

Figure 8.2 (c) Shows the depth-wise variation of normalized longitudinal velocity for 'y3', point (Experimental and Simulation)

The depth-wise distribution of normalized vertical velocity for experimental runs 3R, 5R and 7R are shown in Figures 8.3 and 8.4. The vertical velocity is negative at points upstream of the bar. The negative vertical velocity indicates the downflow at these points (Figure 8.3). For region upstream of mid-channel bar, the magnitude of vertical velocity is greatest at point closest to the mid-channel bar i.e. "x1". The presence of mid-channel bar causes negative vertical flow velocity in the proximity of bar.

The vertical velocity is also negative for points downstream of mid-channel bar (Figure 8.4). At points downstream of mid-channel bar, the magnitude of negative vertical velocity is greater as compared to the upstream points (Figures 8.3 and 8.4). The magnitude of negative vertical velocity is greater for high submergence ratio. This indicates that the increase in mid-channel bar height causes increase in the magnitude of downflow.

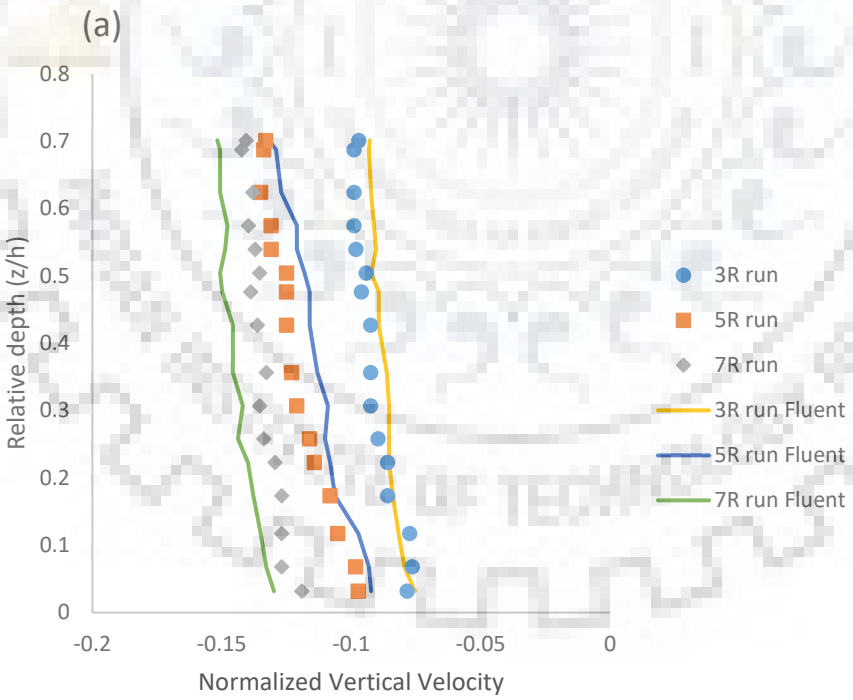

Figure 8.3 (a) Show the depth-wise variation of normalized vertical velocity for 'x1' point (Experimental and Simulation)

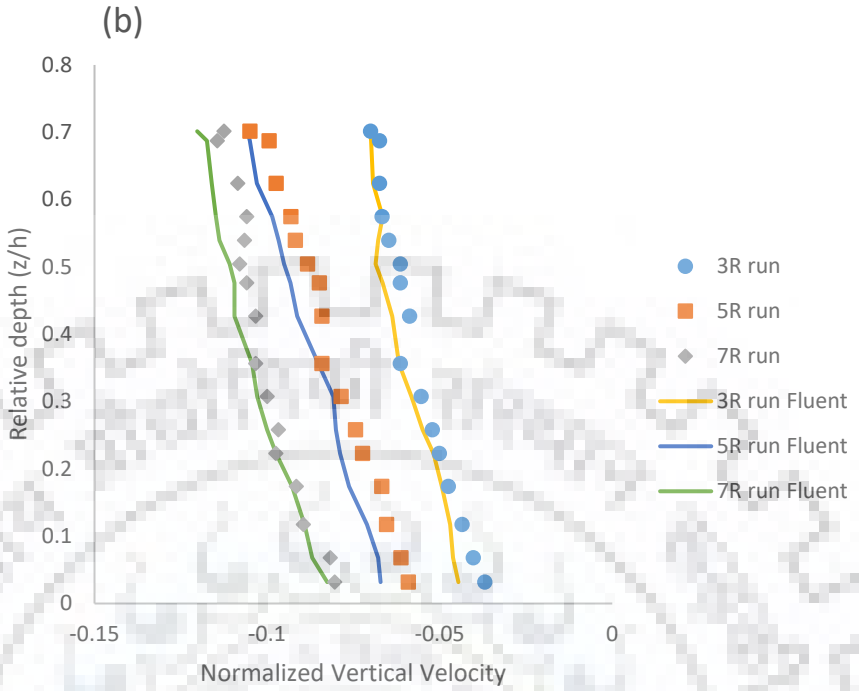

Figure 8.3 (b) Show the depth-wise variation of normalized vertical velocity for 'x2' point (Experimental and Simulation)

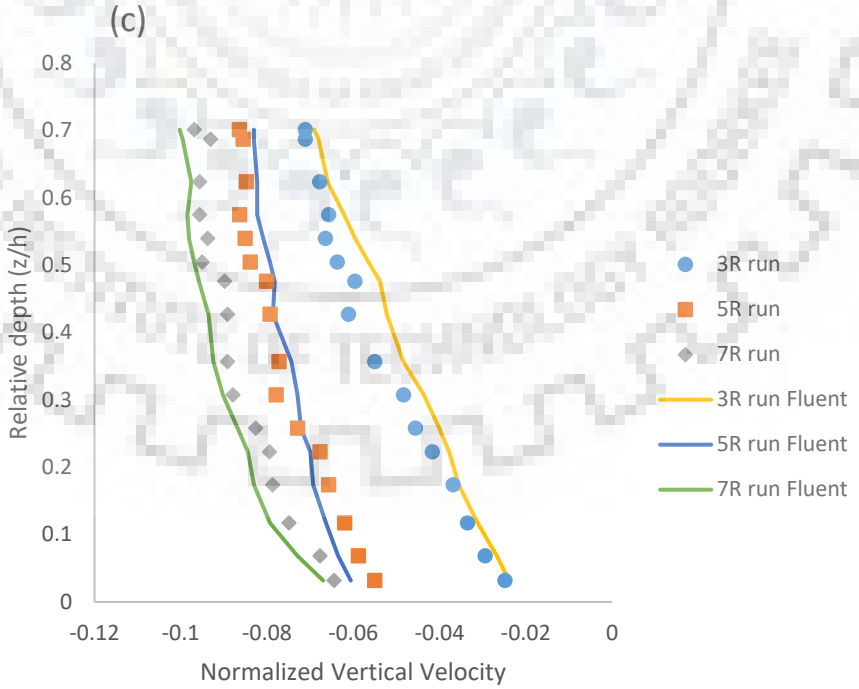

Figure 8.3 (c) Show the depth-wise variation of normalized vertical velocity for 'x3' point (Experimental and Simulation)

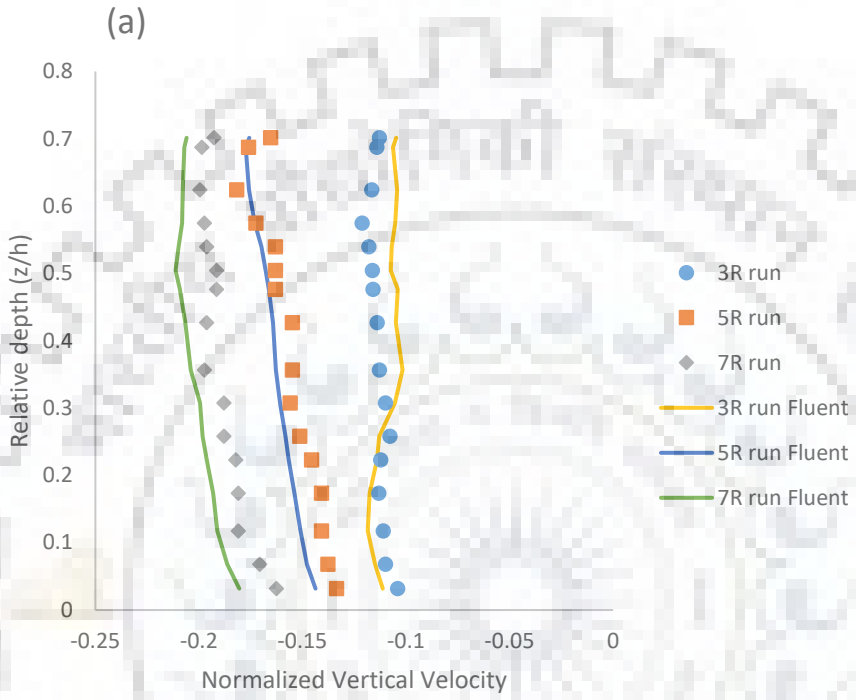

Figure 8.4 (a) Shows the depth-wise variation of normalized vertical velocity for 'y1' point (Experimental and Simulation)

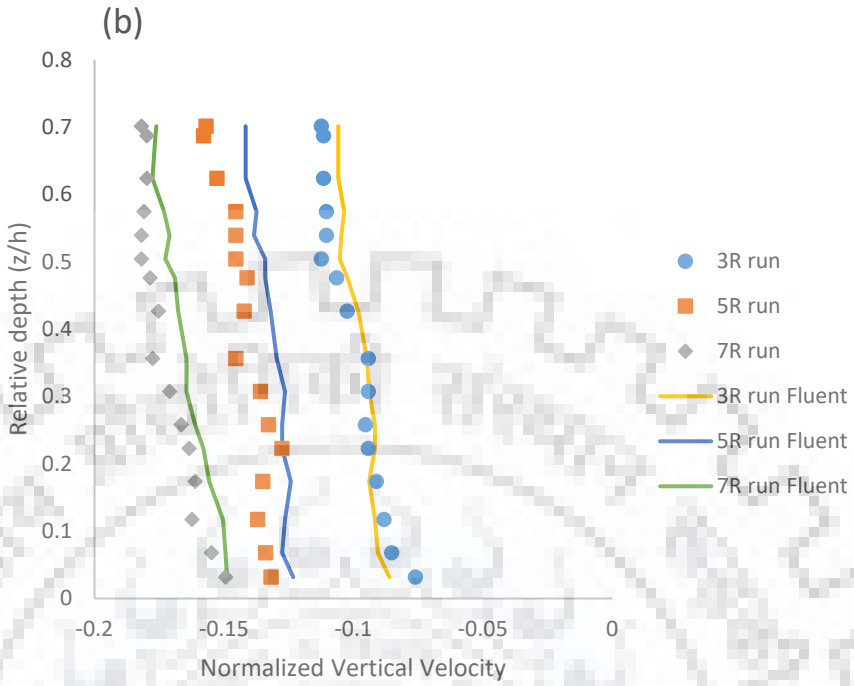

Figure 8.4 (b) Shows the depth-wise variation of normalized vertical velocity for 'y2' point (Experimental and Simulation)

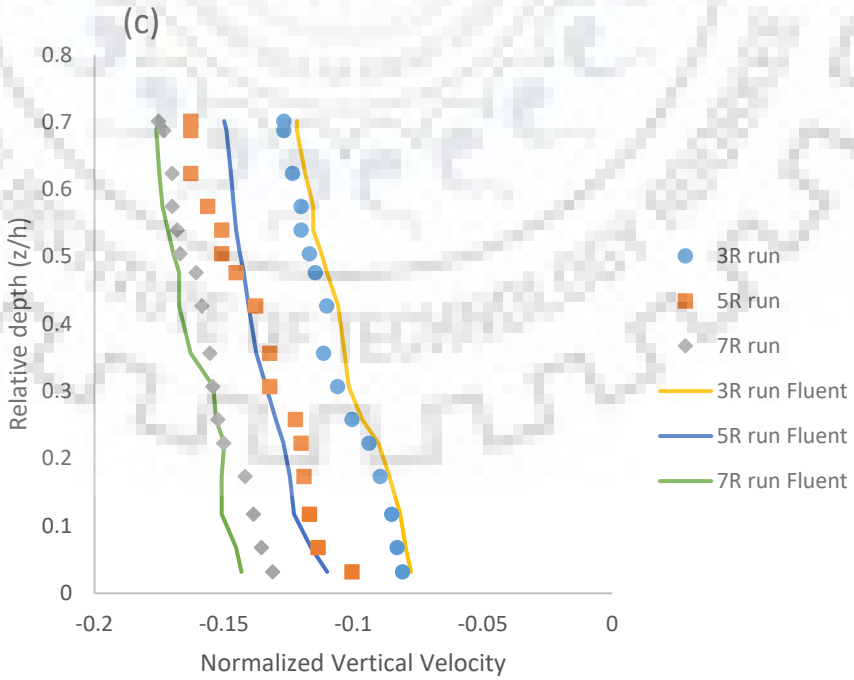

Figure 8.4 (c) Shows the depth-wise variation of normalized vertical velocity for 'y3' point (Experimental and Simulation)

The depth-wise distribution of normalized transverse velocity for experimental runs 3R ,5R and 7R are shown in Figures 8.5 and 8.6. At points upstream of mid-channel bar, the magnitude of transverse velocity is less as compared to the downstream points (Figures 8.5 and 8.6). The magnitude of transverse velocity is significant at points downstream of mid-channel bar (Figure 8.6). This indicates that the flow is three dimensional at downstream region of mid-channel bar. At downstream of mid-channel bar, the transverse velocity is greatest at point closest to the bar i.e. 'y1' (Figure 8.6). The transverse velocity is greater for higher submergence ratio. This indicates that the increase in mid-channel bar height causes increase in the transverse velocity.

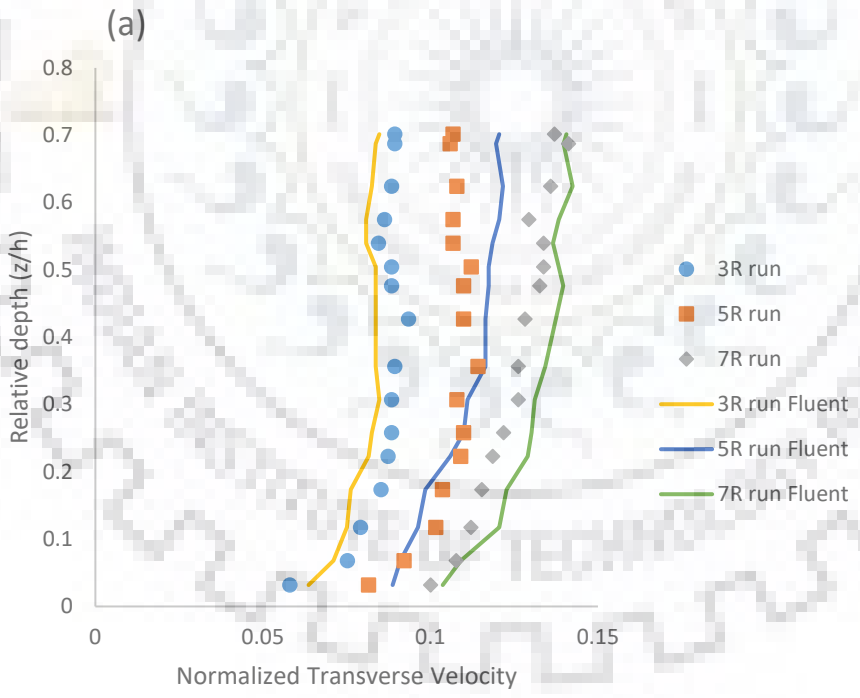

Figure 8.5 (a) Shows the depth-wise variation of normalized transverse velocity for 'x1' point (Experimental and Simulation)

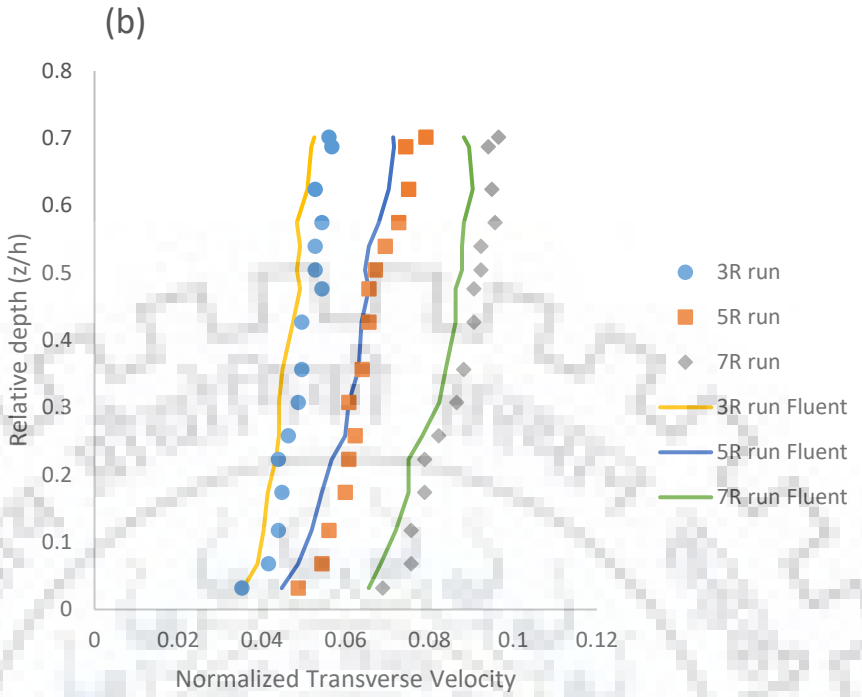

Figure 8.5 (b) Shows the depth-wise variation of normalized transverse velocity for 'x2' point (Experimental and Simulation)

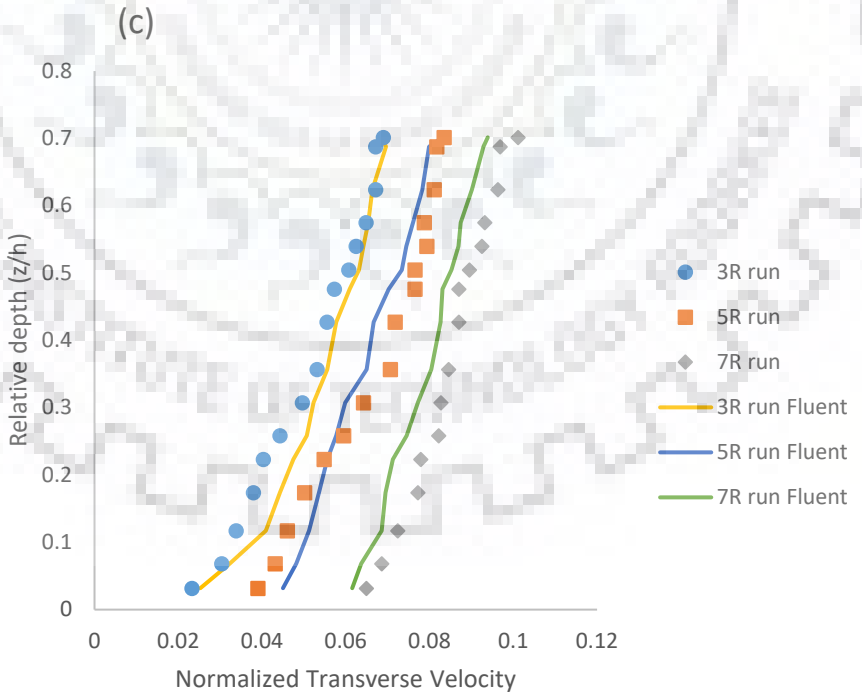

Figure 8.5 (c) Shows the depth-wise variation of normalized transverse velocity for 'x3' point (Experimental and Simulation)

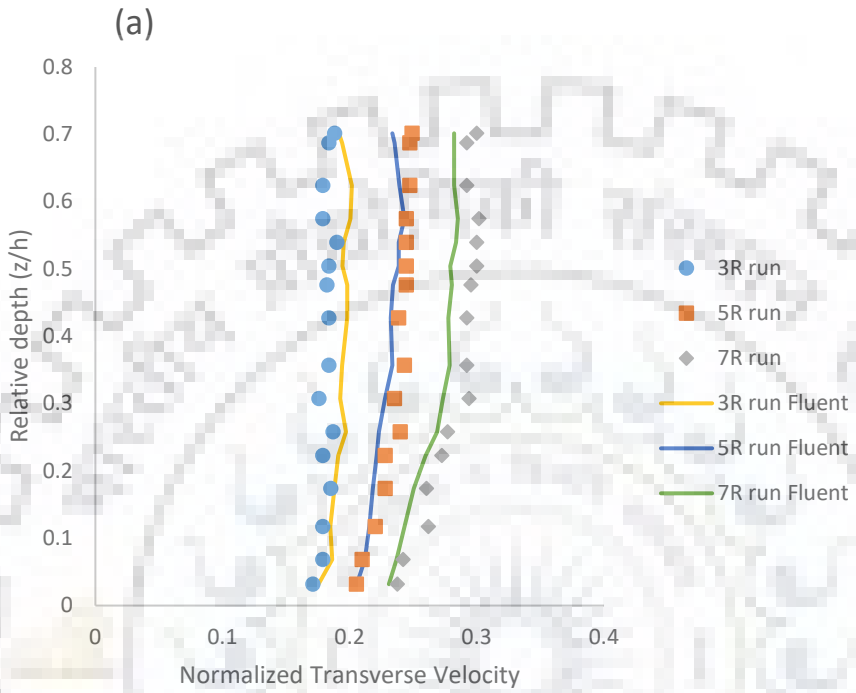

Figure 8.6 (a) Shows the depth-wise variation of normalized transverse velocity for 'y1' point (Experimental and Simulation)

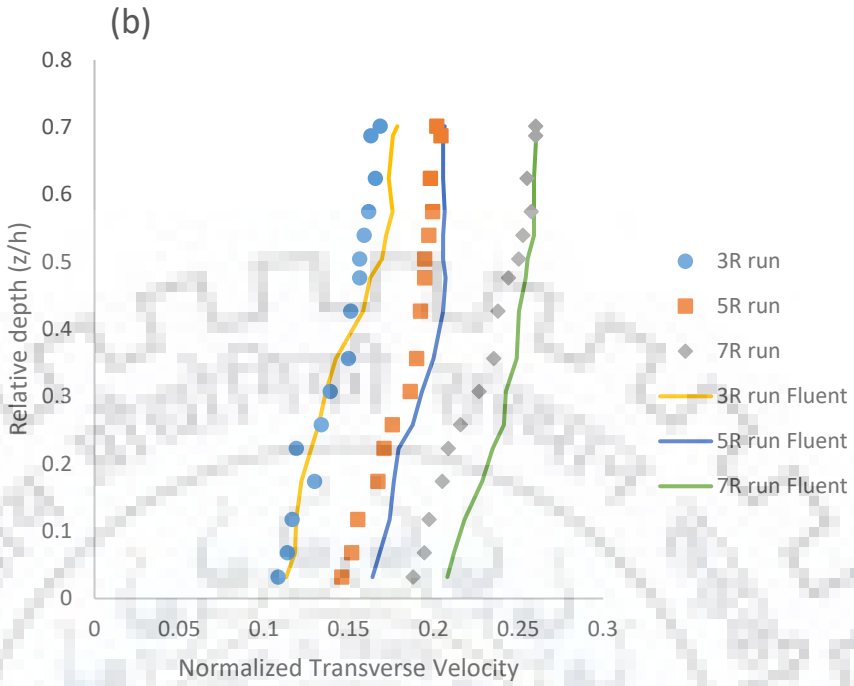

Figure 8.6 (b) Shows the depth-wise variation of normalized transverse velocity for 'y2' point (Experimental and Simulation)

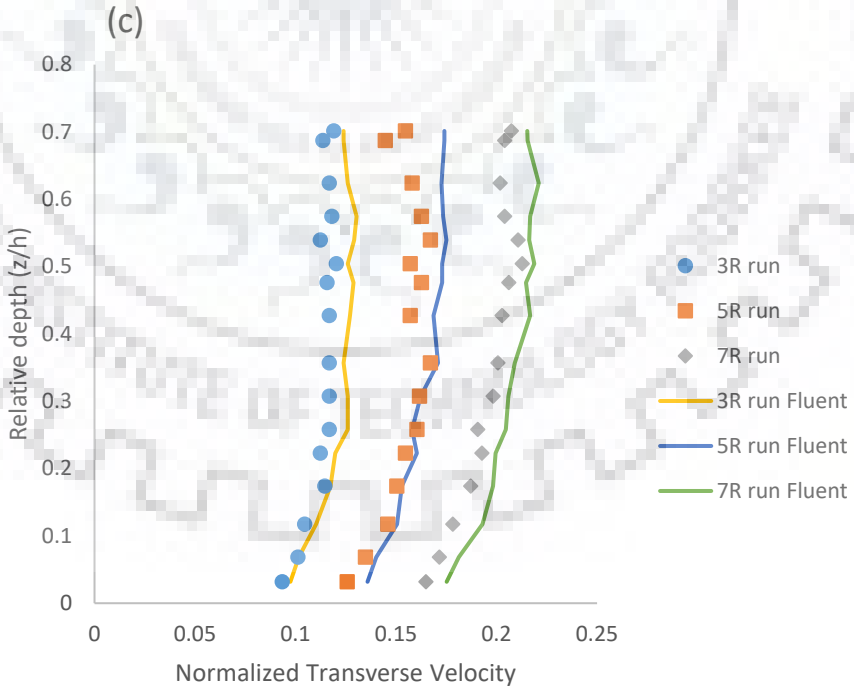

Figure 8.6 (c) Shows the depth-wise variation of normalized transverse velocity for 'y3' point (Experimental and Simulation)

For validating the experimental results, the commercial CFD code Fluent is used. Flow simulations are carried out using the Reynolds stress model as recommended by Sarkar and Ratha (2014). The experimental velocity profile is plotted along with the simulated profile obtained from the Reynolds stress model inbuilt in the Fluent Software. The experimental profiles are lying very close to the simulation profiles. This indicates that the Reynolds stress model results are in agreement with the experimental data profiles.

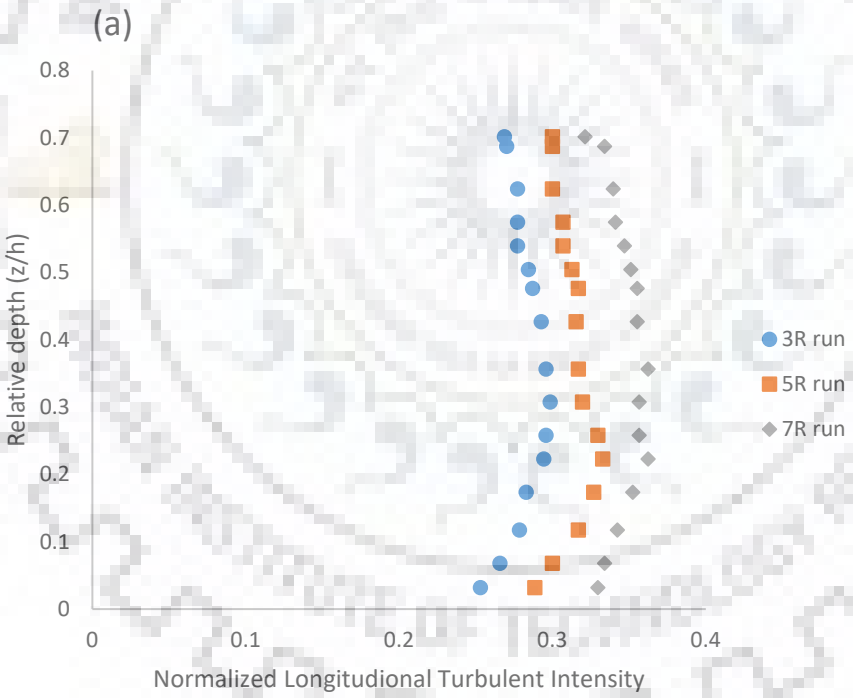

Figure 8.7 (a) Shows the depth-wise variation of normalized longitudinal turbulent intensity for 'x1' point

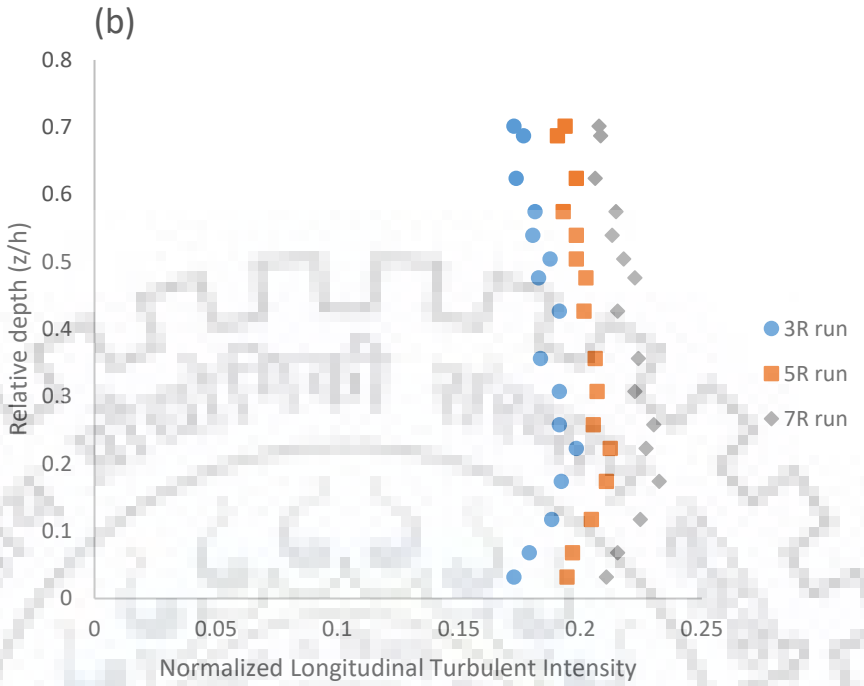

Figure 8.7 (b) Shows the depth-wise variation of normalized longitudinal turbulent intensity for 'x2' point

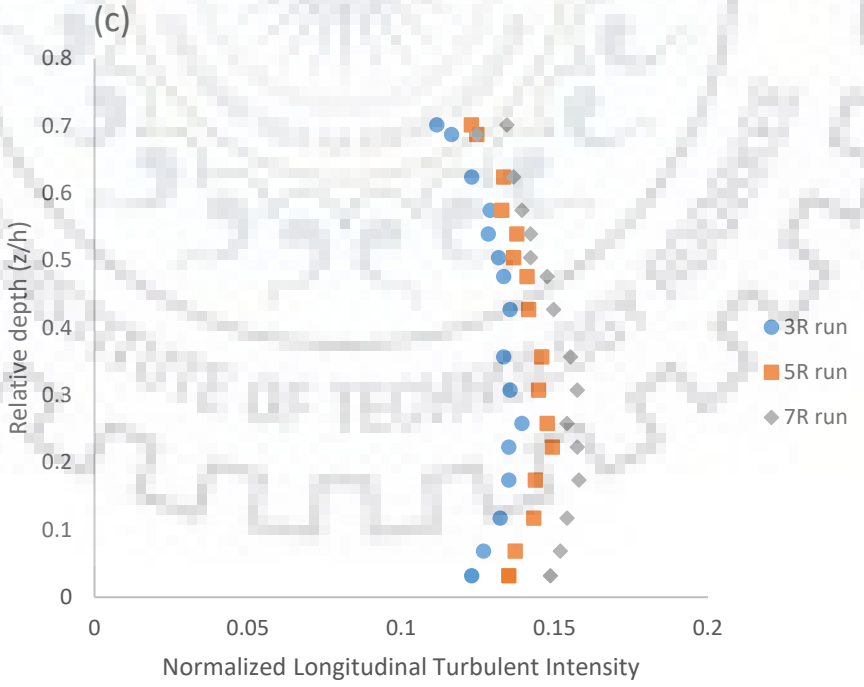

Figure 8.7 (c) Shows the depth-wise variation of normalized longitudinal turbulent intensity for 'x3' point

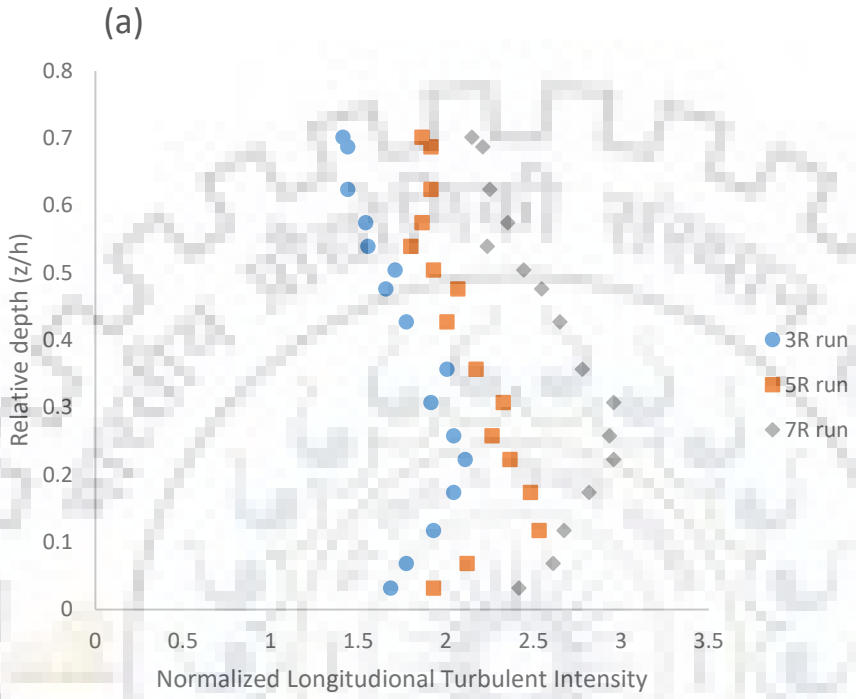

Figure 8.8 (a) Shows the depth-wise variation of normalized longitudinal turbulent intensity for 'y1' point

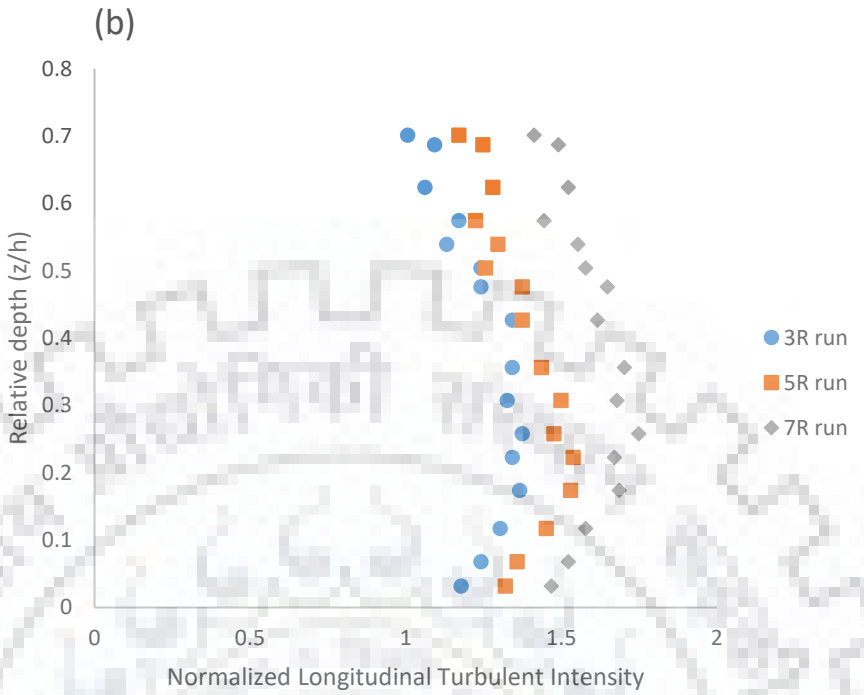

Figure 8.8 (b) Shows the depth-wise variation of normalized longitudinal turbulent intensity for 'y2' point

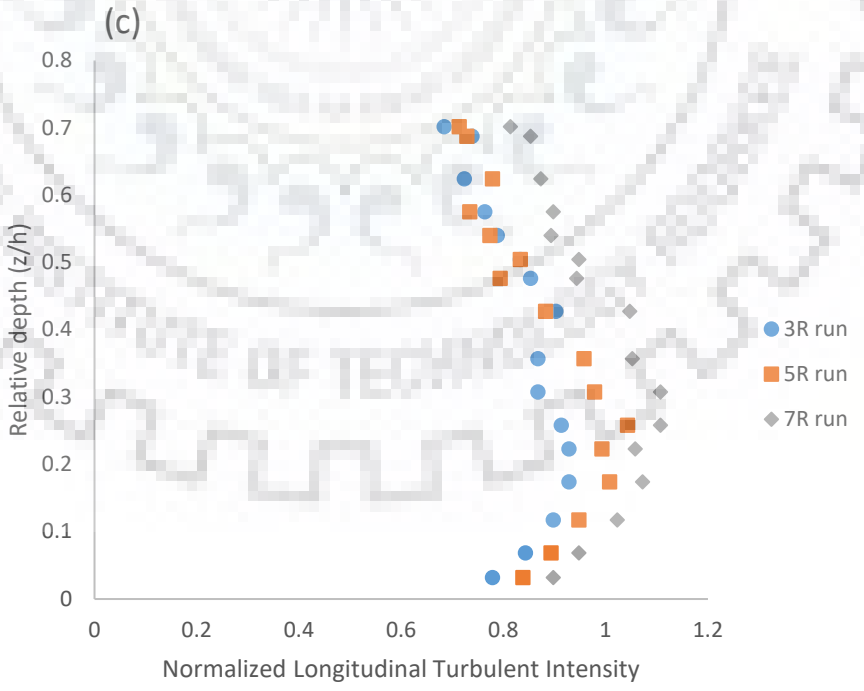

Figure 8.8 (c) Shows the depth-wise variation of normalized longitudinal turbulent intensity for 'y3' point

8.2.2 Turbulent Intensity Distributions

The depth-wise distribution of turbulence parameters helps in analysing the turbulent flow structures generated by the fluid and mid-channel bar interaction. The depth-wise distributions of turbulence parameters are studied in detail in this section. The determination of normalized turbulent intensities is explained in Section 5.2

The vertical distribution of the normalized longitudinal turbulent intensity (Ti_u) is shown in Figures 8.7 and 8.8. At upstream of mid-channel bar, the value of Ti_u is maximum for point present at closest proximity of bar i.e. 'x1" (Figure 8.7). The value of Ti_u is more for points in the vicinity of mid-channel bar. This indicates that the presence of mid-channel bar causes increase in the magnitude of Ti_u. The value of Ti_u at points downstream of mid-channel bar are much more as compared to upstream points (Figures 8.7 and 8.8). This is mainly due to the interaction of surface wave with the downstream flow. The increase in Ti_u value at locations downstream of submerged body is also reported by the Sarkar and Ratha (2014). For downstream points, the maximum value of Ti_u is observed for 'y1' point. The Ti_uvalue is greater for higher submergence ratio (Figures 8.7 and 8.8). This indicates that the increase in height of mid-channel bar causes increase in the magnitude of Ti_u.

The depth-wise distribution of normalized vertical and transverse components of turbulent intensity is illustrated in (Figures 8.9 to 8.12). The increase in normalized vertical and transverse component of turbulent intensity is observed for higher submergence ratio. At points upstream of mid-channel bar, the normalized vertical and transverse components of turbulent intensity are much lesser as compared to the downstream points (Figures 8.9 to 8.12). For downstream points, the transverse and vertical components of turbulent intensity have significant values (Figures 8.10 and 8.12).

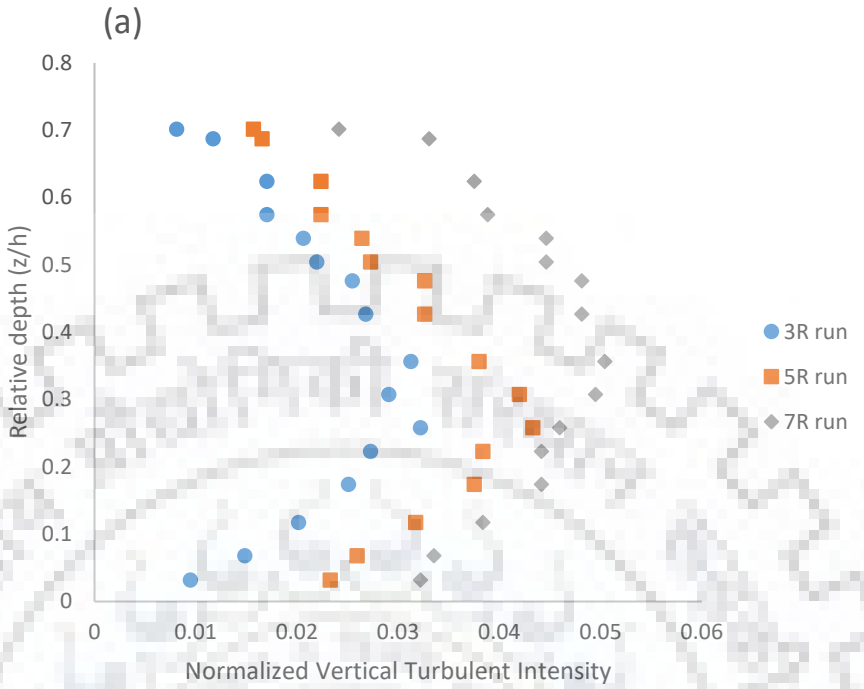

Figure 8.9 (a) Shows the depth-wise variation of normalized vertical turbulent intensity for 'x1' point

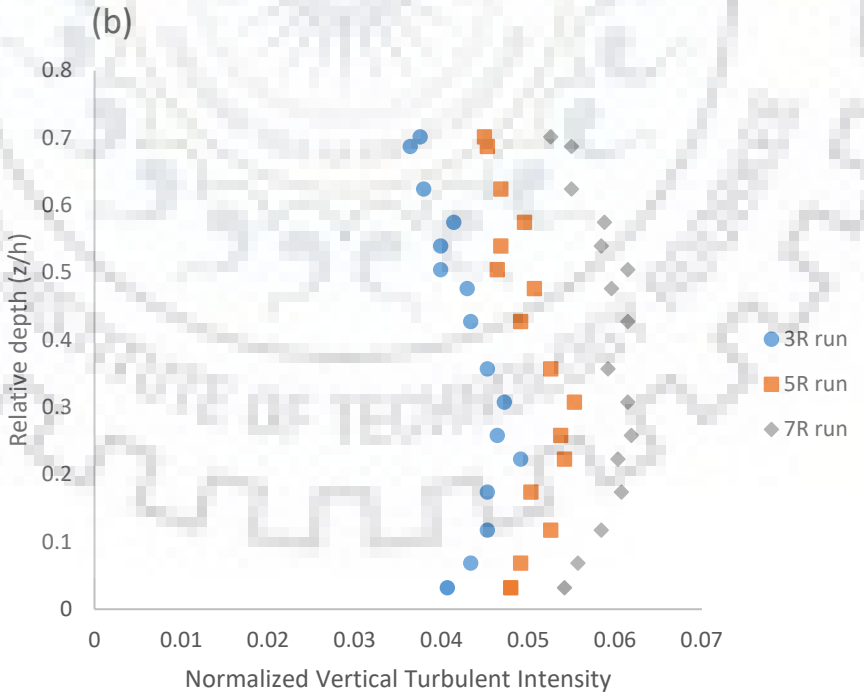

Figure 8.9 (b) Shows the depth-wise variation of normalized vertical turbulent intensity for 'x2' point

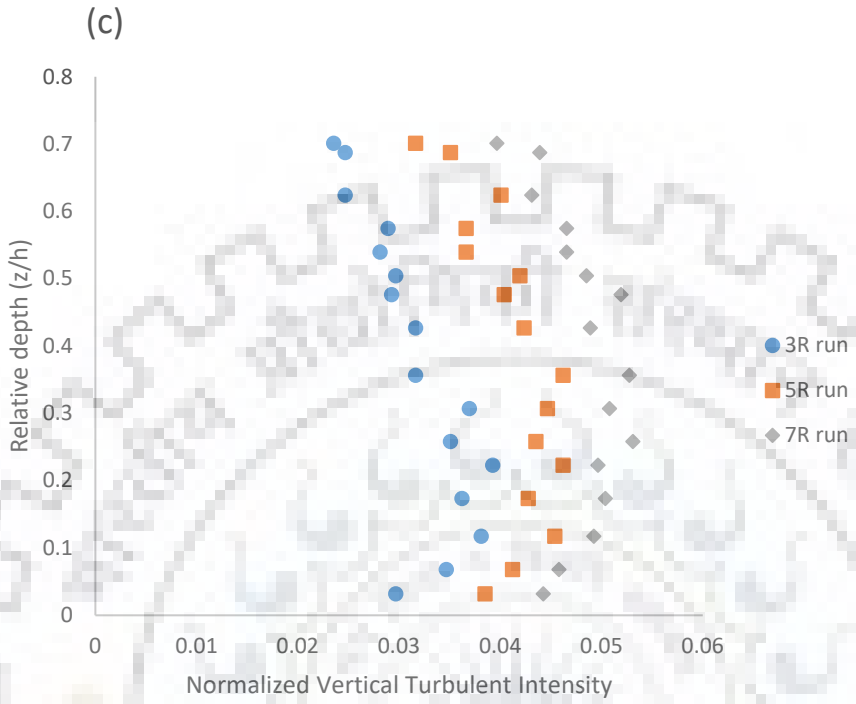

Figure 8.9 (c) Shows the depth-wise variation of normalized vertical turbulent intensity for 'x3' point

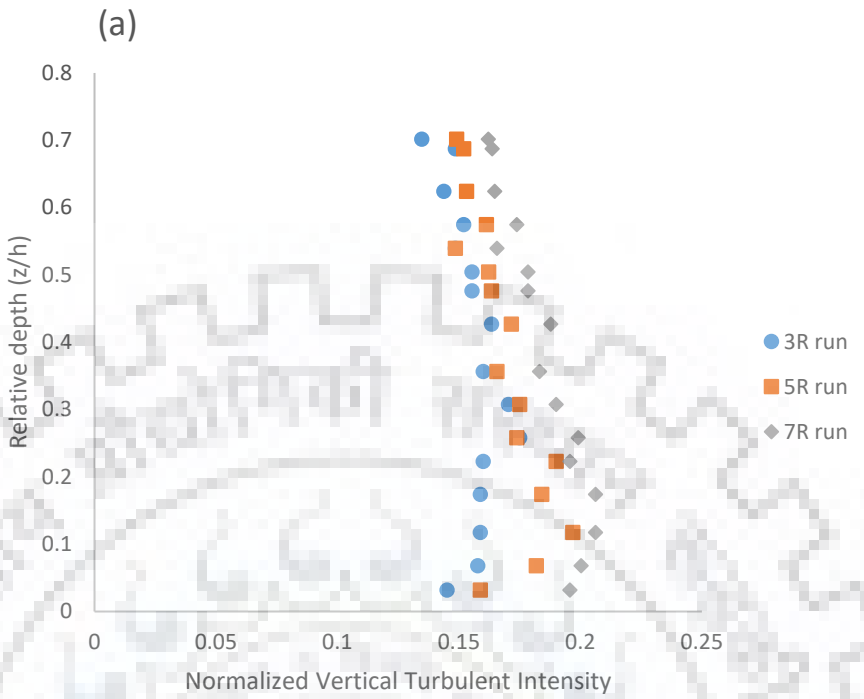

Figure 8.10 (a) Shows the depth-wise variation of normalized vertical turbulent intensity for 'y1' point

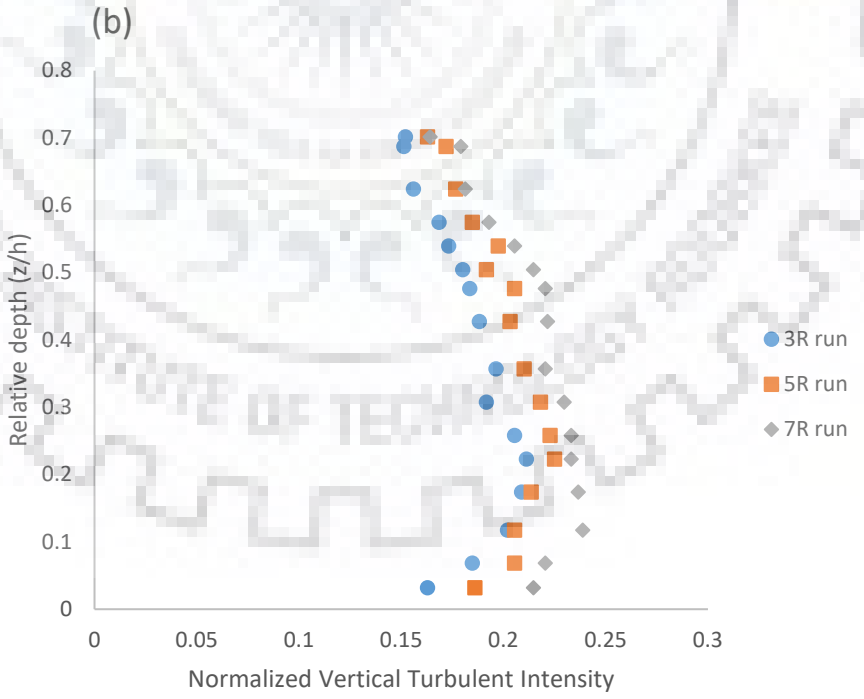

Figure 8.10 (b) Shows the depth-wise variation of normalized vertical turbulent intensity for 'y2' point

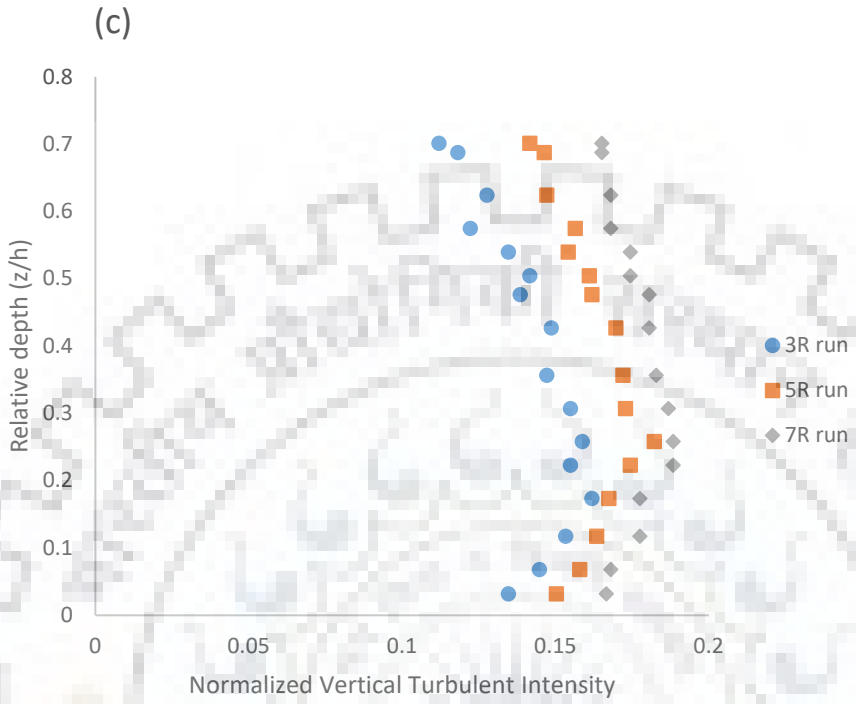

Figure 8.10 (c) Shows the depth-wise variation of normalized vertical turbulent intensity for 'y3' point

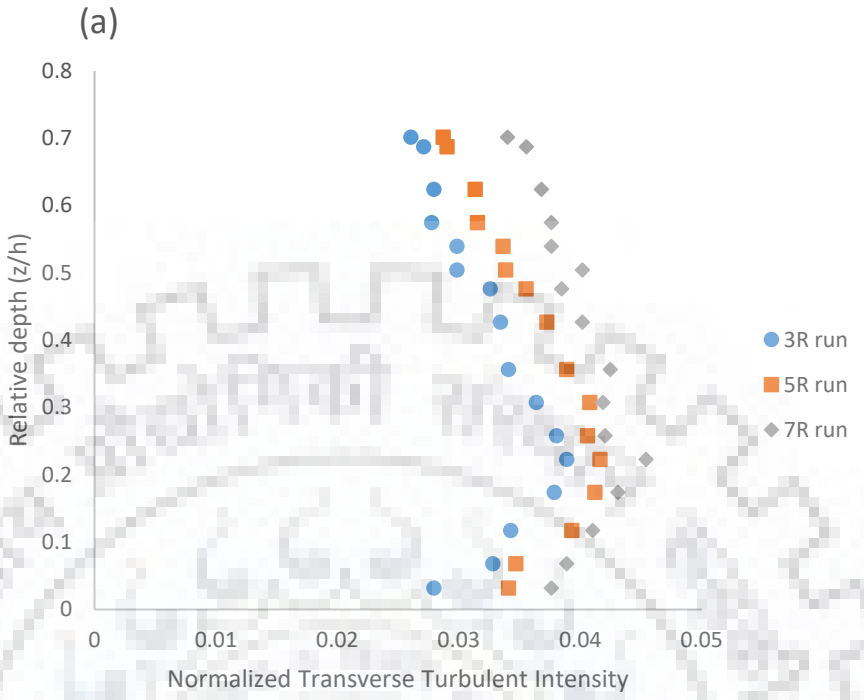

Figure 8.11 (a) Shows the depth-wise variation of normalized transverse turbulent intensity for 'x1' point

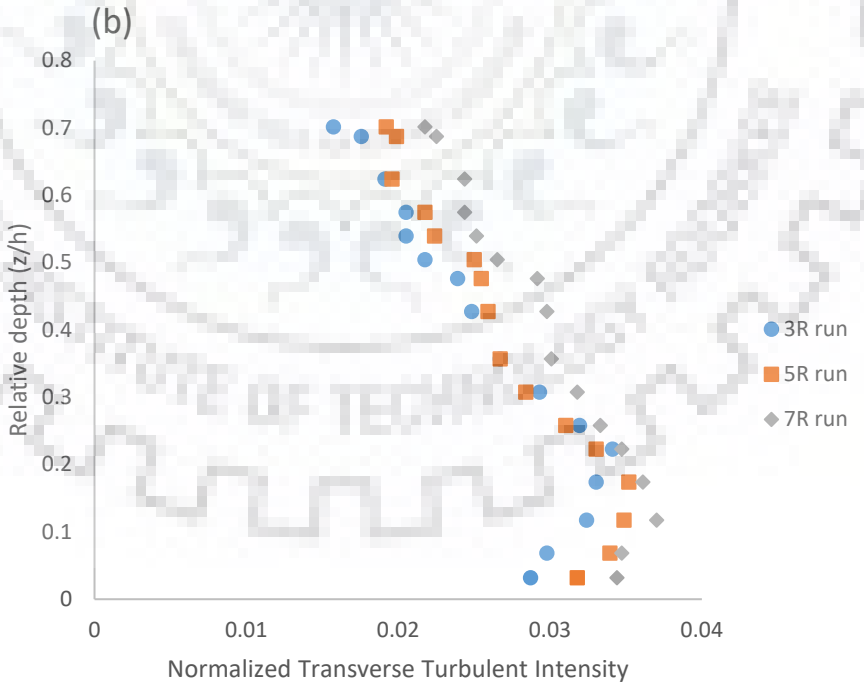

Figure 8.11 (b) Shows the depth-wise variation of normalized transverse turbulent intensity for 'x2' point

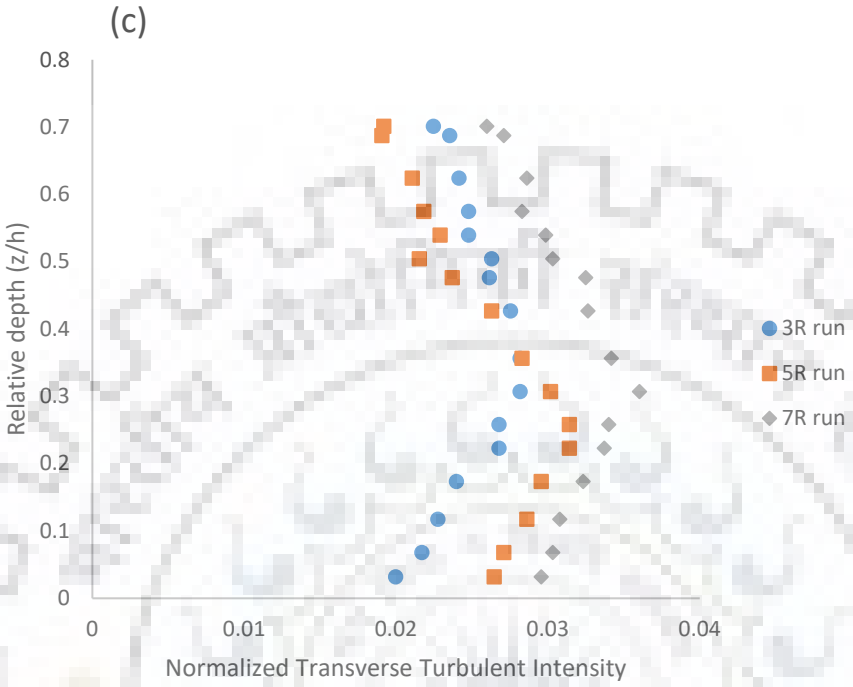

Figure 8.11 (c) Shows the depth-wise variation of normalized transverse turbulent intensity for 'x3' point

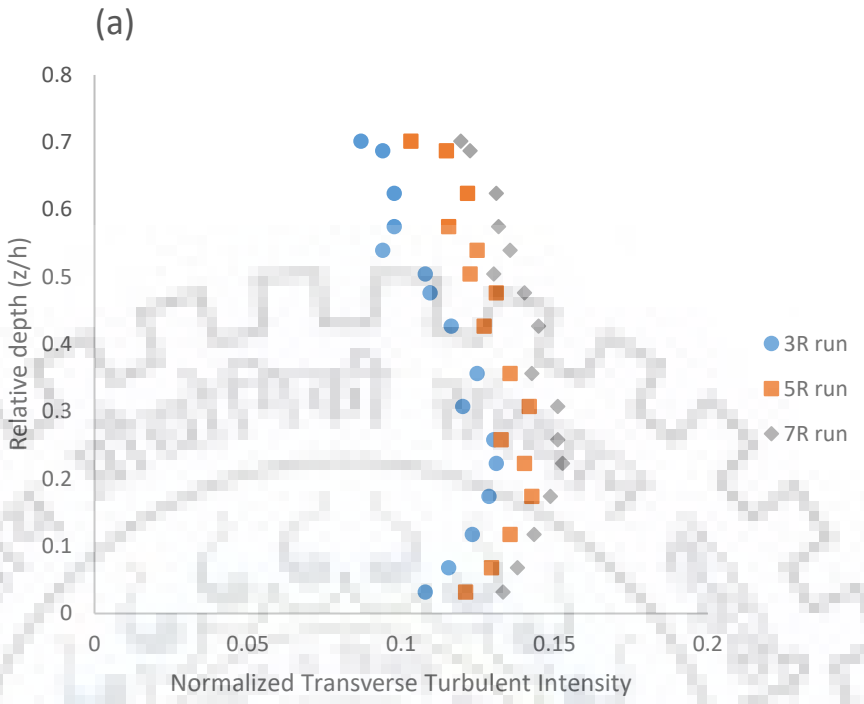

Figure 8.12 (a) Shows the depth-wise variation of normalized transverse turbulent intensity for 'y1' point

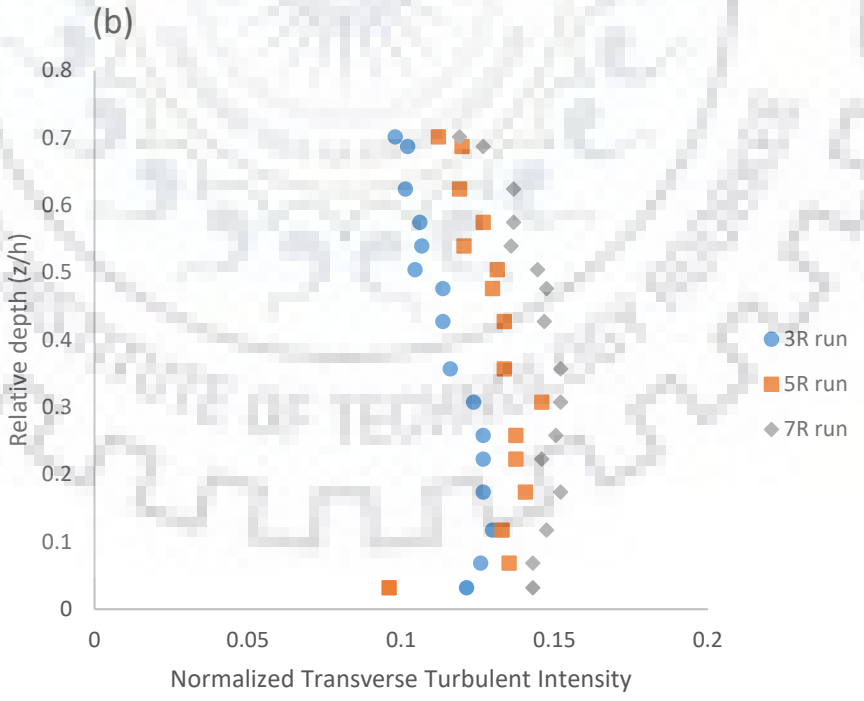

Figure 8.12 (b) Shows the depth-wise variation of normalized transverse turbulent intensity for 'y2' point

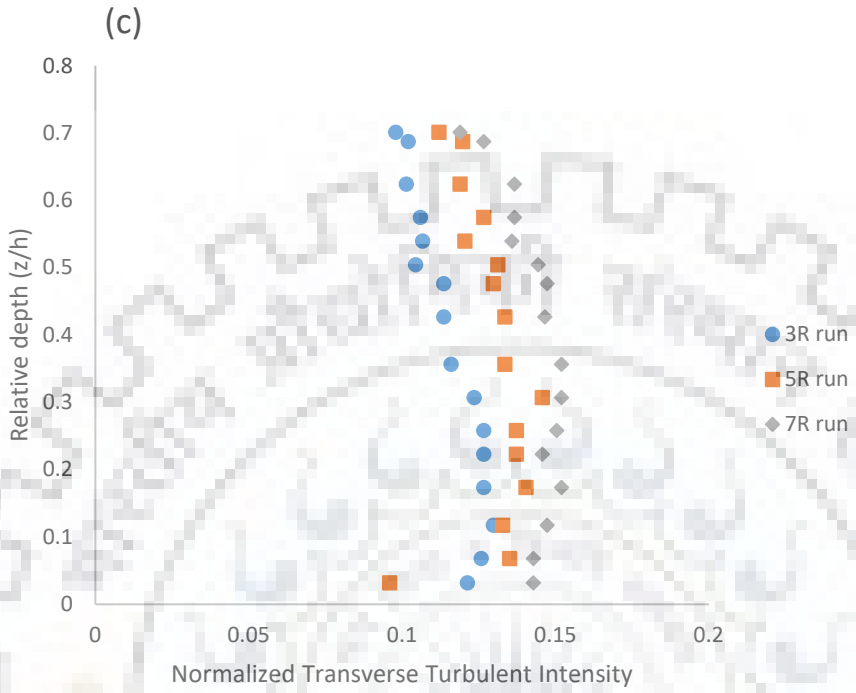

Figure 8.12 (c) Shows the depth-wise variation of normalized transverse turbulent intensity for 'y3' point

Total turbulent intensity is the summation of turbulent intensity in all three directions (Equation 8.1).

$$Ti_{total} = Ti_u + Ti_v + Ti_w \quad (8.1)$$

The total turbulent intensity(Ti_{total}) is plotted against the relative depth of flow (z/h) (Figures 8.13 and 8.14).

The longitudinal turbulent intensity is much greater than the vertical and transverse turbulent intensity. Thus, the distribution of total turbulent intensity distribution is similar to the longitudinal turbulent intensity distribution. The Reynolds stress model of Fluent software does not provide the detail of turbulent intensity of each direction. It only provides the detail of total turbulent intensity. Thus, the total turbulent intensity computed from the experiments are plotted along with the simulation profiles obtained from Reynolds stress model results of Fluent. The value and pattern of simulation results are almost similar to the experimental results (Figures 8.13 and 8.14). This

indicates that the experimental results are reasonably validated by the Reynolds stress model simulations of Fluent Software.

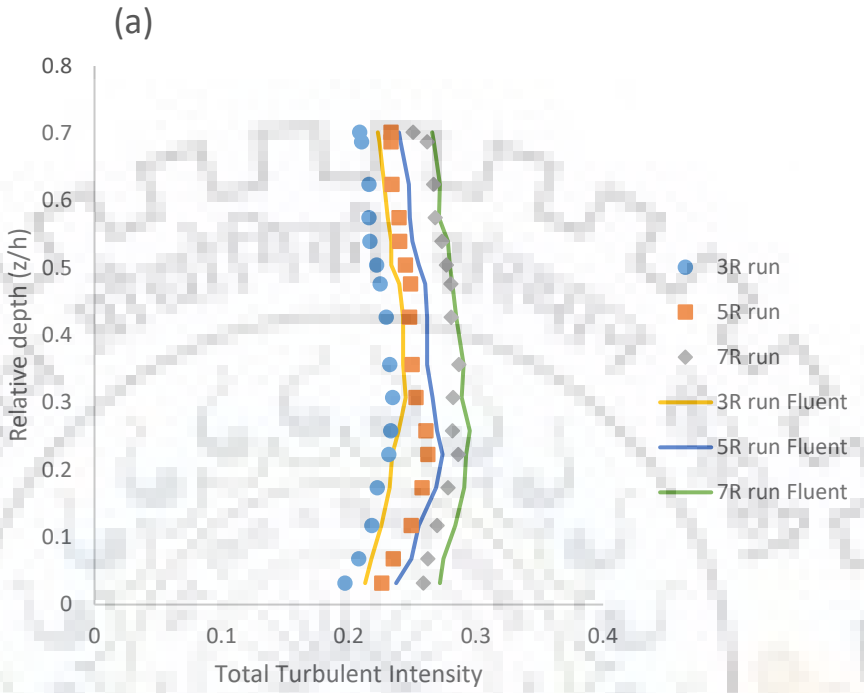

Figure 8.13 (a) Shows the depth-wise variation of total turbulent intensity for 'x1' point (Experimental and Simulation)

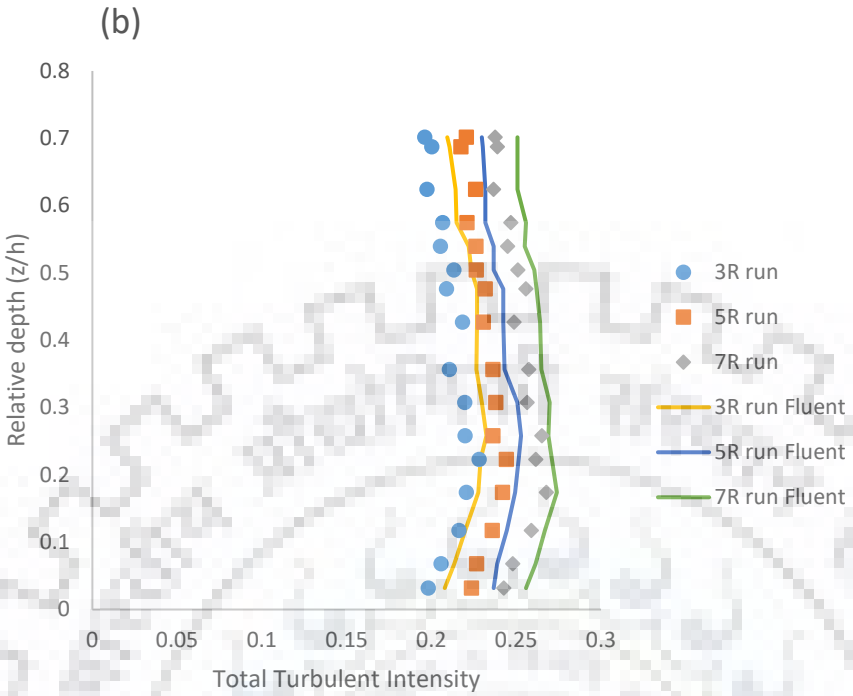

Figure 8.13 (b) Shows the depth-wise variation of total turbulent intensity for 'x2' point (Experimental and Simulation)

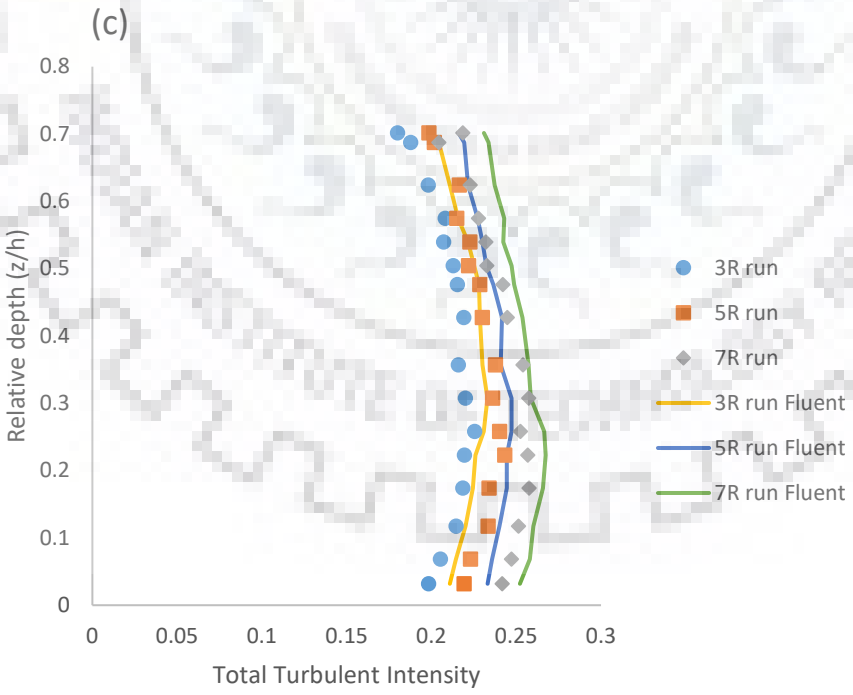

Figure 8.13 (c) Shows the depth-wise variation of total turbulent intensity for 'x3' point (Experimental and Simulation)

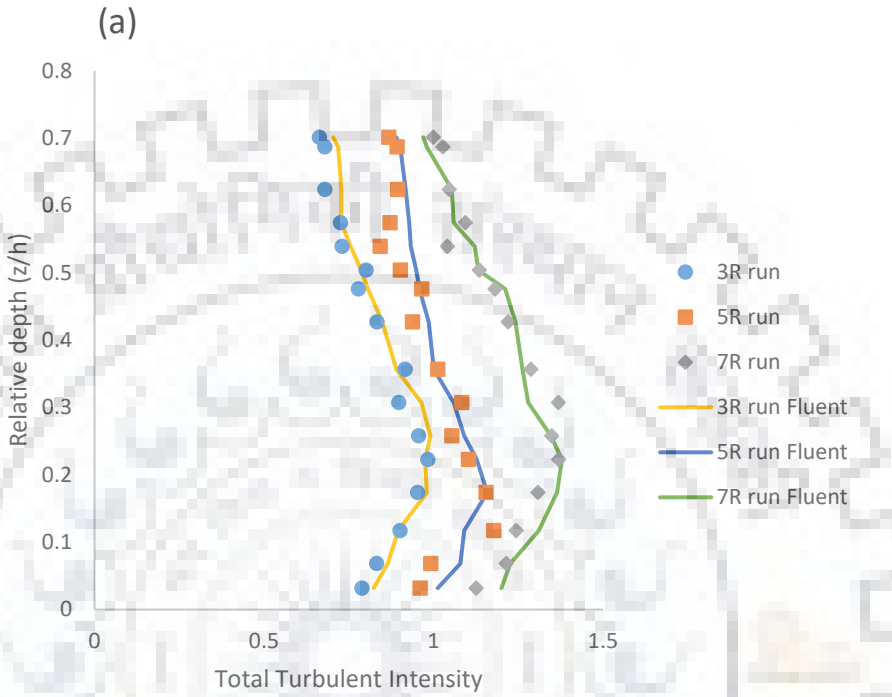

Figure 8.14 (a) Shows the depth-wise variation of normalized total turbulent intensity for 'y1' point (Experimental and Simulation)

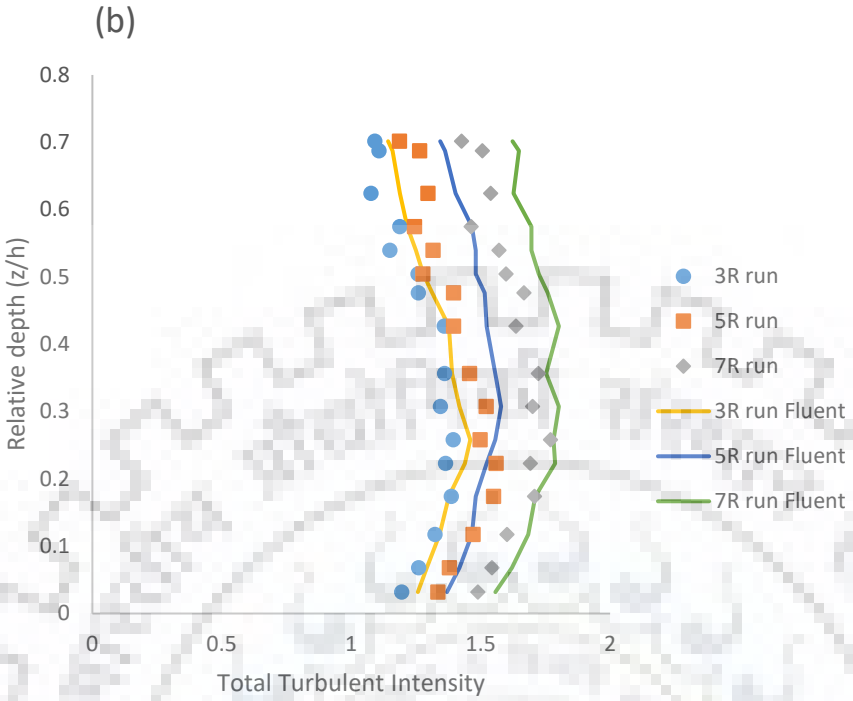

Figure 8.14 (b) Shows the depth-wise variation of normalized total turbulent intensity for 'y2' point (Experimental and Simulation)

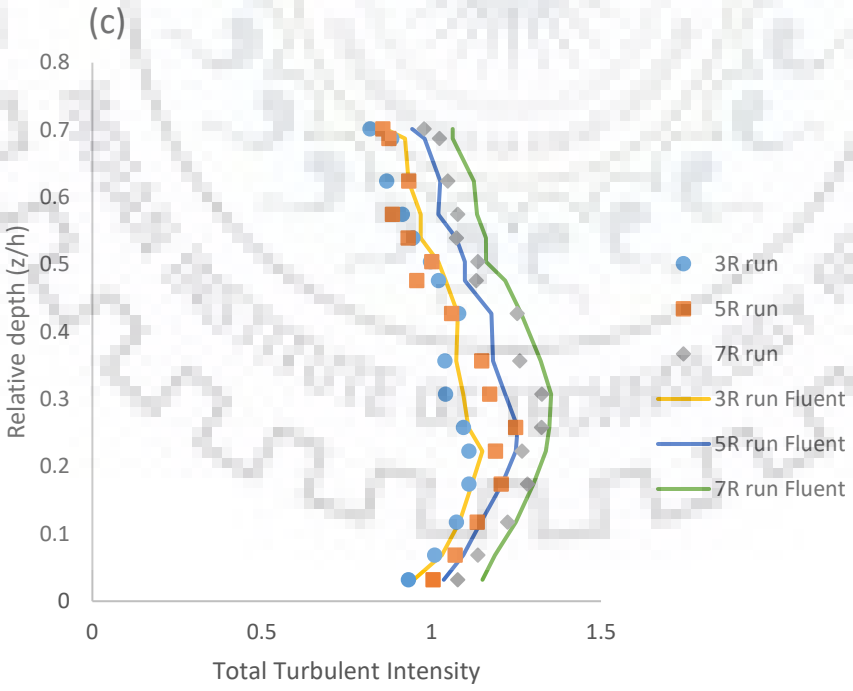

Figure 8.14 (c) Shows the depth-wise variation of normalized total turbulent intensity for 'y3' point (Experimental and Simulation)

8.3 Wake flow Analysis

The wake flow characteristics in the vicinity of mid-channel bar is analysed by plotting the U/u_* against the dimensionless parameter $\frac{zu_*}{\vartheta}$ for three different experimental conditions (Figure 8.15). Here, U is the mean velocity of flow, u_* is shear velocity of approaching flow, ϑ is dynamic viscosity of water and z is vertical distance from the bed. In Figure 8.15, the straight line follows the Prandtl-Karman log law distribution shown by Equation 8.2.

$$\frac{U}{u_*} = \frac{1}{k} ln\left(\frac{z}{y_0}\right) \tag{8.2}$$

Here, k is the von Karman's constant and its value is 0.41 for clear water. y_0 is zero velocity level. As mentioned in Van Rijn(1993), the expression of y_0 is given by Equation 8.3.

$$y_0 = \frac{\vartheta}{9.1u_*} \tag{8.3}$$

The deviation of velocity profile from the log law distribution indicate the presence of wake vortices (Purtell et al. 1981).

The velocity profile is plotted for four points located downstream of the mid-channel bar (Figure 8.15). Dey et al. (2008), Shamloo et al. (2001) observed that the wake flow is observed at downstream region of submerged structure. Thus, the points downstream of mid-channel bar are selected for analysis of log law distribution. The deviation of velocity profile from the log law distribution indicates the presence of wake flow (Figure 8.15).

The deviation from log law is more for points located at close vicinity of the mid-channel bar. The maximum deviation from the log law line is observed for 'y1' point. The greater deviation of experimental data from the log law for points close to the mid-channel bar may occur due to the formation of wake vortices. The deviations of experimental data from log law line increases as the submergence ratio increase (Figure 8.15).

(a)

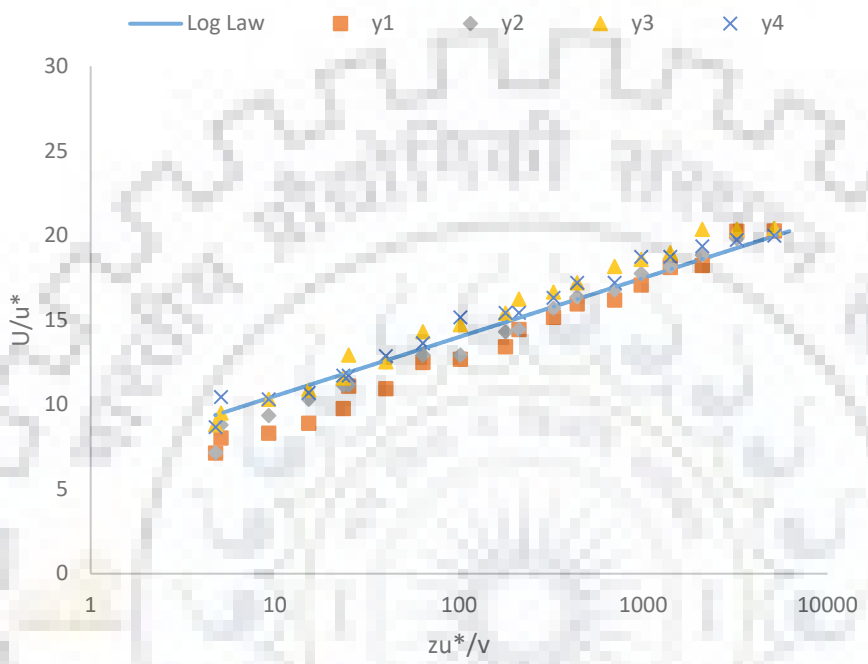

Figure 8.15(a) Showing the variations of U/u_* versus $\frac{zu_*}{\vartheta}$ for different points located at downstream of mid-channel bar (3R Experimental run)

(b)

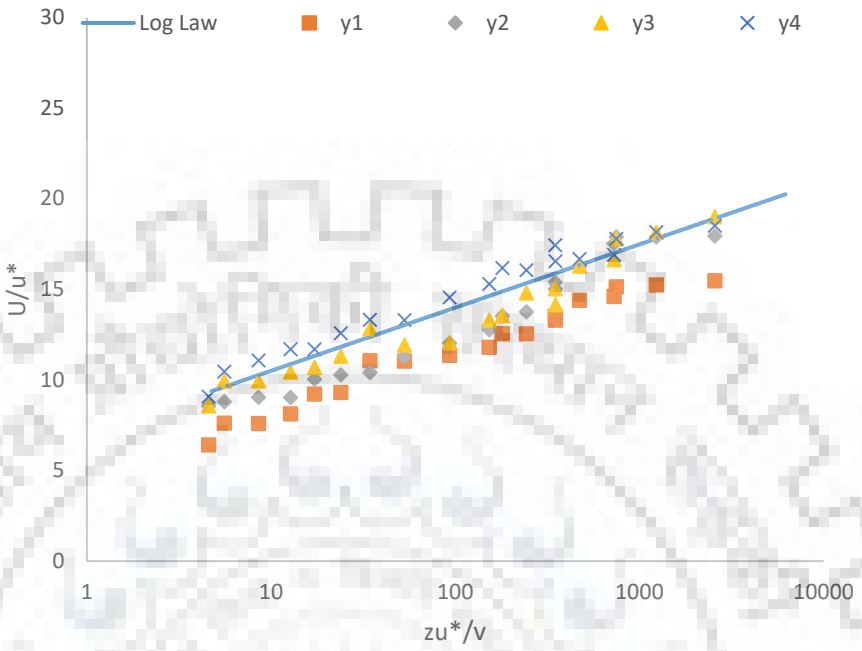

Figure 8.15(b) Showing the variations of U/u_* versus $\frac{zu_*}{\vartheta}$ for different points located at downstream of mid-channel bar (5R Experimental run)

(c)

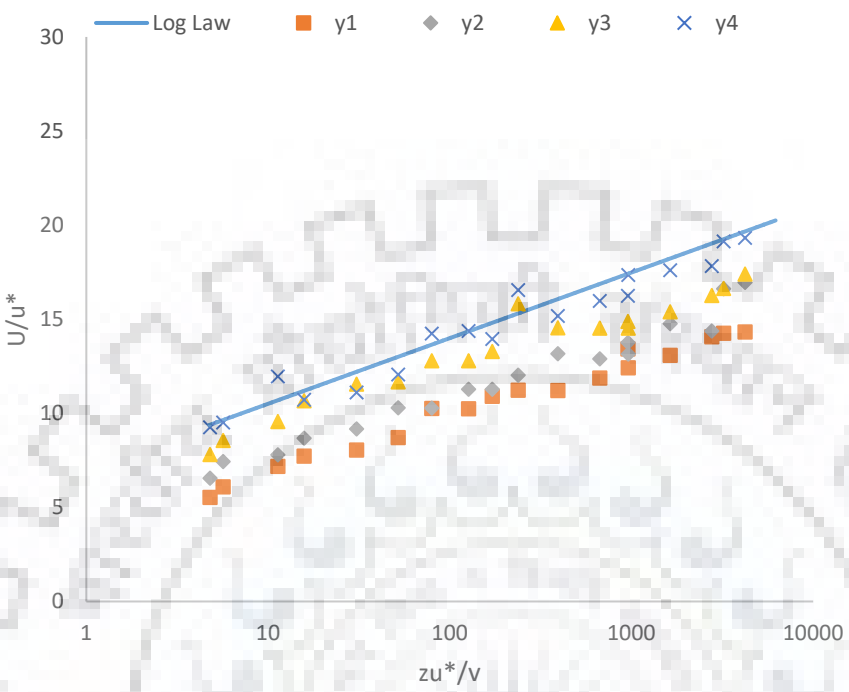

Figure 8.15(c) Showing the variations of U/u_* versus $\frac{zu_*}{\vartheta}$ for different points located at downstream of mid-channel bar (7R Experimental run)

CHAPTER-9 STUDY OF THIRD ORDER MOMENTS OF VELOCITY FLUCTUATIONS CHARACTERISTICS IN THE VICINITY OF MID-CHANNEL BAR

9.1 Third Order Moments

Third order moments of velocity fluctuations provide the information about skewness of velocity fluctuations with respect to the mean velocity. Third order moments are closely related to the coherent structure due to the preservation of their signs. These third order moments of velocity fluctuations transmit the stochastic information of the turbulent fluctuations in terms of flux and advection of turbulent stresses (Balachandar and Bhuiyan 2007; Bey et al. 2007; Gad-el-Hak and Bandyopadhyay 1994). In this chapter, the characteristics of third order moments of velocity fluctuations are studied in detail. For analysing the third order moment, the turbulent fluctuations in longitudinal and vertical directions are used. The turbulent fluctuation in transverse direction is not considered in this chapter.

9.1.1 Skewness Coefficients

The skewness coefficient provides a measure of skewness which is an important criterion for measuring the degree of symmetry of the distribution of velocity fluctuations with respect to the mean velocity components. The positive and negative values of skewness represent the useful statistical information of the distribution in term of right and left tail respectively (Dey et al. 2011). The skewness coefficients in the longitudinal and vertical directions are given by $S_u=\frac{\overline{u'^3}}{(\overline{u'})^3}$, $S_w = \frac{\overline{w'^3}}{(\overline{w'})^3}$ respectively (Dey et al. 2011). Here, u' and w' are velocity fluctuations in the longitudinal and vertical directions respectively. $\overline{u'}$ and $\overline{w'}$ are the mean values of u' and w' fluctuations respectively.

The depth-wise distribution of S_u is plotted at six different points for 3R, 5R and 7R experimental runs (Figures 9.1 and 9.2).

The detail of experimental runs is given in Table 3.4. The location of measuring points is shown in Figure 3.4. At point 'x3', the value of S_u is positive up to the relative depth (z/h) of 0.5, changing

over to a negative value afterward. At ‘x1’and ‘x2’ points, the value of S_u is positive in the near bed region (z/h<0.15), changes sign between (0.15>z/h<0.2) and stay negative for the remaining depth of flow (Figure 9.1). For points downstream of mid-channel bar, the S_u is negative for (z/h<0.2) and becomes positive afterward (Figure 9.2).

For (z/h<0.2), the magnitude of S_u is greater for points in the close vicinity of mid-channel bar ‘x1’ and ‘y1’ (Figures 9.1 and 9.2). This indicates that the presence of mid-channel bar causes increase of skewness in the longitudinal velocity distribution.

The value of S_u is greater for higher submergence ratio. This indicates that the high submergence ratio creates greater skewness of longitudinal velocity. The effect of submergence ratio is mainly predominant for z/h<0.2.

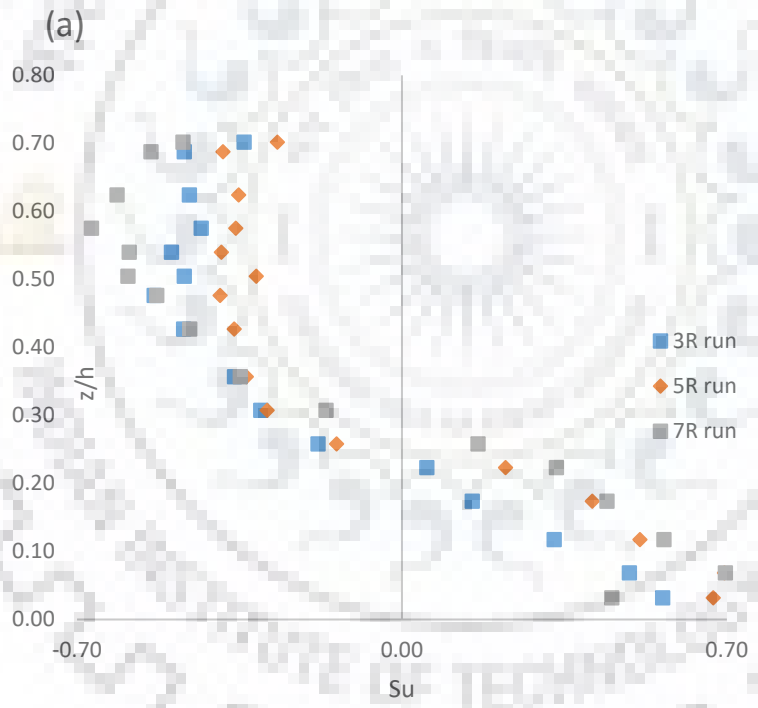

Figure 9.1 (a) Shows the depth-wise variation of S_u for ‘x1’ point

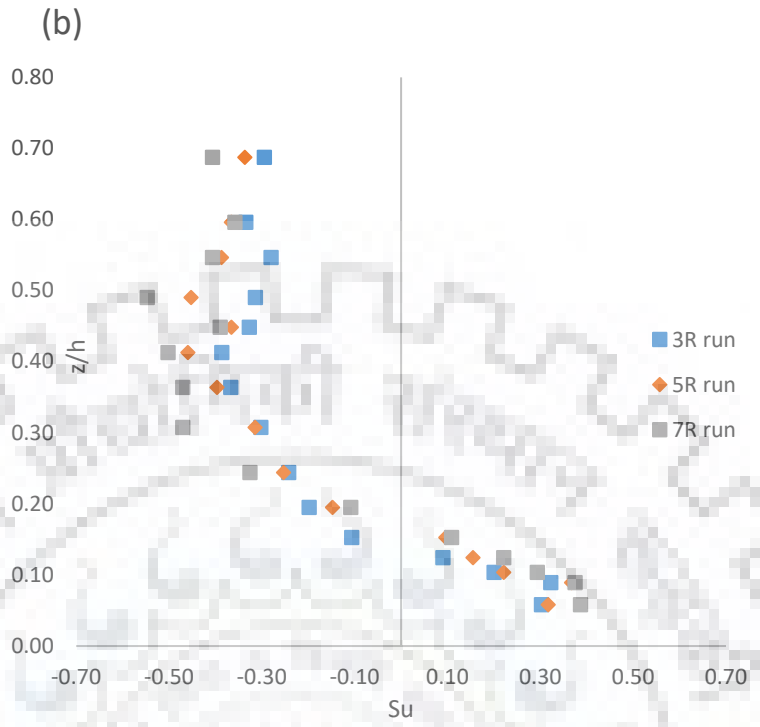

Figure 9.1 (b) Shows the depth-wise variation of S_u for 'x2' point

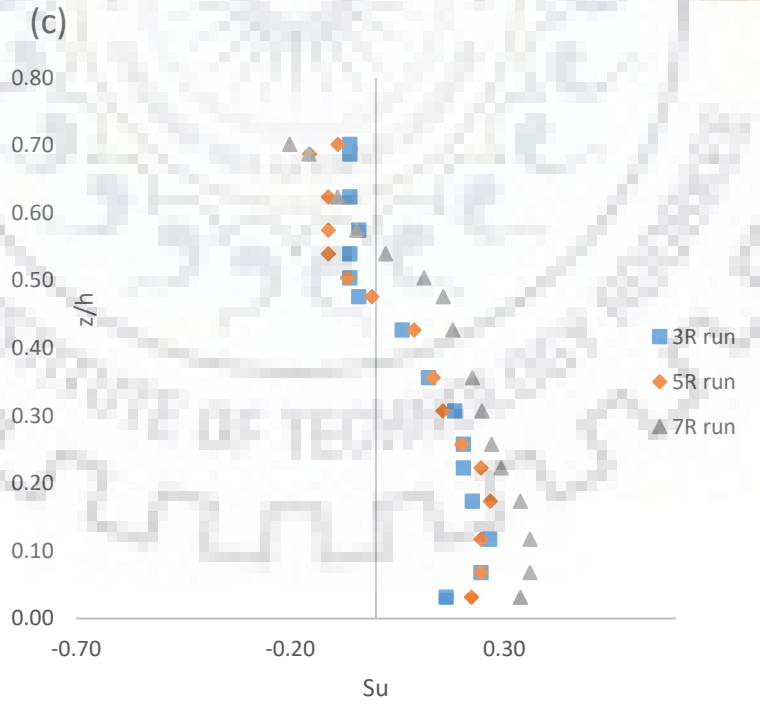

Figure 9.1 (c) Shows the depth-wise variation of S_u for 'x3' point

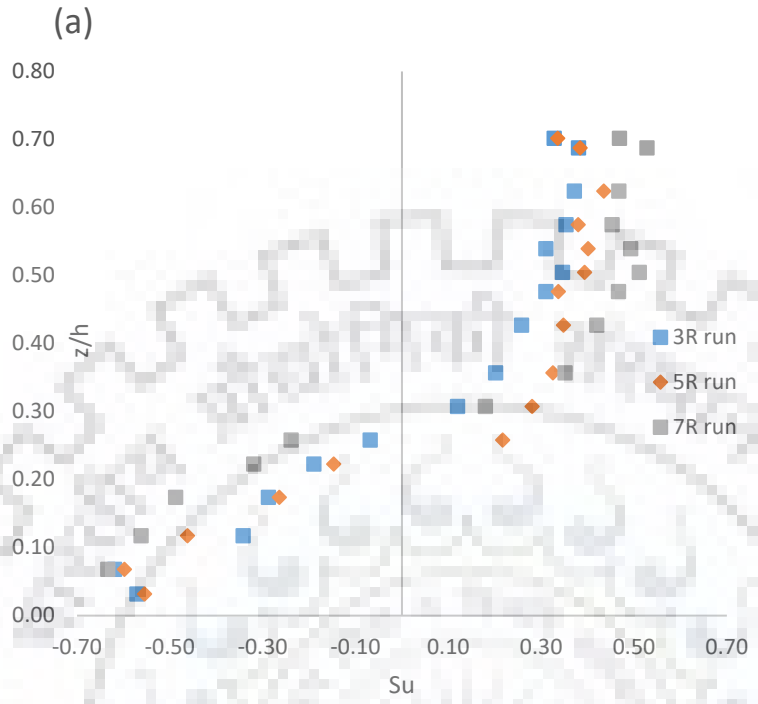

Figure 9.2 (a) Shows the depth-wise variation of S_u for 'y1' point

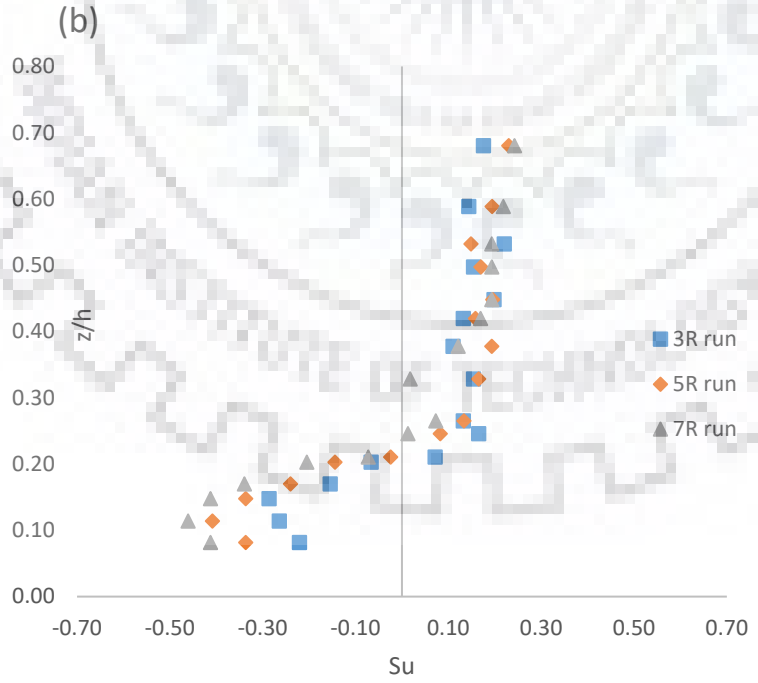

Figure 9.2 (b) Shows the depth-wise variation of S_u for 'y2' point

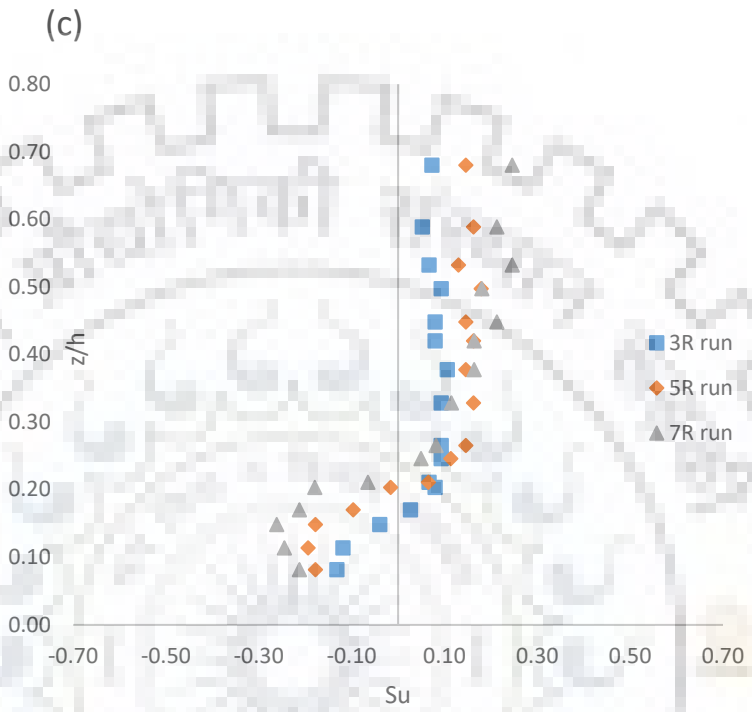

Figure 9.2 (c) Shows the depth-wise variation of S_u for 'y3' point

The S_w is plotted at six different points and for three different experimental conditions (Figures 9.3 and 9.4). For point 'x3', the value of S_w is negative throughout the flow depth. At 'x1' and 'x2' points, the value of S_w is negative for region z/h<0.2 and become positive afterward (Figure 9.3). For 'y1', 'y2'and 'y3' points, the value of S_w is positive for z/h<0.2 and then it becomes negative (Figure 9.4). The magnitude of S_w is more at points in the close vicinity of mid-channel bar 'x1' and 'y1' (Figures 9.3 and 9.4). This indicates that the presence of mid-channel bar causes greater skewness in the vertical velocity distribution.

Near the bed, the value of S_w is negative for points upstream of mid-channel bar and positive for points downstream of mid-channel bar (Figures 9.3 and 9.4). The value of S_w is more for higher submergence ratio. This shows that the higher submergence ratio causes greater skewness in the transverse velocity distribution.

For near bed region, the positive value of S_u and negative value of S_w at points upstream of mid-channel bar mean that the value of u' and w' are positive and negative respectively (Figures 9.1 and 9.3). Positive value of u' and negative value of w' contributes to the sweep event (Figure 2.4). Similarly at downstream points, the negative value of S_u and positive value of S_w indicate the dominance of ejection event (Figures 9.2 and 9.4).

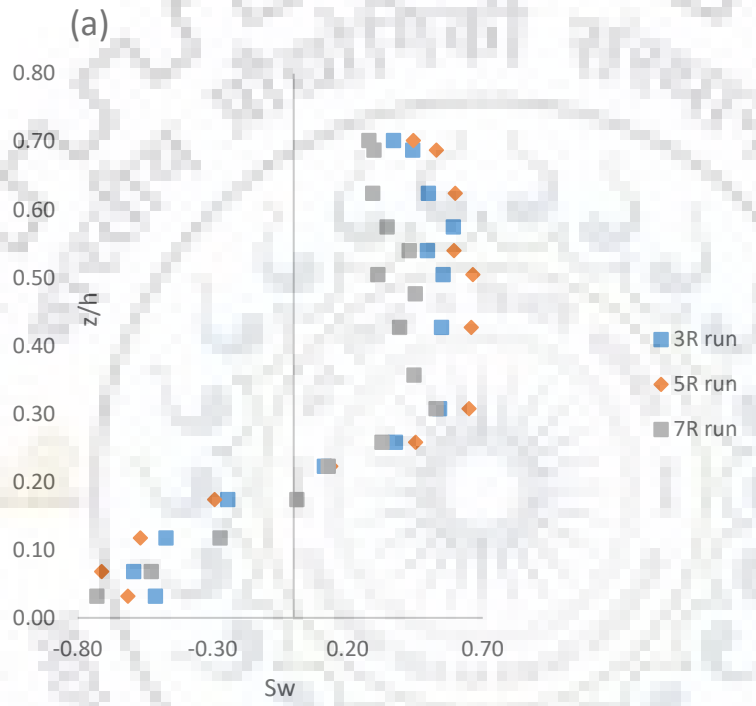

Figure 9.3 (a) Shows the depth-wise variation of S_w for 'x1' point

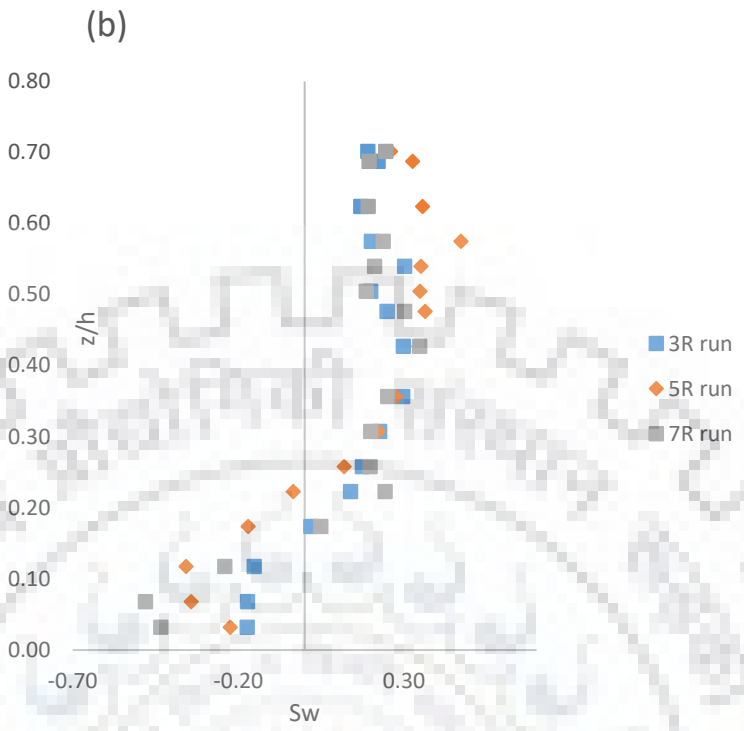

Figure 9.3 (b) Shows the depth-wise variation of S_w for 'x2' point

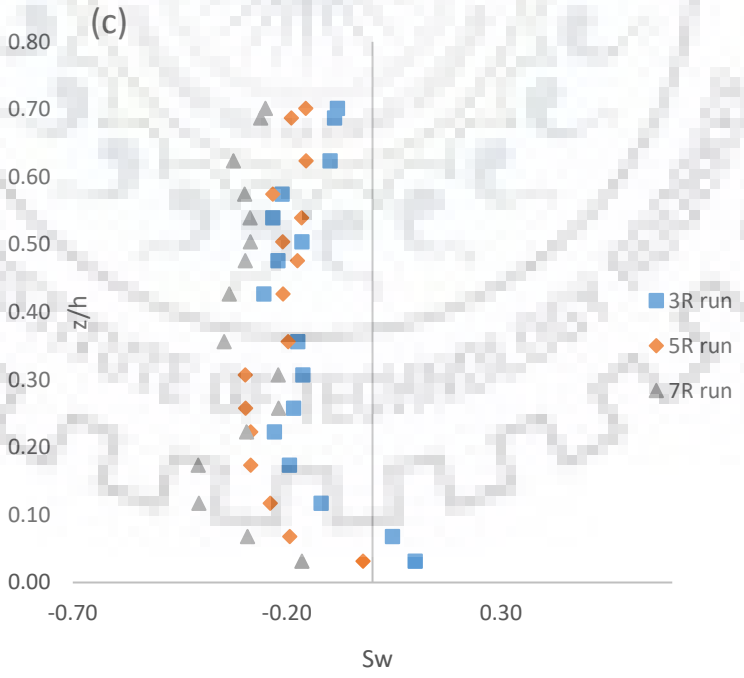

Figure 9.3 (c) Shows the depth-wise variation of S_w for 'x3' point

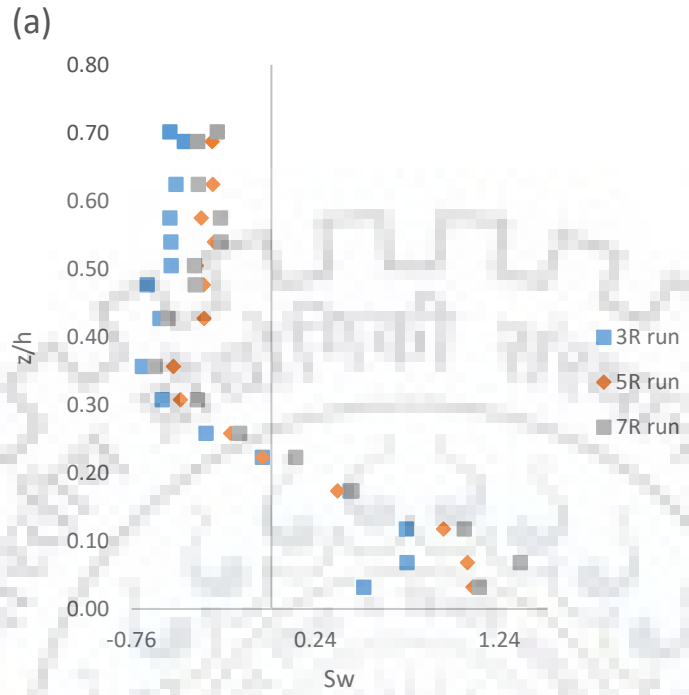

Figure 9.4 (a) Shows the depth-wise variation of S_w for 'y1' point

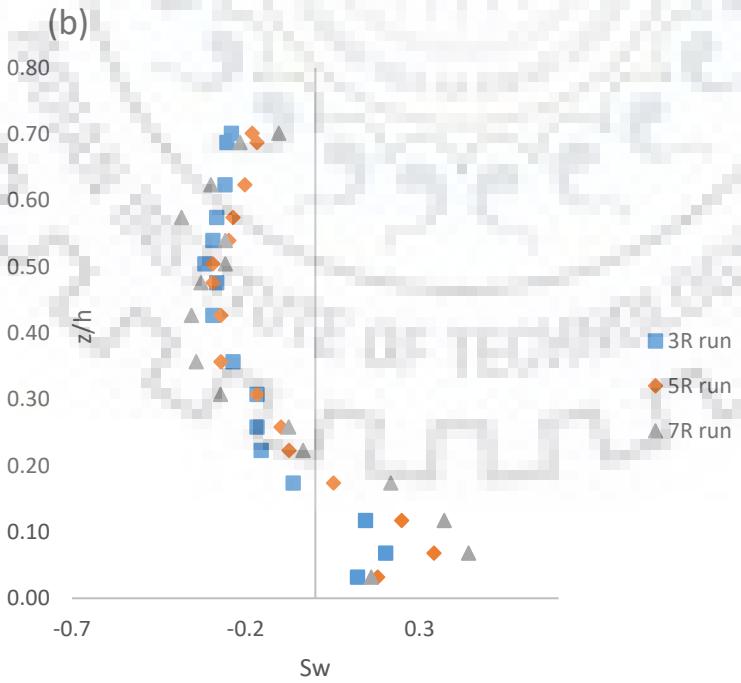

Figure 9.4 (b) Shows the depth-wise variation of S_w for 'y2' point

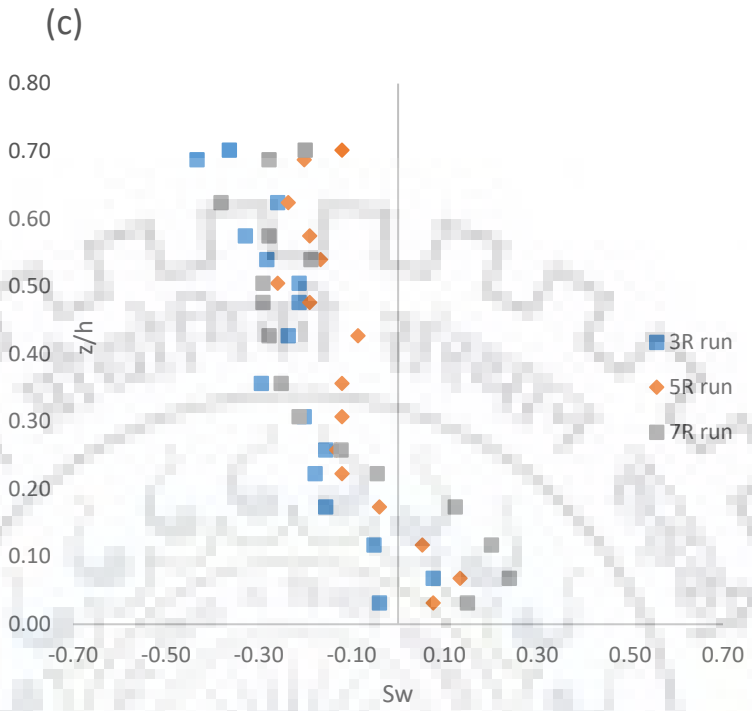

Figure 9.4 (c) Shows the depth-wise variation of S_w for 'y3' point

9.1.2 Stream-wise and Vertical Fluxes of turbulent kinetic energy

The depth-wise distribution of stream-wise and vertical fluxes of the turbulent kinetic energy are plotted. The stream wise and vertical fluxes of turbulent kinetic energy are expressed as $fku = 0.75(\overline{u'u'u'} + \overline{u'w'w'})$ and $fkw = 0.75(\overline{w'w'w'} + \overline{w'u'u'})$ respectively (Bey et al. 2007; Krogstadt and Antonia 1999). The stream wise and vertical fluxes of turbulent kinetic energy are normalized by the $(\overline{u'})^3$ and $(\overline{w'})^3$ respectively. The normalized stream-wise and vertical fluxes are expressed as $Fku = \frac{0.75(\overline{u'u'u'}+\overline{u'w'w'})}{(\overline{u'})^3}$, $Fkw = \frac{0.75(\overline{w'w'w'}+\overline{w'u'u})}{(\overline{w'})^3}$ respectively.

At point 'x3', the value of Fku is positive throughout the flow depth. For 'x2' point, the value of Fku is positive for (z/h<0.2) , it became negative for (0.2<z/h<0.4) and after it again becomes positive. For 'x1' point, the value of Fku is positive throughout the depth (Figure 9.5).

For 'y1', 'y2' and 'y3' points, the value of Fku is negative throughout the flow depth (Figure 9.6). Negative and positive values of Fku indicate the transport of energy in the backward and forward direction respectively (Dey et al. 2011). The negative value of Fku for downstream points indicates

the transfer of energy in the negative longitudinal direction (Figure 9.6). The magnitude of Fku is greater for higher submergence ratio. This indicates that the greater energy transfer takes place for higher submergence ratio (Figures 9.5 and 9.6). The effect for submergence ratio is mainly found in the lower layer of flow (z/h<0.2).

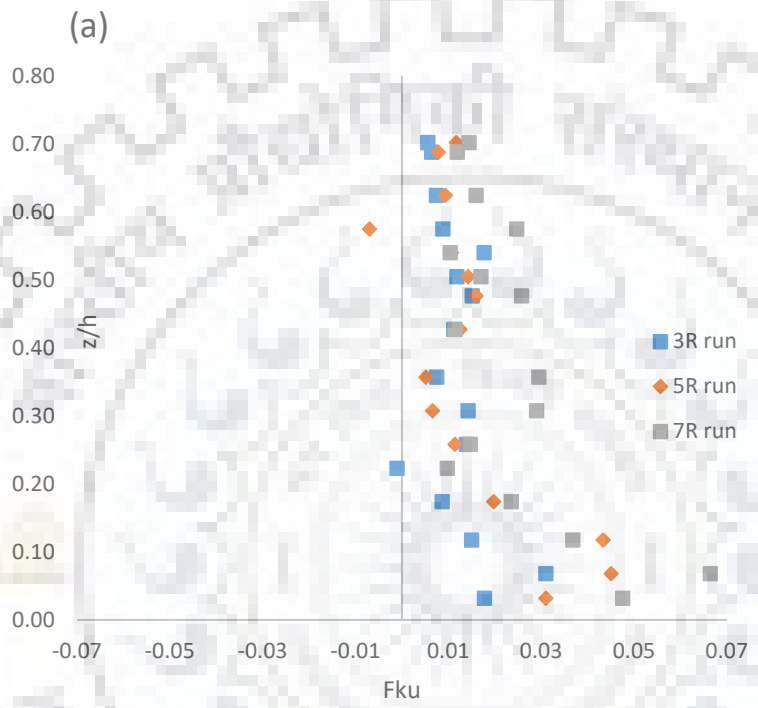

Figure 9.5 (a) Shows the depth-wise variation of Fku for 'x1' point

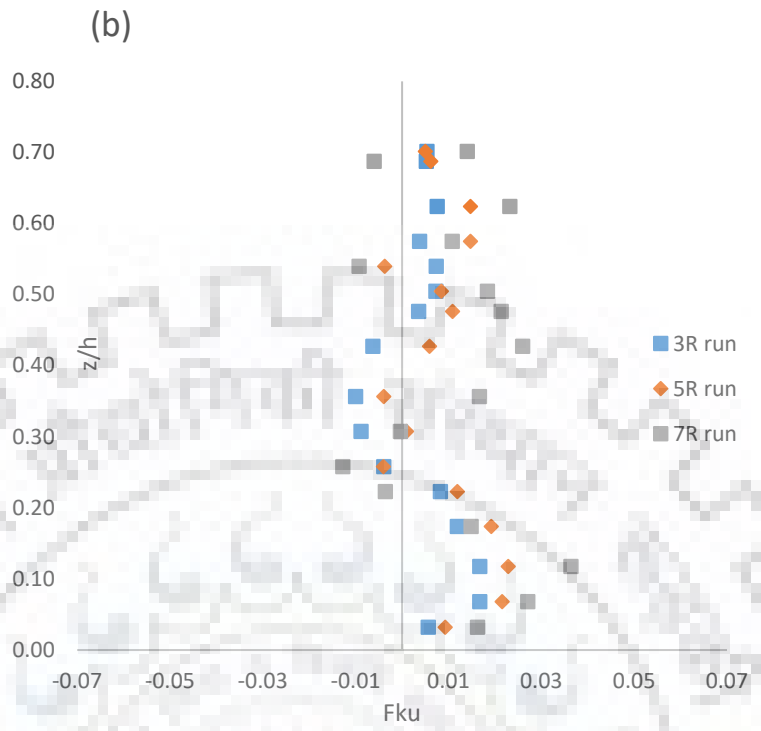

Figure 9.5 (b) Shows the depth-wise variation of Fku for 'x2' point

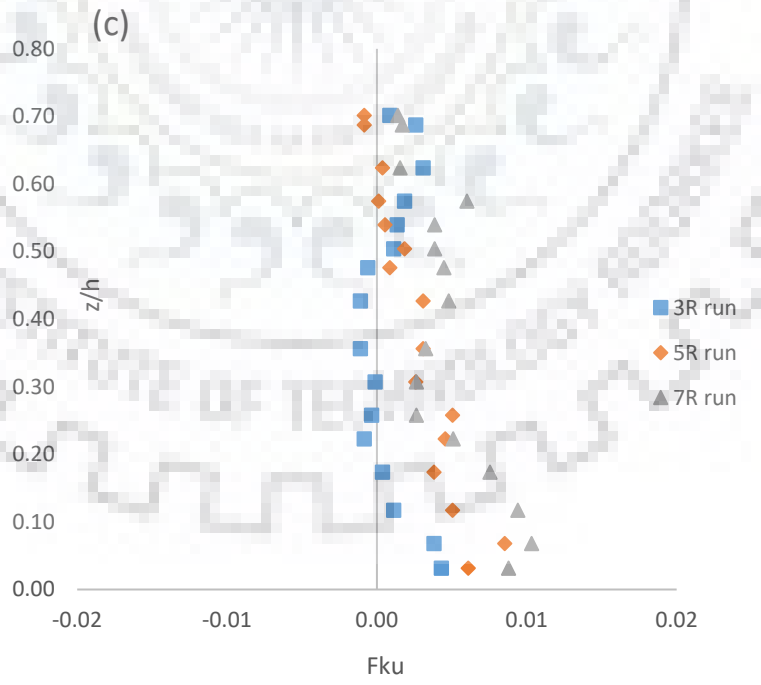

Figure 9.5 (c) Shows the depth-wise variation of Fku for 'x3' point

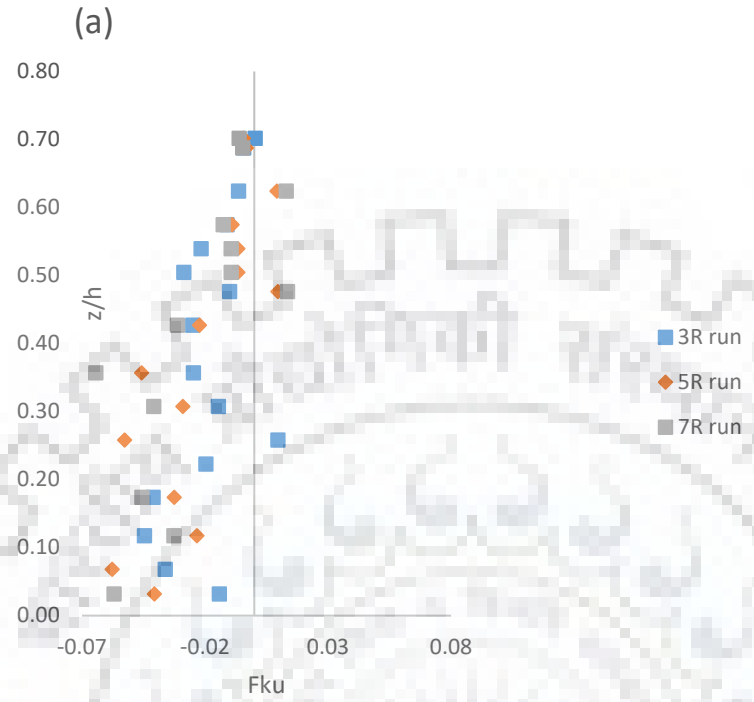

Figure 9.6 (a) Shows the depth-wise variation of Fku for 'y1' point

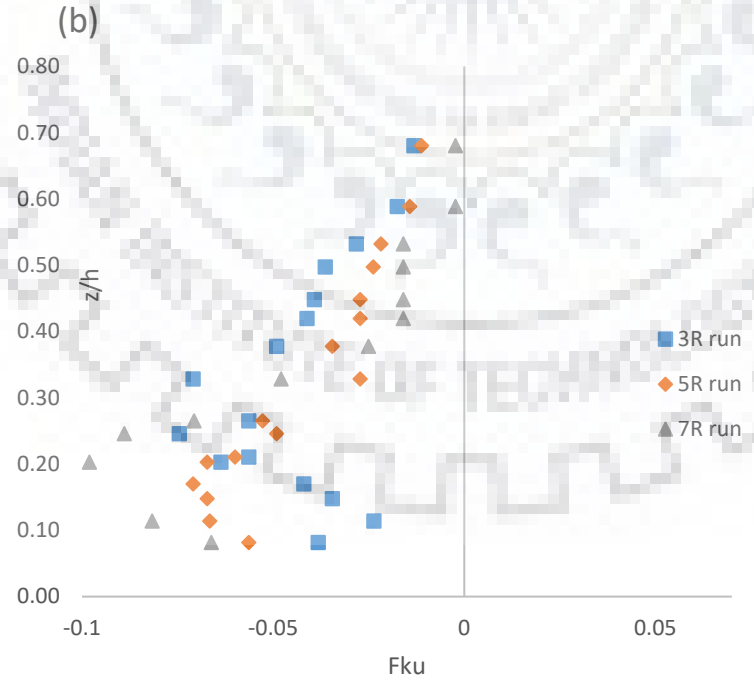

Figure 9.6 (b) Shows the depth-wise variation of Fku for 'y2' point

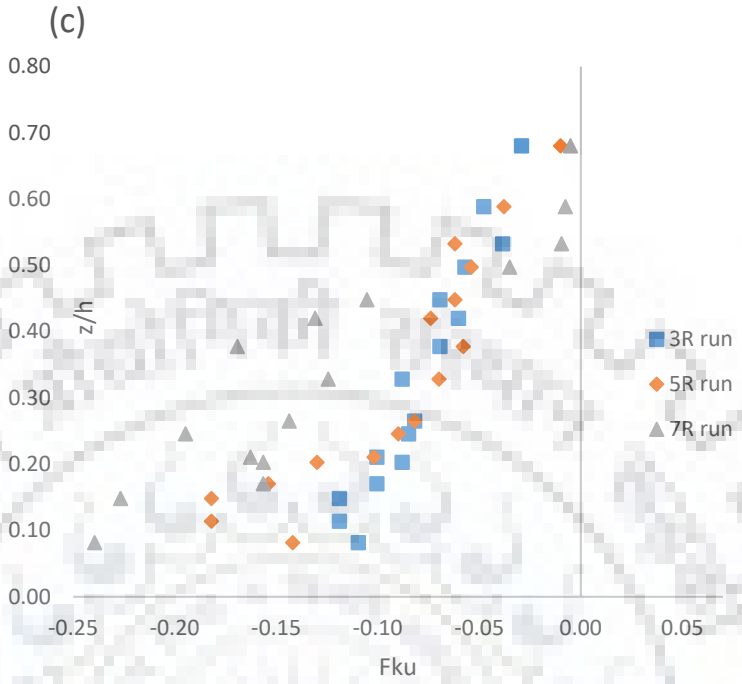

Figure 9.6 (c) Shows the depth-wise variation of Fku for 'y3' point

The depth-wise distribution of Fkw is also plotted (Figures 9.7 and 9.8). At point 'x3', the Fkw is positive almost throughout the flow depth. At 'x2' and 'x3' points, the value of Fkw is negative for (z/h <0.2) and stays positive for remaining depth of flow (Figure 9.7). The negative and positive values of Fkw indicate the transport of energy in the downward and upward direction respectively (Dey et al. 2011). The magnitude of Fkw increases with increase in the submergence ratio (Figures 9.7 and 9.8). This indicates that the higher energy transport in vertical direction takes places for higher submergence ratio.

Presence of mid-channel bar causes redistribution of Fku and Fkw coefficients. At 'y2' and 'y3' points, the negative value of Fku and positive value of Fkw indicate the transport of energy in backward and upward direction respectively (Figures 9.6 and 9.8). At upstream points for (z/h< 0.2), the positive value of Fku and negative value of Fkw indicate the transport of energy in forward and downward direction respectively (Figures 9.5 and 9.7).

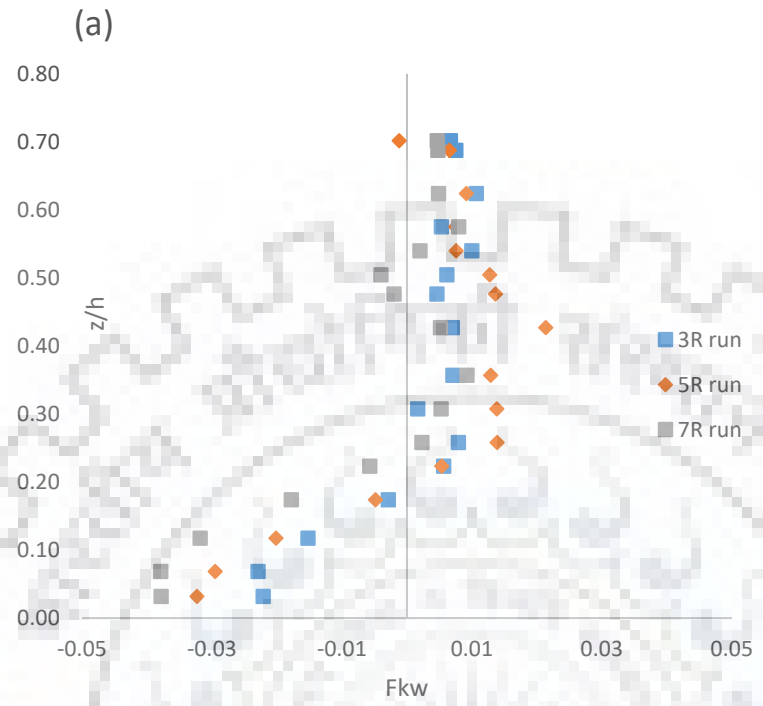

Figure 9.7 (a) Shows the depth-wise variation of Fkw for 'x1' point respectively

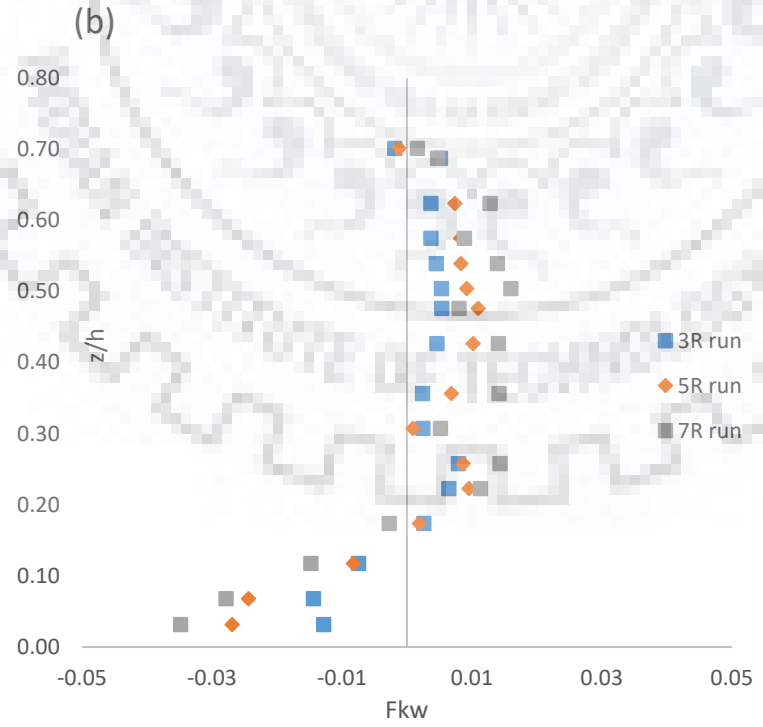

Figure 9.7 (b) Shows the depth-wise variation of Fkw for 'x2' point respectively

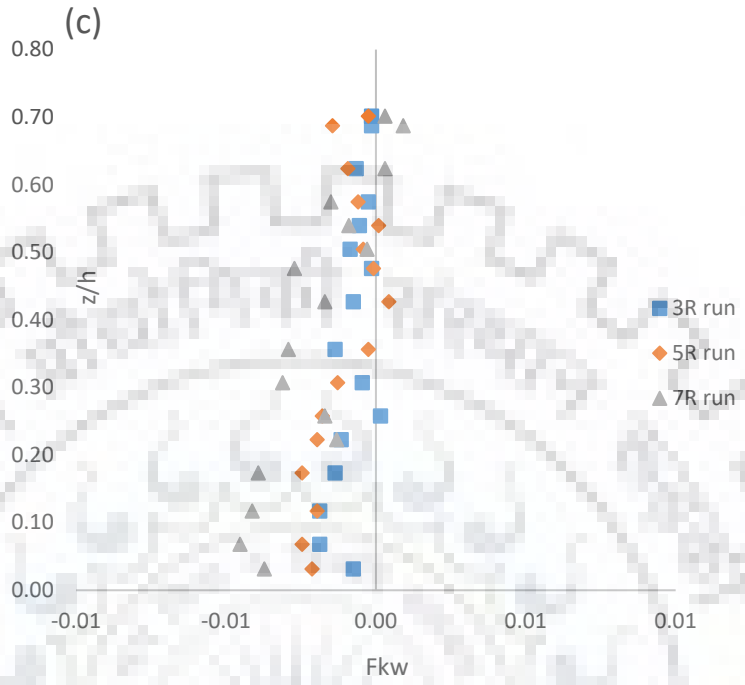

Figure 9.7 (c) Shows the depth-wise variation of Fkw for 'x3' point respectively

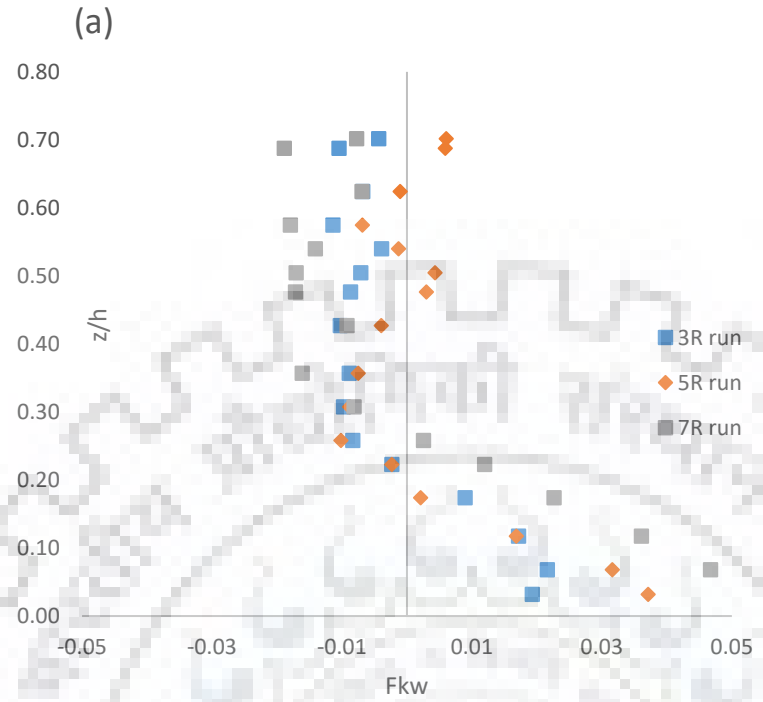

Figure 9.8 (a) Shows the depth-wise variation of Fkw for 'y1' point

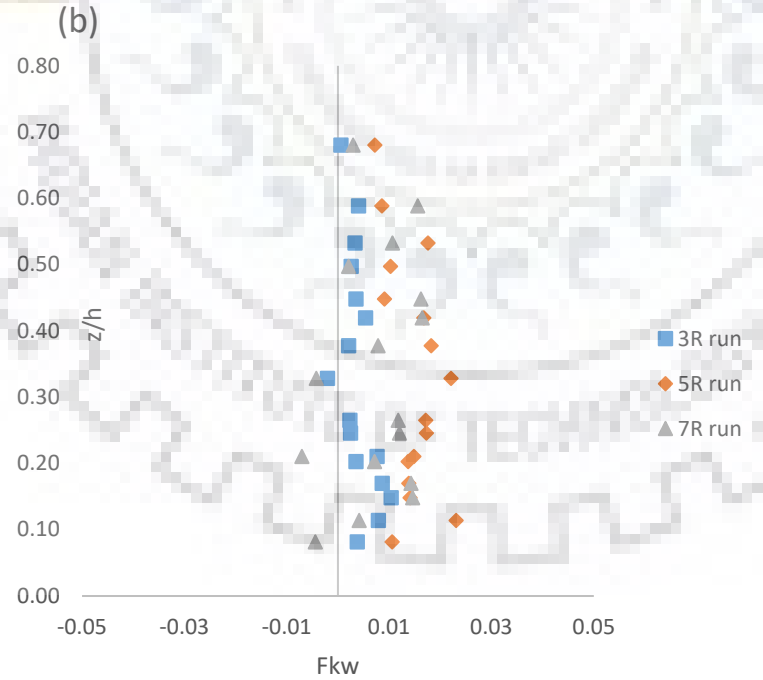

Figure 9.8 (b) Shows the depth-wise variation of Fkw for 'y2' point

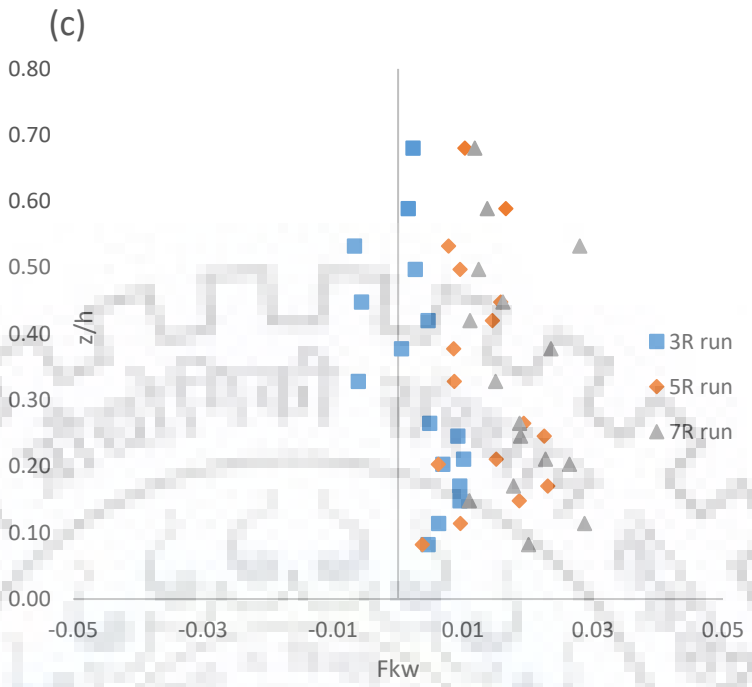

Figure 9.8 (c) Shows the depth-wise variation of Fkw for 'y3' point

CHAPTER-10 SUMMARY, CONCLUSIONS AND RECOMMENDATIONS

10.1 Summary of Research Work

In the present research, extensive laboratory investigations have been conducted to study in depth the turbulent flow hydraulics in the vicinity of mid-channel bar of alluvial stream. The experimental study is divided into two phases.

In first phase of study, the flow behaviour along the side of mid-channel bar is investigated. The changes induced in turbulent flow structure by the mid-channel bar are examined. The turbulent flow structures are analysed using the quadrant and octant techniques.

In the second phase of study, the velocity and turbulence parameters are thoroughly investigated at locations upstream and downstream of mid-channel bar. The main aim of performing second phase of experiments is to analyse the effect of mid-channel bar on the flow structure and to study the effect of mid-channel bar height on the turbulent structure of flow.

Quadrant technique is employed for analysing the joint probability distribution of bursting events. The velocity fluctuations are modelled using the Gram-Charlier method. The variation of bursting events with the Hole size is also analysed using the quadrant technique. The Hole size concept is used to segregate extreme events from low intensity events. The transverse flow component is found to make significant contribution to turbulent bursts in the vicinity of mid-channel bar. Thus, the three-dimensional bursting analysis is carried out in this study. The joint probability analysis of 3-D bursting events will be very complex from mathematical point of view. Although the two-dimensional joint probability analysis will not fully represent the flow structure in the vicinity of mid-channel bar, it will still give an idea of bursting events distribution in the vicinity of mid-channel bar. Hence, the joint probability distribution of bursting events is analysed using the quadrant technique.

The occurrence probabilities of three-dimensional octant events are computed using the method given by Keshavarzi and Gheisi (2006). The results indicate that the even octant events are related to the scouring and odd octant events are associated to the deposition observed in the vicinity of mid-

channel bar. Thus, in order to club the effect of bursting events on the flow characteristics in the vicinity of mid-channel bar, a new parameter 3-Dimensional Burst Index (3DBI) is introduced in the present study. It is the ratio of summation of odd events to the summation of even events. The 3DBI exhibits linear relationship with the scouring/deposition phenomenon observed in the vicinity of mid-channel bar with Coefficient of Determination and Pearson R value equal to 0.94 and 0.97 respectively. The high value of correlation coefficients indicates that the 3DBI is closely related with the local stream bed elevation change occurred in the proximity of mid-channel bar. Researches have been done on the effect of Hole size on two-dimensional bursting events. The Hole size concept for octant events is not yet defined in the literature. At region where the flow is three dimensional, the Hole size concept for octant events is necessary for segregating the extreme octant events from the low intensity octant events. Therefore, for defining the Hole size concept for octant events, a new parameter '3- Dimensional Hole Size'(3DHS) is proposed in this study. For studying the interaction between the sweep and ejection events, a new parameter 3-Dimensional Dominance function (3DDF)=$\frac{P_{2,H}+P_{6,H}}{P_{4,H}+P_{8,H}}$ is introduced which is the ratio of summation of ejection events to the summation of sweep events. The high rate of scouring is observed in the area of interaction due to the kolks-boils phenomenon. First order Markov chain process is used in this study for transitional movements modelling as per Keshavarzi and Gheisi (2006).

The depth averaged values of transition probability of stable movements are plotted for bar condition. Results indicate that the higher values of $p_{2\to2}$, $p_{4\to4}$, $p_{6\to6}$, $p_{8\to8}$ are observed at scouring points and higher values of $p_{1\to1}$, $p_{3\to3}$, $p_{5\to5}$, $p_{7\to7}$ are observed at depositional points. Thus, the odd stable movements are related to deposition and even stable movements are related to the scouring which occur in the vicinity of mid-channel bar. In the present study, the new parameter Transition Ratio (TR) is proposed. This parameter takes into account the effect of stable transition movements on the local stream bed elevation change that occurred in the proximity of mid-channel bar. In this study the relationships have been developed for Class A and Class B stable movements using the Nonlinear Fit toolbox of MATLAB Software.

From literature survey, it could be found that the turbulent flow structure in the vicinity of a mid-channel bar is not much researched in the past. Therefore, for validating the experimental results, the commercial CFD code Fluent is used. Steady state simulations are carried out using the Reynolds stress model of Fluent Software on the basis of the study by Sarkar and Ratha (2014). The flow

structure in the vicinity of mid-channel bar is greatly affected by the mid-channel bar. The depth-averaged contours of turbulence parameters are analysed for bar and no bar conditions. The depth-wise distributions of velocities and turbulence parameters are plotted for different submergence ratio. The effects of submergence ratio on the turbulent flow structure are analysed. The characteristics of third order moments of velocity fluctuations are studied in detail.

The present study contributes towards better comprehension of the intricate linkage of turbulent burst events with the local stream bed elevation changes that are observed in the vicinity of mid-channel bar. New parameters are developed for an insight into the turbulent flow structure in the vicinity of mid- channel bar. The concept of Hole size is proposed for the three-dimensional octant events in this study. The newly introduced Three-Dimensional Hole Size in this research helps in minutely studying the turbulent flow structure. Not many prominent studies have been done on the flow structure in the vicinity of mid-channel bar. Due to the lack of experimental data on this topic, the Reynolds stress modelling is done for validating the experimental results using the CFD code of Fluent software. The effect of submergence ratio on the turbulent flow structure in the vicinity of mid-channel bar are analysed. Effect of fluid-bar interaction on the third order moments of velocity fluctuations is investigated.

10.2 Conclusions

The following prime results and conclusions have been drawn from the study:

1. The results indicate that the extreme events are observed at sections near the upstream end of mid-channel bar. These extreme turbulent bursts are triggered by the fluid bar interaction. The sweep events are found to be dominant near the boundary and ejection events are observed to be dominant away upward from the boundary. From the results, it was found that the dominance of sweep events decreases as the hyperbolic Hole size increases. The results bring out that the higher stresses are produced mainly due to ejection events.
2. The presence of the mid-channel bar causes redistribution of turbulent bursts with high occurrence probability for even events at location near upstream end of mid-channel bar. The high magnitude of turbulent burst generated due to the fluid bar interaction causes scouring at these locations. The zone of high probability becomes more eccentric toward the dominant quadrants as the Hole size increases from 0 to 1.5.

3. The presence of mid-channel bar causes non-homogeneity in the contours pattern of turbulent intensities. High level turbulent intensities are observed at region near upstream end of mid-channel bar and level of turbulent intensities decreases with increase in distance from the upstream end of mid-channel bar. The high level of turbulent intensities at region near upstream end of mid-channel bar is responsible for occurrence of scouring at that region. For no bar condition, the turbulent intensities contours have lesser spatial variation.
4. The presence of mid-channel bar induces a series of critical changes to the turbulent flow structure, where high Reynolds stresses are generated at region near upstream end of mid-channel bar. These high Reynolds stresses may be expected to generate increased stream bed scouring.
5. The magnitude of turbulent kinetic energy for each individual direction is computed. The results show that the transverse flow component is significant for bar condition. The contribution of Tke_y for bar condition is almost 1.5 times as compared to the no bar condition. This indicates that the transfer of turbulent energy takes place from longitudinal to the lateral direction due to the presence of mid-channel bar.
6. The new parameters 3DBI and TR are evolved in this research to reflect streambed elevation changes and stable transitional movements. These parameters show linear relationships with the scouring/deposition occurred in the vicinity of mid-channel bar. These two parameters are closely related with the local stream bed elevation changes that occurred in the vicinity of mid-channel bar.
7. The new parameter 3DHS is defined in the present research to closely examine high intensity 3-Dimensional bursts with Hole size for fluid bar interaction. This parameter has defined the Hole size concept for three-dimensional flow. The 3DHS helps in segregating the extreme octant events from the low intensity octant events. The variations of octant events with the 3DHS are analysed. The results indicate that the presence of mid-channel bar leads to the creation of high intensity turbulent burst. The one more notable conclusion drawn from this analysis is that the dominant events become more dominant with increase in the 3DHS value.
8. Another new parameter 3DDF formulated in this research brings out the relative dominance and interaction between sweep and ejection events in three-dimensional bursting process. “kolks-boils” phenomenon is observed due to the interaction of sweep and ejection events.

The results indicate that the 3DDF parameter is successful in predicting the high scouring region.

9. The three-dimensional transitional movements of bursting events are modelled using the first order Markov chain. The transition probabilities of stable movements are closely related to the Scouring/Deposition that occurred in the vicinity of mid- channel bar. The relationships have been developed for Class A and Class B stable movements using the Nonlinear Fit toolbox of MATLAB Software. The high value of correlation for these expressions indicates that they are correctly predicting the relationship between the stable movements.
10. The literature survey brings out that the turbulent flow structure in the vicinity of the mid-channel bar is not investigated in the past. Therefore, the computational fluid dynamic CFD code Fluent is used for validating the present experimental results of the study. The flow simulations are carried out using the Reynolds stress model. The value and pattern of simulation results are almost similar to the experimental results. Hence, the Reynolds stress model is successfully predicting the depth-wise profile of turbulent and velocity distributions.
11. The longitudinal velocity is lesser for higher submergence ratio. This indicates that the increase in the height of mid-channel bar causes greater reduction in longitudinal velocity. The vertical velocity is negative at sections upstream of the mid-channel bar. The negative vertical velocity indicates the downflow at these sections. The magnitude of transverse velocity is significant at sections downstream of mid-channel bar. This highlights that the flow structure is three dimensional at downstream region of the mid-channel bar.
12. The longitudinal turbulent intensity is greater for higher submergence ratio. This indicates that the increase in height of mid-channel bar causes increase in the magnitude of longitudinal turbulent intensity. The longitudinal turbulent intensity at sections downstream of mid-channel bar is much more pronounced as compared to the upstream sections. This is mainly due to the interaction of surface wave with the downstream flow. The increase in vertical and transverse component of turbulent intensity is observed for higher submergence ratio.
13. The deviation of velocity profile from logarithmic law is more discernible for sections located in close vicinity of the mid-channel bar. The deviations from logarithmic profile increases as the submergence ratio increases.

14. The presence of mid-channel bar causes increase of skewness in the longitudinal velocity distribution. The value of S_u is greater for higher submergence ratio. This indicates that the high submergence ratio creates greater skewness of longitudinal velocity. The magnitude of S_w is more at sections in the close vicinity of mid-channel bar. This highlights that the presence of mid-channel bar causes greater skewness in the vertical velocity distribution.
15. Presence of mid-channel bar causes redistribution of Fku and Fkw coefficients. The magnitude of Fku and Fkw are greater for higher submergence ratio. This indicates that the greater energy transfer takes place for higher submergence ratio.

10.3 Future Scope of the Study

The present study utilized the bursting phenomena for investigating the turbulence in the vicinity of mid-channel bar. Hydraulic parameters are proposed for relating the three-dimensional bursting events with the local stream bed elevation changes observed in the vicinity of mid-channel bar. The bursting approach is applied for only one Aspect Ratio of mid-channel bar with an oval like shape. For greater insight into the turbulent flow structure, the present study may be extended for different sizes with varying Aspect Ratios and shapes of mid-channel bar. The present experiments were carried out for only one bed material. The future study can be extended for different sizes of bed material.

BIBLIOGRAPHY

Afzal, B., Faruque, M. A., and Balachandar, R. (2009). "Effect of Reynolds number, near-wall perturbation and turbulence on smooth open-channel flows." Journal of Hydraulic Research, 47(1), 66-81.

Ahrens, B. (2006). "Distance in spatial interpolation of daily rain gauge data." Hydrology and Earth System Sciences Discussions, 10(2), 197-208.

Akhtar, M., Sharma, N., and Ojha, C. (2011). "Braiding process and bank erosion in the Brahmaputra River." International Journal of Sediment Research, 26(4), 431-444.

Ali, S., Ghani, U., and Latif, A. (2013). "Study of turbulent kinetic energy and reattachment length downstream the obstruction in an open channel." Life Sci. J, 10.

Amsler, M. L., Garcia, M. H., Neill, C. R., Julien, P. Y., and Klaassen, G. J. (1997). "Discussions and Closure: Sand-Dune Geometry of Large Rivers during Floods." Journal of Hydraulic Engineering, 123(6), 582-585.

Ashmore, P. (1991). "Channel morphology and bed load pulses in braided, gravel-bed streams." Geografiska Annaler: Series A, Physical Geography, 73(1), 37-52.

Ashmore, P. E. (1982). "Laboratory modelling of gravel braided stream morphology." Earth Surface Processes and Landforms, 7(3), 201-225.

Ashmore, P. E. (1988). "Bed load transport in braided gravel-bed stream models." Earth Surface Processes and Landforms, 13(8), 677-695.

Ashmore, P. E. (1991). "How do gravel-bed rivers braid?" Canadian journal of earth sciences, 28(3), 326-341.

Ashmore, P., and Parker, G. (1983). "Confluence scour in coarse braided streams." Water Resources Research, 19(2), 392-402.

Ashworth, P. J. (1996). "Mid-channel bar growth and its relationship to local flow strength and direction." Earth Surface Processes and Landforms, 21(2), 103-123.

Ashworth, P. J., Best, J. L., Roden, J. E., Bristow, C. S., and Klaassen, G. J. (2000). "Morphological evolution and dynamics of a large, sand braid-bar, Jamuna River, Bangladesh." Sedimentology, 47(3), 533-555.

Ashworth, P. J., Sambrook Smith, G. H., Best, J. L., Bridge, J. S., Lane, S. N., Lunt, I. A., Reesink, A. J., Simpson, C. J., and Thomas, R. E. (2011). "Evolution and sedimentology of a channel fill in the sandy braided South Saskatchewan River and its comparison to the deposits of an adjacent compound bar." Sedimentology, 58(7), 1860-1883.

Ashworth, P., Ferguson, R., and Powell, M. (1992). "Bedload transport and sorting in braided channels, Dynamics of Gravel-Bed Rivers P. Billi, et al., 497–515." John Wiley, New York.

Baki, A. B. M., and Gan, T. Y. (2012). "Riverbank migration and island dynamics of the braided Jamuna River of the Ganges–Brahmaputra basin using multi-temporal Landsat images." Quaternary International, 263, 148-161.

Balachandar, R., and Bhuiyan, F. (2007). "Higher-order moments of velocity fluctuations in an open-channel flow with large bottom roughness." Journal of Hydraulic Engineering, 133(1), 77-87.

Barman, K., Debnath, K., and Mazumder, B. S. (2017). "Higher-order turbulence statistics of wave–current flow over a submerged hemisphere." Fluid Dynamics Research, 49(2), 025504.

Bathurst, J. C. (1985). "Flow resistance estimation in mountain rivers." Journal of Hydraulic Engineering, 111(4), 625-643.

Bergé, P., Pomeau, Y., and Vidal, C. (1984). Order within chaos, Wiley and Sons NY.

Best, J. L. (1986). "The morphology of river channel confluences." Progress in Physical Geography, 10(2), 157-174.

Best, J. L., Ashworth, P. J., Sarker, M. H., Roden, J. E., and Gupta, A. (2007). "The Brahmaputra-Jamuna River, Bangladesh." Large rivers: geomorphology and management, 395-430.

Bey, A., Faruque, M., and Balachandar, R. (2007). "Two-dimensional scour hole problem: role of fluid structures." Journal of Hydraulic Engineering, 133(4), 414-430.

Bhosekar, V., Deolalikar, P., and Sridevi, M. (2007). "Hydraulic design aspects for swirling flow at vertical drop shaft spillways." ISH Journal of Hydraulic Engineering, 13(3), 78-89.

Bhosekar, V., Jothiprakash, V., and Deolalikar, P. (2011). "Orifice spillway aerator: Hydraulic design." Journal of Hydraulic Engineering, 138(6), 563-572.

Blanckaert, K., and De Vriend, H. J. (2005). "Turbulence structure in sharp open-channel bends." Journal of Fluid Mechanics, 536, 27-48.

Bluck, B. (1979). "Structure of coarse grained braided stream alluvium." Earth and Environmental Science Transactions of The Royal Society of Edinburgh, 70(10-12), 181-221.

Bogard, D., and Tiederman, W. (1986). "Burst detection with single-point velocity measurements." Journal of Fluid Mechanics, 162, 389-413.

Box, G. E., and Cox, D. R. (1964). "An analysis of transformations." Journal of the Royal Statistical Society. Series B (Methodological), 211-252.

Brice, J. (1960). "Index for description of channel braiding." Geological Society of America Bulletin, 71, 1833.

Bridge, J. S. (1993). "The interaction between channel geometry, water flow, sediment transport and deposition in braided rivers." Geological Society, London, Special Publications, 75(1), 13-71.

Bridge, J., Smith, N., Trent, F., Gabel, S., and Bernstein, P. (1986). "Sedimentology and morphology of a low-sinuosity river: Calamus River, Nebraska Sand Hills." Sedimentology, 33(6), 851-870.

Bristow, C. S. (1993). "Sedimentary structures exposed in bar tops in the Brahmaputra River, Bangladesh." Geological Society, London, Special Publications, 75(1), 277-289.

Bristow, C. S., Best, J., and Roy, A. (1993). "Morphology and facies models of channel confluences." Alluvial Sedimentation, 89-100.

Bristow, C., and Best, J. (1993). "Braided rivers: perspectives and problems." Geological Society, London, Special Publications, 75(1), 1-11.

Callander, R. (1969). "Instability and river channels." Journal of Fluid Mechanics, 36(3), 465-480.

Cambon, C., Jacquin, L., and Lubrano, J. (1992). "Toward a new Reynolds stress model for rotating turbulent flows." Physics of Fluids A: Fluid Dynamics, 4(4), 812-824.

Cant, D. J., and Walker, R. G. (1978). "Fluvial processes and facies sequences in the sandy braided South Saskatchewan River, Canada." Sedimentology, 25(5), 625-648.

Cea, L., Puertas, J., and Pena, L. (2007). "Velocity measurements on highly turbulent free surface flow using ADV." Experiments in fluids, 42(3), 333-348.

Cellino, M., and Lemmin, U. (2004). "Influence of coherent flow structures on the dynamics of suspended sediment transport in open-channel flow." Journal of Hydraulic Engineering, 130(11), 1077-1088.

Chahar, B. R. (2007). "Optimal design of a special class of curvilinear bottomed channel section." Journal of Hydraulic Engineering, 133(5), 571-576.

Church, M., and Ferguson, R. (2015). "Morphodynamics: Rivers beyond steady state." Water Resources Research, 51(4), 1883-1897.

Church, M., and Jones, D. (1982). "Gravel-bed rivers." Sediment Cascades: An Integrated Approach, 241-269.

Coleman, J. M. (1969). "Brahmaputra River: channel processes and sedimentation." Sedimentary Geology, 3(2-3), 129-239.

Crosato, A., Mosselman, E., Beidmariam Desta, F., and Uijttewaal, W. S. (2011). "Experimental and numerical evidence for intrinsic nonmigrating bars in alluvial channels." Water Resources Research, 47(3).

Cuthbertson, A., and Ervine, D. (2007). "Experimental study of fine sand particle settling in turbulent open channel flows over rough porous beds." Journal of Hydraulic Engineering, 133(8), 905-916.

Czernuszenko, W., and Rowiński, P. (2008). "Shear stress statistics in a compound channel flow." Arch Hydro-Engin Environ Mech, 55(1-2), 3-27.

Detert, M., Weitbrecht, V., and Jirka, G. (2007). "Simultaneous velocity and pressure measurements using PIV and multi layer pressure sensor arrays in gravel bed flows." HMEM, Lake Placid.

Dey, S., Bose, S. K., and Sastry, G. L. (1995). "Clear water scour at circular piers: a model." Journal of Hydraulic Engineering, 121(12), 869-876.

Dey, S., Raikar, R. V., and Roy, A. (2008). "Scour at submerged cylindrical obstacles under steady flow." Journal of Hydraulic Engineering, 134(1), 105-109.

Dey, S., Sarkar, S., and Solari, L. (2011). "Near-bed turbulence characteristics at the entrainment threshold of sediment beds." Journal of Hydraulic Engineering, 137(9), 945-959.

Dobler, A., and Ahrens, B. (2008). "Precipitation by a regional climate model and bias correction in Europe and South Asia." Meteorologische Zeitschrift, 17(4), 499-509.

Drake, T. G., Shreve, R. L., Dietrich, W. E., Whiting, P. J., and Leopold, L. B. (1988). "Bedload transport of fine gravel observed by motion-picture photography." Journal of Fluid Mechanics, 192, 193-217.

Durbin, P. (1993). "A Reynolds stress model for near-wall turbulence." Journal of Fluid Mechanics, 249, 465-498.

Eaton, B. C., Millar, R. G., and Davidson, S. (2010). "Channel patterns: braided, anabranching, and single-thread." Geomorphology, 120(3-4), 353-364.

Federici, B., and Paola, C. (2003). "Dynamics of channel bifurcations in noncohesive sediments." Water Resources Research, 39(6).

Ferguson, R. (1993). "Understanding braiding processes in gravel-bed rivers: progress and unsolved problems." Geological Society, London, Special Publications, 75(1), 74-87.

Ferguson, R. I., and Werritty, A. (1983). "Bar development and channel changes in the gravelly River Feshie, Scotland." Modern and ancient fluvial systems, 181-193.

Finelli, C. M., Hart, D. D., and Fonseca, D. M. (1999). "Evaluating the spatial resolution of an acoustic Doppler velocimeter and the consequences for measuring near-bed flows." Limnology and Oceanography, 44(7), 1793-1801.

Flügel, W. A. (1995). "Delineating hydrological response units by geographical information system analyses for regional hydrological modelling using PRMS/MMS in the drainage basin of the River Bröl, Germany." Hydrological Processes, 9(3-4), 423-436.

Franca, M., and Lemmin, U. (2006). "Eliminating velocity aliasing in acoustic Doppler velocity profiler data." Measurement Science and Technology, 17(2), 313.

Gad-el-Hak, M., and Bandyopadhyay, P. R. (1994). "Reynolds number effects in wall-bounded turbulent flows." Appl. Mech. Rev, 47(8), 307-365.

Gaur, S., Chahar, B. R., and Graillot, D. (2011). "Analytic elements method and particle swarm optimization based simulation–optimization model for groundwater management." Journal of hydrology, 402(3), 217-227.

Gheisi, A. R., Alavimoghaddam, M. R., and Dadrasmoghaddam, A. (2006). "Markovian–Octant analysis based stable turbulent shear stresses in near-bed bursting phenomena of vortex settling chamber." Environmental Fluid Mechanics, 6(6), 549-572.

Girija, T., Mahanta, C., and Chandramouli, V. (2007). "Water quality assessment of an untreated effluent impacted urban stream: the Bharalu tributary of the Brahmaputra River, India." Environmental Monitoring and Assessment, 130(1), 221-236.

Goel, A. "Estimation of scour downstream of spillways using SVM modeling." Proc., Proceedings of the World Congress on Engineering and Computer Science WCECS, October, 22-24.

Goel, A. (2008). "Design of stilling basin for circular pipe outlets." Canadian Journal of Civil Engineering, 35(12), 1365-1374.

Goff, J. R., and Ashmore, P. (1994). "Gravel transport and morphological change in braided Sunwapta River, Alberta, Canada." Earth Surface Processes and Landforms, 19(3), 195-212.

Hein, F. J., and Walker, R. G. (1977). "Bar evolution and development of stratification in the gravelly, braided, Kicking Horse River, British Columbia." Canadian Journal of Earth Sciences, 14(4), 562-570.

Howard, A. D., Keetch, M. E., and Vincent, C. L. (1970). "Topological and geometrical properties of braided streams." Water Resources Research, 6(6), 1674-1688.

Hussain, A. F. (1983). "Coherent structures—reality and myth." The Physics of fluids, 26(10), 2816-2850.

Jang, C.-L., and Shimizu, Y. (2007). "Vegetation effects on the morphological behavior of alluvial channels." Journal of Hydraulic Research, 45(6), 763-772.

Jennifer, D., Li, H., Guangqian, W., and Xudong, F. (2011). "Turbulent burst around experimental spur dike." International Journal of Sediment Research, 26(4), 471-523.

Joglekar, J., and Gedam, S. S. (2012). "Area based image matching methods—A survey." Int. J. Emerg. Technol. Adv. Eng, 2(1), 130-136.

Julien, P. Y., and Klaassen, G. J. (1995). "Sand-dune geometry of large rivers during floods." Journal of Hydraulic Engineering, 121(9), 657-663.

Izadinia, E., Heidarpour, M., and Schleiss, A. J. (2013). "Investigation of turbulence flow and sediment entrainment around a bridge pier." Stochastic environmental research and risk assessment, 27(6), 1303-1314.

Kang, S., Xu, Y., You, Q., Flügel, W.-A., Pepin, N., and Yao, T. (2010). "Review of climate and cryospheric change in the Tibetan Plateau." Environmental Research Letters, 5(1), 015101.

Katul, G., Kuhn, G., Schieldge, J., and Hsieh, C.-I. (1997). "The ejection-sweep character of scalar fluxes in the unstable surface layer." Boundary-Layer Meteorology, 83(1), 1-26.

Keshavarzi, A. R., and Gheisi, A. R. (2006). "Stochastic nature of three dimensional bursting events and sediment entrainment in vortex chamber." Stochastic Environmental Research and Risk Assessment, 21(1), 75-87.

Keshavarzi, A. R., Ziaei, A. N., Homayoun, E., and Shirvani, A. (2005). "Fractal-Markovian scaling of turbulent bursting process in open channel flow." Chaos, Solitons & Fractals, 25(2), 307-318.

Keshavarzi, A., and Gheisi, A. (2007). "Three-dimensional fractal scaling of bursting events and their transition probability near the bed of vortex chamber." Chaos, Solitons & Fractals, 33(2), 342-357.

Keshavarzi, A., and Shirvani, A. "Probability analysis of instantaneous shear stress and entraind particles from the bed." Proc., Proceedings of the CSCE/EWRI of ASCE Environmental engineering conference, Niagara.

Keshavarzi, A., Melville, B., and Ball, J. (2014). "Three-dimensional analysis of coherent turbulent flow structure around a single circular bridge pier." Environmental Fluid Mechanics, 14(4), 821-847.

Keshavarzy, A. (1997). Entrainment of sediment particles from a flat mobile bed with the influence of near-wall turbulence, University of New South Wales.

Khan, M. A., Sharma, N., and Singhal, G. D. (2016). "Experimental study on bursting events around a bar in physical model of a braided channel." ISH Journal of Hydraulic Engineering, 1-8.

Kim, J. (1985). "Turbulence structures associated with the bursting event." Physics of Fluids (1958-1988), 28(1), 52-58.

Klaasen, G. (1999). "Flow structure and transport of sand-grade suspended sediment around an evolving braid bar, Jamuna River, Bangladesh."

Kleinhans, M. G. (2010). "Sorting out river channel patterns." Progress in Physical Geography, 34(3), 287-326.

Kleinhans, M. G., and van den Berg, J. H. (2011). "River channel and bar patterns explained and predicted by an empirical and a physics-based method." Earth Surface Processes and Landforms, 36(6), 721-738.

Kline, S., Reynolds, W., Schraub, F., and Runstadler, P. (1967). "The structure of turbulent boundary layers." J. Fluid Mech, 30(4), 741-773.

Kostaschuk, R., and Ilersich, S. (1995). "Dune geometry and sediment transport: Fraser River, British Columbia." River geomorphology, 19-36.

Kostaschuk, R., and Villard, P. (1996). "Flow and sediment transport over large subaqueous dunes: Fraser River, Canada." Sedimentology, 43(5), 849-863.

Kozioł, A. (2015). "Scales of turbulent eddies in a compound channel." Acta Geophysica, 63(2), 514-532.

Krogstadt, P.-Å., and Antonia, R. (1999). "Surface roughness effects in turbulent boundary layers." Experiments in fluids, 27(5), 450-460.

Kumar, A., Kothyari, U. C., and Raju, K. G. R. (2012). "Flow structure and scour around circular compound bridge piers–A review." Journal of Hydro-environment Research, 6(4), 251-265.

Lane, E. W. (1957). A study of the shape of channels formed by natural streams flowing in erodible material, US Army Engineer Division, Missouri River.

Leopold, L., and Wolman, M. (1957). "River channel patterns." Fluv Geom: Geom Crit Conc Vol, 3.

Lewin, J. (1976). "Initiation of bed forms and meanders in coarse-grained sediment." Geological Society of America Bulletin, 87(2), 281-285.

Li, S.-G., Venkataraman, L., and mclaughlin, D. (1992). "Stochastic theory for irregular stream modeling. Part I: flow resistance." Journal of Hydraulic Engineering, 118(8), 1079-1090.

Lien, R.-C., and D'Asaro, E. A. (2006). "Measurement of turbulent kinetic energy dissipation rate with a Lagrangian float." Journal of Atmospheric and Oceanic Technology, 23(7), 964-976.

Lu, S., and Willmarth, W. (1973). "Measurements of the structure of the Reynolds stress in a turbulent boundary layer." Journal of Fluid Mechanics, 60(03), 481-511.

Luchi, R., Zolezzi, G., and Tubino, M. (2010). "Modelling mid-channel bars in meandering channels." Earth Surface Processes and Landforms, 35(8), 902-917.

Lunt, I., and Bridge, J. (2004). "Evolution and deposits of a gravelly braid bar, Sagavanirktok River, Alaska." Sedimentology, 51(3), 415-432.

Lunt, I., Bridge, J., and Tye, R. (2004). "A quantitative, three-dimensional depositional model of gravelly braided rivers." Sedimentology, 51(3), 377-414.

Mahanta, C. (2010). "India's north east and hydropower development: Future security challenges." South Asian Survey, 17(1), 131-146.

Mao, Y. (2003). "The effects of turbulent bursting on the sediment movement in suspension." International Journal of Sediment Research, 18(2), 148-157.

Matthes, G. H. (1947). "Macroturbulence in natural stream flow." Eos, Transactions American Geophysical Union, 28(2), 255-265.

Mazumder, B., and Ojha, S. P. (2007). "Turbulence statistics of flow due to wave–current interaction." Flow Measurement and Instrumentation, 18(3), 129-138.

Mianaei, S. J., and Keshavarzi, A. R. (2008). "Spatio-temporal variation of transition probability of bursting events over the ripples at the bed of open channel." Stochastic Environmental Research and Risk Assessment, 22(2), 257-264.

Mori, N., Suzuki, T., and Kakuno, S. (2007). "Experimental study of air bubbles and turbulence characteristics in the surf zone." Journal of Geophysical Research: Oceans, 112(C5).

Mosley, M. P. (1976). "An experimental study of channel confluences." The journal of geology, 535-562.

Mosselman, E. (2009). "Bank protection and river training along the braided Brahmaputra-Jamuna River, Bangladesh." Braided Rivers: Process, Deposition, Ecology and Management, edited by: Smith, GHS, Best, JL, Bristow, CS, and Petts, GE, Blackwell, Oxford, UK, 277-287.

Murray, A. B., and Paola, C. (1994). "A cellular model of braided rivers."

Nagano, Y., and Tagawa, M. (1988). "Statistical characteristics of wall turbulence with a passive scalar." Journal of Fluid Mechanics, 196, 157-185.

Nakagawa, H., and Nezu, I. (1978). "Bursting phenomenon near the wall in open-channel flows and its simple mathematical model." Kyoto University Faculty Engineering Memoirs, 40, 213-240.

Nakagawa, H., and Nezu, I. (1981). "Structure of space-time correlations of bursting phenomena in an open-channel flow." Journal of Fluid Mechanics, 104, 1-43.

Nakagawa, H., Nezu, I., and Ueda, H. (1975). "Turbulence of open channel flow over smooth and rough beds." 土木学会論文報告集, 1975(241), 155-168.

Naot, D., Nezu, I., and Nakagawa, H. (1993). "Hydrodynamic behavior of compound rectangular open channels." Journal of Hydraulic Engineering, 119(3), 390-408.

Neary, V. S., and Odgaard, A. J. (1993). "Three-dimensional flow structure at open-channel diversions." Journal of Hydraulic Engineering, 119(11), 1223-1230.

Nelson, J. M., Shreve, R. L., mclean, S. R., and Drake, T. G. (1995). "Role of near-bed turbulence structure in bed load transport and bed form mechanics." Water Resources Research, 31(8), 2071-2086.

Nezu, I., and Nakagawa, H. (1989). "Turbulent structure of backward-facing step flow and coherent vortex shedding from reattachment in open-channel flows." Turbulent shear flows 6, Springer, 313-337.

Nezu, I., Nakagawa, H., and Jirka, G. H. (1994). "Turbulence in open-channel flows." Journal of Hydraulic Engineering, 120(10), 1235-1237.

Nikora, V., and Goring, D. (2000). "Flow turbulence over fixed and weakly mobile gravel beds." Journal of Hydraulic Engineering, 126(9), 679-690.

Offen, G., and Kline, S. (1975). "A proposed model of the bursting process in turbulent boundary layers." Journal of Fluid Mechanics, 70(02), 209-228.

Ojha, S. P., and Mazumder, B. (2008). "Turbulence characteristics of flow region over a series of 2-D dune shaped structures." Advances in Water Resources, 31(3), 561-576.

Ojha, S. P., and Mazumder, B. (2010). "Turbulence characteristics of flow over a series of 2-D bed forms in the presence of surface waves." Journal of Geophysical Research: Earth Surface, 115(F4).

Ore, H. T. (1964). "Some criteria for recognition of braided stream deposits." Rocky Mountain Geology, 3(1), 1-14.

Parker, G. (1976). "On the cause and characteristic scales of meandering and braiding in rivers." Journal of fluid mechanics, 76(3), 457-480.

Purtell, L., Klebanoff, P., and Buckley, F. (1981). "Turbulent boundary layer at low Reynolds number." The Physics of Fluids, 24(5), 802-811.

Rice, S. P., Church, M., Wooldridge, C. L., and Hickin, E. J. (2009). "Morphology and evolution of bars in a wandering gravel-bed river; lower Fraser river, British Columbia, Canada." Sedimentology, 56(3), 709-736.

Richardson, W. R., and Thorne, C. R. (1998). "Secondary currents around braid bar in Brahmaputra River, Bangladesh." Journal of hydraulic engineering, 124(3), 325-328.

Richardson, W. R., and Thorne, C. R. (2001). "Multiple thread flow and channel bifurcation in a braided river: Brahmaputra–Jamuna River, Bangladesh." Geomorphology, 38(3), 185-196.

Rosgen, D. L. "A stream classification system." Proc., Riparian Ecosystems and Their Management. First North American Riparian Conference. Rocky Mountain Forest and Range Experiment Station, RM-120, 91-95.

Roy, A. G., Buffin-Belanger, T., Lamarre, H., and Kirkbride, A. D. (2004). "Size, shape and dynamics of large-scale turbulent flow structures in a gravel-bed river." Journal of Fluid Mechanics, 500, 1-27.

Roy, A., and Bergeron, N. (1990). "Flow and particle paths at a natural river confluence with coarse bed material." Geomorphology, 3(2), 99-112.

Rust, B. R. (1977). "Depositional models for braided alluvium."

Sankhua, R., Sharma, N., Garg, P., and Pandey, A. (2005). "Use of remote sensing and ANN in assessment of erosion activities in Majuli, the world's largest river island." International Journal of Remote Sensing, 26(20), 4445-4454.

Sapozhnikov, V., and Foufoula-Georgiou, E. (1996). "Self-affinity in braided rivers." Water Resources Research, 32(5), 1429-1439.

Sarkar, A., and Ratha, D. (2014). "Flow around submerged structures subjected to shallow submergence over plane bed." Journal of Fluids and Structures, 44, 166-181.

Sarma, J. (2005). "Fluvial process and morphology of the Brahmaputra River in Assam, India." Geomorphology, 70(3-4), 226-256.

Sarma, J., and Phukan, M. (2006). "Bank erosion and bankline migration of the Brahmaputra River in Assam during the twentieth century." JOURNAL-GEOLOGICAL SOCIETY OF INDIA, 68(6), 1023.

Schumm, S. A., and Lichty, R. W. (1963). "Channel widening and flood-plain construction along Cimarron River in southwestern Kansas."

Schumm, S., and Khan, H. (1972). "Experimental study of channel patterns." Geological Society of America Bulletin, 83(6), 1755-1770.

Shamloo, H., Rajaratnam, N., and Katopodis, C. (2001). "Hydraulics of simple habitat structures." Journal of Hydraulic Research, 39(4), 351-366.

Sharma, N. (2004). "Mathematical modelling and braid indicators." The Brahmaputra basin water resources, Springer, 229-260.

Shvidchenko, A. B., and Pender, G. (2001). "Macroturbulent structure of open-channel flow over gravel beds." Water Resources Research, 37(3), 709-719.

Singh, A., Krause, P., Panda, S. N., and Flugel, W.-A. (2010). "Rising water table: A threat to sustainable agriculture in an irrigated semi-arid region of Haryana, India." Agricultural water management, 97(10), 1443-1451.

Smith, N. (1970). "The braided stream depositional environment: comparison of the Platte River with some Silurian clastic rocks, north-central Appalachians." Geological Society of America Bulletin, 81(10), 2993-3014.

Sumer, B. M., and Deigaard, R. (1981). "Particle motions near the bottom in turbulent flow in an open channel. Part 2." Journal of Fluid Mechanics, 109, 311-337.

Surian, N. (2015). "Fluvial Processes in Braided Rivers." Rivers–Physical, Fluvial and Environmental Processes, Springer, 403-425.

Szupiany, R. N., Amsler, M. L., Parsons, D. R., and Best, J. L. (2009). "Morphology, flow structure, and suspended bed sediment transport at two large braid-bar confluences." Water Resources Research, 45(5).

Thorne, C. R., and Tovey, N. K. (1981). "Stability of composite river banks." Earth Surface Processes and Landforms, 6(5), 469-484.

Thorne, C. R., Russell, A. P., and Alam, M. K. (1993). "Planform pattern and channel evolution of the Brahmaputra River, Bangladesh." Geological Society, London, Special Publications, 75(1), 257-276.

Tiwari, H., and Sharma, N. (2014). "Statistical study of turbulence near piano key weir: a review." Journal of Experimental & Applied Mechanics, 5(3), 16-28.

Van der Wegen, M., and Roelvink, J. (2008). "Long-term morphodynamic evolution of a tidal embayment using a two-dimensional, process-based model." Journal of Geophysical Research: Oceans, 113(C3).

Van Rijn, L. C. (1993). Principles of sediment transport in rivers, estuaries and coastal seas, Aqua publications Amsterdam.

Voulgaris, G., and Trowbridge, J. H. (1998). "Evaluation of the acoustic Doppler velocimeter (ADV) for turbulence measurements*." Journal of Atmospheric and Oceanic Technology, 15(1), 272-289.

Wallace, J. M., Eckelmann, H., and Brodkey, R. S. (1972). "The wall region in turbulent shear flow." Journal of Fluid Mechanics, 54(01), 39-48.

Wang, X., Yang, Q., Lu, W. (2012). "Experimental study of near-wall turbulent characteristics in an open-channel with gravel bed using an acoustic Doppler velocimeter." Experiments in fluids, 52(1), 85-94.

Williams, J. J., Thorne, P. D., and Heathershaw, A. D. (1989). "Comparisons between acoustic measurements and predictions of the bedload transport of marine gravels." Sedimentology, 36(6), 973-979.

Wohl, E. E. (2000). Mountain rivers, Amer Geophysical Union.

Wu, F.-C., and Jiang, M.-R. (2007). "Numerical investigation of the role of turbulent bursting in sediment entrainment." Journal of Hydraulic Engineering, 133(3), 329-334.

Yalin, M. (1992). "River mechanics. Eds." Pergamon Press, Oxford, England.

ANNEX-I

MATLAB codes for computing the relationships between the stable transition movements

```
% Program by Mohammad Amir Khan
% Program for Ph.D Thesis
% For developing the relationships between the stable transitional movements
% Program for Class A stable transitional movements
% Reading Excel File
d=xlsread('D:\excel for transition prob.xlsx');
[RR,C]=size(d);
%defining the Data
i=d(:,4);  ii=d(:,5); iii=d(:,6); iv=d(:,7); v=d(:,8); vi=d(:,9); vii=d(:,10);
viii=d(:,11);
% i represent the transition probability of P1→1 movements. Similarly, other
stable transition movements are defined.
% Defining the dependent variables
a1=ii;
a2=iii;
a3=iv;
a=[a1,a2,a3];
% Defining the independent variable
p=ia;
% Defining the dependent variables
b1=i;
b2=iii;
b3=iv;
b=[b1,b2,b3];
% Defining the independent variable
q=ii;
% Defining the dependent variables
c1=i;
c2=ii;
c3=iv;
c=[c1,c2,c3];
% Defining the independent variable
r=iii;
% Defining the dependent variables
e1=i;
e2=ii;
```

```
e3=iii;
e=[e1,e2,e3];
% Defining the independent variable
s=iva;
% beta function for developing the relationships
% All initial values are taken as one for first iteration
beta0 =[1.0 1.0 1.0 1.0 1.0 1.0];
% brate Function defined later
% “nlinfit” MATLAB Toolbox for performing the Nonlinear fitting
betaa= nlinfit(a,p,'brate',beta0);
coefft1=[betaa];
phat = brate(betaa,a);
% computing the coefficients of brate function
betab= nlinfit(b,q,'brate',beta0);
coefft2=[betab];
qhat = brate(betab,b);
betac= nlinfit(c,r,'brate',beta0);
coefft3=[betac];
rhat = brate(betac,c);
betad= nlinfit(e,s,'brate',beta0);
coefft4=[betad];
shat = brate(betad,e);
% Figures for displaying the relating between the exact values and computed
values
for i=1:1
  figure(i)
  [m1,b1,r1] = postreg(phat,p);
end
for i=2:2
  figure(i)
  [m1,b1,r1] = postreg(qhat,q);
end
for i=3:3
  figure(i)
  [m1,b1,r1] = postreg(rhat,r);
end
for i=4:4
  figure(i)
  [m1,b1,r1] = postreg(shat,s);
```

```
end
% for testing and fitting of experimental data
iifit = [1:10:RR,2:10:RR,3:10:RR, 4:10:RR, 6:10:RR, 7:10:RR, 8:10:RR,9:10:RR];
iitst = [5:10:RR, 10:10:RR];
a1fit=iia(iifit,:);
a2fit=iiia(iifit,:);
a3fit=iva(iifit,:);

b1fit=ia(iifit,:);
b2fit=iiia(iifit,:);
b3fit=iva(iifit,:);

c1fit=ia(iifit,:);
c2fit=iia(iifit,:);
c3fit=iva(iifit,:);

e1fit=ia(iifit,:);
e2fit=iia(iifit,:);
e3fit=iiia(iifit,:);

afit=[a1fit,a2fit,a3fit];
bfit=[b1fit,b2fit,b3fit];
cfit=[c1fit,c2fit,c3fit];
efit=[e1fit,e2fit,e3fit];

pfit=ia(iifit,:);
qfit=iia(iifit,:);
rfit=iiia(iifit,:);
sfit=iva(iifit,:);
phatfit = brate(betaa,afit);
qhatfit = brate(betab,bfit);
rhatfit = brate(betac,cfit);
shatfit = brate(betad,efit);


a1tst=iia(iitst,:);
a2tst=iiia(iitst,:);
a3tst=iva(iitst,:);
```

```
b1tst=ia(iitst,:);
b2tst=iiia(iitst,:);
b3tst=iva(iitst,:);

c1tst=ia(iitst,:);
c2tst=iia(iitst,:);
c3tst=iva(iitst,:);

e1tst=ia(iitst,:);
e2tst=iia(iitst,:);
e3tst=iiia(iitst,:);

atst=[a1tst,a2tst,a3tst];
btst=[b1tst,b2tst,b3tst];
ctst=[c1tst,c2tst,c3tst];
etst=[e1tst,e2tst,e3tst];

ptst=ia(iitst,:);
qtst=iia(iitst,:);
rtst=iiia(iitst,:);
stst=iva(iitst,:);
phattst = brate(betaa,atst);
qhattst = brate(betab,btst);
rhattst = brate(betac,ctst);
shattst = brate(betad,etst);


% For doing the performance analysis
xx1=[pfit,phatfit];
xx2=[qfit,qhatfit];
xx3=[rfit,rhatfit];
xx4=[sfit,shatfit];
perfit1=performance(xx1);
perfit2=performance(xx2);
perfit3=performance(xx3);
perfit4=performance(xx4);

xx5=[ptst,phattst];
xx6=[qtst,qhattst];
```

```
xx7=[rtst,rhattst];
xx8=[stst,shattst];
pertst1=performance(xx5);
pertst2=performance(xx6);
pertst3=performance(xx7);
pertst4=performance(xx8);
perf_Column=[perfit1;perfit2;perfit3;perfit4;pertst1;pertst2;pertst3;pertst4];
fclose('all');

% Program for Class B stable transition movements
% Reading Excel File
d=xlsread('D:\excel for transition prob.xlsx');
[RR,C]=size(d);
%defining the Data
v=d(:,8); vi=d(:,9); vii=d(:,10); viii=d(:,11);
defining the dependent variables
a1=vi;
a2=vii;
a3=viii;
a=[a1,a2,a3];
defining the independent variable
p=v;
defining the dependent variables
b1=v;
b2=vii;
b3=viii;
b=[b1,b2,b3];
defining the independent variable
q=vi;
defining the dependent variables
c1=v;
c2=vi;
c3=viii;
c=[c1,c2,c3];
defining the independent variable
r=vii;
defining the dependent variables
e1=v;
e2=vi;
```

```
e3=vii;
e=[e1,e2,e3];
defining the independent variable
s=viii;
% beta function for developing relationships between the class b transition
movements
% all initial values are taken as one for first iteration

beta0 =[1.0 1.0 1.0 1.0 1.0 1.0];
% “nlinfit” MATLAB toolbox for performing the Nonlinear fitting

betaa= nlinfit(a,p,'brate',beta0);
% Computing the coefficients of brate function
coefft1=[betaa];
phat = brate(betaa,a);
betab= nlinfit(b,q,'brate',beta0);
coefft2=[betab];
qhat = brate(betab,b);
betac= nlinfit(c,r,'brate',beta0);
coefft3=[betac];
rhat = brate(betac,c);
betad= nlinfit(e,s,'brate',beta0);
coefft4=[betad];
shat = brate(betad,e);
% Figures for displaying the relating between the exact values and computed
values

for i=1:1
  figure(i)
  [m1,b1,r1] = postreg(phat,p);
end
for i=2:2
  figure(i)
  [m1,b1,r1] = postreg(qhat,q);
end
for i=3:3
  figure(i)
  [m1,b1,r1] = postreg(rhat,r);
end
```

```
for i=4:4
  figure(i)
  [m1,b1,r1] = postreg(shat,s);
end
% for testing and fitting of experimental data
iifit = [1:10:RR,2:10:RR,3:10:RR, 4:10:RR, 6:10:RR, 7:10:RR, 8:10:RR,9:10:RR];
iitst = [5:10:RR, 10:10:RR];
a1fit=iib(iifit,:);
a2fit=iiib(iifit,:);
a3fit=ivb(iifit,:);

b1fit=ib(iifit,:);
b2fit=iiib(iifit,:);
b3fit=ivb(iifit,:);

c1fit=ib(iifit,:);
c2fit=iib(iifit,:);
c3fit=ivb(iifit,:);

e1fit=ib(iifit,:);
e2fit=iib(iifit,:);
e3fit=iiib(iifit,:);

afit=[a1fit,a2fit,a3fit];
bfit=[b1fit,b2fit,b3fit];
cfit=[c1fit,c2fit,c3fit];
efit=[e1fit,e2fit,e3fit];

pfit=ib(iifit,:);
qfit=iib(iifit,:);
rfit=iiib(iifit,:);
sfit=ivb(iifit,:);
phatfit = brate(betaa,afit);
qhatfit = brate(betab,bfit);
rhatfit = brate(betac,cfit);
shatfit = brate(betad,efit);


a1tst=iib(iitst,:);
```

```
a2tst=iiib(iitst,:);
a3tst=ivb(iitst,:);

b1tst=ib(iitst,:);
b2tst=iiib(iitst,:);
b3tst=ivb(iitst,:);

c1tst=ib(iitst,:);
c2tst=iib(iitst,:);
c3tst=ivb(iitst,:);

e1tst=ib(iitst,:);
e2tst=iib(iitst,:);
e3tst=iiib(iitst,:);

atst=[a1tst,a2tst,a3tst];
btst=[b1tst,b2tst,b3tst];
ctst=[c1tst,c2tst,c3tst];
etst=[e1tst,e2tst,e3tst];

ptst=ib(iitst,:);
qtst=iib(iitst,:);
rtst=iiib(iitst,:);
stst=ivb(iitst,:);
phattst = brate(betaa,atst);
qhattst = brate(betab,btst);
rhattst = brate(betac,ctst);
shattst = brate(betad,etst);

% For doing the performance analysis
xx1=[pfit,phatfit];
xx2=[qfit,qhatfit];
xx3=[rfit,rhatfit];
xx4=[sfit,shatfit];
perfit1=performance(xx1);
perfit2=performance(xx2);
perfit3=performance(xx3);
perfit4=performance(xx4);
```

```
xx5=[ptst,phattst];
xx6=[qtst,qhattst];
xx7=[rtst,rhattst];
xx8=[stst,shattst];
pertst1=performance(xx5);
pertst2=performance(xx6);
pertst3=performance(xx7);
pertst4=performance(xx8);
perf_Column=[perfit1;perfit2;perfit3;perfit4;pertst1;pertst2;pertst3;pertst4];f
close('all');
% Brate Function for performing Nonlinear fitting
function yhat =brate(beta,x)
b1 = beta(1);
b2 = beta(2);
b3 = beta(3);
b4 = beta(4);
b5 = beta(5);
b6 = beta(6);

x1 = x(:,1);
x2 = x(:,2);
x3 = x(:,3);
%yhat=b1.*(x1.^b2.)*(x2.^b3.)*(x3^b4.)+b5.;MOHSIN
%yhat=b1.*(x1.^b2).*(x2.^b3).*(x3.^b4).*(x4.^b5);
%yhat=(x1.^b1).*(x2.^b2).*(x3.^b3).*(x4.^b4)+b5;
yhat=b1.*(x1.^b2)+b3.*(x2.^b4)+b5.*(x3.^b6):
```

ANNEX-II

JOURNALS

1. **Khan Amir** and S. Nayan (2016), Experimental study on coherent structure around a bar in physical model of a braided channel, ISH Journal of Hydraulic Research, **Taylor and Francis** London, Vol. 23, pp. 63-70.
2. **Khan Amir** and S. Nayan (2017), Analysis of turbulent flow characteristics in the vicinity of Mid-Channel Bar, Korean Society of Civil Engineering, **Springer**, pp. 1-10.
3. **Khan Amir** and S. Nayan (2017), Study of turbulent characteristics of flow around island in a braided river model using quadrant technique, ISH Journal of Hydraulic Research, **Taylor and Francis** London, Vol.24, pp. 1-8.
4. **Khan Amir**, S. Nayan and S.Gopal (2017), Analysis of turbulent dynamics in the vicinity of braided bar, ISH Journal of Hydraulic Research, **Taylor and Francis** London, 2017, Vol. 23, pp.267-275.
5. **Khan Amir** and S. Nayan (2017): Braided River: Aspects and Issues, Journal of Water Resource Engineering and Management, Vol 4, pp.1-7.
6. **Khan Amir** and S. Nayan (2017), Turbulence burst analysis around bar in a braided river model, Water Resources Journal, **Springer** (accepted for publication).

INTERNATIONAL CONFERENCES

1. **Khan Amir** and S. Nayan (2015), A review of Reynolds Stress Model for Turbulent Flow, Hydro, International conference on Hydraulic Research, IIT Roorkee.
2. **Khan Amir** and S. Nayan (2016), Flow Characteristics near the braided island, National Conference on "Water Resources & Hydropower-2016, UPES, Dehradoon.
3. **Khan Amir** and S. Nayan (2016), A study of Stream Braiding, India Water week, International conference on Water Research 2016, Vigyan Bhawan New Delhi.
4. **Khan Amir** and S. Nayan (2018), Experimental study of coherent structure at close proximity of mid channel bar, International Conference on Sustainable Technologies for Intelligent Water Management, IIT Roorkee.

PAPER UNDER REVIEW

1. (**Khan Amir**, S. Nayan and J.Odgaard), Study of stream flow turbulent burst in the vicinity of Mid-Channel bar, Stochastic Environmental Research and Risk Assessment, **Springer**.
2. (**Khan Amir**, S. Nayan), Experimental investigation of coherent flow structures in the vicinity of bar, Journal of Environmental Fluid mechanics, **Springer**.
3. (**Khan Amir**, S. Nayan), Experimental study of turbulence structure near the mid-channel bar, Sadhana Journal, **Springer**.